UNIVERSITY OF THE
WITWATERSRAND,
JOHANNESBURG

THERMO–PHOTOCATALYTIC PRODUCTION OF HYDROGEN FROM WATER WITH METHANOL/ FORMALDEHYDE AS SACRIFICIAL AGENT UNDER MILD CONDITIONS

by

Nancy Akoth Nyamai

Student Number: 2391056

A THESIS

Submitted in fulfilment of the requirements for the degree of

DOCTOR OF PHILOSOPHY

in

CHEMISTRY

in the Faculty of Science, University of the Witwatersrand, Johannesburg, South Africa

OCTOBER 2024

DECLARATION

I declare that this thesis is my own, unaided work. It is being submitted for the Degree of Philosophy in Chemistry at the University of the Witwatersrand, Johannesburg. It has not been submitted before for any degree or examination at any other University.

_____

(Candidate)

_22_day of _October__2024_at_14:15 pm

ABSTRACT

Fossil fuels are the main source of energy for modern society to this decade. The awareness of scarcity of fossil fuels and the environmental degradation accompanying their use has motivated researchers to conduct extensive research in other forms of energy for mitigation. Hydrogen has the potential to replace the traditional fuels for transportation application and other uses. Comparatively, hydrogen has higher energy (143 MJ/kg) than the conventional fossil fuels (natural gas: 53.6 MJ/kg, petrol: 46.4 MJ/kg, diesel: 45.4 MJ/kg) moreover, its environmental friendly as it produces water as the only by-product of its combustion. In spite of its superiority, public acceptance of hydrogen based technologies are still undermined. Following the main finding of water-based photoelectrolysis in 1972, scientists, engineers and environmental activists have intensified research on the production of hydrogen via photocatalytic water splitting adopting different modifications of semiconducting materials such as titanium dioxide, TiO_2, cadmium sulphide, graphitic carbon nitride and using sunlight to fragment water molecules to produce hydrogen gas. Titanium is one of the most attractive d-block transition metals in use as water splitting photocatalyst. It is preferred because of its low density, high strength, corrosion resistance, availability and cost effectiveness. However, efficient water splitting using visible light and TO_2 has been a challenge. TO_2 has a setback of wide bandgap, 3.0 – 3.2 eV, which lowers its prospective for visible light absorption. This study outlines the development and the testing of efficient catalytic materials for the thermo-photocatalytic production of hydrogen from water. Methanol-water mixture was also tested under mild conditions. TiO_2 composited with carbon nanofibers, CNFs at different loadings (0, 10 and 20%) and co-catalysts platinum (Pt), gold (Au), iridium (Ir), zinc (Zn) and copper (Cu) were synthesized and used in the photocatalytic water splitting and appreciable quantities of hydrogen were obtained. Additionally, 10% methanol was also used as sacrificial reagent with

water and tested for hydrogen evolution but the results were not significantly different when compared to the results obtained from the use of photocatalysts without methanol addition. The photocatalysts were tested for hydrogen production using water, and the most active photocatalyst, F_CNFs/20% _TiO_2/6%Pt exhibited an activity of 0.45 mol g^{-1} h^{-1}. This was followed by F_CNFs/10% _TiO_2/5%Au and F_CNFs/20% _TiO_2/1%Ir with activities of 0.28 mol g^{-1} h^{-1}, and 0.21 mol g^{-1} h^{-1} respectively. In another section of this study, the focus was on the fabrication of nanomaterials for advanced photocatalytic water splitting as a result, structures of TiO_2/CNFs, Cu/TiO_2/CNFs, and Zn/ TiO_2/CNFs nanocomposites of mesoporous nature were synthesized using CNFs and surfactant wrapping sol-gel/hydrothermal method. Impregnation technique was used in copper and zinc loading while characterization of the synthesized catalysts was achieved by XRD, Raman, FESEM, TEM, UV/DRS, BET, FTIR, XPS, and PL techniques. Water splitting was performed by UV light irradiation and the effect of compositing TiO_2/CNFs-Cu/Zn evaluated. 10%_TiO_2/CNFs/5%Zn composite was the most efficient photocatalyst for hydrogen production when compared with the rest of the samples. The most efficient photocatalyst, 10%_TiO_2/CNFs/5%Zn, produced 0.53 mol (h g cat.)$^{-1}$ of H_2 which was 90-100 folds the amount generated over commercial TiO_2 - P25, and pure TiO_2 photocatalysts. The improved photo-activity of the TiO_2/CNFs, Pt/TiO_2/CNFs, Au/TiO_2/CNFs, Ir/TiO_2/CNFs, Cu/TiO_2/CNFs, and Zn/ TiO_2/CNFs composites were due to the synergistic effect between Pt, Au, Ir, Cu, Zn, and CNFs, greater BET surface area, suitable band structure and reduced recombination rate of the photo-generated charge carriers. This work gives promising route for fabricating TiO_2/CNFs/metal (Pt, Au, Ir, Cu, and Zn) composites for advanced H_2 production using UV- radiation.

DEDICATION

Blessed memory of my loving parents

Augustinus Nyamai and Hulda Omollo Nyamai

ACKNOWLEDGEMENT

I am grateful for the support I received from Prof Neil Coville, Prof Nithaya Chetty, Prof Moira Bode, Prof Charles De Koning, Prof Dean Brady, Prof Nosipho Moloto, Prof Andreas Lemmerer, Dr John Moma, Dr Zikhona Tetana, Dr Cebisa Linganiso, Dr Siziwe Gqoba, Dr Manoko Maubane, Dr Grant Demas, Mr Tshepo Phaphedi Mashoene, Mr Fitsum Hailu, Khwezi Ndawonde, Miss Liz Dodo, Paul – Mercy, Clinton Masemola, Andrew Van Der Riet, Prof Rudolph Erasmus and Dr Tumelo Phaahlamohlaka,

TABLE OF CONTENTS

LIST OF FIGURES

LIST OF TABLES

NOMENCLATURE

CB - Conduction band

CQD - Carbon quantum dots

CMM - Carbon nanomaterials

CNFs – Carbon Nano Fibers

CNTs – Carbon Nano Tubes

FESEM - Field Emission Scanning Electron Microscopy

F_CNF – Functionalized Carbon Nano Fibers

E_g - Band gap Energy

FTIR - Fourier Transform Infrared

eV - Electron Volts

VB - Valence band

h^+_{vb} - Valence band hole

e^-_{cb} - Conduction band electron

STH - Solar to hydrogen

TGA - Thermogravimetric analysis

TEM - Transmission Electron Microscopy

BET - Brunauer – Emmett – Teller

PEC - Photoelectrochemical cell

O_v – Oxygen Vaccanies

UV – Ultraviolet

PV - Photovoltaic

XRD - X-ray diffraction

XPS - X – ray photoelectron spectroscopy

CHAPTER ONE

Introduction

1.1 Background

The use of fossil fuels is a serious problem to the world. The fossil fuel consumption increases the atmospheric greenhouse gases, which leads to global warming and the melting of glaciers. Availability of fossil fuels is also a concern, and their continuous consumption will lead to their fast depletion. The environmental and availability aspects of the fossil fuels are a serious threat to the developing world. The use of hydro power, nuclear power, and wind, solar and tidal power are increasing and progressively replacing the use of fossil fuels such as coal for stationary power generation. But for transportation or mobile applications, there is a demand for an energy source which can replace the fossil fuels. Hydrogen has the potential to replace the traditional fuels for transportation application and other uses. Comparatively, hydrogen has higher energy than the conventional fossil fuels and produces water as the only by-product of its combustion. In spite of its superiority as regards energy content and zero green-house gas emissions to the atmosphere, public acceptance of hydrogen based technologies are still undermined. Subsequent to the principal discovery of water-based photoelectrolysis in 1972, scientists, engineers and environmental activists have intensified research on the production of hydrogen through photocatalytic water splitting adopting different modifications of semiconducting materials such as titanium dioxide, TiO_2, cadmium sulphide, graphitic carbon nitride and using sunlight to fragment water molecules to produce hydrogen gas [1]–[6]. Taking into account the fact that hydrogen is basically a zero-emission green-house gas, a lot of research work has been based on splitting water, aided by various photocatalysts, including the addition of sacrificial agents (electron donors or electron-acceptors) into the processing system [6]. Despite the fact that a catalyst can facilitate reactions with the help of sacrificial agents, this may not be adequate for the absolute separation of water. However, in reactions where

sacrificial agents are involved in the development of hydrogen reactions primarily aim to boost the hydrogen and oxygen yields under such environments. The efficiency is dependent on the catalyst together with the sacrificial agent used [5]. In this study, a section has discussed the production of hydrogen from water using heterogeneous catalysts. The use of methanol/formaldehyde (sacrificial reagents) under mild conditions has also been discussed.

1.2 Problem statement

Indiscriminate use of fossil fuels (coal and petroleum oil) is a major problem for the world. It increases the atmospheric greenhouse gases, which eventually lead to global warming and melting of glaciers [7]–[10]. Availability of these fossil fuels is also a concern, and their continuous consumption will lead to their fast depletion [7], [8], [11]–[13]. Both these issues are serious, and a threat to the development of the modern society. Share of hydro power, nuclear power, wind, solar and tidal power are increasing and progressively replacing the use of fossil fuels such as coal for stationary power generation. But for transportation or mobile applications, there is a demand for an energy source which can replace the fossil fuels such as petrol, diesel. Hydrogen has the potential to replace the traditional fuels for transportation application. Hydrogen has higher specific energy (143 MJ/kg) in comparison to conventional fossil fuels (natural gas: 53.6 MJ/kg, petrol: 46.4 MJ/kg, diesel: 45.4 MJ/kg), hydrogen is very good and produces water as the only by-product of its combustion [14]–[19]. In spite of its superiority in regard to energy content and zero greenhouse gas emissions to the atmosphere, public acceptance of hydrogen based technologies are still undermined. Secondly, finding a way to store large quantity of hydrogen in a portable volume is also a challenge. Even if the storage issue is solved, distribution of hydrogen requires a massive new infrastructure similar to petroleum products to the millions of potential users [20]–[22]. Furthermore, hydrogen is still produced by technologies which require severe process conditions [23]–[29]. Therefore,

hydrogen needs to be generated in a non-flammable liquid, which is safer for transportation and other uses. Besides, systems need to be developed that can use hydrogen directly as it's produced to reduce production and storage costs.

1.3 Justification

To successfully address the problem of fossil fuels depletion and environmental pollution arising from their combustion, the world needs a new form of energy that is renewable, cheap, clean, and safe. Furthermore, hydrogen is a potential substitute to fossil fuels and nuclear energy. Hydrogen production from water with methanol (low concentration), also known as water splitting is conceivably a better route for obtaining a renewable energy compared to conventional technologies such as photovoltaic (PV). Photocatalytic dissociation of water using semiconductors and solar energy was discovered in 1972 and since has become an interesting field to researchers, and photocatalytic materials in the form of metal (oxy) sulphides, metal, non-metal nitrides, metal oxides, metal sulphides, and metal (oxy) nitrides having a cation with d^0 or d^{10} have been studied for this type of work [30], [31]. In photocatalytic water splitting, the photocatalysts used can potentially use inexhaustible solar energy, sacrificial agents, methanol/formaldehyde, and mild conditions, and still operate at low temperatures without additional power sources such as coal and electricity to produce hydrogen. Water splitting is divided into three: (1) thermochemical (2) photobiological and (3) photocatalytic [32]–[38].

Studies have been carried out on hydrogen production from systems consisting of semiconductor particles suspended in aqueous solutions and dissolved organic compounds. The compounds are generally known as sacrificial reagents/agents. For instance, in a Pt/TiO_2-water- methanol system, methanol is oxidized by means of the photo-generated valence band (VB) holes on the metal-decorated photocatalyst hence allowing the reduction of water to

hydrogen by photogenerated electrons in the conduction band (CB) [39]–[44]. The sacrificial reagents/agents then react irreversibly with the photogenerated holes and promote accordingly the electron/hole separation. This technique can be used in the photocatalytic production of hydrogen with simultaneous decomposition of pollutants (water treatment) or what is referred to as photo reforming [45].

Hence, in photo reforming systems, the organic substance gets oxidized by the photogenerated hole at the photocatalyst surface while water will be reduced accepting the photogenerated CB electrons according to equation, (Eq.1) [45].

$$C_xH_yO_z + (2_x - z)H_2O \rightarrow (2_x + y/2 - z)H_2 + xCO_2 \quad (1)$$

Methanol: $H_2O + CH_3OH \rightarrow CO_2 + 3H_2, \quad \Delta H^0 = 49.3$ kJ/mol (2)

Formaldehyde: $H_2O + HCHO \rightarrow CO_2 + 2H_2, \quad \Delta H^0 = -43.1$ kJ/mol (3)

In this work, noble co-catalyst(s) iridium (Ir), platinum (Pt), gold (Au) nanoparticles (co-catalysts) will be developed to help in proton reduction and water oxidation in the photocatalytic water splitting processes (overcome the overpotential necessary for hydrogen formation). Methanol/formaldehyde will be used as sacrificial agents under mild conditions, ambient temperature and normal pressure in the presence of a suitable catalyst as shown below [(Eqns (4)-(7)] [44], [46], [47]. Methanol, CH_3OH will be oxidized to formaldehyde, HCHO, HCHO to formic acid, HCO_2H, and HCO_2H to carbon dioxide, CO_2 and H_2. Equations 5 – 7 are different steps involved in water splitting using sacrificial agents [1], [6], [48]–[50] and further discussions are ahead.

$$CH_3OH \xrightarrow{hv,\ cat.} HCHO + H_2 \quad (4)$$

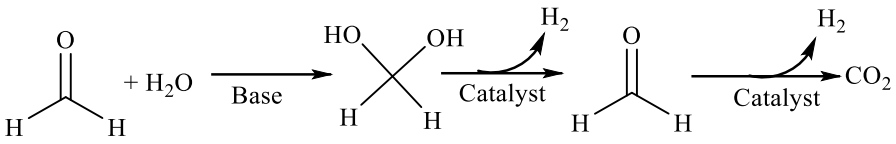

(5)

$$HCHO + H2O \xrightarrow{hv,\ cat.} HCO_2H + H_2 \quad (6)$$

$$HCO_2H \xrightarrow{hv,\ cat.} CO_2 + H_2 \quad (7)$$

Taking into account the fact that formaldehyde/para-formaldehyde and methanediol are products of methanol, H_2 production experiments from formaldehyde/para-formaldehyde as starting materials were successfully conducted using ruthenium, Ru based catalyst by Heim et al. [51] and iridium, Ir based catalyst by Suenobu et al. [52]. These two are the only literature available on the production of hydrogen from water with formaldehyde/paraformaldehyde as sacrificial agent under mild conditions. Both the groups have successfully conducted one-pot dehydrogenation of formaldehyde in aqueous media where water acts as a hydrogen source as well [eqn (5)]. It has been suggested that dehydrogenation of methanediol occurs in a two-step reaction, where methanediol is converted to formic acid with the evolution of hydrogen in the first step and then formic acid is converted into carbon dioxide and hydrogen in the second step [eqn (5)] [51]. It has been observed that this process yields two moles of hydrogen and one mole of carbon dioxide in pure form, equation 3. Moreover, production of hydrogen from water with formaldehyde/para-formaldehyde as sacrificial agent is found to be more advantageous as the oxygen formed during water splitting reaction is tapped in the form

of carbon dioxide which is not possible to happen in the case of homogeneous water splitting experiments where hydrogen and oxygen exists in the same mixture, explosion limits for H_2/O_2 are dependent on initial pressures and temperatures and therefore, they vary according to pressure and temperature [53]. Hence, the oxygen is not available for oxidation and thus formation of explosive mixture of hydrogen and oxygen is avoided. Using this noble method, hydrogen is generated in a non-flammable liquid, which is safer for mobile applications. Moreover, hydrogen and carbon dioxide are easier to handle and to separate than an oxygen-hydrogen mixture and can be used directly in various systems such as hydrogenation reactions, IC engine, fuel cell among others [20], [44], [47], [54].

Although the production of H_2 was successfully achieved from aqueous formaldehyde/para-formaldehyde using Ru and Ir based homogeneous organometallic catalysts, it would be ideal if the catalysts will be replaced by heterogeneous and/or cheap catalytic materials. Secondly, the use of base in the reaction for the formation of methanediol from formaldehyde/ paraformaldehyde needs to be minimized/ stopped (It has been suggested that dehydrogenation of methanediol occurs in a two-step reaction, where methanediol is converted to formic acid with the evolution of hydrogen in the first step and then formic acid is converted into carbon dioxide and hydrogen in the second step [eqn (5)] [51]). This is possible if the catalyst is capable of activating formaldehyde and water molecules to form methanediol. This will definitely enhance the hydrogen yield efficiency and hence its practicability as shown by eqn (5), eqn (6) and eqn (7). Heterogeneous catalysts can offer engineers opportunity to design a system where fuel (aqueous solution aldehyde/ methanol) can be passed directly to the heterogeneous catalyst bed to produce hydrogen to be used on site [20], [44], [47], [52], [54].

Dehydrogenation of hydrocarbons is an industrially important reaction which follows oxidative (leading to formation of water) and non-oxidative (leading to formation of molecular hydrogen) pathways. Oxidative dehydration of alkanes (such as ethane, a by-product of petroleum

processing and present in natural gas) to olefins (such as ethylene, butene, and butadiene) is in great demand from chemical industry. Vanadium pentoxide or supported (SiO_2, $A1_2O_3$, etc.) vanadium based catalysts are capable of dehydrogenation, but the hydrogen is eliminated in the form of water which is a net loss of energy [55], [56]. Various other metals such as Pt, Pd, Ni, Fe, Mo etc. are used as active catalysts for dehydrogenation of hydrocarbons (such as ethane and propane) with evolution of molecular hydrogen but the temperature requirement is high (>400 °C) and it suffers from carbon deposition[31]. Metal sulphides (Mo, Mn, Cu, Ni, Fe, Co) supported on silica (SiO_2) were also reported to be active for the dehydrogenation of isobutane to isobutene and found to be better than Al_2O_3 supported Pt and Cr based commercial catalysts [57].

Very recently, Lin et.al. [58] has reported base free production of hydrogen over atomically dispersed platinum (Pt) on α-molybdenum carbide (α-MoC) at 150-190 °C through aqueous-phase reforming of methanol (APRM). In this, α-MoC induces water dissociation and Pt in combination with α-MoC activate methanol to reform it to produce hydrogen. In another study, Yu et. al. [59] has reported the production of hydrogen and carbon dioxide over CuZnGaOx by steam reforming of methanol at 150-200 °C with no detectable CO (below detection limit of 1 ppm).

Although CuZnGaOx by steam reforming of methanol is able to produce hydrogen at temperature 150-200 °C but production of CO cannot be denied at this temperature range. From thermodynamic study carried out using CuZnGaOx by steam reforming of methanol, it is found that CO formation is zero at 100 °C. Rh and Ir show promising results towards the formation of hydrogen at 90-110 °C but it requires base and catalytic system is homogeneous. Observation of Lin et.al. [58] has also showed promising results for water dissociation using

α-MoC. Considering all the facts, a catalytic system can be developed which can produce hydrogen without the formation of CO.

Designing heterogeneous catalysts for the production of hydrogen from water with alcohol/aldehyde is complicated as the non-oxidative dehydrogenation involves several steps as discussed in the above sections. It is highly challenging to overcome these difficulties (Designing heterogeneous catalysts for the production of hydrogen from water with alcohol/aldehyde is complicated as the non-oxidative dehydrogenation involves several steps as discussed in the above sections) but at the same time highly desirable to produce molecular hydrogen under mild reaction conditions. In the recent past, it has been shown that *in-situ* studies can be successfully used for unravelling the mechanism of catalytic processes as well for designing tailor made catalysts. This important information from the *in-situ* studies can be the key and helpful for designing the final catalyst for the hydrogen generation.

The aim of the study is to develop efficient catalytic materials for the thermo-photocatalytic production of hydrogen from water with methanol and its oxidation products (formaldehyde/ formic acid) in aqueous medium under mild conditions.

1.4 Aim and objectives

1.4.1 Aim

The aim of this project was to develop efficient catalytic materials for the thermo-photocatalytic reaction for the production of hydrogen from water with methanol and its oxidation products (formaldehyde/ formic acid) in aqueous medium under mild conditions and recommend further study on related work.

1.4.2 Objectives

The objectives of the study were divided as follows:

1. Development of supported Pt, Ir, Au, Cu, Zn, and their bimetallic combination catalysts for the production of hydrogen from water with methanol/formaldehyde at low concentrations as sacrificial agent(s).

2. Synthesis of carbon nanofibers, CNFs, titanium dioxide, TiO_2 and TiO_2/CNFs composites for thermo-photocatalytic hydrogen production from water with methanol/formaldehyde at low concentrations as sacrificial agents.

3. Preparation of carbon nanomaterials and titania-carbon nanomaterials as composite support materials for Pt, Au, Ir, Cu and Zn catalysts.

4. Fundamental understanding of the production of hydrogen from water using methanol/formaldehyde as a sacrificial agent(s) through various physical-chemical techniques such as FT-IR, SEM, TEM, Raman spectroscopy, UV-Vis, PL, BET, XPS, etc. which will provide critical information on reactant/product surface interaction.

1.5 Outline of the thesis

The outline of this thesis will be organized as follows:

Chapter 2: This chapter gives a literature review of related work. There is an abstract summarizing the work covered, where fossil fuels are still considered as the major form of energy to this decade. Further the scarcity of fossil fuels and the environmental impact of their use are discussed under the introduction. The production of hydrogen using sacrificial

agents (half-reactions using sacrificial electron donors and acceptors), basic principles of water splitting on a semiconductor particle, development history of water splitting, titanium dioxide (TiO_2) as a photocatalyst and photocatalytic materials for hydrogen production are also discussed.

Chapter 3: The chapter explains a facile synthesis method used in the preparation of copper oxide nanoparticles. It also gives the details of the experimental work and characterization techniques used in achieving the copper oxide nanoparticles and the catalytic use of the prepared coper oxide nanoparticles to synthesize high quality carbon nanofibers, CNFs using catalytic chemical vapour deposition method, CCVD. In addition, the synthesis of high quality carbon nanofibers and their functionalization are discussed step by step before characterizing them. The work was carried out under; preparation of copper oxide nanoparticles, preparation of carbon nanofibers, acid treatment of carbon nanofibers, characterization of copper oxide nanoparticles, and carbon nanofibers

Chapter 4: Gives comparison between TiO_2 and TiO_2 composited with CNFs used in photocatalytic water splitting. It further covers the use of sacrificial agent, methanol at low concentration together with the prepared composites of CNFs/TiO_2. This chapter gives the steps used to achieve water splitting using the prepared photocatalysts. The discussion of the work was captured under introduction to the work, experimental and the characterization techniques employed in the work. The most active photocatalyst was identified as CNFs/20%TiO_2. The introduction of TiO_2 – P25 (commercial TiO_2) was necessary to help with the discussion of the results.

Chapter 5: This chapter discusses the photocatalytic hydrogen production of TiO_2/CNFs doped with Pt, Au and Ir nanoparticles. The methods of synthesizing the F_CNFs/20%TiO_2/Pt, F_CNFs/20%TiO_2/Au, and F_CNFs/20%TiO_2/Ir nanostructures and the various characterization techniques used in their study are discussed. There is also the photocatalytic studies presentation and the conclusion.

Chapter 6: The chapter is based on the hydrogen production via water splitting over Zn/TiO_2/CNFs and Cu/TiO_2/CNFs nanocomposites. The chapter covers full synthesis methods used and the characterization techniques employed in the study. Further, the mechanism of the photocatalytic water splitting is also discussed. An evaluation of the most active photocatalyst was achieved before concluding the work.

Chapter 7: This chapter summarizes the findings of this study and gives conclusions and recommendations for future work.

References: The list of references used are presented at the end of each chapter.

1.6 Reference

[1] M. A. Aziz Aljar, M. Zulqarnain, A. Shah, M. S. Akhter, and F. J. Iftikhar, "A review of renewable energy generation using modified titania for photocatalytic water splitting," *AIP Adv.*, vol. 10, no. 7, 2020, doi: 10.1063/5.0006196.

[2] J. Tang, W. Zhou, R. Guo, C. Huang, W. Pan, and P. Liu, "An exploration on in-situ synthesis of europium doped g-C_3N_4 for photocatalytic water splitting," *Energy Procedia*, vol. 158, pp. 1553–1558, 2019, doi: 10.1016/j.egypro.2019.01.365.

[3] M. Solakidou, A. Giannakas, Y. Georgiou, N. Boukos, M. Louloudi, and Y.

Deligiannakis, “Efficient photocatalytic water-splitting performance by ternary CdS/Pt-N-TiO_2 and CdS/Pt-N,F-TiO_2: Interplay between CdS photo corrosion and TiO_2-dopping,” *Appl. Catal. B Environ.*, vol. 254, pp. 194–205, 2019, doi: 10.1016/j.apcatb.2019.04.091.

[4] R. Bashiri *et al.*, “Influence of seeding layer on photoelectrochemical hydrogen production over TiO_2 nanorod decorated with reduced graphene oxide,” *Diam. Relat. Mater.*, vol. 94, pp. 194–202, 2019, doi: 10.1016/j.diamond.2019.03.006.

[5] A. S. Hainer, J. S. Hodgins, V. Sandre, M. Vallieres, A. E. Lanterna, and J. C. Scaiano, “Photocatalytic Hydrogen Generation Using Metal-Decorated TiO_2: Sacrificial Donors vs True Water Splitting,” *ACS Energy Lett.*, vol. 3, no. 3, pp. 542–545, 2018, doi: 10.1021/acsenergylett.8b00152.

[6] E. Can and R. Yildirim, “Data mining in photocatalytic water splitting over perovskites literature for higher hydrogen production,” *Appl. Catal. B Environ.*, vol. 242, pp. 267–283, 2019, doi: 10.1016/j.apcatb.2018.09.104.

[7] B. Xu, R. Fu, and C. K. M. Lau, “Energy market uncertainty and the impact on the crude oil prices,” *J. Environ. Manage.*, vol. 298, pp. 113403, 2021, doi: 10.1016/j.jenvman.2021.113403.

[8] J. Speirs, C. McGlade, and R. Slade, “Uncertainty in the availability of natural resources: Fossil fuels, critical metals and biomass,” *Energy Policy*, vol. 87, pp. 654–664, 2015, doi: 10.1016/j.enpol.2015.02.031.

[9] A. Berger, Q. Yin, H. Nifenecker, and J. Poitou, “Slowdown of global surface air temperature increase and acceleration of ice melting,” *Earth’s Futur.*, vol. 5, no. 7, pp. 811–822, 2017, doi: 10.1002/2017EF000554.

[10] F. M. Toma, A. J. Cowan, M. Sugiyama, L. Wang, and K. Xi, “Solar to fuel: Recent developments in conversion of sunlight into high value chemicals,” *APL Mater.*, vol. 8,

no. 12, pp. 8–11, 2020, doi: 10.1063/5.0038968.

[11] I. Mouratiadou, G. Luderer, N. Bauer, and E. Kriegler, “Emissions and their drivers: sensitivity to economic growth and fossil fuel availability across world regions,” *Clim. Change*, vol. 136, no. 1, pp. 23–37, 2016, doi: 10.1007/s10584-015-1368-4.

[12] N. Bauer *et al.*, “Global fossil energy markets and climate change mitigation – an analysis with REMIND,” *Clim. Change*, vol. 136, no. 1, pp. 69–82, 2016, doi: 10.1007/s10584-013-0901-6.

[13] E. Kriegler *et al.*, “Will economic growth and fossil fuel scarcity help or hinder climate stabilization?: Overview of the RoSE multi-model study,” *Clim. Change*, vol. 136, no. 1, pp. 7–22, 2016, doi: 10.1007/s10584-016-1668-3.

[14] X. Zhou *et al.*, “An overview on energy router based on various forms of energy,” *Proc. 28th Chinese Control Decis. Conf. CCDC 2016*, no. 50877053, pp. 2901–2906, 2016, doi: 10.1109/CCDC.2016.7531478.

[15] M. C. RAO, “Sustainable and Renewable Energy Resources — Alternative Forms of Energy,” *Int. J. Mod. Phys. Conf. Ser.*, vol. 22, pp. 385–390, 2013, doi: 10.1142/s2010194513010416.

[16] A. R. Hansen, F. Friis, M. H. Jacobsen, and K. Gram-Hanssen, “Three forms of energy prosumer engagement and their impact on time-shifting electricity consumption,” *Eceee Summer Study Proc.*, vol. 2019-June, no. March 2020, pp. 39–46, 2019.

[17] B. Vogel-Heuser, B. Weißenberger, H. Meyer, and J. Plössnig, “Modeling of Power Consumption in Manufacturing,” *2014 IEEE Int. Conf. Ind. Technol. (ICIT), Busan, Korea*, pp. 659–663, 2014. https://doi.org/10.3182/20130619-3-RU-3018.00056.

[18] F. E. Osterloh, “Photocatalysis versus Photosynthesis: A Sensitivity Analysis of Devices for Solar Energy Conversion and Chemical Transformations,” *ACS Energy Lett.*, vol. 2, no. 2, pp. 445–453, 2017, doi: 10.1021/acsenergylett.6b00665.

[19] K. Mazloomi and C. Gomes, “Hydrogen as an energy carrier: Prospects and challenges,” *Renew. Sustain. Energy Rev.*, vol. 16, no. 5, pp. 3024–3033, 2012, doi: 10.1016/j.rser.2012.02.028.

[20] L. Schlapbach and A. Züttel, “Hydrogen-storage materials for mobile applications,” *Nature*, vol. 414, no. 6861, pp. 353–358, 2001, doi: 10.1038/35104634.

[21] M. H. G. Prechtl and S. Sahler, “Hydrogen Storage Using Ionic Liquid Media,” *Curr. Org. Chem.*, vol. 17, no. 3, pp. 220–228, 2013, doi: 10.2174/1385272811317030004.

[22] F. Schüth, “Challenges in hydrogen storage,” *Eur. Phys. J. Spec. Top.*, vol. 176, pp. 155–166, 2009, doi: 10.1140/epjst/e2009-01155-x.

[23] I. Dincer and C. Acar, “Review and evaluation of hydrogen production methods for better sustainability,” *Int. J. Hydrogen Energy*, vol. 40, no. 34, pp. 11094–11111, 2014, doi: 10.1016/j.ijhydene.2014.12.035.

[24] T. Sinigaglia, F. Lewiski, M. E. Santos Martins, and J. C. Mairesse Siluk, “Production, storage, fuel stations of hydrogen and its utilization in automotive applications-a review,” *Int. J. Hydrogen Energy*, vol. 42, no. 39, pp. 24597–24611, 2017, doi: 10.1016/j.ijhydene.2017.08.063.

[25] T. da Silva Veras, T. S. Mozer, D. da Costa Rubim Messeder dos Santos, and A. da Silva César, “Hydrogen: Trends, production and characterization of the main process worldwide,” *Int. J. Hydrogen Energy*, vol. 42, no. 4, pp. 2018–2033, 2017, doi: 10.1016/j.ijhydene.2016.08.219.

[26] H. T. Hwang and A. Varma, “Hydrogen storage for fuel cell vehicles,” *Curr. Opin. Chem. Eng.*, vol. 5, pp. 42–48, 2014, doi: 10.1016/j.coche.2014.04.004.

[27] H. Ishaq and I. Dincer, “Comparative assessment of renewable energy-based hydrogen production methods,” *Renew. Sustain. Energy Rev.*, vol. 135, 2021, doi: 10.1016/j.rser.2020.110192.

[28] R. Kumar, A. Kumar, and A. Pal, “An overview of conventional and non-conventional hydrogen production methods,” *Mater. Today Proc.*, vol. 46, pp. 5353–5359, 2020, doi: 10.1016/j.matpr.2020.08.793.

[29] T. Varadarajan, B. Viswanathan, and M. Sastri, “Catalytic Decomposition of Formic Acid on Zinc Molybdate,” *Indian J. Chem.*, vol. 15, no. 3, pp. 202–204, 1977.

[30] J. Schneider *et al.*, “ Understanding TiO_2 Photocatalysis Mechanisms and Materials” *Chem. Rev.*, vol. 114, no. 9, p. 9919−9986, 2014, doi: 10.1021/cr5001892.

[31] N. M. Gupta, “Factors affecting the efficiency of a water splitting photocatalyst: A perspective,” *Renewable and Sustainable Energy Reviews*, vol. 71, pp. 585–601, 2017, doi: 10.1016/j.rser.2016.12.086.

[32] C. Agrafiotis *et al.*, “Solar water splitting for hydrogen production with monolithic reactors,” *Sol. Energy*, vol. 79, no. 4, pp. 409–421, 2005, doi: 10.1016/j.solener.2005.02.026.

[33] S. Chen, T. Takata, and K. Domen, “Particulate photocatalysts for overall water splitting,” *Nat. Rev. Mater.*, vol. 2, pp. 1–17, 2017, doi: 10.1038/natrevmats.2017.50.

[34] J. Zhang, J. Shi, Z. Cui, S. Chu, Y. Wang, and Z. Zou, “Highly efficient hydrogen evolution from water splitting on heptazine polymer with three types of defects,” *Appl. Surf. Sci.*, vol. 580, 2022, doi: 10.1016/j.apsusc.2021.152070.

[35] P. W. Menezes *et al.*, “Helical cobalt borophosphates to master durable overall water-splitting,” *Energy Environ. Sci.*, vol. 12, no. 3, pp. 988–999, 2019, doi: 10.1039/c8ee01669k.

[36] P. M. Rajaitha *et al.*, “Multifunctional materials for photo-electrochemical water splitting,” *J. Mater. Chem. A*, vol. 10, no. 30, pp. 15906–15931, 2022, doi: 10.1039/d2ta01869a.

[37] B. Y. Alfaifi, H. Ullah, S. Alfaifi, A. A. Tahir, and T. K. Mallick,

"Photoelectrochemical solar water splitting: From basic principles to advanced devices," *Veruscript Funct. Nanomater.*, vol. 2, 2018, doi: 10.22261/fnan.bdjoc3.

[38] K. Maeda, "Photocatalytic water splitting using semiconductor particles: History and recent developments," *J. Photochem. Photobiol. C Photochem. Rev.*, vol. 12, no. 4, pp. 237–268, 2011, doi: 10.1016/j.jphotochemrev.2011.07.001.

[39] Y. Ma, X. Wang, Y. Jia, X. Chen, H. Han, and C. Li, "Titanium dioxide-based nanomaterials for photocatalytic fuel generations," *Chem. Rev.*, vol. 114, no. 19, pp. 9987–10043, 2014, doi: 10.1021/cr500008u.

[40] W. Tu *et al.*, "State-of-the-art advancements of crystal facet-exposed photocatalysts beyond TiO_2: Design and dependent performance for solar energy conversion and environment applications," *Mater. Today*, vol. 33, pp. 75–86, 2020, doi: 10.1016/j.mattod.2019.09.003.

[41] Y. Li and S. C. E. Tsang, "Recent progress and strategies for enhancing photocatalytic water splitting," *Mater. Today Sustain.*, vol. 9, 2020, doi: 10.1016/j.mtsust.2020.100032.

[42] K. H. Ng, S. Y. Lai, C. K. Cheng, Y. W. Cheng, and C. C. Chong, "Photocatalytic water splitting for solving energy crisis: Myth, Fact or Busted?," *Chem. Eng. J.*, vol. 417, 2021, doi: 10.1016/j.cej.2021.128847.

[43] N. Fajrina and M. Tahir, "A critical review in strategies to improve photocatalytic water splitting towards hydrogen production," *Int. J. Hydrogen Energy*, vol. 44, no. 2, pp. 540–577, 2019, doi: 10.1016/j.ijhydene.2018.10.200.

[44] G. Commentary, "Undesired Role of Sacrificial Reagents in Photocatalysis," J. Phys. Chem. Lett., vol. 4, pp. 3479−3483, 2013, doi: 10.1021/jz4018199.

[45] A. Hakki, Y. AlSalka, C. B. Mendive, J. Ubogui, P. C. Dos Santos Claro, and D. Bahnemann, "Hydrogen production by heterogeneous photocatalysis," *Encycl.*

Interfacial Chem. Surf. Sci. Electrochem., pp. 413–419, 2018, doi: 10.1016/B978-0-12-409547-2.13795-3.

[46] A. Galińska and J. Walendziewski, "Photocatalytic water splitting over Pt-TiO_2 in the presence of sacrificial reagents," *Energy and Fuels*, vol. 19, no. 3, pp. 1143–1147, May 2005, doi: 10.1021/ef0400619.

[47] B. Tomoji Kawai and T. Sakata, "Photocatalytic Hydrogen Production from Liquid Methanol and Water," *J. Chem. Soc., Chem. Commun.*, PP. 694-695, 1980, https://doi.org/10.1039/C39800000694.

[48] S. ichiro Fujita, H. Kawamori, D. Honda, H. Yoshida, and M. Arai, "Photocatalytic hydrogen production from aqueous glycerol solution using NiO/TiO_2 catalysts: Effects of preparation and reaction conditions," *Appl. Catal. B Environ.*, vol. 181, pp. 818–824, 2016, doi: 10.1016/j.apcatb.2015.08.048.

[49] M. El ouardi *et al.*, "Review of photoelectrochemical water splitting: From quantitative approaches to effect of sacrificial agents, oxygen vacancies, thermal and magnetic field on (photo)electrolysis," *Int. J. Hydrogen Energy*, vol. 51, pp. 1044–1067, 2024, doi: 10.1016/j.ijhydene.2023.09.111.

[50] T. Zhang and S. Lu, "Sacrificial agents for photocatalytic hydrogen production: Effects, cost, and development," *Chem Catal.*, vol. 2, no. 7, pp. 1502–1505, 2022, doi: 10.1016/j.checat.2022.06.023.

[51] L. E. Heim, N. E. Schlörer, J. H. Choi, and M. H. G. Prechtl, "Selective and mild hydrogen production using water and formaldehyde," *Nat. Commun.*, vol. 5, 2014, doi: 10.1038/ncomms4621.

[52] T. Suenobu, Y. Isaka, S. Shibata, and S. Fukuzumi, "Catalytic hydrogen production from paraformaldehyde and water using an organoiridium complex," *Chem. Commun*, vol. 51, pp. 1670, 2015, doi: 10.1039/c4cc06581f.

[53] V. Schroeder and K. Holtappels, “Explosion Characteristics of Hydrogen-Air and Hydrogen-Oxygen Mixtures at Elevated Pressures,” *Int. Conf. Hydrog. Saf.*, 2005, https://h2tools.org/bibliography/explosion-characteristics-hydrogen-air-and-hydrogen-oxygen-mixtures-elevated-pressures.

[54] A. Galińska and J. Walendziewski, “Photocatalytic water splitting over Pt-TiO_2 in the presence of sacrificial reagents,” *Energy and Fuels*, vol. 19, no. 3, pp. 1143–1147, 2005, doi: 10.1021/ef0400619.

[55] A. Khodakov, B. Olthof, A. T. Bell, and E. Iglesia, “Structure and catalytic properties of supported vanadium oxides: Support effects on oxidative dehydrogenation reactions,” *J. Catal.*, vol. 181, no. 2, pp. 205–216, 1999, doi: 10.1006/jcat.1998.2295.

[56] A. H. S. Kootenaei, J. Towfighi, A. Khodadadi, and Y. Mortazavi, “Stability and catalytic performance of vanadia supported on nanostructured titania catalyst in oxidative dehydrogenation of propane,” *Appl. Surf. Sci.*, vol. 298, pp. 26–35, 2014, doi: 10.1016/j.apsusc.2013.12.172.

[57] G. Wang, C. Li, and H. Shan, “Highly Efficient Metal Sulfide Catalysts for Selective Dehydrogenation of Isobutane to Isobutene,” *ACS Catal.*, vol. 4, no. 4, pp. 1139–1143, 2014, doi: 10.1021/cs5000944.

[58] L. Lin *et al.*, “Low-temperature hydrogen production from water and methanol using Pt/α-MoC catalysts,” *Nat. Publ. Gr.*, vol. 544, 2017, doi: 10.1038/nature21672.

[59] K. Man *et al.*, “Non-syngas direct steam reforming of methanol to hydrogen and carbon dioxide at low temperature,” *Nat. Commun.*, vol. 3, no. 1230, 2012, doi: 10.1038/ncomms2242.

CHAPTER TWO

Photocatalytic water splitting for Hydrogen production – A review

Molecular Sciences Institute, School of Chemistry, University of the Witwatersrand, Johannesburg 2050, South Africa

Abstract

Fossil fuels are the major form of energy for modern society to this decade. Cognizance about fossil fuels scarcity and their related environmental destruction which has led to global warming through the emission of greenhouse gases has inspired researchers, particularly scientists and engineers to engage in intensive research in other forms of energy for mitigation. Photocatalysis in which inexhaustible, clean and safe solar energy can be harvested for sustainable, non-hazardous, and low-cost technologies, is a significant advance in obtaining clean energy. Photocatalytic water splitting for hydrogen production systems are alternative routes to clean and cost effective energy. The trapping of solar energy and the use of the abundant water on the earth's surface to produce hydrogen fuel will lead reduce the fossil fuels scarcity and environmental pollution to manageable levels. The power from hydrogen production can be used in transportation and industries. This work covers the progress on Photocatalytic water splitting for hydrogen production and recommends the use of water splitting technologies via the development of inexpensive and non-toxic, recyclable, photostable and corrosion resistant photocatalysts as the way forward for future work.

Keywords: Photoelectrolysis; sacrificial reagents; titanium dioxide; H_2 production; semiconductor particle.

2.1 Introduction

Photocatalytic hydrogen production using water and solar energy is a better route towards renewable energy as compared to other technologies such as photovoltaic (PV) systems. In photovoltaic technology, a PV cell, electrolyser and other components are needed to set up a working system while in photocatalytic hydrogen production, these expensive components are not required because systems can be developed that can use hydrogen directly as it's produced to reduce production costs. Concerning process driving energy sources, the types of energy are mechanical, electrical, thermal, biological, or photonic. In general, hydrogen can be generated by water splitting reaction. Water-based photoelectrolysis using sunlight to fragment water molecules to produce hydrogen has gained a lot of attention because it's environmentally friendly and there is also renewable supply of energy. The method is classified into three categories; (1) thermochemical water splitting, (2) photobiological water splitting, and (3) photocatalytic water splitting [1]–[4]. Thermochemical water splitting employs the harvesting of heat from sunlight by solar concentrators to split the water. Whilst photobiological and photocatalytic water splitting make use of bacteria either aerobically or anaerobically, and photocatalysts respectively, in the conversion of the light energy into chemical energy.

According to the thermodynamics of this type of reactions, Bard and Nozik [2], [5]–[13] grouped in photocatalytic systems as those in which photon absorption promotes a reaction with $\Delta G < 0$ (ΔG – change in Gibbs free energy), figure 1, therefore there is no net storage of chemical charge, however the radiant energy is needed by the system for the reaction to occur or else the reaction would be extremely slow without photocatalyst. Conversely, in the photosynthetic system, the radiant energy is required thus it provides the required Gibbs free energy with $\Delta G > 0$ [1], [2], [9], [14], [15] as shown in figure 1.

Since the products of photosynthetic system have elevated free energy than the reagents, the reverse photosynthetic reaction is thermodynamically favoured. Thus, photosynthetic systems as well must be able to overcome this reverse photosynthetic reaction [2]. Consequently, the two systems can (1) absorb light-generating charge carriers, electrons and holes (active sites), and (2) deliver these charge carriers to the adsorbed chemical species at their surface to enhance redox reactions. Photocatalysts are the light absorbing materials, which in the heterogeneous systems are normally semiconductors [3], [13], [14], [16], [17].

Extensive research has been carried out on hydrogen production from systems consisting of semiconductor particles suspended in aqueous solutions and dissolved organic compounds. The compounds are generally known as sacrificial reagents/agents. For instance, in a Pt/TiO_2-water- methanol system, methanol is oxidized by means of the photo-generated valence band (VB) holes on the metal-decorated photocatalyst hence allowing the reduction of water to hydrogen by photogenerated electrons in the conduction band (CB). The sacrificial reagents/agents react irreversibly with the photogenerated holes and promote accordingly the electron/hole separation. This technique can be used in the photocatalytic production of hydrogen with simultaneous decomposition of pollutants (water treatment) or what is referred to as photo reforming [16], [18], [19], [28]–[37], [20], [38]–[47], [21]–[27].

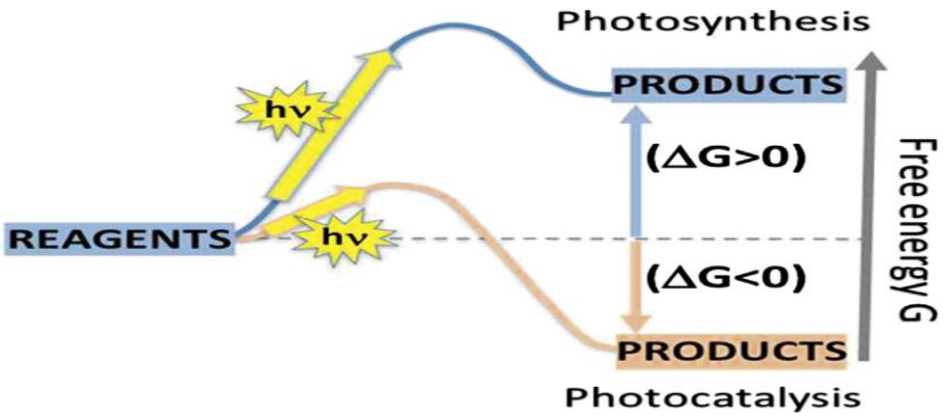

Fig. 1. Primary processes involved in photocatalysis and photosynthesis, an illustration of the absorption of light in order to trigger a thermodynamically more (photocatalysis) or less (photosynthesis) stable product as compared to the reagents [2].

On the other hand, radiative and non-radiative recombination of the excited charge carriers may occur at a shorter time scale thereby limiting the quantum efficiency. Furthermore, the photogenerated carriers could interact with the lattice and surface defects together with impurities substituting the lattice sites of a semiconductor photocatalyst [3], [14], [17], [48], [49].

2.2 Basic principles of water splitting on a semiconductor particle

As shown in figure 2, the basic principles of overall water splitting on a semiconductor particle is primarily identical to a water splitting photo electrochemical cell (PEC). Upon irradiation with an energy equivalent to or greater than the band gap of the semiconductor photocatalyst, electrons in the valence band are excited into the conduction band, leaving holes in the valence band. These electrons and holes which are photogenerated cause reduction and oxidation reactions, respectively. To accomplish overall water splitting, the bottom of the conduction band must be more negative than the reduction potential of H^+ to H_2 (0V vs NHE at pH = 0), whilst the top of the valence band must be more positive than the oxidation potential of H_2O to

O_2 (1.23V vs NHE). Consequently, it would seem possible to employ the entire spectral range of visible light ($400 < \lambda < 800$ nm). Nonetheless, there is an activation barrier in the charge transfer process between the photocatalyst and water molecules, necessitating a photon energy greater than the band gap of the photocatalyst to promote the overall water splitting reaction at a suitable rate. Moreover. The backward reaction: i.e., water formation from H_2 to O_2, has to be strictly inhibited, and the photocatalyst must be stable in the reaction. Additionally, even though there are large number of materials that possess suitable band gap potentials, there are limited number that work as photocatalyst for overall water splitting [1], [9], [55]–[57], [14], [15], [17], [50]–[54]. As illustrated in figure 3, overall water splitting on a semiconductor photocatalyst takes place in 3 steps: (1) the photocatalyst absorbs photon energy greater than, the bandgap energy of the material and generates photo excited electron-hole pairs in the bulk (2) the photo excited carriers separate and migrate to the surface without recombination, and (3) the adsorbed species are reduced and oxidized by the photogenerated electrons and holes to produce H_2 and O_2, respectively. Research has shown that the first 2 steps are strongly dependent on the structural and electronic properties of the photocatalyst. In principle, high crystallinity promotes activity, since the density of defects, which act as recombining centres between photogenerated carriers, decrease with increasing crystallinity. Better photocatalytic activity can also be obtained by reducing the particle size of a photocatalyst to reduce the diffusion length for the photogenerated electron – hole pairs. Step 3, however, is promoted by a solid cocatalyst. The cocatalyst, is normally a noble metal (Pt, Rh) or transition metal oxide (e.g. NiO_x, RuO_2) which is loaded onto the photocatalyst surface as a dispersion of nanoparticles to produce active sites and reduce the activation energy for H_2 gas evolution. Predominantly, cocatalysts are loaded for the promotion of H_2 evolution because most photocatalysts are unable to activate hydrogen (in large quantities) on the surface. Hence, it is

important to design both the bulk and surface properties of the material correctly to obtain a high activity for a given photocatalytic reaction [14], [16], [49], [51], [52], [58]–[62].

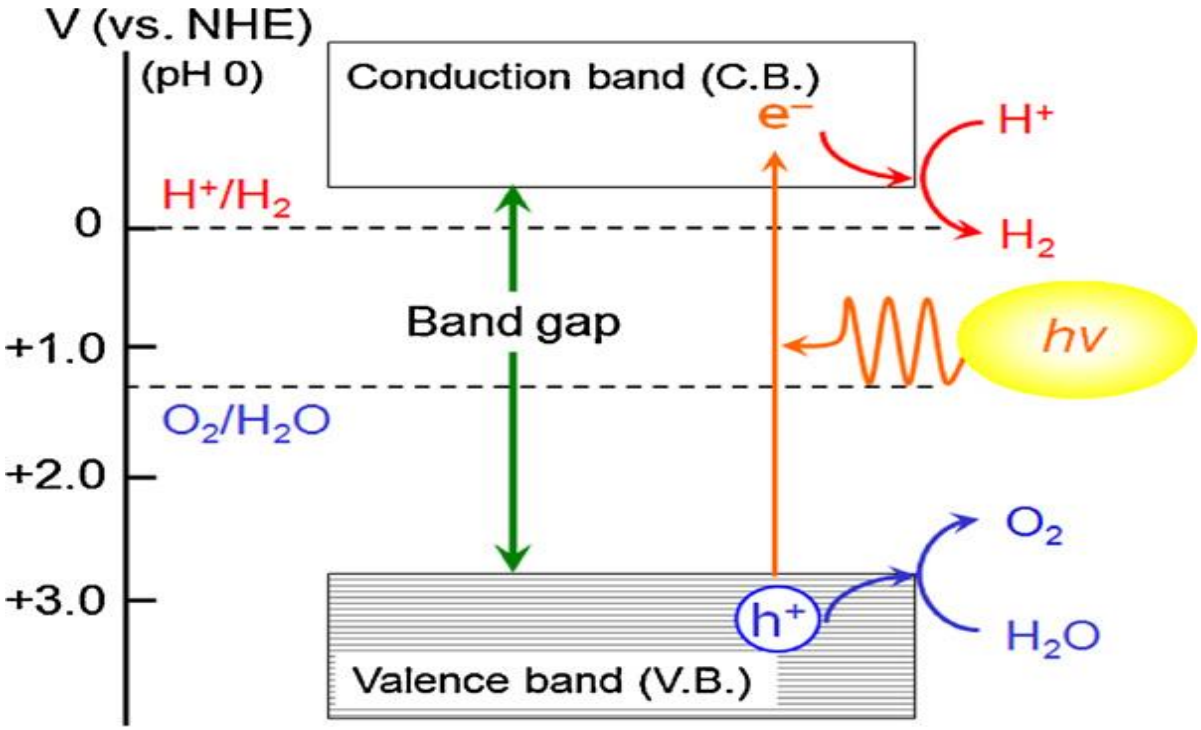

Fig. 2. Basic principle of overall water splitting on a semiconductor particle[9], [52].

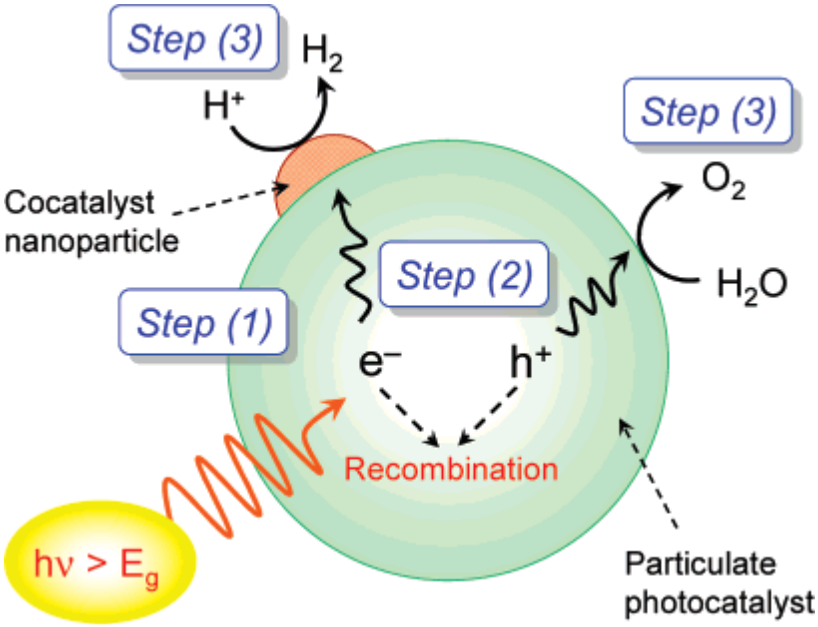

Fig. 3. Processes involved in photocatalytic overall water splitting on a heterogeneous photocatalyst[52].

Fundamentally, accelerated charge separation must be enhanced by fabricating hetero/homo-junctions to maximize the photocatalytic efficiency [62]–[64]. The final step comprises the electrons, which migrate from the CB to the photocatalyst surface to take part in a reduction reaction and produce hydrogen, while the holes move from the VB to the surface of the catalyst to be involved in oxidation reaction forming oxygen. As a result of the high activation energy of water splitting, only a few of the photogenerated electron- hole pairs reaching the photocatalyst facet can be involved in the water splitting reaction in good time, hence surface recombination occurs thereby greatly reducing the photocatalytic overall water splitting efficiency [65]–[69]. The reduction and oxidation (redox) processes on the surface of the catalysts are shown as follows [62], [70];

$$\text{Photo - reduction: } 2H_2O + 2e^- \rightarrow H_2 + 2OH^- \quad (1)$$

$$\text{Photo - oxidation: } 2H_2O \rightarrow O_2 + 4H^+ + 4e^- \quad (2)$$

$$\text{Overall reaction: } H_2O + 1.23eV\ (h\nu) \rightarrow H_2 + 1/2O_2 \quad (3)$$

To accelerate the surface redox response, numerous techniques of inserting cocatalysts on the photocatalysts have been established, including impregnation [71], photodeposition, and others [72]–[75]. Suitable cocatalysts composited with photocatalysts function as active sites and catalyse the process by enhancing charge separation, together with relocation caused by the heterojunction existing in the midst of semiconductor photocatalyst and the cocatalyst [64], [69], [76]–[79].

2.3 Half-reactions using sacrificial electron donors and acceptors

Whenever the photocatalytic reaction is conducted in the presence of an electron donor such as methanol, the photogenerated holes in the valence band irreversibly oxidize methanol instead of H_2O, as a result facilitating water reduction by conduction band electrons if the bottom of the conduction band of the photocatalyst is located above the water reduction potential. In spite of this, it should be understood that the ability of a photocatalyst to both reduce and oxidize water separately does not make it automatically suitable or qualify to achieve overall water splitting without sacrificial reagents, figure 4 [9], [14], [87], [88], [62], [80]–[86]

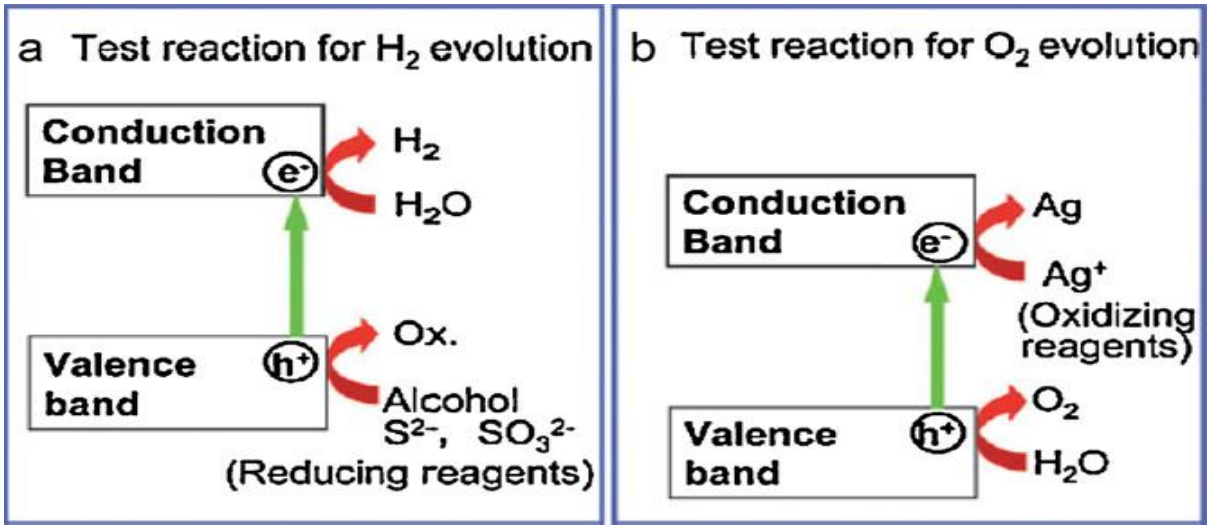

Fig. 4. H_2 or O_2 evolution reaction in the presence of sacrificial reagents—Half reactions of water splitting [62].

The environmental friendliness of hydrogen (a zero-emitter of greenhouse gases) has triggered a lot of interest in research related to its production through water splitting, accelerated by a diversity of photocatalysts and sacrificial reagents in the production processes. Admitting the role of the photocatalysts together with the use of electron/hole separators, sacrificial electron donors and acceptor, achieving absolute water splitting is still unfeasible [1], [4], [80], [89]–[91]. However, sacrificial reagents are used in the production of hydrogen in cases where there is need for enhancement of the yields (hydrogen and oxygen yields) under such states. The success of the use of sacrificial reagents relies on photocatalyst and the sacrificial reagent used [92], [93].

During photocatalysis, the charge carriers are abundantly produced as a result of the photon absorption as the irradiation is employed on the photocatalyst. The generated electron-hole pairs migrate to the reaction centers which are on the facet of the photocatalysts. On the photocatalyst surface, water molecules are reduced to H_2 while oxidation occurs to form O_2 [6], [41], [82], [84], [85], [93]–[96]. Different opinions have emerged concerning the benefits derived from the use of sacrificial reagents. This, however has made TiO_2-based catalysts when used together with sacrificial reagents an emerging area of interest to researchers as divided hypotheses have come up. Most research indicate that information gained in one research is not transferable to another. Hence, the type of sacrificial reagent to be used in water splitting together with photocatalysts such as TiO_2 need to be investigated further. To this moment, there is no correlation between the photocatalyst ability to split water and the presence of sacrificial reagents [6], [41], [82], [84], [85], [93], [95]–[97].

2.4 Development history of water splitting photocatalysts

Particulate photocatalytic systems, with particle sizes of a few micrometres to hundred nanometres for overall water splitting was first demonstrated in 1980 [98], [99]. TiO_2 and $SrTiO_3$ were developed for the splitting of water vapour [98], [100]. It was noted that

suppressing the reverse reaction (water formation from H_2 and O_2) on the loaded cocatalyst is a prerequisite, and that adsorbed water molecules are essential for the evolution of H_2 and O_2. For instance, Pt-loaded TiO_2 exhibits little water splitting activity resulting from rapid water formation from H_2 and O_2. The coating of Pt/TiO_2 with NaOH, conversely, results in higher stoichiometric H_2 and O_2 evolution ($H_2/O_2 = 2$)[8], [88], [99]. It was deduced that the NaOH coating suppressed H_2-O_2 recombination on Pt and to hold water molecules near the catalyst surface. Following this work, however, most photocatalytic water splitting reactions have been designed for aqueous solution is basically faster than in the gaseous phase [41], [88], [101]–[108]. The two important parameters which are used to evaluate the photocatalytic water splitting performance of a chosen material are solar to hydrogen (STH) conversion efficiency and apparent quantum efficiency (AQE), or apparent quantum yield (AQY [109]–[111]).

The most widely used carbon nanomaterials, CNMs for the synthesis of photocatalysts such as carbon nanotubes, graphene, carbon quantum dots (CQDs), fullerene and graphitic carbon nitride have received a lot of attention because of their great physiochemical stability, earth abundant, and low cost of synthesis. In addition, the electronic structure, and photocatalytic properties of CNMs can be controlled through morphology and interfacial modulation. To overcome rapid recombination of electron-hole pair and narrow visible light adsorption is to construct heterojunction via assembly of CNMs with semiconductors. Particularly, the modified CNMs-based Z-scheme heterojunction, the benefits include improved light harvesting, spatially separated electron and hole sites and strong redox ability [109], [110], .

On the other hand, apart from structure modification of the Z-scheme heterojunction, the introduced CNMs also serve as electron mediator between two semiconductors, which helps to reduce the resistance and improve the charge separation and stability [1], [109], [112].

Recent research has shown that CQDs have also been used as electron mediator in building solid state Z-scheme heterojunction. In 2019, a CQD-based Z- scheme heterojunction was fabricated by Liu et al. by bridging TiO_2 and $Cd_{0.5}Zn_{0.5}S$ with CQDs, which display super photocatalytic activity for H_2 evolution. Further, Pan et al. framed a sandwich-type structure where CQDs were encapsulated between CdS and BiOCl. The formed CdS/CQDs/BiOCl heterojunction exhibited much higher photocatalytic activity on the degradation of RhB and phenol under visible and UV light irradiation compared to BiOCl, CdS/BiOCl, and CQDs/BiOCl [109], [112]–[114].

Currently, researchers are targeting the use of carbon-based nanomaterials like helices (CNFs), CNTs and fullerenes (C_{60}) doped with semiconductor photocatalysts to enhance the effectiveness of the composite materials in water splitting [15], [109], [115], [116]. The importance of this technique is perceived to be associated with the delocalization processes of the combined structure present in the carbon allotropes that act as electron reservoirs that will necessitate the transfer and splitting of the photogenerated electrons. Additionally, there is improvement of the adsorptive properties of the photocatalysts and this gives rise to catalytic sites on the photocatalyst surfaces [117], [118]. Other methods have been used to extend TiO_2 photocatalytic properties to electromagnetic radiation regions by capping it with carbon. This technique of doping TiO_2 with CNFs has combined effect thereby improving the efficiency of the photocatalyst and proposed various mechanisms which still require justification [1], [97], [119]–[121].

Despite the uncertainty, the enhanced compositing of CNFs with TiO_2 (TiO_2/CNFs) materials helps to advance the catalytic effect of TiO_2. Studies have shown that CNFs/CNTs have the potential to act as an electron reservoir to separate electron-hole pairs successfully. Moreover, similar studies have suggested the photosensitizing properties of CNFs/CNTs in which they directly inject electrons into the TiO_2 conductive band, CB [15], [72], [96], [121], [122].

2.5 Titanium dioxide (TiO_2) as a photocatalyst

Titanium dioxide, titanium (IV) oxide or titania, is the naturally occurring oxide of titanium, TiO_2. Primarily, it is obtained from ilmenite, rutile, and anatase. It is used in paints, sunscreen, Photocatalysis, and food colouring etc [9], [11], [123]. Photocatalysis in which inexhaustible, clean and safe solar energy can be harvested for sustainable, non-hazardous, and low-cost technologies, is a major advance in obtaining clean energy. Titanium oxide materials in different types and forms have proved to be essential photocatalysts for a range of significant reaction because of their chemical stability, nontoxicity and high reactivity. Extensive research has led to the development of varied Ti-oxide based photocatalytic materials. Especially, photocatalysts have been used for applications such as the purification of polluted water and air, self-cleaning glasses, tiles, and tents coated with Ti-oxide materials with distinct photo-induced superhydrophilicity, and bone-implant fixation etc [9], [11], [123].

Titanium dioxide, TiO_2 and its morphological variants are the most researched photocatalysts for thermo-splitting of water for and removal of organic contaminants from the environment. In the last decade, TiO_2 has been one of the most investigated semiconductor [6], [77], [129]–[132], [103], [104], [123]–[128]. This is associated with its high reactivity, high hydrophilicity, low cost, and availability, chemical and physical stability, resistance to photo-corrosion, optical electronic and optical capacity [133]–[135]. TiO_2 is a transition-metal oxide semiconductor consisting of Ti^{4+} atoms and six O^{2-} coordinated together forming a TiO_6, octahedron [123], [136]. Similar to other metal oxides, TiO_2 is often non-stoichiometric with oxygen vacancies (O_v) as main defects at the near-atmospheric oxygen pressure, according to the properties of an intrinsic n-type semiconductor [1], [14], [123]. The oxygen vacancies (O_v) at the surface of the n-type appear as extra unpaired electrons in CB, which function as donor like states. This generates an accumulation layer in the surface, hence, a downward band bending [9], [81].

TiO_2 consists of three crystal phases: anatase, rutile, and bookite. Although anatase and rutile exhibit the same tetragonal crystal structure, bookite has an orthorhombic structure. The three polymorphs also differ in the energy bandgap (E_g) values, with 3.2eV, 3.0eV, and 3.3eV for anatase, rutile, and bookite, respectively [123], [133], [137]. Anatase has been generally considered as the most active phase of the three TiO_2 polymorphs for photocatalytic work.

Studies show that in the presence of alcohols, faster and irreversible hole scavenging was achieved on anatase than in the rutile, resulting in the generation of long-lived electrons ($t \approx 0.7s$) The lower activity of rutile caused the deficiency of rutile holes to drive efficient and irreversible alcohol oxidation and not the differences in recombination kinetics. It has also been found by other researchers [123] that only anatase generates OH● radicals, thus, the photocatalytic oxidation on rutile is limited to adsorbed species.

Research has also been carried out focusing on the improvement of visible light-responsive Ti-oxide photocatalysts by introducing little amounts of components such as cations and metal oxides by chemical doping and physical ion-implantation methods [3], [17], [80].

Besides, Ti-oxide photocatalysts which operate effectively under natural sunlight irradiation have been prepared.

The splitting of H_2O for the evolution of H_2 and O_2 is undergoing development using visible light-responsive titanium oxide thin film photocatalysts under sunlight irradiation. It has also been reported that Ti-oxide single site photocatalysts constructed within zeolite frameworks can induce the reduction of CO_2 with water to form hydrocarbons and O_2 [11], [16], [41]

By 1960s, many researchers studied the photo induced phenomena activities on semiconducting solids such as TiO_2 and ZnO under UV light irradiation. They observed that some molecules such as O_2 and water are adsorbed on or desorbed from the solid

semiconductor surfaces under UV illumination depending on the respective surface conditions. The photocatalytic decomposition of water on powdered TiO_2 photocatalysts loaded with small amounts of Pt or Rh metal particles has been reported. This led to the development of Pt/TiO_2 catalysts, the electron, photo-formed in TiO_2 moved to the Pt metal site where they induce reduction reactions, while photo-formed holes remain in the TiO_2 particle and migrate to its surface where they induce oxidation reactions [9], [11]. Hence the charge separation of electrons and holes is the most important process in photocatalysis employing semiconducting materials, photo electrochemical mechanism.

Substantive efforts have been devoted to the design of photocatalytic systems displaying a high conversion efficiency of light into chemical energy such as splitting of water into H_2 and O_2. Others have focused on colloidal semiconductors and others on semiconductors incorporated on inert supports such as porous glass, or zeolites. Besides, binary oxide catalysts have also been shown to be promising photocatalysts.

An earlier description of the photocatalytic properties of some metal oxides was given in1955 by Markham who worked with ZnO, Sb_2O_3 and TiO_2, and the different types of photochemical changes that these oxides may undergo such as catalytic oxidation of organic compounds under UV irradiation. At a later time, in 1972, Fujishioma and Honda showed that water could be photolyzed electrochemically at an illuminated TiO_2 and Pt electrode combination to give H_2 and O_2 [16], [41].

Since this discovery there has been a series of studies in search of the photocatalytic materials to produce Hydrogen fuel, hydrogen economy. A lot of semiconductors have showed photocatalytic properties like MoS_2, WO_3, $BiFeO_3$, Fe_2O_3 and CdTe, though only a few of them fulfil the thermodynamic requirements for overall water splitting, much like $KTaO_3$, $SrTiO_3$, TiO_3, ZnS, and SiC. What may be perceived as a simple basic function like the excitation of

the semiconductor by absorption of light results in the formation of charge carriers, the valence band holes, h_{vb}^{+}, and the conduction band electrons, e_{cb}^{-}. But, because of the strong oxidation potential of h_{vb}^{+} and reactive oxygen species such as ●OH, ●OOH, and H_2O_2 which are formed from the h_{vb}^{+} oxidation of water and e_{cb}^{-} reduction of O_2, most organic compounds like methanol, formaldehyde, formic acid can be oxidized, also, they can be mineralized to CO_2 and H_2O in the photocatalytic systems [1], [14], [123].

As a result of the challenges facing the overall water splitting, an alternative approach is to combine light-induced splitting of water and photooxidation of organic substrates, (i.e. methanol, formaldehyde, formic acid) into a single process known as photocatalytic reforming.

TiO_2 has been extensively studied as photocatalyst, there was an argument in many aspects such as the nature of the oxidative agent (●H radicals vs h^+), the site at which the reaction takes place (surface vs bulk solution), how to improve performance and efficiency of TiO_2 photocatalytic properties. Unfavourably, TiO_2 has a relatively large bandgap (3.2eV) as a result, only UV radiation can activate it, its conduction band is a bit positive relative to the redox potential for H_2 evolution. Evidently, new semiconductor-based nanostructured materials are needed that would use lower-energy photons available in the visible spectral region. Currently, there is development of strategies to push the absorption of photons by TiO_2 toward longer wavelengths ($\geq$ 387 nm) by doping TiO_2 with anions and/or cations (N, C, S, F, and metal ions) [11], [17], [123]. TiO_2 has been widely used because of its many advantages namely non-toxicity, high photochemical stability, abundance, low cost and high stability against photo corrosion [138]–[141]. In spite of the many studies on TiO_2, there is no other metal oxide that has been found to act as an efficient photoanode with valence and conduction band edges that embrace the redox potentials of water and organic pollutants.

2.6 Water splitting in the presence of sacrificial reagents

Reliable conversions of solar energy have been a challenging problem and varied studies have been undertaken to try resolve the issue. For example: Biomass conversion, photocatalytic cells, and photocatalytic water splitting. Studies have shown that some metal oxides like TiO_2, $SrTiO_2$, ZrO_2, $BaTi_4O_9$, and CeO_2, have capability for water splitting into hydrogen and oxygen in the stoichiometric ratio under ultraviolet (UV) and visible light irradiation [80], [82], [96], [123], [142]–[144].

TiO_2 has been extensively used in photocatalysis, due to its favourable bandgap energy (3.2 eV in anatase) and its high stability in aqueous solution under UV irradiation.

The process of photocatalysis over TiO_2 is triggered by the absorption of a photon with energy equal to or greater than the forbidden band gap of the semiconductor. Accompanying light irradiation, the electron-hole pairs are generated. The photogenerated electrons move to the conduction band, where they reduce H^+ to H_2 and the holes on the surface of semiconductor break up water to O_2 and H^+.

It has been noted that pure TiO_2 cannot achieve the splitting of water into H_2 and O_2 in aqueous suspension system. The challenging problem is the fast, undesired electron-hole recombination reaction, which is thermodynamically favoured. Thus, it is vital to inhibit the electron-hole recombination process. The use of sacrificial reagent helps to control the process.

Photo-efficiency of the process can be enhanced by the addition of sacrificial reagents which act as electron donors or electron-acceptor scavengers. In photocatalytic water splitting, the photocatalysts used can potentially use inexhaustible solar energy, sacrificial agents, and still operate at low temperatures without additional power sources such as coal and electricity to produce hydrogen [53], [88], [145]–[149]. Studies have been carried out on hydrogen production from systems consisting of semiconductor particles suspended in aqueous solutions

and dissolved organic compounds. The compounds are generally known as sacrificial reagents/agents. For instance, in a Pt/TiO_2- water- methanol system, methanol is oxidized by means of the photo-generated valence band (VB) holes on the metal-decorated photocatalyst hence allowing the reduction of water to hydrogen by photogenerated electrons in the conduction band (CB) [55], [81], [121], [150]–[152]. The sacrificial reagents/agents then react irreversibly with the photogenerated holes and promote accordingly the electron/hole separation. This technique can be used in the photocatalytic production of hydrogen with simultaneous decomposition of pollutants (water treatment) or what is referred to as photo reforming [9], [123]. The examples of scavengers (sacrificial agents) that have been in use are; Ethanol, Methanol, 4-nitrophenol, Na_2S, Na2SO4, glucose, glycerol, Ethylene diamine tetra-acetic acid, EDTA, I^- and IO_3^-, CN^-, and Fe^{3+} ions [62], [81], [114], [123], [153] and the most appropriate for water splitting are glycerol and glucose [153]. It has also been reported that organic pollutants (like oxalic acid, formic acid, and formaldehyde) act as electron donors in waste water [4], [123].

2.7 Photocatalytic materials for hydrogen production

Traditional and extensively studied binary transition-metal-semiconductors such as TiO_2 and WO_3, are easy to prepare and are stable under photo electrochemical operations, but their bandgaps are large to absorb a substantive fraction of the solar spectrum. Thus, the search for more and better materials to efficiently catalyze water splitting reaction is in progress. Various metal oxides, sulphides, nitrides, and phosphates which comprise of metal cations with d^0 and d^{10} configurations with smaller bandgaps can be considered as photocatalysts. Transition metal oxides based on d^0 and d^{10} bands have valence-band energy levels dominated wholly by the O_2 p levels, making the VB at ca +3V or higher (vs NHE), figure2, which is appropriate to oxidize water. Their high ionic character dictates a large separation between the band edges. But, if the bottom of the CB of a given metal oxide is located at a potential more negative than the water

reduction potential, the bandgap of the material will automatically become larger than 3eV, which is too large for efficient solar energy harvesting [1], [9], [14], [76], [120], [154]–[161] .

Group I and Group II metals together with some lanthanides form perovskite materials, also semiconductor catalysts coupled with carbon materials are promising for this type of work [9], [162].

By evaluating the semiconductors that are suitable for photocatalysis, TiO_2 has been widely used because of its many advantages namely non-toxicity, high photochemical stability, abundance, low cost and high stability against photo corrosion [140], [141]. Nevertheless, TO_2 also has a setback of wide bandgap, 3.0 – 3.2 eV, which lowers its prospective for visible light absorption [163]–[165]. Owing to the structural and chemical properties of TiO_2, it is feasible to construct the bandgap, recombination rate, and light absorption properties by controlling and improving the electrical properties [1], [6], [17], [129], [166]. There are different polymorphs of TiO_2 with dissimilar behaviours. The common and most important ones are anatase, rutile and brookite. Anatase and rutile TiO_2 polymorphs are primarily used for photocatalytic water splitting; though some research have been done with amorphous TiO_2 [167], [168].

Carbon was first proposed by A. L. Lavoisier in 1789 from charcoal. It is one of the most available elements on earth. Besides, it is capable of forming several compounds [169]. Carbon has proved to have distinctive physicochemical and thermal properties [11]. Eminently, during photocatalytic water splitting, the material can capably play several roles, including co-catalyst, supporting material and electron acceptor [170]. The aforementioned functions of carbon basically enhance the surface reaction sites, visible light capturing as well as competently transferring the electrons to the surface reaction sites in TiO_2 [171], [172]. Additionally, carbon also promotes the segregation of the photogenerated electron-hole pairs of TiO_2 showing that carbon has gained electron storage potential [173]–[177]. Other studies by Gao et al., also

reported the compositing of TiO_2 carbon for H_2 evolution upon illumination with visible light [173]. Also, it turned out that the inclusion of carbon in TiO_2 photocatalysts helps to advance the photocatalytic stability [178], [179]. Other studies show that Chengwu et al., prepared carbon-TiO_2 composite with sheets coated on the shell type TiC (TiC/TiO_2-C) by thermal growth process [176], [180]. The TiC/TiO_2-C principal covering produced enhanced hydrogen evolution results than the neat TiO_2 (P-25) as a result of the principal covering structure that helped to shift the band edge of TiO_2 which resulted from the retardation of the photogenerated electron- hole pair recombination efficiency.

Semiconductor materials have been used for solar energy conversions as colloids, powders, electrodes, and thin films while hydrogen production is by electrochemical, biological, photochemistry (semiconductor electrode) and photocatalytic (using semiconductor powders) processes [9], [17], [181].

Table 1: Outline of the photocatalytic activity of photocatalysts for water splitting

Photocatalyst	**Reactant & sacrificial agents**	**Parameter (Light source)**	**Activity (H_2 evolution)**	**Ref**
rGO/TiO_2	Methanol	300 W Xenon lamp	149 μmol g^{-1} h^{-1}	[177]
NiO_X/ TiO_2	Glycerol (16.6%)	500 W Hg lamp	900 μmol g^{-1} h^{-1}	[182]
rGO/g-C_3N_4/TiO_2	Glycerol (5%)	UV – Visible light 250 W	23143 μmol g^{-1} h^{-1}	[183]
Cu/TiO_2-G	Methanol	300 W high pressure Hg/500 W Xe lamp	TiO_2 – 500 μmol g^{-1} h^{-1} G-TiO_2 – 1900 μmol g^{-1} h^{-1} Cu/G-TiO_2 – 10,000 μmol g^{-1} h^{-1}	[184]
TiO_2 (P-25)/RGO	Methanol	UV - vis	Hydrothermol - 78 TiO_2/ RGO – 200 μmol g^{-1} h^{-1} TiO_2 – 20 μmol g^{-1} h^{-1}	[185]

P25-Graphene	Methanol	Metal halide lamp	TiO_2/Graphene – 350 μmol g^{-1} h^{-1}	[186]
TiO_2/g-C_3N_4		UV	18200 μmol h^{-1}	[187]
Black TiO_2		UV	0.4 μmol h^{-1}	[188]
Cu/TiO_2 nanorods	Methanol, 20 vol %	300 W Xe lamp	1023.8 μmol g^{-1} h^{-1}	[189]
Rh-Nb/TiO_2 NRs	Methanol, 10 vol %	300 W Xe lamp	7850 μmol g^{-1} h^{-1}	[190]
rGO/TiO_2	Methanol	300 W Xe lamp	149 μmol g^{-1} h^{-1}	[177]
3 wt% Ni-TiO_2/CdS	Ethanol, 25 wt%	300 W Xe lamp, 420 cut off filter	33.63 μmol /g-cat^{-1} h^{-1}	[191]
Ru/CdS-ZnS	Formic acid, methanol, ethanol	300 W Xe lamp	266 mmol/m^2 h	[192]
Au/TiO_2	Ethanol	4 UV-LED lights, 12 W each	15.8 μmol /min g-cat.	[91]
SiFe co doped TiO_2	540 ml distilled H_2O, 60 ml ethanol	500 W	320 μmol g^{-1} h^{-1}	[54]
GaN:ZnO (Mn_3O_4.Rh/Cr_2O_3	Distilled H_2O NaI		20 μmol g^{-1} h^{-1}	[54]
TiO_2	Distilled H_2O 10% methanol	300 W Xe lamp	42.00 μmol g^{-1} h^{-1}	[54][193]
Au/ TiO_2		300 W Xe lamp	3550 μmol g^{-1} h^{-1}	[194]
2 wt% NiO - loaded TiO_2		500 W Hg lamp	1230 μmol g^{-1} h^{-1}	[195]
MoS_2/TiO_2		300 W Xe arc lamp	8.43 μmol g^{-1} h^{-1}	[196]

Acknowledgement

I thank the University of the Witwatersrand for the support.

Declaration of competing interests

The author has no conflicts of interest to declare.

Reference

[1] M. B. Tahir, A. M. Asiri, and T. Nawaz, "A perspective on the fabrication of heterogeneous photocatalysts for enhanced hydrogen production," *Int. J. Hydrogen Energy*, vol. 45, no. 46, pp. 24544–24557, 2020, doi: 10.1016/j.ijhydene.2020.06.301.

[2] F. E. Osterloh, "Photocatalysis versus Photosynthesis: A Sensitivity Analysis of Devices for Solar Energy Conversion and Chemical Transformations," *ACS Energy Lett.* 2017, 2, 2, 445–453, doi: 10.1021/acsenergylett.6b00665.

[3] C. Ros, T. Andreu, and J. R. Morante, "Photoelectrochemical water splitting: a road from stable metal oxides to protected thin film solar cells," *J. Mater. Chem. A*, 2020,8, 10625-10669, doi: 10.1039/d0ta02755c.

[4] Y. Zhou, X. Ye, and D. Lin, "Enhance photocatalytic hydrogen evolution by using alkaline pretreated corn stover as a sacrificial agent," *Int. J. Energy Re*s. 2020, 44:4616–4628, doi: 10.1002/er.5242.

[5] J. S. Jang, H. G. Kim, and J. S. Lee, "Heterojunction semiconductors: A strategy to develop efficient photocatalytic materials for visible light water splitting," *Catal. Today*, vol. 185, no. 1, pp. 270–277, 2012, doi: 10.1016/j.cattod.2011.07.008.

[6] M. Ijaz and M. Zafar, "Titanium dioxide nanostructures as efficient photocatalyst: Progress, challenges and perspective," *Int. J. Energy Res.*, vol. 45, no. 3, pp. 3569–3589, 2021, doi: 10.1002/er.6079.

[7] A. L. Linsebigler, G. Lu, and J. T. Yates, "Photocatalysis on $Ti0_2$ Surfaces: Principles, Mechanisms, and Selected Results," *Chem. Rev*., vol. 95, no. 3, pp. 735–758, 1995, https://pubs.acs.org/sharingguidelines.

[8] K. Yamaguti and S. Sato, "Photolysis of water over metallized powdered titanium

dioxide," *J. Chem. Soc., Faraday Trans*. vol. I, no. 81, pp. 1237-1246, 1985, doi: 10.1039/F19858101237.

[9] A. Hakki, Y. AlSalka, C. B. Mendive, J. Ubogui, P. C. Dos Santos Claro, and D. Bahnemann, "Hydrogen production by heterogeneous photocatalysis,"

Encycl. Interfacial Chem. Surf. Sci. Electrochem., pp. 413–419, 2018, doi: 10.1016/B978-0-12-409547-2.13795-3.

[10] K. Sivula and R. Van De Krol, "Semiconducting materials for photoelectrochemical energy conversion,"*Nature Reviews Materials*, vol. 1, no. 15010 (2016). doi: 10.1038/natrevmats.2016.10.

[11] J. Schneider *et al.*, "Understanding TiO_2 Photocatalysis Mechanisms and Materials," *Chem. Rev.*, vol. 114, no. 9, p. 9919−9986, 2014, doi:10.1021/cr5001892.

[12] M. Ghorbanloo *et al.*, "BN/Cs_2CO_3/TiO_2 composite nanofibers to improve hydrogen generation," *J. Alloys Compd.*, vol. 945, p. 169218, 2023, doi: 10.1016/j.jallcom.2023.169218.

[13] Q. Wang and K. Domen, "Particulate Photocatalysts for Light-Driven Water Splitting: Mechanisms, Challenges, and Design Strategies," *Chemical Reviews*, vol. 120, no. 2. 2020. doi: 10.1021/acs.chemrev.9b00201.

[14] M. A. Nadeem, M. A. Khan, A. A. Ziani, and H. Idriss, "An overview of the photocatalytic water splitting over suspended particles," *Catalysts*, vol. 11, no. 1, pp. 1–25, 2021, doi: 10.3390/catal11010060.

[15] M. S. Nasir, G. Yang, I. Ayub, A. Nasir, and W. Yan, "Higher hydrogen production by photocatalytic water splitting using a hollow tubular graphitic carbon nitride-zinc telluride

composite," *Environ. Chem. Lett.*, vol. 20, no. 1, pp. 19–26, 2022, doi: 10.1007/s10311-021-01301-z.

[16] H. Park, H. Il Kim, G. H. Moon, and W. Choi, "Photoinduced charge transfer processes in solar photocatalysis based on modified TiO_2," *Energy Environ. Sci.*, vol. 9, no. 2, pp. 411–433, 2016, doi: 10.1039/c5ee02575c.

[17] N. M. Gupta, "Factors affecting the efficiency of a water splitting photocatalyst: A perspective," *Renewable and Sustainable Energy Reviews*, vol. 71, pp. 585–601, May 01, 2017. doi: 10.1016/j.rser.2016.12.086.

[18] L. Wu *et al.*, "A library of polytypic copper-based quaternary sulfide nanocrystals enables efficient solar-to-hydrogen conversion," *Nat. Commun.*, vol. 13, no. 1, p. 5414, 2022, doi: 10.1038/s41467-022-33065-7.

[19] B. Qiu, L. Cai, N. Zhang, X. Tao, and Y. Chai, "A Ternary Dumbbell Structure with Spatially Separated Catalytic Sites for Photocatalytic Overall Water Splitting," *Adv. Sci.*, vol. 7, no. 17, pp. 1–8, 2020, doi: 10.1002/advs.201903568.

[20] M. Yuan *et al.*, "Cu_2ZnSnS_4-CdS heterostructured nanocrystals for enhanced photocatalytic hydrogen production," *Catal. Sci. Technol.*, vol. 7, no. 18, pp. 3980–3984, 2017, doi: 10.1039/c7cy01360d.

[21] D. Zhao *et al.*, "Boron-doped nitrogen-deficient carbon nitride-based Z-scheme heterostructures for photocatalytic overall water splitting," *Nat. Energy*, vol. 6, no. 4, pp. 388–397, 2021, doi: 10.1038/s41560-021-00795-9.

[22] M. Ebihara, T. Ikeda, S. Okunaka, H. Tokudome, K. Domen, and K. Katayama, "Charge carrier mapping for Z-scheme photocatalytic water-splitting sheet via categorization of microscopic time-resolved image sequences," *Nat. Commun.*, vol. 12, no. 1, pp. 1–9, 2021,

doi: 10.1038/s41467-021-24061-4.

[23] W. Yang *et al.*, “Electron Accumulation Induces Efficiency Bottleneck for Hydrogen Production in Carbon Nitride Photocatalysts,” *J. Am. Chem. Soc.*, vol. 141, no. 28, pp. 11219–11229, 2019, doi: 10.1021/jacs.9b04556.

[24] X. Yu, A. Shavel, X. An, Z. Luo, and A. Cabot, “Cu_2ZnSnS_4 - Pt and Cu_2ZnSnS_4 - Au Heterostructured Nanoparticles for Photocatalytic Water Splitting and Pollutant Degradation,” *J. Am. Chem. Soc.*, vol. 136, no. 26, pp. 9236–9239, 2014.

[25] S. Maiti *et al.*, “Dye-Sensitized Ternary Copper Chalcogenide Nanocrystals: Optoelectronic Properties, Air Stability, and Photosensitivity,” *Chem. Mater.*, vol. 31, no. 7, pp. 2443–2449, 2019, doi: 10.1021/acs.chemmater.8b05108.

[26] H. Zhang *et al.*, “Direct probing of atomically dispersed Ru species over multi-edged TiO_2 for highly efficient photocatalytic hydrogen evolution,” *Sci. Adv.*, vol. 6, no. 39, pp. 2–10, 2020, doi: 10.1126/sciadv.abb9823.

[27] E. Ha, L. Y. S. Lee, J. Wang, F. Li, K. Y. Wong, and S. C. E. Tsang, “Significant enhancement in photocatalytic reduction of water to hydrogen by Au/Cu_2ZnSnS_4 nanostructure,” *Adv. Mater.*, vol. 26, no. 21, pp. 3496–3500, 2014, doi: 10.1002/adma.201400243.

[28] R. Shi *et al.*, “Achieving an exceptionally high loading of isolated cobalt single atoms on a porous carbon matrix for efficient visible-light-driven photocatalytic hydrogen production,” *Chem. Sci.*, vol. 10, no. 9, pp. 2585–2591, 2019, doi: 10.1039/c8sc05540h.

[29] Y. Zhao *et al.*, “A Hydrogen Farm Strategy for Scalable Solar Hydrogen Production with Particulate Photocatalysts,” *Angew. Chemie - Int. Ed.*, vol. 59, no. 24, pp. 9653–9658, 2020, doi: 10.1002/anie.202001438.

[30] K. Maeda and K. Domen, “Photocatalytic water splitting: Recent progress and future challenges,” *J. Phys. Chem. Lett.*, vol. 1, no. 18, pp. 2655–2661, 2010, doi: 10.1021/jz1007966.

[31] C. Cheng, B. He, J. Fan, B. Cheng, S. Cao, and J. Yu, “An Inorganic/Organic S-Scheme Heterojunction H_2-Production Photocatalyst and its Charge Transfer Mechanism,” *Adv. Mater.*, vol. 33, no. 22, pp. 1–8, 2021, doi: 10.1002/adma.202100317.

[32] J. Ran *et al.*, “2D Metal Organic Framework Nanosheet: A Universal Platform Promoting Highly Efficient Visible-Light-Induced Hydrogen Production,” *Adv. Energy Mater.*, vol. 9, no. 11, 2019, doi: 10.1002/aenm.201803402.

[33] X. Chen, J. Wang, Y. Chai, Z. Zhang, and Y. Zhu, “Efficient Photocatalytic Overall Water Splitting Induced by the Giant Internal Electric Field of a g-C_3N_4/rGO/PDIP Z-Scheme Heterojunction,” *Adv. Mater.*, vol. 33, no. 7, pp. 1–7, 2021, doi: 10.1002/adma.202007479.

[34] A. Galińska and J. Walendziewski, “Photocatalytic water splitting over Pt-TiO_2 in the presence of sacrificial reagents,” *Energy and Fuels*, vol. 19, no. 3, pp. 1143–1147, 2005, doi: 10.1021/ef0400619.

[35] K. Villa, J. R. Galán-Mascarós, N. López, and E. Palomares, “Photocatalytic water splitting: advantages and challenges,” *Sustain. Energy Fuels*, vol. 5, no. 18, pp. 4560–4569, 2021, doi: 10.1039/d1se00808k.

[36] M. Liu, D. Jing, Z. Zhou, and L. Guo, “Twin-induced one-dimensional homojunctions yield high quantum efficiency for solar hydrogen generation,” *Nat. Commun.*, vol. 4, pp. 1–8, 2013, doi: 10.1038/ncomms3278.

[37] C. Feng *et al.*, “Significantly enhanced photocatalytic hydrogen production performance of g-C_3N_4/CNTs/CdZnS with carbon nanotubes as the electron mediators,” *J.*

Mater. Sci. Technol., vol. 80, pp. 75–83, 2021, doi: 10.1016/j.jmst.2020.11.047.

[38] X. L. Yin *et al.*, "MoS_2/CdS Nanosheets-on-Nanorod Heterostructure for Highly Efficient Photocatalytic H_2 Generation under Visible Light Irradiation," *ACS Appl. Mater. Interfaces*, vol. 8, no. 24, 2016, doi: 10.1021/acsami.6b02687.

[39] I. Tsuji, H. Kato, H. Kobayashi, and A. Kudo, "Photocatalytic H_2 evolution under visible-light irradiation over band-structure-controlled (CuIn)xZn_2(1-x)S_2 solid solutions," *J. Phys. Chem. B*, vol. 109, no. 15, 2005, doi: 10.1021/jp044722e.

[40] S. Chen *et al.*, "Surface Modifications of (ZnSe)0.5(CuGa2.5Se4.25)0.5to Promote Photocatalytic Z-Scheme Overall Water Splitting," *J. Am. Chem. Soc.*, vol. 143, no. 28, 2021, doi: 10.1021/jacs.1c03555.

[41] D. Kobayashi *et al.*, "Significant Enhancement of Hydrogen Evolution Reaction Activity by Negatively Charged Pt through Light Doping of W," *J. Am. Chem. Soc.*, vol. 142, no. 41, 2020, doi: 10.1021/jacs.0c07143.

[42] F. Ozel, E. Aslan, B. Istanbullu, O. Akay, and I. Hatay Patir, "Photocatalytic hydrogen evolution based on Cu_2ZnSnS_4, Cu_2NiSnS_4 and Cu_2CoSnS_4 nanocrystals," *Appl. Catal. B Environ.*, vol. 198, pp. 67–73, 2016, doi: 10.1016/j.apcatb.2016.05.053.

[43] Y. Li *et al.*, "Significant Enhancement of Hydrogen Production in MoS_2/Cu_2ZnSnS_4 Nanoparticles," *Part. Part. Syst. Charact.*, vol. 35, no. 6, pp. 2–7, 2018, doi: 10.1002/ppsc.201700472.

[44] A. M. Huerta-Flores *et al.*, "Enhanced Photocatalytic Hydrogen Evolution from Water Splitting on Ta_2O_5/$SrZrO_3$ Heterostructures Decorated with CuxO/RuO_2 Cocatalysts," *ACS Appl. Mater. Interfaces*, vol. 14, no. 28, pp. 31767–31781, 2022, doi: 10.1021/acsami.2c02520.

[45] J. Ran *et al.*, "$NiPS_3$ ultrathin nanosheets as versatile platform advancing highly active photocatalytic H_2 production," *Nat. Commun.*, vol. 13, no. 1, pp. 1–17, 2022, doi: 10.1038/s41467-022-32256-6.

[46] Y. Kageshima *et al.*, "Photocatalytic and Photoelectrochemical Hydrogen Evolution from Water over $Cu_2SnxGe1\text{-}xS_3$ Particles," *J. Am. Chem. Soc.*, vol. 143, no. 15, pp. 5698–5708, 2021, doi: 10.1021/jacs.0c12140.

[47] F. Ozel *et al.*, "Earth-Abundant Cu_2CoSnS_4 Nanofibers for Highly Efficient H_2 Evolution at Soft Interfaces," *ChemNanoMat*, vol. 1, no. 7, pp. 477–481, 2015, doi: 10.1002/cnma.201500113.

[48] T. Setoyama, T. Takewaki, K. Domen, and T. Tatsumi, "The challenges of solar hydrogen in chemical industry: How to provide, and how to apply?," *Faraday Discuss.*, vol. 198, pp. 509–527, 2017, doi: 10.1039/c6fd00196c.

[49] M. Qureshi and K. Takanabe, "Insights on measuring and reporting heterogeneous photocatalysis: Efficiency definitions and setup examples," *Chem. Mater.*, vol. 29, no. 1, pp. 158–167, 2017, doi: 10.1021/acs.chemmater.6b02907.

[50] N. Fajrina and M. Tahir, "A critical review in strategies to improve photocatalytic water splitting towards hydrogen production," *Int. J. Hydrogen Energy*, vol. 44, no. 2, pp. 540–577, 2019, doi: 10.1016/j.ijhydene.2018.10.200.

[51] T. Takata, C. Pan, and K. Domen, "Recent progress in oxynitride photocatalysts for visible-light-driven water splitting," *Sci. Technol. Adv. Mater.*, vol. 16, no. 3, 2015, doi: 10.1088/1468-6996/16/3/033506.

[52] Y. Li, Y. L. Li, B. Sa, and R. Ahuja, "Review of two-dimensional materials for photocatalytic water splitting from a theoretical perspective," *Catal. Sci. Technol.*, vol. 7, no.

3, pp. 545–559, 2017, doi: 10.1039/c6cy02178f.

[53] Y.-J. Yuan, D. Chen, Z.-T. Yu, and Z.-G. Zou, “Cadmium sulfide-based nanomaterials for photocatalytic hydrogen production,” *J. Mater. Chem. A*, vol. 6, no. 25, pp. 11606–11630, 2018, doi: 10.1039/C8TA00671G.

[54] C. Ros, T. Andreu, and J. R. Morante, “Photoelectrochemical water splitting: a road from stable metal oxides to protected thin film solar cells,” *J. Mater. Chem. A*, vol. 8, no. 21, pp. 10625–10669, 2020, doi: 10.1039/d0ta02755c.

[55] K. Maeda and K. Domen, “Nano-particulate photocatalysts for overall water splitting under visible light,” *Theor. Comput. Chem.*, vol. 18, pp. 301–315, 2007, doi: 10.1016/S1380-7323(06)80014-2.

[56] B. Y. Alfaifi, H. Ullah, S. Alfaifi, A. A. Tahir, and T. K. Mallick, “Photoelectrochemical solar water splitting: From basic principles to advanced devices,” *Veruscript Funct. Nanomater.*, vol. 2, 2018, doi: 10.22261/fnan.bdjoc3.

[57] R. D. Tentu and S. Basu, “Photocatalytic water splitting for hydrogen production,” *Curr. Opin. Electrochem.*, vol. 5, no. 1, pp. 56–62, 2017, doi: 10.1016/j.coelec.2017.10.019.

[58] S. C. Warren *et al.*, “Identifying champion nanostructures for solar water-splitting,” *Nat. Mater.*, vol. 12, no. 9, pp. 842–849, 2013, doi: 10.1038/nmat3684.

[59] M. S. Reza, N. B. H. Ahmad, S. Afroze, J. Taweekun, M. Sharifpur, and A. K. Azad, “Hydrogen Production from Water Splitting through Photocatalytic Activity of Carbon-Based Materials,” *Chem. Eng. Technol*., vol. 46, No. 3, 420–434, 2023, doi: 10.1002/ceat.202100513.

[60] A. R. Alharbi, I. M. Alarifi, W. S. Khan, and R. Asmatulu, “Semiconductor Nanomaterials for Water Splitting,” *Advances in Materials Science Research,* no. 316, pp. 1–22, 2015, https://www.researchgate.net/publication/322487050.

[61] E. W. Marcelino, D. D. O. Silva, and R. R. Riehl, “A REVIEW ON THE INFLUENCE OF NANOPARTICLE SIZE IN THERMAL ENHANCEMENT OF CuO-WATER NANOFLUIDS AND THEIR CHARACTERISTICS.” ITherm 2016, Las Vegas, NV USA, May 31 - June 3, 2016, https://www.researchgate.net/publication/322775565.

[62] A. Kudo and Y. Miseki, “Heterogeneous photocatalyst materials for water splitting,” *Chem. Soc. Rev.*, vol. 38, no. 1, pp. 253–278, 2009, doi: 10.1039/b800489g.

[63] X. Guan, S. Zong, and S. Shen, “Homojunction photocatalysts for water splitting,” *Nano Res.*, vol. 15, no. 12, pp. 10171–10184, 2022, doi: 10.1007/s12274-022-4704-9.

[64] D. Zhao, X. Guan, and S. Shen, “Design of polymeric carbon nitride-based heterojunctions for photocatalytic water splitting: a review,” *Environ. Chem. Lett.*, vol. 20, no. 6, pp. 3505–3523, 2022, doi: 10.1007/s10311-022-01429-6.

[65] N. L. Reddy, S. Kumar, V. Krishnan, M. Sathish, and M. V. Shankar, “Multifunctional Cu/Ag quantum dots on TiO_2 nanotubes as highly efficient photocatalysts for enhanced solar hydrogen evolution,” *J. Catal.*, vol. 350, pp. 226–239, 2017, doi: 10.1016/j.jcat.2017.02.032.

[66] M. Y. Xie, K. Y. Su, X. Y. Peng, R. J. Wu, M. Chavali, and W. C. Chang, “Hydrogen production by photocatalytic water-splitting on Pt-doped TiO_2–ZnO under visible light,” *J. Taiwan Inst. Chem. Eng.*, vol. 70, pp. 161–167, 2017, doi: 10.1016/j.jtice.2016.10.034.

[67] J. Zhang, Y. Wu, M. Xing, S. A. K. Leghari, and S. Sajjad, “Development of modified N doped TiO_2 photocatalyst with metals, nonmetals and metal oxides,” *Energy Environ. Sci.*, vol. 3, no. 6, pp. 715–726, 2010, doi: 10.1039/b927575d.

[68] A. Meng, L. Zhang, B. Cheng, and J. Yu, “Dual Cocatalysts in TiO_2 Photocatalysis,” *Adv. Mater.*, vol. 31, no. 30, pp. 1–31, 2019, doi: 10.1002/adma.201807660.

[69] G. Zhao and X. Xu, “Cocatalysts from types, preparation to applications in the field of photocatalysis,” *Nanoscale*, vol. 13, no. 24, pp. 10649–10667, 2021, doi: 10.1039/d1nr02464g.

[70] H. Wang, S. Dong, Y. Chang, and J. L. Faria, “Enhancing the photocatalytic properties of TiO_2 by coupling with carbon nanotubes and supporting gold,” *J. Hazard. Mater.*, vol. 235–236, pp. 230–236, 2012, doi: 10.1016/j.jhazmat.2012.07.050.

[71] T. K. Townsend, N. D. Browning, and F. E. Osterloh, “Nanoscale strontium titanate photocatalysts for overall water splitting,” *ACS Nano*, vol. 6, no. 8, pp. 7420–7426, 2012, doi: 10.1021/nn302647u.

[72] Q. Wang *et al.*, “Oxysulfide photocatalyst for visible-light-driven overall water splitting,” *Nat. Mater.*, vol. 18, no. 8, pp. 827–832, 2019, doi: 10.1038/s41563-019-0399-z.

[73] T. Takata *et al.*, “Photocatalytic water splitting with a quantum efficiency of almost unity,” *Nature*, vol. 581, no. 7809, pp. 411–414, 2020, doi: 10.1038/s41586-020-2278-9.

[74] A. Aguirre-Astrain, E. Luévano-Hipólito, and L. M. Torres-Martínez, “Integration of 2D printing technologies for AV_2O_6 (A=Ca, Sr, Ba)-MO (M=Cu, Ni, Zn) photocatalyst manufacturing to solar fuels production using seawater,” *Int. J. Hydrogen Energy*, vol. 46, no. 75, pp. 37294–37310, 2021, doi: 10.1016/j.ijhydene.2021.09.007.

[75] Y. Liu, X. Zhou, Y. Zhou, and G. Chen, “Construction of Ag decorated 2D rGO/SnS_2 nanostructure towards synergistically enabling overall water splitting,” *Chem. Eng. J.*, vol. 433, no. 2, 2022, doi: 10.1016/j.cej.2021.133198.

[76] A. Gupta, B. Likozar, R. Jana, W. C. Chanu, and M. K. Singh, “A review of hydrogen production processes by photocatalytic water splitting – From atomistic catalysis design to optimal reactor engineering,” *Int. J. Hydrogen Energy*, vol. 7, 2022, doi: 10.1016/j.ijhydene.2022.07.210.

[77] Y. Zhao *et al.*, “Classification and catalytic mechanisms of heterojunction photocatalysts and the application of titanium dioxide (TiO_2)-based heterojunctions in environmental remediation,” *J. Environ. Chem. Eng.*, vol. 10, no. 3, 2022, doi: 10.1016/j.jece.2022.108077.

[78] T. Gong, J. Zhang, Y. Liu, L. Hou, J. Deng, and C. Yuan, “Construction of hetero-phase Mo_2C-CoO@N-CNFs film as a self-supported Bi-functional catalyst towards overall water splitting,” *Chem. Eng. J.*, vol. 451, no. 4, 2023, doi: 10.1016/j.cej.2022.139025.

[79] H. Zhao *et al.*, “Transition-Metal-Based Cocatalysts for Photocatalytic Water Splitting,” *Small Struct.*, vol. 3, no. 7, 2022, doi: 10.1002/sstr.202100229.

[80] X. Li, J. Yu, and C. Jiang, “Principle and surface science of photocatalysis,” *Interface Sci. Technol.*, vol. 31, pp. 1–38, Jan. 2020, doi: 10.1016/B978-0-08-102890-2.00001-4.

[81] K. Maeda, “Photocatalytic water splitting using semiconductor particles: History and recent developments,” *J. Photochem. Photobiol. C Photochem. Rev.*, vol. 12, no. 4, pp. 237–268, 2011, doi: 10.1016/j.jphotochemrev.2011.07.001.

[82] A. Galińska and J. Walendziewski, “Photocatalytic water splitting over Pt-TiO_2 in the presence of sacrificial reagents,” *Energy and Fuels*, vol. 19, no. 3, pp. 1143–1147, May 2005, doi: 10.1021/ef0400619.

[83] G. Commentary, “Undesired Role of Sacrificial Reagents in Photocatalysis,” *J. Phys. Chem. Lett.*, vol. 4, no. 20, pp. 3479–3483, 2013, doi.org/10.1021/jz4018199.

[84] F. Costantino and P. V. Kamat, “Do Sacrificial Donors Donate H_2 in Photocatalysis?,” *ACS Energy Lett.*, vol. 7, no. 1, pp. 242–246, 2022, doi: 10.1021/acsenergylett.1c02487.

[85] L. Z. Wu, B. Chen, Z. J. Li, and C. H. Tung, “Enhancement of the efficiency of photocatalytic reduction of protons to hydrogen via molecular assembly,” *Acc. Chem. Res.*, vol. 47, no. 7, pp. 2177–2185, 2014, doi: 10.1021/ar500140r.

[86] M. Wang, S. Shen, L. Li, Z. Tang, and J. Yang, “Effects of sacrificial reagents on photocatalytic hydrogen evolution over different photocatalysts,” *J. Mater. Sci.*, vol. 52, no. 9, pp. 5155–5164, 2017, doi: 10.1007/s10853-017-0752-z.

[87] P. Chowdhury, H. Gomaa, and A. K. Ray, “Sacrificial hydrogen generation from aqueous triethanolamine with Eosin Y-sensitized Pt/TiO_2 photocatalyst in UV, visible and solar light irradiation,” *Chemosphere*, vol. 121, pp. 54–61, 2015, doi: 10.1016/j.chemosphere.2014.10.076.

[88] A. T. Hubbard, “Surface Science of Photocatalysis,”*Interface Science and Technology*, vol. 31, p. 602, 2020.

[89] T. Zhang and S. Lu, “Sacrificial agents for photocatalytic hydrogen production: Effects, cost, and development,” *Chem Catal.*, vol. 2, no. 7, pp. 1502–1505, 2022, doi: 10.1016/j.checat.2022.06.023.

[90] M. El ouardi *et al.*, “Review of photoelectrochemical water splitting: From quantitative approaches to effect of sacrificial agents, oxygen vacancies, thermal and magnetic field on (photo)electrolysis,” *Int. J. Hydrogen Energy*, vol. 51, pp. 1044–1067, 2024, doi: 10.1016/j.ijhydene.2023.09.111.

[91] E. Taboada, I. Angurell, and J. Llorca, “Dynamic photocatalytic hydrogen production from ethanol-water mixtures in an optical fiber honeycomb reactor loaded with Au/TiO_2,” *J.*

Catal., vol. 309, pp. 460–467, 2014, doi: 10.1016/j.jcat.2013.10.025.

[92] V. Kumaravel *et al.*, "Photocatalytic hydrogen production: Role of sacrificial reagents on the activity of oxide, carbon, and sulfide catalysts," *Catalysts*, vol. 9, no. 3, Mar. 2019, doi: 10.3390/catal9030276.

[93] A. S. Hainer, J. S. Hodgins, V. Sandre, M. Vallieres, A. E. Lanterna, and J. C. Scaiano, "Photocatalytic Hydrogen Generation Using Metal-Decorated TiO_2: Sacrificial Donors vs True Water Splitting," *ACS Energy Lett.*, vol. 3, no. 3, pp. 542–545, 2018, doi: 10.1021/acsenergylett.8b00152.

[94] W.-T. Chen, Y. Dong, P. Yadav, R. D. Aughterson, D. Sun-Waterhouse, and G. I. N. Waterhouse, "Effect of alcohol sacrificial agent on the performance of Cu/TiO_2 photocatalysts for UV-driven hydrogen production," *Appl. Catal. A Gen.*, vol. 602, p. 117703, 2020, doi: https://doi.org/10.1016/j.apcata.2020.117703.

[95] H. Husin *et al.*, "Efficient hydrogen production by microwave-assisted catalysis for glycerol-water solutions via NiO/zeolite-CaO catalyst," *South African J. Chem. Eng.*, vol. 41, pp. 43–50, 2022, doi: 10.1016/j.sajce.2022.04.004.

[96] A. Bratovcic, "A Recent Developments in Photocatalytic Water Splitting by TiO_2 Modified Photocatalysts," *Res. Dev. Mater. Sci.*, vol. 14, no. 1, pp. 1491–1498, 2020, doi: 10.31031/rdms.2020.14.000827.

[97] T. Jafari, E. Moharreri, A. S. Amin, R. Miao, W. Song, and S. L. Suib, "Photocatalytic water splitting - The untamed dream: A review of recent advances," *Molecules*, vol. 21, no. 7, 2016, doi: 10.3390/molecules21070900.

[98] A. Kudo, K. Domen, K. ichi Maruya, and T. Onishi, "Photocatalytic activities of TiO_2 loaded with NiO," *Chem. Phys. Lett.*, vol. 133, no. 6, pp. 517–519, 1987, doi: 10.1016/0009-

2614(87)80070-2.

[99] S. Sato and J. M. White, “Photodecomposition of water over Pt/TiO_2 catalysts,” *Chem. Phys. Lett.*, vol. 72, no. 1, pp. 83–86, 1980, doi: 10.1016/0009-2614(80)80246-6.

[100] J.-M. Lehn and R. Ziessel, “Photochemical generation of carbon monoxide and hydrogen by reduction of carbon dioxide and water under visible light irradiation,” *Proc. Natl. Acad. Sci.*, vol. 79, no. 2, pp. 701–704, 1982, doi: 10.1073/pnas.79.2.701.

[101] B. J. Ng, L. K. Putri, X. Y. Kong, Y. W. Teh, P. Pasbakhsh, and S. P. Chai, “Z-Scheme Photocatalytic Systems for Solar Water Splitting,” *Adv. Sci.*, vol. 7, no. 7, 2020, doi: 10.1002/advs.201903171.

[102] T. Hisatomi and K. Domen, “Reaction systems for solar hydrogen production via water splitting with particulate semiconductor photocatalysts,” *Nat. Catal.*, vol. 2, no. 5, pp. 387–399, 2019, doi: 10.1038/s41929-019-0242-6.

[103] P. Arunachalam, K. Nagai, M. S. Amer, M. A. Ghanem, R. J. Ramalingam, and A. M. Al-Mayouf, “Recent developments in the use of heterogeneous semiconductor photocatalyst based materials for a visible-light-induced water-splitting system-a brief review,” *Catalysts*, vol. 11, no. 2, pp. 1–27, 2021, doi: 10.3390/catal11020160.

[104] F. Opoku, K. K. Govender, C. G. C. E. van Sittert, and P. P. Govender, “Recent Progress in the Development of Semiconductor-Based Photocatalyst Materials for Applications in Photocatalytic Water Splitting and Degradation of Pollutants,” *Adv. Sustain. Syst.*, vol. 1, no. 7, pp. 1–24, 2017, doi: 10.1002/adsu.201700006.

[105] T. Kawawaki, M. Kawachi, D. Yazaki, Y. Akinaga, D. Hirayama, and Y. Negishi, “Development and Functionalization of Visible-Light-Driven Water-Splitting Photocatalysts,” *Nanomaterials*, vol. 12, no. 3, p. 344, 2022, doi: 10.3390/nano12030344.

[106] T. Yamada and K. Domen, “Development of sunlight driven water splitting devices towards future artificial photosynthetic industry,” *Chem. Engineering*, vol. 2, no. 3, pp. 1–18, 2018, doi: 10.3390/chemengineering2030036.

[107] J. Ran, J. Zhang, J. Yu, M. Jaroniec, and S. Z. Qiao, “Earth-abundant cocatalysts for semiconductor-based photocatalytic water splitting,” *Chem. Soc. Rev.*, vol. 43, no. 22, pp. 7787–7812, 2014, doi: 10.1039/c3cs60425j.

[108] S. Wang, J. Zhang, B. Li, H. Sun, and S. Wang, “Engineered Graphitic Carbon Nitride-Based Photocatalysts for Visible-Light-Driven Water Splitting: A Review,” *Energy and Fuels*, vol. 35, no. 8, pp. 6504–6526, 2021, doi: 10.1021/acs.energyfuels.1c00503.

[109] S. Kundu, K. Bramhaiah, and S. Bhattacharyya, “Carbon-based nanomaterials: In the quest of alternative metal-free photocatalysts for solar water splitting,” *Nanoscale Adv.*, vol. 2, no. 11, pp. 5130–5151, 2020, doi: 10.1039/d0na00569j.

[110] H. Lan, Y. Xia, K. Feng, A. Wei, Z. Kang, and J. Zhong, “Co-doped carbon layer to lower the onset potential of hematite for solar water oxidation,” *Appl. Catal. B Environ.*, vol. 258, no. January, p. 117962, 2019, doi: 10.1016/j.apcatb.2019.117962.

[111] P. Raizada, A. Sudhaik, P. Singh, P. Shandilya, P. Thakur, and H. Jung, “Visible light assisted photodegradation of 2,4-dinitrophenol using Ag_2CO_3 loaded phosphorus and sulphur co-doped graphitic carbon nitride nanosheets in simulated wastewater,” *Arab. J. Chem.*, vol. 13, no. 1, pp. 3196–3209, 2020, doi: 10.1016/j.arabjc.2018.10.004.

[112] H. Yu *et al.*, “Carbon-Based Nanomaterials via Heterojunction Serving as Photocatalyst,” *Front. Chem.,* vol. 7, p. 713, 2019, doi: 10.3389/fchem.2019.00713.

[113] J. Zhong, L. Chen, and L. Zhang, “High-throughput determination of high-quality interdiffusion coefficients in metallic solids: a review,” *J. Mater. Sci.*, vol. 55, no. 24, pp.

10303–10338, 2020, doi: 10.1007/s10853-020-04805-1.

[114] A. R. Marlinda, N. Yusoff, S. Sagadevan, and M. R. Johan, “Recent developments in reduced graphene oxide nanocomposites for photoelectrochemical water-splitting applications,” *International Journal of Hydrogen Energy*, vol. 45, no. 21. pp. 11976–11994, Apr. 17, 2020. doi: 10.1016/j.ijhydene.2020.02.096.

[115] L. S. Salah, N. Ouslimani, D. Bousba, I. Huynen, Y. Danleé, and H. Aksas, “Carbon Nanotubes (CNTs) from Synthesis to Functionalized (CNTs) Using Conventional and New Chemical Approaches,” *J. Nanomater.*, vol. 2021, 2021, doi: 10.1155/2021/4972770.

[116] M. M. Sabzehmeidani, S. Mahnaee, M. Ghaedi, H. Heidari, and V. A. L. Roy, “Carbon based materials: A review of adsorbents for inorganic and organic compounds,” *Mater. Adv.*, vol. 2, no. 2, pp. 598–627, 2021, doi: 10.1039/d0ma00087f.

[117] L. K. Putri, W. J. Ong, W. S. Chang, and S. P. Chai, “Heteroatom doped graphene in photocatalysis: A review,” *Appl. Surf. Sci.*, vol. 358, pp. 2–14, 2015, doi: 10.1016/j.apsusc.2015.08.177.

[118] H. Esmaili, E. Kowsari, S. Sarabadani Tafreshi, S. Ramakrishna, N. H. de Leeuw, and M. Abdouss, “TiO_2 nanoarrays modification by a novel Cobalt-heteroatom doped graphene complex for photoelectrochemical water splitting: An experimental and theoretical study,” *J. Mol. Liq.*, vol. 356, p. 118960, 2022, doi: 10.1016/j.molliq.2022.118960.

[119] H. M. Moustafa, M. S. Mahmoud, and M. M. Nassar, “Photon-induced water splitting experimental and kinetic studies with a hydrothermally prepared TiO_2-doped rGO photocatalyst,” *Inorg. Chem. Commun.*, vol. 141, 2022, doi: 10.1016/j.inoche.2022.109546.

[120] K. C. Christoforidis and P. Fornasiero, “Photocatalytic Hydrogen Production: A Rift into the Future Energy Supply,” *Chem. Cat. Chem.*, vol. 9, no. 9, pp. 1523–1544, 2017, doi:

10.1002/cctc.201601659.

[121] Y. Li and S. C. E. Tsang, “Recent progress and strategies for enhancing photocatalytic water splitting,” *Mater. Today Sustain.*, vol. 9, 2020, doi: 10.1016/j.mtsust.2020.100032.

[122] I. Dincer and C. Acar, “Review and evaluation of hydrogen production methods for better sustainability,” *Int. J. Hydrogen Energy*, vol. 40, no. 34, pp. 11094–11111, 2014, doi: 10.1016/j.ijhydene.2014.12.035.

[123] O. Al-Madanat, Y. Alsalka, W. Ramadan, and D. W. Bahnemann, “WTiO_2 photocatalysis for the transformation of aromatic water pollutants into fuels,” *Catalysts*, vol. 11, no. 3, pp. 1–45, 2021, doi: 10.3390/catal11030317.

[124] P. V. Govardhana Reddy *et al.*, “A review on multicomponent reactions catalysed by zero-dimensional/one-dimensional titanium dioxide (TiO_2) nanomaterials: Promising green methodologies in organic chemistry,” *J. Environ. Manage.*, vol. 279, 2021, doi: 10.1016/j.jenvman.2020.111603.

[125] A. Tayel, A. R. Ramadan, and O. A. El Seoud, “Titanium dioxide/graphene and titanium dioxide/graphene oxide nanocomposites: Synthesis, characterization and photocatalytic applications for water decontamination,” *Catalysts*, vol. 8, no. 11, 2018, doi: 10.3390/catal8110491.

[126] M. A. Aziz Aljar, M. Zulqarnain, A. Shah, M. S. Akhter, and F. J. Iftikhar, “A review of renewable energy generation using modified titania for photocatalytic water splitting,” *AIP Adv.*, vol. 10, no. 7, 2020, doi: 10.1063/5.0006196.

[127] B. Zhang, S. Cao, M. Du, X. Ye, Y. Wang, and J. Ye, “Titanium dioxide (TiO_2) mesocrystals: Synthesis, growth mechanisms and photocatalytic properties,” *Catalysts*, vol. 9, no. 1, 2019, doi: 10.3390/catal9010091.

[128] A. J. Haider, Z. N. Jameel, and I. H. M. Al-Hussaini, “Review on: Titanium dioxide applications,” *Energy Procedia*, vol. 157, pp. 17–29, 2019, doi: 10.1016/j.egypro.2018.11.159.

[129] M. Nasr, C. Eid, R. Habchi, P. Miele, and M. Bechelany, “Recent Progress on Titanium Dioxide Nanomaterials for Photocatalytic Applications,” *ChemSusChem*, vol. 11, no. 18, pp. 3023–3047, 2018, doi: 10.1002/cssc.201800874.

[130] K. Vikrant, S. Weon, K. H. Kim, and M. Sillanpää, “Platinized titanium dioxide (Pt/TiO_2) as a multi-functional catalyst for thermocatalysis, photocatalysis, and photothermal catalysis for removing air pollutants,” *Appl. Mater. Today*, vol. 23, 2021, doi: 10.1016/j.apmt.2021.100993.

[131] E. T. Bekele, B. A. Gonfa, F. K. Sabir, and F. Kedir, “Use of Different Natural Products to Control Growth of Titanium Oxide Nanoparticles in Green Solvent Emulsion, Characterization, and Their Photocatalytic Application,” *Bioinorganic Chemistry and Applications,* vol. 2021, doi: 10.1155/2021/6626313.

[132] S. A. Ansari, M. M. Khan, M. O. Ansari, and M. H. Cho, “Nitrogen-doped titanium dioxide (N-doped TiO_2) for visible light photocatalysis,” *New J. Chem.*, vol. 40, no. 4, pp. 3000–3009, 2016, doi: 10.1039/c5nj03478g.

[133] J. Zhang, P. Zhou, J. Liu, and J. Yu, “New understanding of the difference of photocatalytic activity among anatase, rutile and brookite TiO_2,” *Phys. Chem. Chem. Phys.*, vol. 16, no. 38, pp. 20382–20386, 2014, doi: 10.1039/c4cp02201g.

[134] E. Friehs *et al.*, “Toxicity, phototoxicity and biocidal activity of nanoparticles employed in photocatalysis,” *J. Photochem. Photobiol. C Photochem. Rev.*, vol. 29, pp. 1–28, 2016, doi: 10.1016/j.jphotochemrev.2016.09.001.

[135] B. Bakbolat *et al.*, "Recent developments of TiO_2-based photocatalysis in the hydrogen evolution and photodegradation: A review," *Nanomaterials*, vol. 10, no. 9, pp. 1–16, 2020, doi: 10.3390/nano10091790.

[136] A. Kurt, B. K. Mert, N. Özengin, Ö. Sivrioğlu, and T. Yonar, "Treatment of Antibiotics in Wastewater Using Advanced Oxidation Processes (AOPs)," *Physico-Chemical Wastewater Treat. Resour. Recover.*, 2017, doi: 10.5772/67538.

[137] G. K. R. Angaru *et al.*, "Facile synthesis of economical feasible fly ash–based zeolite–supported nano zerovalent iron and nickel bimetallic composite for the potential removal of heavy metals from industrial effluents," *Chemosphere*, vol. 267, p. 128889, 2021, doi: 10.1016/j.chemosphere.2020.128889.

[138] P. Gao, A. Li, D. D. Sun, and W. J. Ng, "Effects of various TiO_2 nanostructures and graphene oxide on photocatalytic activity of TiO_2," *J. Hazard. Mater.*, vol. 279, pp. 96–104, 2014, doi: 10.1016/j.jhazmat.2014.06.061.

[139] U. G. Akpan and B. H. Hameed, "Parameters affecting the photocatalytic degradation of dyes using TiO_2-based photocatalysts: A review," *J. Hazard. Mater.*, vol. 170, no. 2–3, pp. 520–529, 2009, doi: 10.1016/j.jhazmat.2009.05.039.

[140] M. Tahir, W. Mulewa, N. A. S. Amin, and Z. Y. Zakaria, "Thermodynamic and experimental analysis on ethanol steam reforming for hydrogen production over Ni-modified TiO_2/MMT nanoclay catalyst," *Energy Convers. Manag.*, vol. 154, pp. 25–37, 2017, doi: 10.1016/j.enconman.2017.10.042.

[141] W. Mulewa, M. Tahir, and N. A. S. Amin, "MMT-supported Ni/TiO_2 nanocomposite for low temperature ethanol steam reforming toward hydrogen production," *Chem. Eng. J.*, vol. 326, pp. 956–969, 2017, doi: 10.1016/j.cej.2017.06.012.

[142] J. J. Velázquez, R. Fernández-González, L. Díaz, E. Pulido Melián, V. D. Rodríguez, and P. Núñez, "Effect of reaction temperature and sacrificial agent on the photocatalytic H_2-production of Pt-TiO_2," *J. Alloys Compd.*, vol. 721, pp. 405–410, 2017, doi: 10.1016/j.jallcom.2017.05.314.

[143] F. Safari and I. Dincer, "A review and comparative evaluation of thermochemical water splitting cycles for hydrogen production," *Energy Convers. Manag.*, vol. 205, 2020, doi: 10.1016/j.enconman.2019.112182.

[144] K. Ahmad, H. R. Ghatak, and S. M. Ahuja, "A review on photocatalytic remediation of environmental pollutants and H_2 production through water splitting: A sustainable approach," *Environ. Technol. Innov.*, vol. 19, 2020, doi: 10.1016/j.eti.2020.100893.

[145] C. Agrafiotis *et al.*, "Solar water splitting for hydrogen production with monolithic reactors," *Sol. Energy*, vol. 79, no. 4, pp. 409–421, 2005, doi: 10.1016/j.solener.2005.02.026.

[146] S. Chen, T. Takata, and K. Domen, "Particulate photocatalysts for overall water splitting," *Nat. Rev. Mater.*, vol. 2, pp. 1–17, 2017, doi: 10.1038/natrevmats.2017.50.

[147] J. Zhang, J. Shi, Z. Cui, S. Chu, Y. Wang, and Z. Zou, "Highly efficient hydrogen evolution from water splitting on heptazine polymer with three types of defects," *Appl. Surf. Sci.*, vol. 580, 2022, doi: 10.1016/j.apsusc.2021.152070.

[148] P. M. Rajaitha *et al.*, "Multifunctional materials for photo-electrochemical water splitting," *J. Mater. Chem. A*, vol. 10, no. 30, pp. 15906–15931, 2022, doi: 10.1039/d2ta01869a.

[149] P. W. Menezes *et al.*, "Helical cobalt borophosphates to master durable overall water-splitting," *Energy Environ. Sci.*, vol. 12, no. 3, pp. 988–999, 2019, doi: 10.1039/c8ee01669k.

[150] Y. Ma, X. Wang, Y. Jia, X. Chen, H. Han, and C. Li, “Titanium dioxide-based nanomaterials for photocatalytic fuel generations,” *Chem. Rev.*, vol. 114, no. 19, pp. 9987–10043, 2014, doi: 10.1021/cr500008u.

[151] K. H. Ng, S. Y. Lai, C. K. Cheng, Y. W. Cheng, and C. C. Chong, “Photocatalytic water splitting for solving energy crisis: Myth, Fact or Busted?,” *Chem. Eng. J.*, vol. 417, 2021, doi: 10.1016/j.cej.2021.128847.

[152] W. Tu *et al.*, “State-of-the-art advancements of crystal facet-exposed photocatalysts beyond TiO_2: Design and dependent performance for solar energy conversion and environment applications,” *Mater. Today*, vol. 33, pp. 75–86, 2020, doi: 10.1016/j.mattod.2019.09.003.

[153] A. Speltini *et al.*, “Photocatalytic hydrogen evolution assisted by aqueous (waste) biomass under simulated solar light: Oxidized g-C_3N_4 vs. P25 titanium dioxide,” *Int. J. Hydrogen Energy*, vol. 44, no. 8, pp. 4072–4078, 2019, doi: 10.1016/j.ijhydene.2018.12.126.

[154] P. Ganguly *et al.*, “2D Nanomaterials for Photocatalytic Hydrogen Production,” *ACS Energy Lett.*, vol. 4, no. 7, pp. 1687–1709, 2019, doi: 10.1021/acsenergylett.9b00940.

[155] M. Aziz, A. Darmawan, and F. B. Juangsa, “Hydrogen production from biomasses and wastes: A technological review,” *Int. J. Hydrogen Energy*, vol. 46, no. 68, pp. 33756–33781, 2021, doi: 10.1016/j.ijhydene.2021.07.189.

[156] J. Baloyi, T. Seadira, M. Raphulu, and A. Ochieng, “Preparation, Characterization and Growth Mechanism of Dandelion-like TiO_2 Nanostructures and their Application in Photocatalysis towards Reduction of Cr(VI),” *Mater. Today Proc.*, vol. 2, no. 7, pp. 3973–3987, 2015, doi: 10.1016/j.matpr.2015.08.027.

[157] H. Ishaq, I. Dincer, and C. Crawford, “A review on hydrogen production and

utilization: Challenges and opportunities," *Int. J. Hydrogen Energy*, vol. 47, no. 62, pp. 26238–26264, 2022, doi: 10.1016/j.ijhydene.2021.11.149.

[158] M. D. Bhatt and J. S. Lee, "Nanomaterials for photocatalytic hydrogen production: From theoretical perspectives," *RSC Adv.*, vol. 7, no. 55, pp. 34875–34885, 2017, doi: 10.1039/c7ra03435k.

[159] S. Guo, X. Li, J. Li, and B. Wei, "Boosting photocatalytic hydrogen production from water by photothermally induced biphase systems," *Nat. Commun.*, vol. 12, no. 1, pp. 1–10, 2021, doi: 10.1038/s41467-021-21526-4.

[160] K. A. Davis, S. Yoo, E. W. Shuler, B. D. Sherman, S. Lee, and G. Leem, "Photocatalytic hydrogen evolution from biomass conversion," *Nano Converg.*, vol. 8, no. 1, 2021, doi: 10.1186/s40580-021-00256-9.

[161] E. I. Epelle *et al.*, "A comprehensive review of hydrogen production and storage: A focus on the role of nanomaterials," *Int. J. Hydrogen Energy*, vol. 47, no. 47, pp. 20398–20431, 2022, doi: 10.1016/j.ijhydene.2022.04.227.

[162] W. Wang *et al.*, "An overview on nitride and nitrogen-doped photocatalysts for energy and environmental applications," *Composites Part B: Engineering*, vol. 172, pp. 704–723, Sep. 01, 2019. doi: 10.1016/j.compositesb.2019.05.097.

[163] M. Tahir, "Ni/MMT-promoted TiO_2 nanocatalyst for dynamic photocatalytic H_2 and hydrocarbons production from ethanol-water mixture under UV-light," *Int. J. Hydrogen Energy*, vol. 42, no. 47, pp. 28309–28326, 2017, doi: 10.1016/j.ijhydene.2017.09.116.

[164] B. Wang, S. Shen, and S. S. Mao, "Black TiO_2 for solar hydrogen conversion," *J. Mater.*, vol. 3, no. 2, pp. 96–111, 2017, doi: 10.1016/j.jmat.2017.02.001.

[165] H. Zhao *et al.*, “Blue-edge slow photons promoting visible-light hydrogen production on gradient ternary 3DOM TiO_2-Au-CdS photonic crystals,” *Nano Energy*, vol. 47, pp. 266–274, 2018, doi: 10.1016/j.nanoen.2018.02.052.

[166] X. Chen and S. S. Mao, “Titanium dioxide nanomaterials: Synthesis, properties, modifications and applications,” *Chem. Rev.*, vol. 107, no. 7, pp. 2891–2959, 2007, doi: 10.1021/cr0500535.

[167] K. Kaur and C. V. Singh, “Amorphous TiO_2 as a photocatalyst for hydrogen production: A DFT study of structural and electronic properties,” *Energy Procedia*, vol. 29, pp. 291–299, 2012, doi: 10.1016/j.egypro.2012.09.035.

[168] J. E. S. Haggerty *et al.*, “High-fraction brookite films from amorphous precursors,” *Sci. Rep.*, vol. 7, no. 1, pp. 1–11, 2017, doi: 10.1038/s41598-017-15364-y.

[169] D. Chen, Z. Jiang, J. Geng, Q. Wang, and D. Yang, “Carbon and nitrogen co-doped TiO_2 with enhanced visible-light photocatalytic activity,” *Ind. Eng. Chem. Res.*, vol. 46, no. 9, pp. 2741–2746, 2007, doi: 10.1021/ie061491k.

[170] J. Lu *et al.*, “Coking- and sintering-resistant palladium catalysts achieved through atomic layer deposition,” *Science*, vol. 335, no. 6073, pp. 1205–1208, 2012, doi: 10.1126/science.1212906.

[171] B. Neumann, P. Bogdanoff, H. Tributsch, S. Sakthivel, and H. Kisch, “Electrochemical mass spectroscopic and surface photovoltage studies of catalytic water photooxidation by undoped and carbon-doped titania,” *J. Phys. Chem. B*, vol. 109, no. 35, pp. 16579–16586, 2005, doi: 10.1021/jp051339g.

[172] G. Zhang *et al.*, “Preparation of carbon-TiO_2 nanocomposites by a hydrothermal method and their enhanced photocatalytic activity,” *RSC Adv.*, vol. 3, no. 46, pp. 24644–

24649, 2013, doi: 10.1039/c3ra44950e.

[173] Z. He, W. Que, and Y. He, “Enhanced photocatalytic performance of sensitized mesoporous TiO_2 nanoparticles by carbon mesostructures,” *RSC Adv.*, vol. 4, no. 7, pp. 3332–3339, 2014, doi: 10.1039/c3ra46389c.

[174] F. H. Abdulrazzak, F. H. Hussein, A. F. Alkaim, I. Ivanova, A. V. Emeline, and D. W. Bahnemann, “Sonochemical/hydration-dehydration synthesis of Pt-TiO_2 NPs/decorated carbon nanotubes with enhanced photocatalytic hydrogen production activity,” *Photochem. Photobiol. Sci.*, vol. 15, no. 11, pp. 1347–1357, 2016, doi: 10.1039/c6pp00240d.

[175] B. Pant, G. P. Ojha, Y.-S. Kuk, O. H. Kwon, Y. W. Park, and M. Park, “Synthesis and Characterization of ZnO-TiO_2/Carbon Fiber Composite with Enhanced Photocatalytic Properties”, doi: 10.3390/nano10101960.

[176] C. Yang *et al.*, “Porous carbon-doped TiO_2 on TiC nanostructures for enhanced photocatalytic hydrogen production under visible light,” *J. Catal.*, vol. 347, pp. 36–44, 2017, doi: 10.1016/j.jcat.2016.11.041.

[177] D. Xu, L. Li, R. He, L. Qi, L. Zhang, and B. Cheng, “Noble metal-free RGO/TiO_2 composite nanofiber with enhanced photocatalytic H_2 -production performance,” *Appl. Surf. Sci.*, vol. 434, pp. 620–625, 2018, doi: 10.1016/j.apsusc.2017.10.192.

[178] M. Inagaki, Y. Okada, H. Miura, and H. Konno, “Preparation of carbon-coated transition metal particles from mixtures of metal oxide and Polyvinylchloride,” *Carbon,* vol. 37, no. 2, pp. 329–334, 1999, doi: 10.1016/S0008-6223(98)00200-0.

[179] M. Inagaki, F. Kojin, B. Tryba, and M. Toyoda, “Carbon-coated anatase: The role of the carbon layer for photocatalytic performance,” *Carbon*, vol. 43, no. 8, pp. 1652–1659, 2005, doi: 10.1016/j.carbon.2005.01.043.

[180] B. Rusinque, S. Escobedo, and H. de Lasa, “Hydrogen production via pd-TiO_2 photocatalytic water splitting under near-uv and visible light: Analysis of the reaction mechanism,” *Catalysts*, vol. 11, no. 3, Mar. 2021, doi: 10.3390/catal11030405.

[181] R. Shwetharani, M. Sakar, C. A. N. Fernando, V. Binas, and R. G. Balakrishna, “Recent advances and strategies to tailor the energy levels, active sites and electron mobility in titania and its doped/composite analogues for hydrogen evolution in sunlight,” *Catal. Sci. Technol.*, vol. 9, no. 1, pp. 12–46, 2019, doi: 10.1039/c8cy01395k.

[182] R. Liu, H. Yoshida, S. ichiro Fujita, and M. Arai, “Photocatalytic hydrogen production from glycerol and water with NiOx/TiO_2 catalysts,” *Appl. Catal. B Environ.*, vol. 144, no. 1, pp. 47–45, 2014, doi: 10.1016/j.apcatb.2013.06.024.

[183] H. Y. Hafeez *et al.*, “Construction of ternary hybrid layered reduced graphene oxide supported g-C_3N_4-TiO_2 nanocomposite and its photocatalytic hydrogen production activity,” *Int. J. Hydrogen Energy*, vol. 43, no. 8, pp. 3892–3904, 2018, doi: 10.1016/j.ijhydene.2017.09.048.

[184] X. J. Lv, S. X. Zhou, C. Zhang, H. X. Chang, Y. Chen, and W. F. Fu, “Synergetic effect of Cu and graphene as cocatalyst on TiO_2 for enhanced photocatalytic hydrogen evolution from solar water splitting,” *J. Mater. Chem.*, vol. 22, no. 35, pp. 18542–18549, 2012, doi: 10.1039/c2jm33325b.

[185] W. Fan, Q. Lai, Q. Zhang, and Y. Wang, “Nanocomposites of TiO_2 and reduced graphene oxide as efficient photocatalysts for hydrogen evolution,” *J. Phys. Chem. C*, vol. 115, no. 21, pp. 10694–10701, 2011, doi: 10.1021/jp2008804.

[186] X. J. Lv *et al.*, “Hydrogen evolution from water using semiconductor nanoparticle/graphene composite photocatalysts without noble metals,” *J. Mater. Chem.*, vol.

22, no. 4, pp. 1539–1546, 2012, doi: 10.1039/c1jm14502a.

[187] L. Chen, X. Liang, H. Wang, Q. Xiao, and X. Qiu, “Ultra-thin carbon nitride nanosheets for efficient photocatalytic hydrogen evolution,” *Chem. Eng. J.*, vol. 442, no. 2, p. 136115, 2022, doi: 10.1016/j.cej.2022.136115.

[188] B. Yan, P. Zhou, Q. Xu, X. Zhou, D. Xu, and J. Zhu, “Engineering disorder into exotic electronic 2D TiO_2 nanosheets for enhanced photocatalytic performance,” *RSC Adv.*, vol. 6, no. 8, pp. 6133–6137, 2016, doi: 10.1039/c5ra24126j.

[189] W. Chen *et al.*, “Non-noble metal Cu as a cocatalyst on TiO_2 nanorod for highly efficient photocatalytic hydrogen production,” *Appl. Surf. Sci.*, vol. 445, pp. 527–534, 2018, doi: 10.1016/j.apsusc.2018.03.209.

[190] J. Huang *et al.*, “Efficient photocatalytic hydrogen production over Rh and Nb codoped TiO_2 nanorods,” *Chem. Eng. J.*, vol. 337, pp. 282–289, 2018, doi: 10.1016/j.cej.2017.12.088.

[191] T. T. D. Vu, F. Mighri, A. Ajji, and T. O. Do, “Synthesis of titanium dioxide/cadmium sulfide nanosphere particles for photocatalyst applications,” *Ind. Eng. Chem. Res.*, vol. 53, no. 10, pp. 3888–3897, 2014, doi: 10.1021/ie403718n.

[192] X. Wang, W. C. Peng, and X. Y. Li, “Photocatalytic hydrogen generation with simultaneous organic degradation by composite CdS-ZnS nanoparticles under visible light,” *Int. J. Hydrogen Energy*, vol. 39, no. 25, pp. 13454–13461, 2014, doi: 10.1016/j.ijhydene.2014.04.034.

[193] C. Huang, M. Wu, and V. Nguyen, “Preparation and Characterization of Nanocrystalline TiO_2 on Microsericite for High-Efficiency Photo-Energy conversion of Methanol to Hydrogen,” Crystals, vol. 9, no. 380, 2019, doi:10.3390/cryst9080380.

[194] G. K. Naik, S. M. Majhi, K. U. Jeong, I. H. Lee, and Y. T. Yu, “Nitrogen doping on the core-shell structured Au@TiO_2 nanoparticles and its enhanced photocatalytic hydrogen evolution under visible light irradiation,” *J. Alloys Compd.*, vol. 771, pp. 505–512, 2019, doi: 10.1016/j.jallcom.2018.08.277.

[195] S. ichiro Fujita, H. Kawamori, D. Honda, H. Yoshida, and M. Arai, “Photocatalytic hydrogen production from aqueous glycerol solution using NiO/TiO_2 catalysts: Effects of preparation and reaction conditions,” *Appl. Catal. B Environ.*, vol. 181, pp. 818–824, 2016, doi: 10.1016/j.apcatb.2015.08.048.

[196] Y. Liu *et al.*, “2H- and 1T- mixed phase few-layer MoS_2 as a superior to Pt co-catalyst coated on TiO_2 nanorod arrays for photocatalytic hydrogen evolution,” *Appl. Catal. B Environ.*, vol. 241, no. May 2018, pp. 236–245, 2019, doi: 10.1016/j.apcatb.2018.09.040.

CHAPTER THREE

A facile synthesis of Copper Oxide Nanoparticles for catalytic Preparation of high quality Carbon Nanofibers

Molecular Sciences Institute, School of Chemistry, University of the Witwatersrand, Johannesburg 2050, South Africa

Abstract

Copper oxide nanoparticles synthesis using a simple, novel method at room temperature is reported. X-ray diffraction (XRD) analysis was used to investigate the crystallinity of the CuO nanoparticles. Single-phase monoclinic structure was confirmed. The average crystallite size of CuO NPs was calculated by Scherrer's formula and found to be 11 nm. The as-synthesized CuO nanoparticles were characterized by High Resolution Scanning Electron Microscopy (HR-SEM) whereby the purity of the CuO nanoparticles was analysed using EDX microanalysis and the composition of the elements showed high purity with O and Cu as the only elements. Raman Spectroscopy was used to study the microstructural nature of the CuO nanoparticles. The three Raman active modes, A_g, B_g^1, and B_g^2 of the CuO nanoparticles were detected at 293 cm^{-1}, 335 cm^{-1}, and 629 cm^{-1}, respectively while the multiphonon band was at 1105 cm^{-1}. The Fourier Transform Infrared (FTIR) spectrum of the CuO nanoparticles showed a strong peak of Cu-O symmetrical stretching at 1638 cm^{-1} whereas Cu-O vibrational modes were at 512 cm^{-1} and at 600 cm^{-1}. This confirm the formation of the CuO nanoparticles, and prove the presence of monoclinic phase of the as-synthesized CuO nanoparticles. The thermal stability of the CuO nanoparticles was investigated and the weight loss of 23% which occurred between 175ºC and 230ºC was due to thermal dehydration of the as – synthesized CuO nanoparticles because water was used in the synthesis. Carbon nano fibers were synthesized using the CuO nanoparticles, functionalized and characterized by

FTIR, PXRD, Raman spectroscopy, HR-SEM, TEM, TGA, BET, and found to be of high purity and high thermal stability.

Keywords: Copper Oxide nanoparticles; Carbon Nanofibers; Catalysis; Chemical Vapour Deposition; Semi-conductor.

3.1 Introduction

The potential of copper oxide, CuO as a p-type semiconductor [1]–[3] has contributed to its extensive use in several applications like catalysis [4]–[7], energy conversion [8], [9], gas sensing [10]–[12], and field electron emission [10], [13]–[15]. Their properties can be enhanced by synthesis into nanoparticles like copper oxide nanoparticles [16]–[18]. Previously, several techniques suggested for the synthesis of copper oxide nanoparticles of divergent morphologies; for instance precipitation [15], [19], sonochemical [20]–[22], thermal oxidation [23]–[25] and combustion [26][27]. Additionally, a lot of CuO nanoparticles have been prepared using hydrothermal [28], [29], acid-catalysed sol-gel processes [30], and hydrolysis [31]. Most of these methods require processing conditions such as vacuum filtration, thermal treatment at different temperatures, centrifuging, calcination, and pH monitoring to obtain high quality CuO nanoparticles. Amongst these processes, precipitation method has proved to be excellent because it is quick, simple, and reproducible. The use of potassium hydroxide and Copper (II) nitrate trihydrate, $Cu(NO_3)_2.3H_2O$ in the synthesis of CuO nanoparticles at room temperature is novel and does not involve the use of acids, surfactants, heating or annealing during the synthesis. This method can be employed in many fields due to economic power usage (low heat) at room temperature (25º C), profitable to extensive work with superior products. The method is safe, environmentally friendly and produces CuO nanoparticles of high purity. One remarkable major field in which the p-type semiconductors have had a massive positive impact is

catalysis whereby they are used as catalysts in the production of structures like carbon nanofibers, CNFs, and carbon nanotubes, CNTs.

Following their findings in 1991 [32], CNFs together with CNTs have drawn great attention because of their unique and tuneable electronic conductivity and mechanical strength [33][34]. Their 1D structural property has further favoured their many applications in medical sector and industries [32]–[34]. In this research, we have synthesised CuO nanoparticles using a noble method that, does not depend on pH, heating or calcination to synthesize. The other methods that have been reported for the synthesis of CuO nanoparticles [35]–[43] depend on pH, heating or calcination. $Cu(NO_3)_2$ was the precursor and the as-synthesized CuO nanoparticles were used in the catalytic preparation of the CNFs. The as-synthesized copper oxide nanoparticles and the synthesized carbon nanofibers were characterized by PXRD, HRSEM, TGA, FTIR, Raman spectroscopy, and BET.

3.2 Experimental

3.2.1 Chemical reagents

Copper (II) nitrate trihydrate, $Cu(NO_3)_2.3H_2O$ (99%), potassium hydroxide, anhydrous, KOH, ≥ 99.95% trace metal basis and nitric acid, HNO_3 (55%) were procured from Sigma – Aldrich and used without further purification. Hydrogen and acetylene gases were both purchased from Afrox and distilled water was used.

3.2.2 Procedure for obtaining copper oxide nanoparticles

The CuONPs were prepared by copper nitrate, $Cu(NO_3)_2.3H_2O$. The metal salt was dispersed in 200 mL deionized water forming 0.05M solution of coper nitrate. An equal volume of 0.05M concentration of KOH was added with vigorous stirring for 12 h. Black precipitates were obtained, repeatedly cleaned with distilled water to neutrality before drying in an oven

overnight with heat of 80 ℃. The dried CuO NPs were characterized using PXRD, Raman, HR-SEM, and FTIR.

3.2.3 Preparation of carbon nanofibers

The carbon nanofibers were prepared by synthesized CuONPs as catalyst at 300 ℃ in a quartz tube using chemical vapour deposition, CVD technique [5]. The synthesis method of CNFs employs the breakdown of acetylene, C_2H_2 in a CVD tube furnace, straight and parallel to the ground. The CVD tube furnace was electronically monitored by setting the thermal flow, rise in temperature, and gas throughput. The catalyst, about 0.1g, added into a quartz boat, 120 mm by 15 mm at room temperature (25ºC) and the boat transferred to the middle of the CVD tube furnace. The temperature of the furnace was then increased at 10 ℃ min^{-1} with hydrogen gas, H_2 discharging over the catalyst at 50 mL min^{-1}. Upon attaining heating of 300 ℃, the H_2 flow was retained for 30 minutes before introducing C_2H_2 at a constant flow rate of 50 $mLmin^{-1}$. Afterwards, approximately 30 minutes, the C_2H_2 stream was ceased, and the CVD tube furnace was enabled to loose heat to 25ºC under H_2 gas stream. The quartz boat was later taken out of the CVD tube furnace and the yield, carbon sediment formed along with the catalyst weighed.

3.2.4 Acid treatment of carbon nanofibers

The CNFs were washed with concentrated nitric acid, to separate the remnants of the CuO NPs besides, functionalizing them. Concentrated nitric acid (55%) was introduced to the CNFs in a round bottom flask before refluxing at 110 ℃ for 2 h. The mixture was enabled to loose heat to 25ºC filtered, washed with copious amount of distilled water to neutrality. The washed CNFs were filtered and dried for 12 h in an oven at 80 ℃.

3.2.5 Characterization of Copper Oxide Nanoparticles, and Carbon Nanofibers

Copper oxide nanoparticles and CNFs were distinguished by a range of methodologies. The analysis of the copper oxide nanoparticles along with CNFs have been investigated by Scanning Electron Microscopy, SEM analysis (ZEISS Sigma 300 VP from M/S ZEISS 'Smart SEM' OXFORD INSTRUMENTS x-act PentaFET Precision and 'Oxford INCA', United Kingdom. The same materials have also been analysed by X-ray diffraction (XRD) using a Brucker D2 phaser fitted with Cu – Kα radiation (λ = 1.5405 Å), operating at 30 kV (Voltage) and 10 mA, (Current). A Perkin Elmer TA TGA Q500 has been explored in the determination of the heat resistance of the materials by thermogravimetric analysis. At least 10 mg of the sample was heated up to 900 ℃ with increasing temperature of 10 ℃ min^{-1} under air. FT- IR Spectroscopy, mounted with a Bruker Tensor 27 FT – IR spectrometer (4000 – 500 cm^{-1}) has been employed to identify the functional groups present in the samples. Optical attributes have been analysed by Varian Cary Eclipse EL0410 3870 photoluminescence/ fluorescence Spectrophotometer and a SPECORD 210 plus UV – Vis Spectrophotometer. The specific surface of the samples was determined by Brunauer – Emmett – Teller (BET), N_2 physisorption (Micromeritics ASAP – 2000 Tri - star analyser). Prior to the analysis of the samples, 0.2 g was degassed for 6 h at 150 ℃ concealed by nitrogen stream employing a Micromeritics flow Prep 060.

3.3. Results and Discussions

3.3.1 X-ray diffraction (XRD) analysis

The XRD order of copper oxide nanoparticles as-synthesized is indicated in Fig. 1. The orientation together with crystallinity attributed to more or less spherical copper oxide

nanoparticles are revealed by the XRD pattern. The absence of diffraction patterns of other phases indicates the phase purity of the as-synthesized copper oxide nanoparticles. The position of the peaks with 2θ values of 32.93°, 35.99°, 39.21°, 49.35°, 53.92°, 58.66°, 62.01°, 66.60°, 68.37°, 72.81°, and 75.47° are indexed as (110), (-111), (-202), (020), (202), (-113), (-311), (220), (311), and (004) planes and are within acceptable limits with those of CuO nanoparticles from the standard JCPDS data file No. 89-5895. The main diffraction peaks positioned at 2θ values are 11 nm, classified (-111) and (111) planes respectively[6]. Scherrer equation has been used to calculate the average grain size,

$$D = k\lambda/\beta\cos\theta$$

Where, D is the average grain size, λ – wavelength of the incident beam (1.5405 Å), β is the full width at half maximum (FWHM) and θ is the diffraction angle. Using the equation, the average CuO nanoparticles is 11 nm.

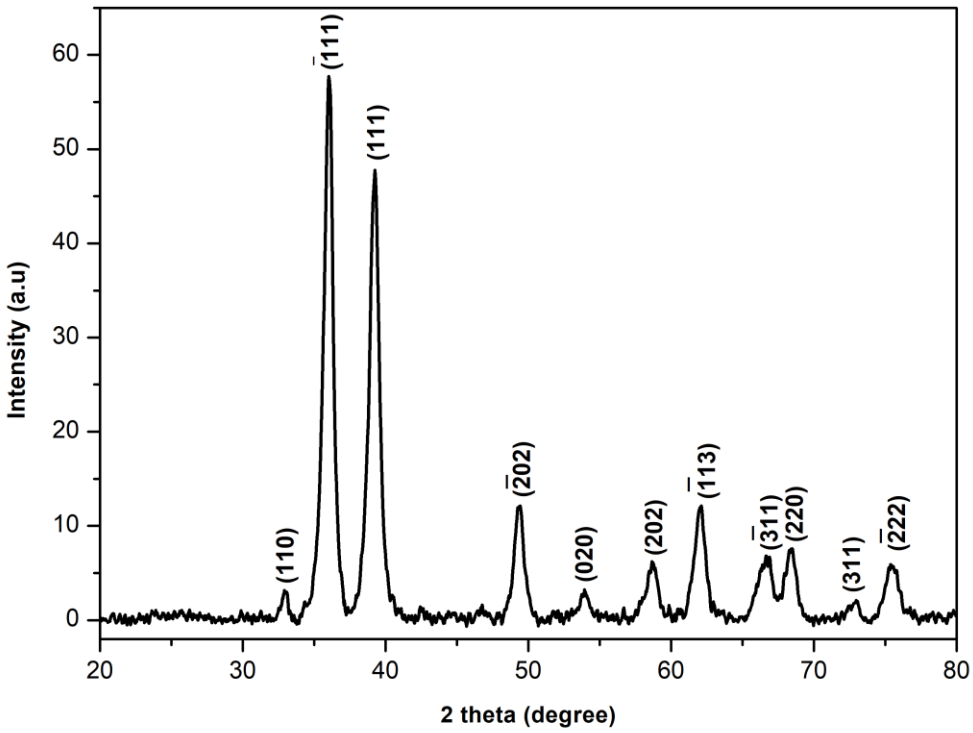

Fig. 1. PXRD patterns of CuO nanoparticles as-synthesized (as-prepared) using novel precipitation method at room temperature without calcination of the CuO nanoparticles.

In addition, PXRD was used in studying the level of crystallinity of the CNFs. The PXRD pattern for CNFs is shown in Fig.2. The broad peak positioned at 11.66º is because of the crystal plane index C(002) which is associated with the orientation of carbon materials. The sharp peak points to a high level of graphiticity in CNFs. Additionally, the high symmetry of the C(002) peak designates the absence of ϒ-bands associated with amorphous carbon [44] A further broad peak is detected at 24.43º, indexed C(100) diffractions of graphitic carbons [45]. The PXRD results indicate that CNFs synthesized by the CuO nanoparticles are highly graphitic, which is preferable for productive exfoliation processes.

Observations on SEM and TGA analyses of the as-prepared carbon nanofibers and cleaned carbon nanofibers were studied in order to further verify obtained information from PXRD

analysis that the functionalized carbon nanofibers did not contain traces of CuONPs.

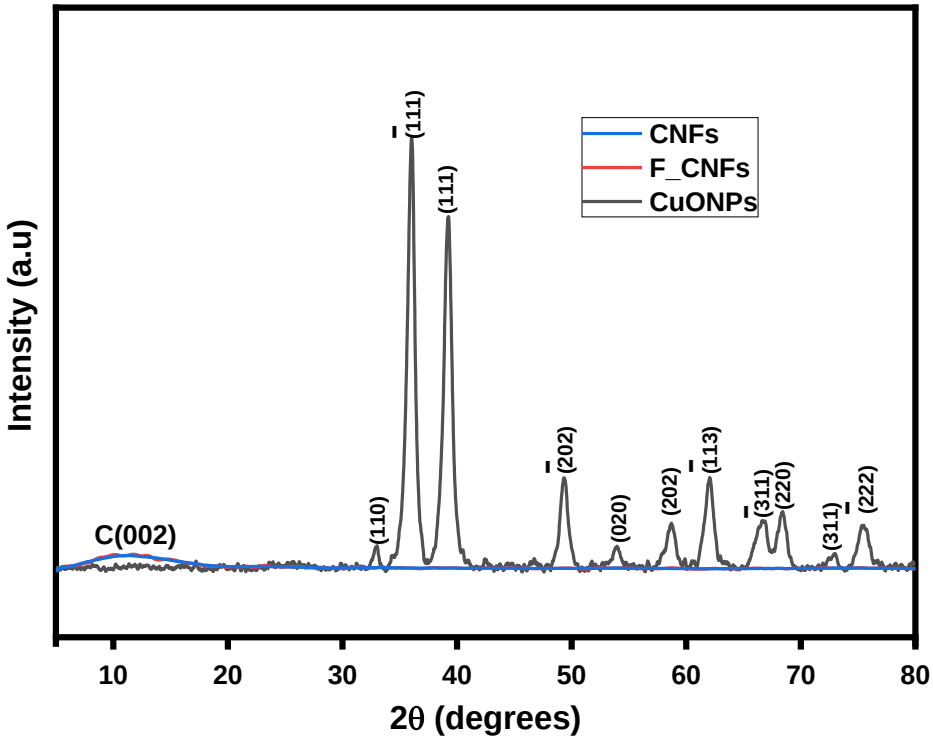

Fig. 2. PXRD spectrum of the copper oxide nanoparticles (CuONPs), carbon nanofibers (CNFs), functionalize carbon nanofibers (F_CNFs) prepared using as-synthesized CuO nanoparticles.

3.3.2 SEM Analysis

The SEM study was used to determine the morphological properties of the CuONPs and the carbon nanofibers (as-synthesized and functionalized CNFs), Figures 3, 5 and 6. The composition of the elements is presented in Table 1. The results indicate high purity with varying sizes and more or less uniform shape for the CuONPs and no aggregation of the particles as shown by Figure 3, Table 1, and Figure 4. High purity was also observed in functionalized CNFs.

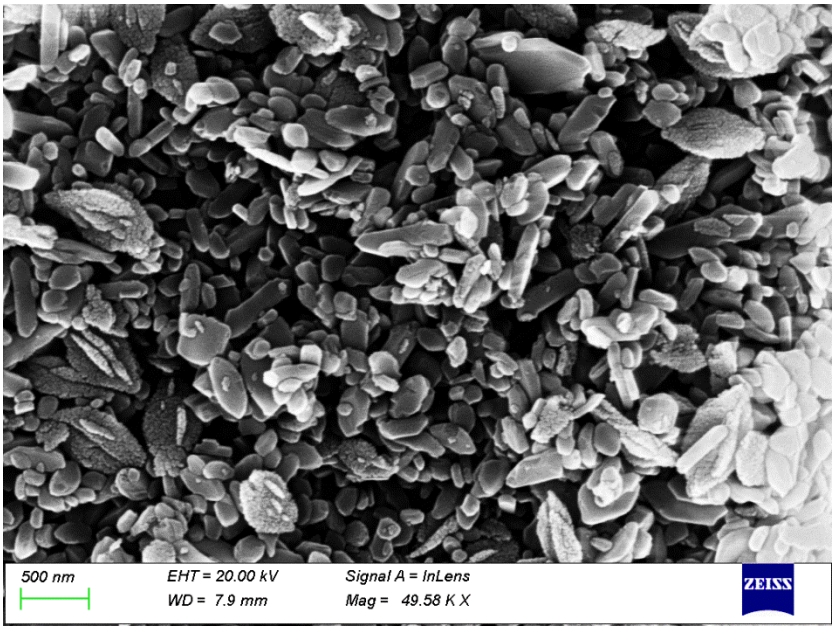

Fig. 3. SEM image of as-synthesized CuO nanoparticles prepared using Novel method at room temperature and without calcination of the synthesized CuO nanoparticles.

TABLE 1. Composition of the elements

Element	Weight%	Atomic%
O K	27.11	59.63
Cu K	72.89	40.37
Totals	100.00	

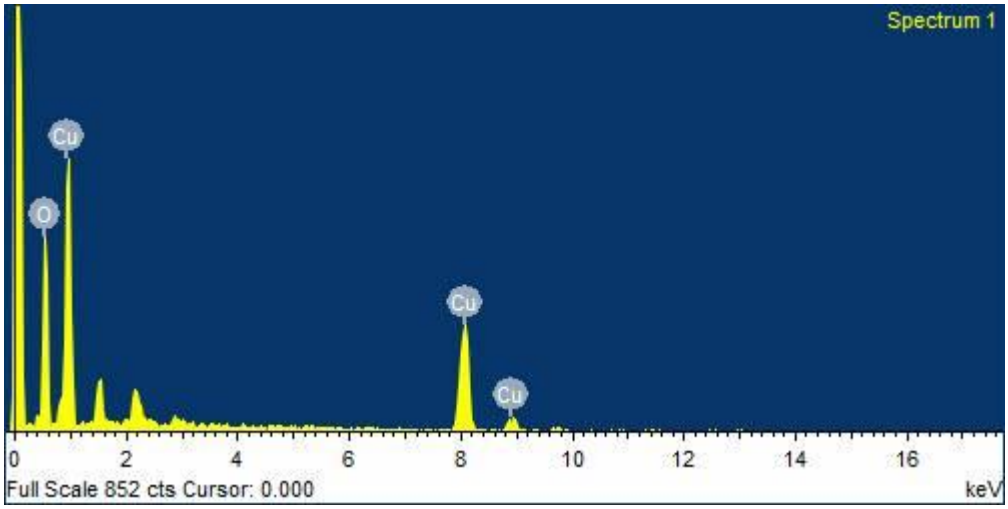

Fig. 4. EDX spectrum of as-synthesized CuO nanoparticles synthesized using Novel method at room temperature and without calcination.

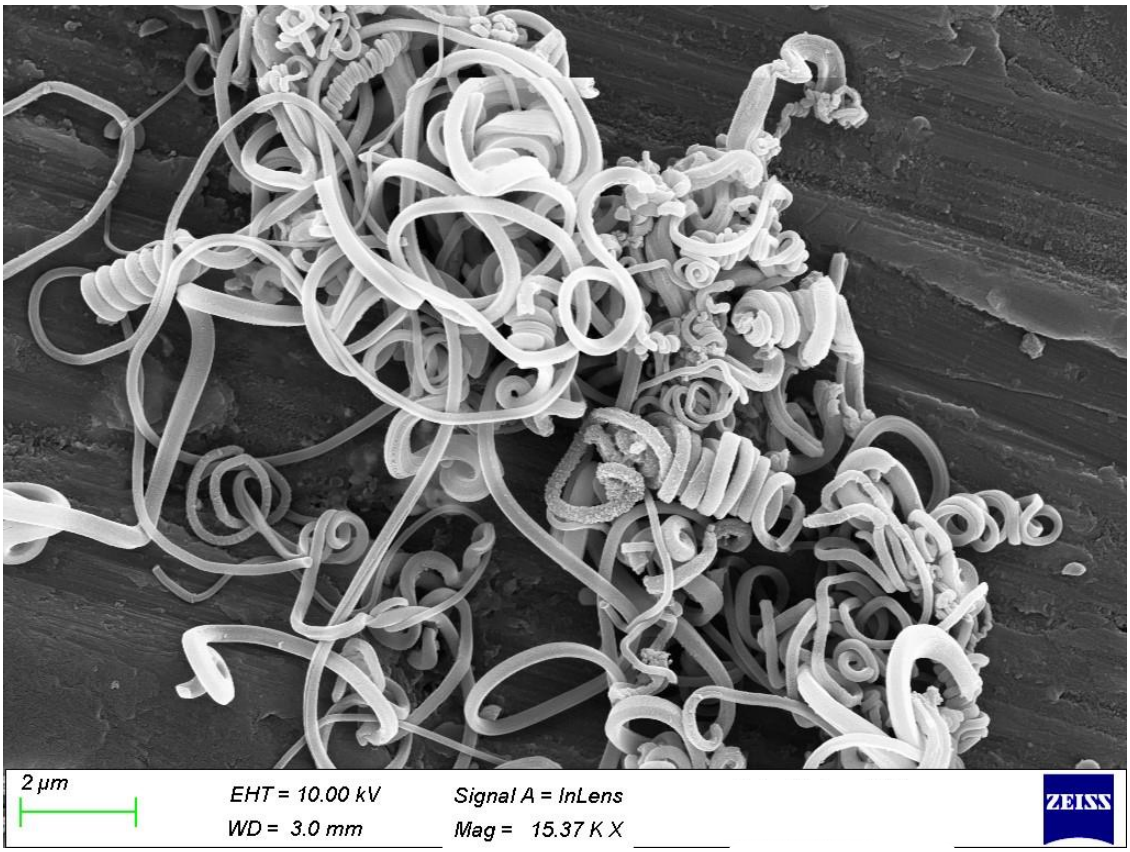

Fig. 5. Scanning Electron Microscopy images of the as-prepared CNFs prepared using as-synthesized copper oxide nanoparticles prepared using Novel method at room temperature and without calcination of the as-prepared copper oxide nanoparticles.

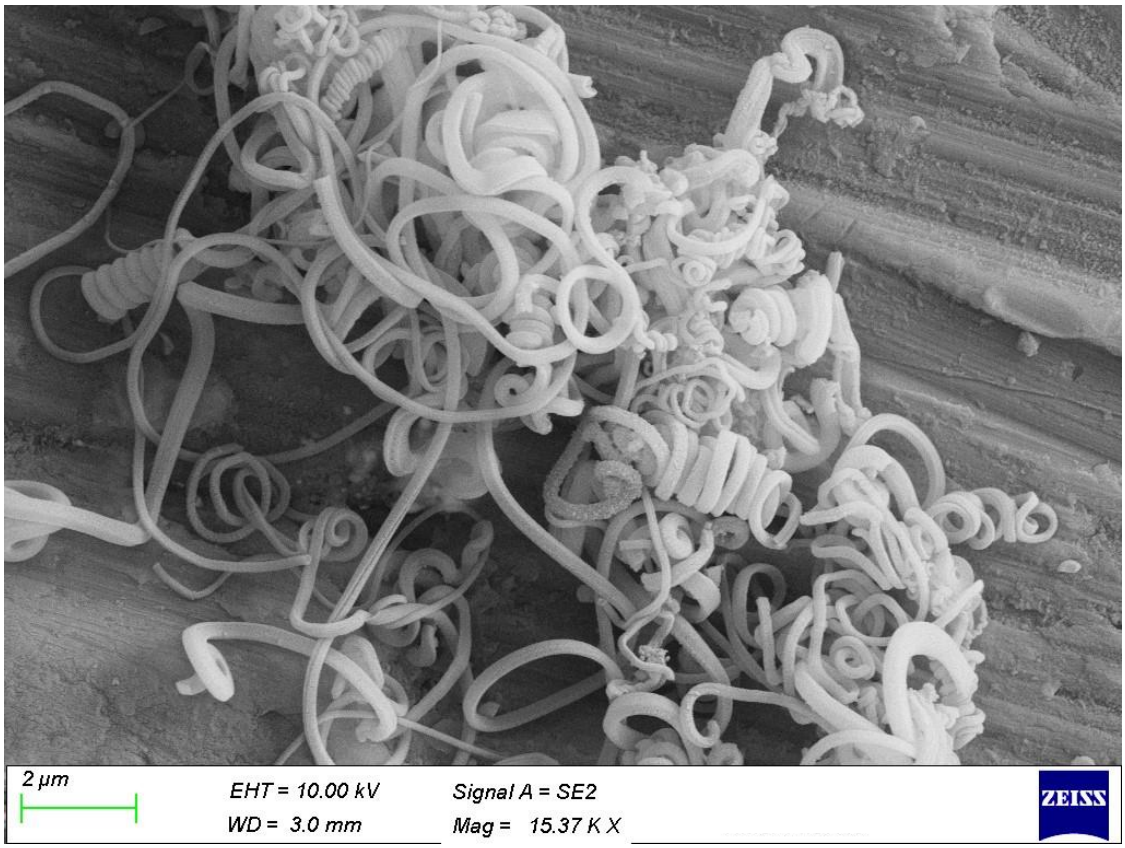

Fig. 6. Scanning Electron Microscopy images of functionalized CNFs.

3.3.3 Thermogravimetric Analysis (TGA)

The heat resistance of the CuO nanoparticles was investigated for comparison with similar work. The experimental TGA graphs of the as-synthesized CuO nanoparticles, CNFs and the functionalized CNFs at heating rates of 10ºC to 900ºC are represented in figure 7. There are three mass-loss sections in the TGA spectra in figure 7. The weight loss of 23% which occurred between 175ºC and 230ºC was due to thermal dehydration of the as – synthesized CuO nanoparticles because water was the only solvent used in the synthesis. The CNFs had thermal decomposition at 185ºC to 530ºC corresponding to weight loss of 93%. And the functionalized CNFs thermally decomposed from 42ºC to 577ºC generating weight loss of 99%. However, functionalized CNFs had a higher thermal stability of 577ºC as compared to

thermal stability of 530ºC for the as-synthesized CNFs. The difference in thermal stability of the CNFs and the functionalized CNFs indicates the presence of CuO nanoparticles in trace amounts in the as-synthesized CNFs thus resulting in the low thermal stability of the CNFs as compared to the functionalized CNFs [46]–[48]. But, the thermogravimetric patterns of the as-prepared carbon nanofibers and functionalized carbon nanofibers were characterized by the thermal induced decomposition from 40ºC to 600ºC.

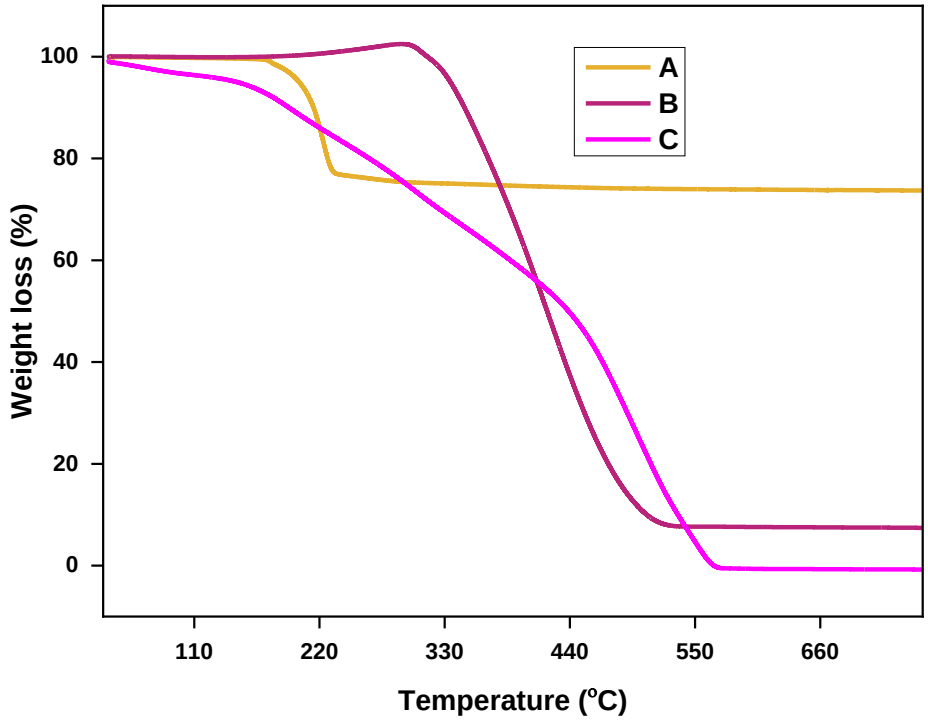

Fig. 7. TGA diagrams of the copper oxide nanoparticles (A), carbon nanofibers (B), and functionalized carbon nanofibers (C).

3.3.4 FT-IR

The FTIR spectrum of CuO nanoparticles prepared at room temperature and without annealing is shown in figure 8. The strong and broad absorption peak at 3466 cm^{-1} resulted

from adsorbed water molecules. By considering the high surface area to volume ratio of the as-synthesized CuO nanoparticles, there were chances of moisture absorption. Normally, the region within 2700 and 3750 cm^{-1} is the OH-stretching region. The strong peak at 1638 cm^{-1} could be attributed to the Cu-O symmetrical stretching. The two strong absorption peaks at 512 cm^{-1} and at 600 cm^{-1} exhibit the vibrational modes of the CuO nanoparticles between 500 -700 cm^{-1}. The peaks marked 512 cm^{-1} and 600 cm^{-1} confirm the formation of the CuO nanoparticles, and also prove the presence of monoclinic phase of the as-synthesized CuO nanoparticles. The absence of an additional IR active mode between 500-700 cm^{-1} eliminates the existence of Cu(I) – O, (Cu_2O) vibration of the CuO nanoparticles. This is in agreement with the other reports of CuO nanoparticles [49]–[51].

The FTIR spectrum of the functionalized CNFs are shown in figure 9. The strong band at 1100 cm^{-1} was associated with C–O stretching vibrations. The IR peak at 3438 cm^{-1} was O-H stretching vibrations. The remainder of the peaks could be the vibrations of aliphatic C-H groups in the range of 3000-2800 cm^{-1}, 2000-1800 cm^{-1}, 1410-1395 cm^{-1}, and 820-790 cm^{-1}.

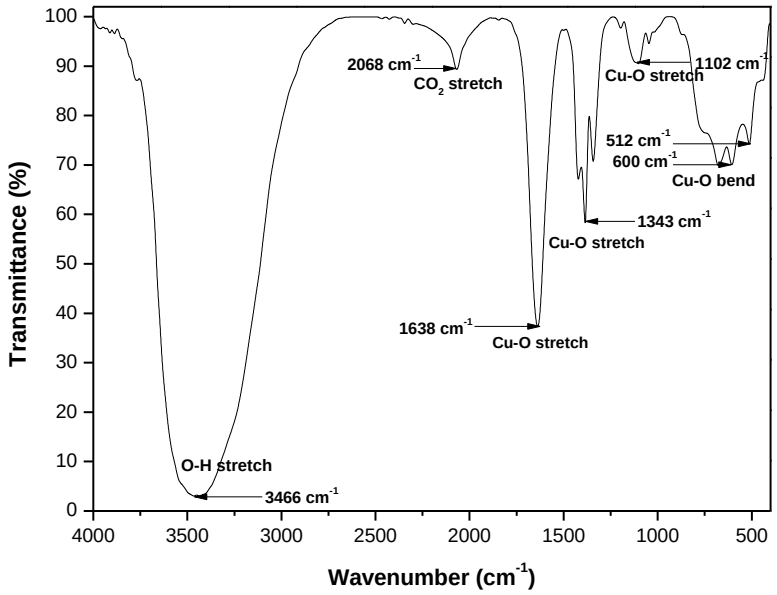

Fig. 8. The FTIR spectrum of the CuO nanoparticles.

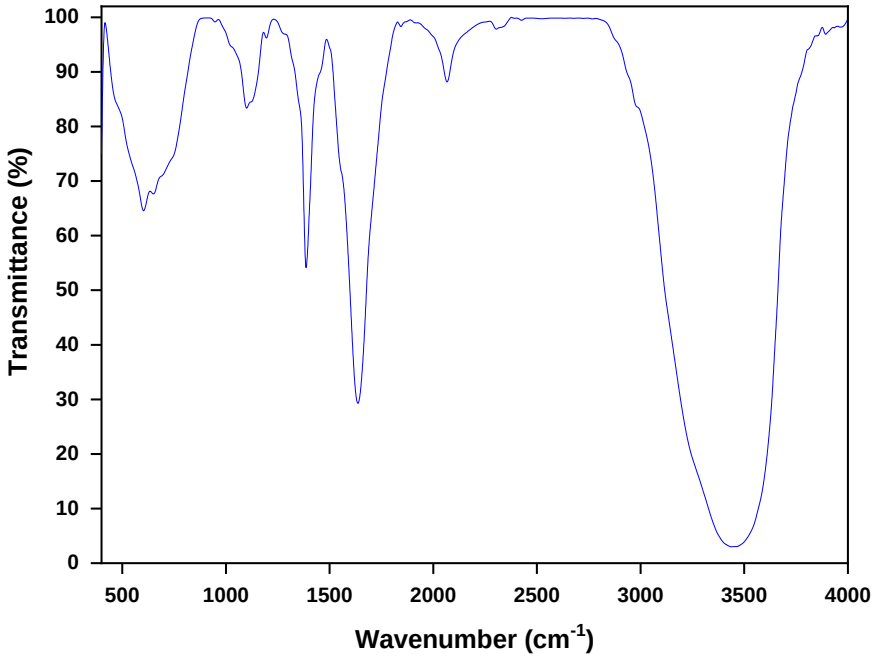

Fig. 9. The FTIR spectrum of the functionalized CNFs.

3.3.5 Raman spectroscopy

The Raman spectroscopy was used to study the microstructural nature of the copper oxide nanoparticles because Raman shifts can be used in the identification of the existence of different phases or crystallinity of Nano sized materials. Therefore, CuO nanoparticles were identified and Cu_2O or $Cu(OH)_2$ were not detected. Figure 10 shows the Raman shifts of the as-prepared copper oxide nanoparticles. The strong and sharp Raman shifts at 293 cm^{-1}, 335 cm^{-1}, and 629 cm^{-1}, with shifts to smaller wavenumbers, red shift was associated with the phonon confinement effect and grain size of the CuO nanoparticles. It has been noted that Raman intensity depends on the grain size; the fine grain sizes give high intensity of stronger and sharper peaks and thus high purity or crystallinity of the test material. From figure 10, the three Raman active modes, A_g, B_g^1, and B_g^2 of the copper oxide nanoparticles were detected at 293 cm^{-1}, 335 cm^{-1}, and 629 cm^{-1}, respectively. The multiphonon band of the CuO nanoparticles in the region 1105 cm^{-1} was associated with the in harmonic coupling between phonons in the CuO nanoparticles matrix.

The Raman spectrum in figure 11 is of the functionalized carbon nanofibers. Raman spectroscopy was used to further evaluate the crystallinity also, to get more details on the defects on F_CNFs. The D-band at 1384 cm^{-1} is a defect's identification on the F_CNFs. And the G-band at 1590 $cm^{-1}$is the C-C stretching in the F_CNFs [52]–[54].

The peak area ratio of the G- to D –bands (1_D /1_G) is 1.54 which indicates high levels of defect in the F_CNFs. The high levels in the material suggests the presence of active sites on the F_CNFs. Normally, presence of defects on the materials results in the formation of landing sites for nano metal particles which are the active species in catalysis. Thus, the higher the ratio, the better is the material for catalysis.

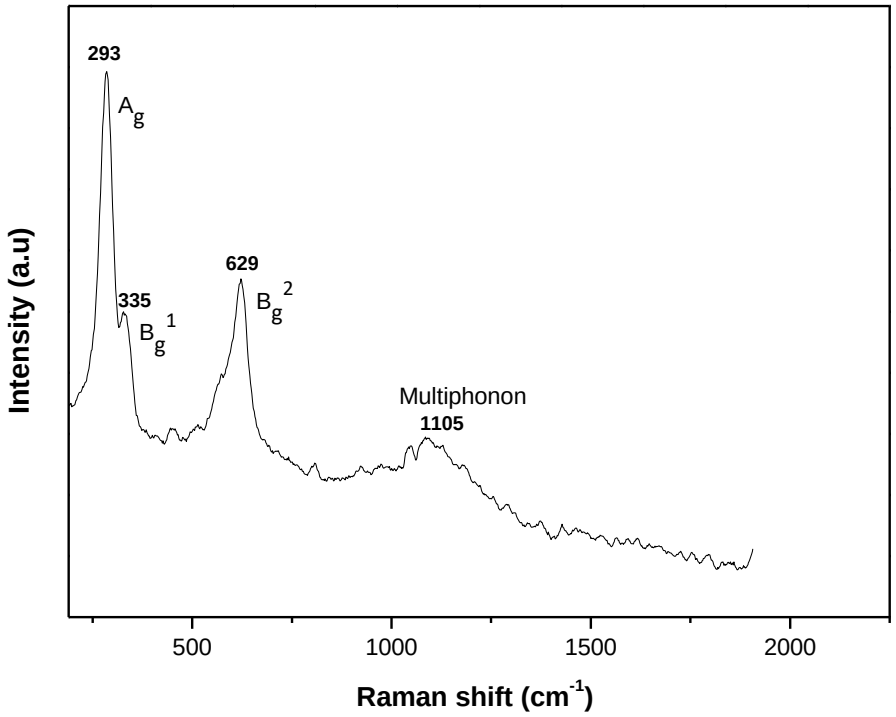

Fig. 10. The Raman shifts of the copper oxide nanoparticles.

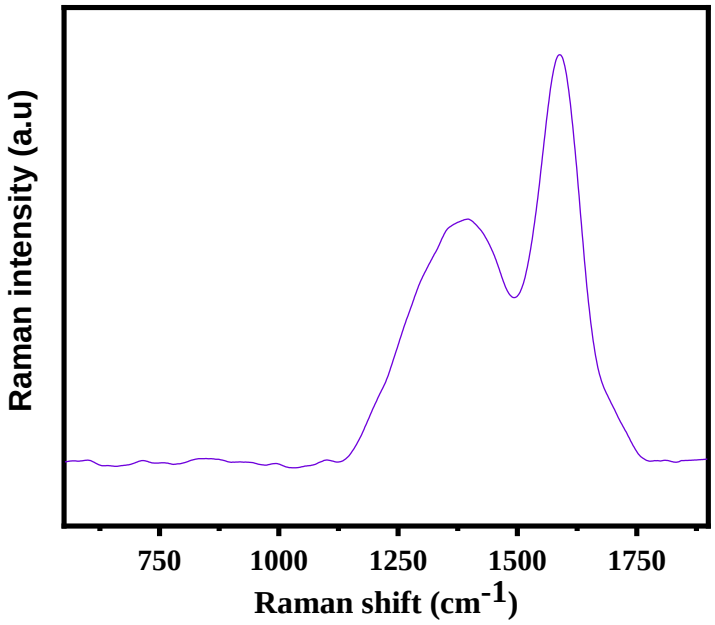

Fig. 11. The Raman shift of the functionalized CNFs.

3.3.6 BET Analysis

The Brunauer – Emmett –Teller (BET) surface area for as-prepared copper oxide nanoparticles was found to be 5.31 m^2g^{-1} while literature values vary, 6.18, 59.1, 58.8, 14.5, 2.79, 1.72 m^2g^{-1} for the F_CNFs was 32 m^2g^{-1} which compared to 38 m^2g^{-1}. It was noted that the surface area of CuO nanoparticles depends on the temperature of the method of preparation. These results suggest that the graphitization scope of carbon nanofibers improve with acid treatment hence the increase in their photocatalytic characteristics [46], [55]–[59].

3.3.7 TEM Analysis

Figure 12 shows the TEM images of the as-prepared copper oxide nanoparticles while the distribution graph in Figure 13 gives the average particle size of 9.940 ± 4.295 nm for the CuO nanoparticles

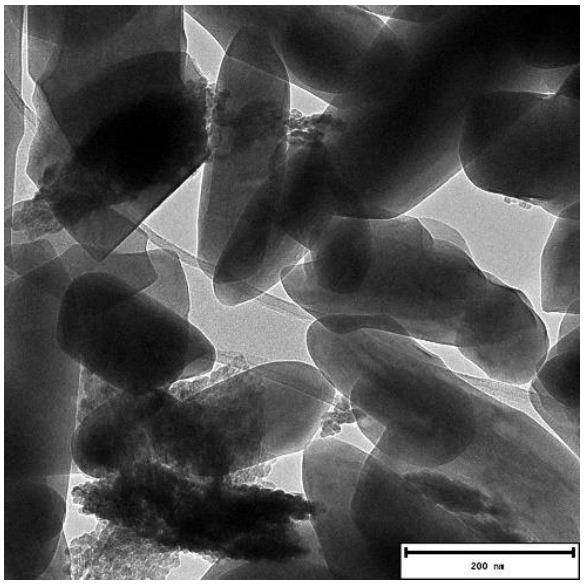

Fig. 12. Transmission Electron Microscopy image of the copper oxide nanoparticles.

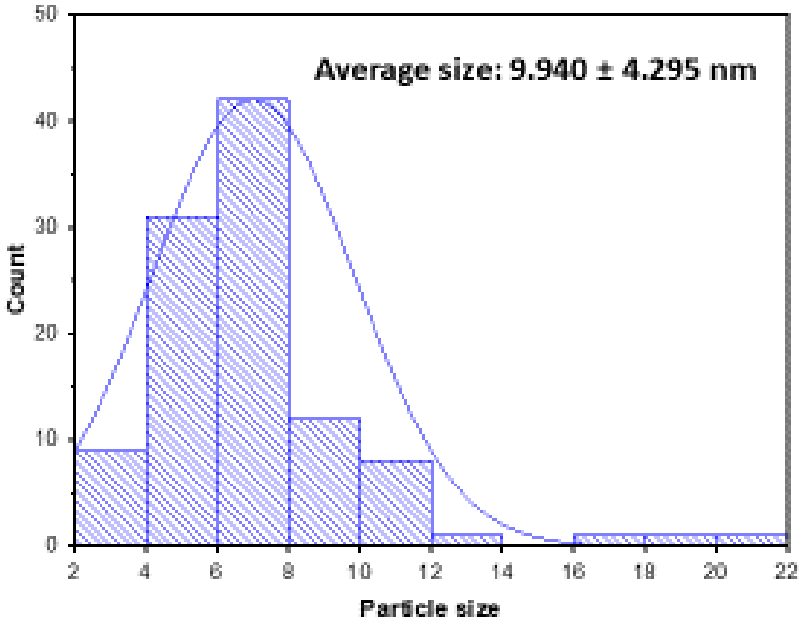

Fig. 13. The distribution graph of the CuONPs.

The TEM image of F_CNFs is presented in Figure 14. The distribution graph of the F_CNFs presented in Figure 15 show that the diameter of the F_CNFs is 73 ± 9.22 nm which is in agreement with what has been reported, 50-200 nm [60].

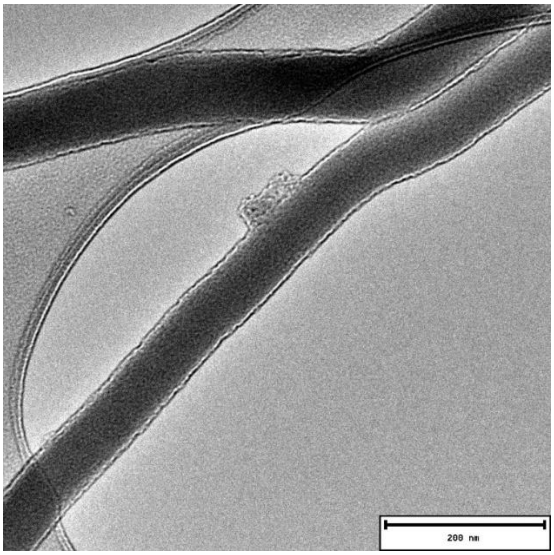

Fig. 14. Transmission Electron Microscopy image of the F_CNFs.

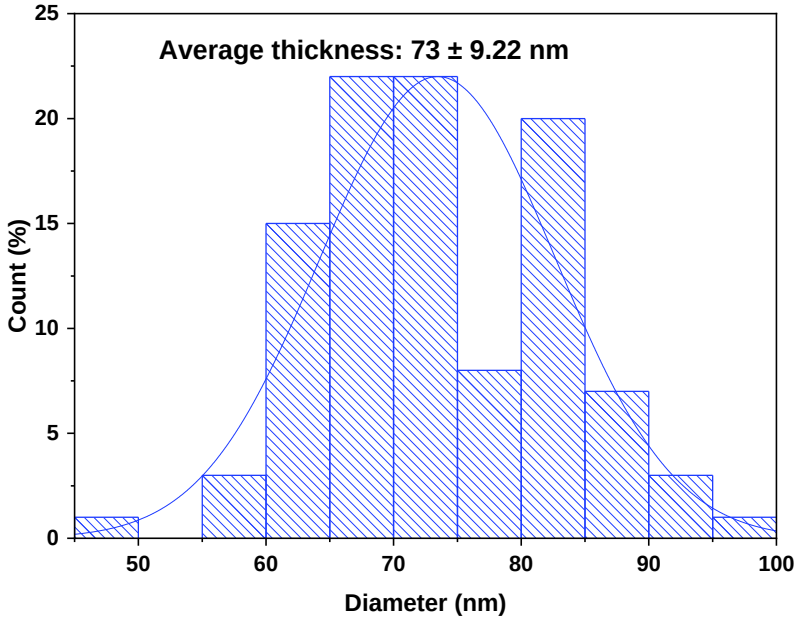

Fig. 15. The distribution graph of the diameter of the F_CNFs.

The electron image and the EDS mapping of the F_CNFs are shown in Figures 16 and 17 respectively.

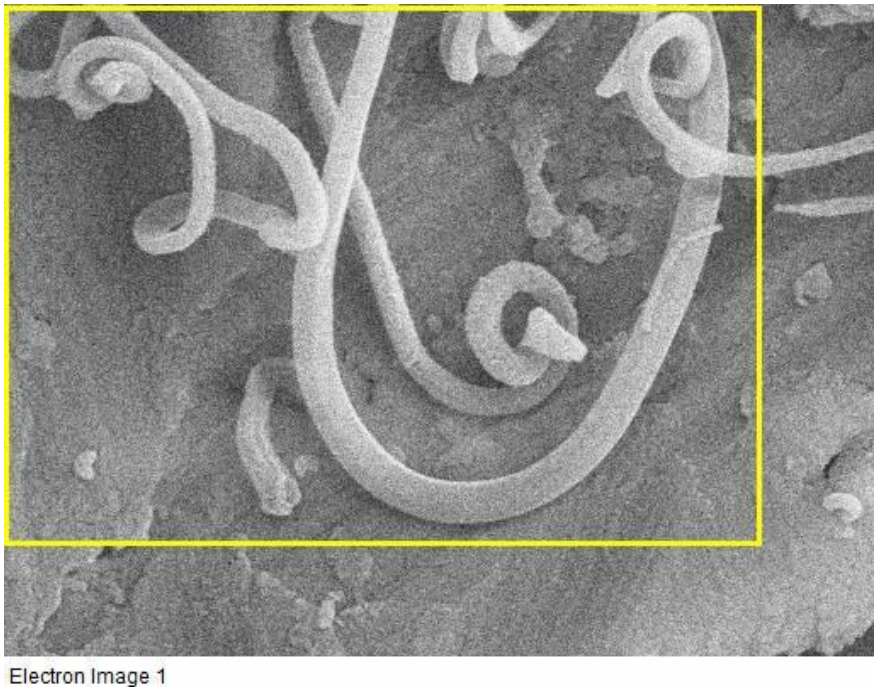

Fig. 16. An electron image of the F_CNFs.

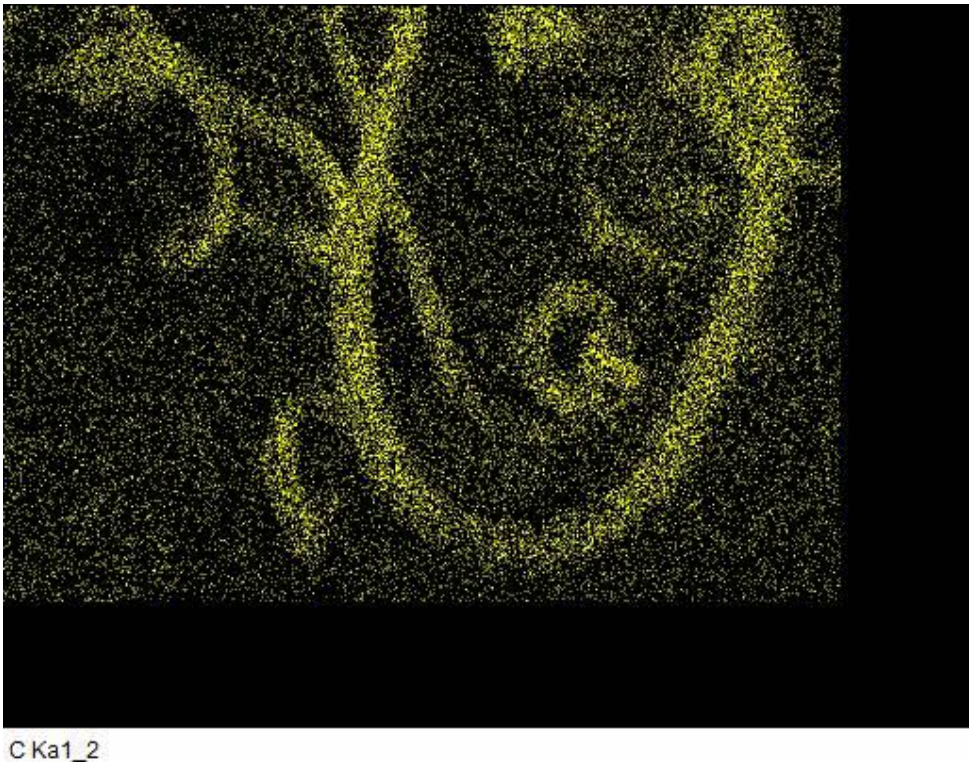

Fig. 17. The EDS mapping of the F_CNFs.

The CuONPs were prepared by copper nitrate, $Cu(NO_3)_2.3H_2O$. The metal salt was dispersed in 200 mL deionized water forming 0.05M solution of coper nitrate. An equal volume of 0.05M concentration of KOH was added with vigorous stirring for 12 h. Black precipitates were obtained, repeatedly cleaned with distilled water to neutrality before drying in an oven overnight with heat of 80 ℃. The dried CuO NPs were characterized using PXRD, Raman, HR-SEM, and FTIR.

The carbon nanofibers were prepared by synthesized CuONPs as catalyst at 300 ℃ in a quartz tube using chemical vapour deposition, CVD technique [5]. The synthesis method of CNFs employs the breakdown of acetylene, C_2H_2 in a CVD tube furnace, straight and parallel to the ground. The CVD tube furnace was electronically monitored by setting the thermal flow, rise in temperature, and gas throughput. The catalyst, about 0.1g, added into a quartz boat, 120 mm by 15 mm at room temperature (25ºC) and the boat transferred to the middle of the CVD tube furnace. The temperature of the furnace was then increased at 10 ℃ min^{-1} with hydrogen gas, H_2 discharging over the catalyst at 50 mL min^{-1}. Upon attaining heating of 300 ℃, the H_2 flow was retained for 30 minutes before introducing C_2H_2 at a constant flow rate of 50 $mLmin^{-1}$. Afterwards, approximately 30 minutes, the C_2H_2 stream was ceased, and the CVD tube furnace was enabled to loose heat to 25ºC under H_2 gas stream. The quartz boat was later taken out of the CVD tube furnace and the yield, carbon sediment formed along with the catalyst weighed.

The CNFs were washed with concentrated nitric acid, to separate the remnants of the CuO NPs besides, functionalizing them. Concentrated nitric acid (55%) was introduced to the CNFs in a round bottom flask before refluxing at 110 ℃ for 2 h. The mixture was enabled to loose heat to 25ºC filtered, washed with copious amount of distilled water to neutrality. The washed CNFs were filtered and dried for 12 h in an oven at 80 ℃.

3.4 Conclusion

In the course of this research, CuO nanoparticles were synthesized via a simple, novel, one-step and highly reproducible method at room temperature. The novel method does not require calcination or annealing of the as-prepared copper oxide nanoparticles which the other methods presently in use need. The CuO nanoparticles synthesized by this novel method was further tested in the catalytic preparation of CNFs and the results prove that the CNFs that were prepared using this method were of high purity as shown by Raman shifts. The Raman spectrum shows the G-band of the functionalized carbon nanofibers at 1596 cm^{-1}, while the presence of the D- band is at about 1387 cm^{-1} indicating the pristine nature of the F_CNFs. The characterization of the as-prepared copper oxide nanoparticles validated features of the copper oxide nanoparticles, and these particles were averagely 11 nm as compared to what has been reported, 6, 10 and 27nm. Additionally, the synthesized CNFs were functionalized and found to be of high purity and of high thermal stability, 577ºC. The results compare well with the CNFs synthesized by other methods.

Declaration of competing interest

There are no competing interest.

Acknowledgement

We, the authors are indebted to the University of the Witwatersrand for financial assistance.

APPENDIX 1

Photoluminescence data

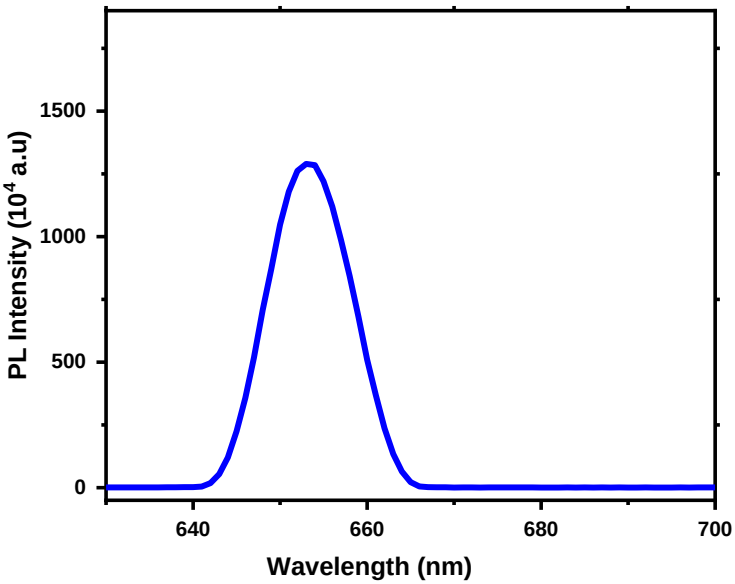

Fig. 1. Photoluminescence spectrum of the F_CNFs.

TGA data

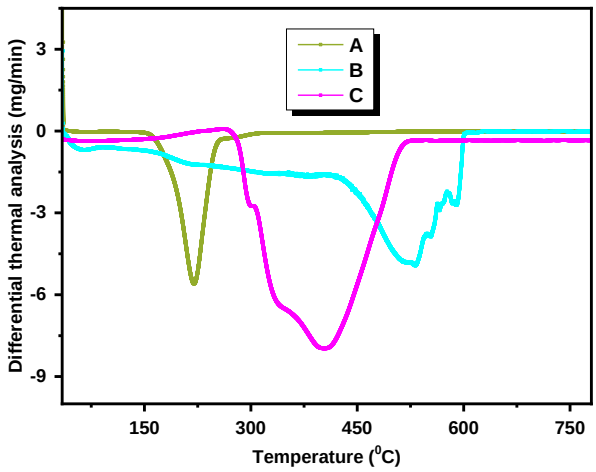

Fig. 2. The DTA diagrams of the copper oxide nanoparticles (A), functionalized carbon nanofibers, F_CNFs (B), and carbon nanofibers (C).

Reference

[1] A. Al Baroot, M. Alheshibri, Q. A. Drmosh, S. Akhtar, E. Kotb, and K. A. Elsayed, "A novel approach for fabrication ZnO/CuO nanocomposite via laser ablation in liquid and its antibacterial activity: A novel approach for fabrication ZnO/CuO nanocomposite," *Arab. J. Chem.*, vol. 15, no. 2, 2022, doi: 10.1016/j.arabjc.2021.103606.

[2] T. H. Tran and V. T. Nguyen, "Copper Oxide Nanomaterials Prepared by Solution Methods, Some Properties, and Potential Applications: A Brief Review," *Int. Sch. Res. Not.*, vol. 2014, pp. 1–14, Dec. 2014, doi: 10.1155/2014/856592.

[3] A. Bhaduri and Kajal, "Facile synthesis and characterization of cupric oxide (CuO) nanoparticles: Inexpensive and abundant candidate for light harvesting," *AIP Conf. Proc.*, vol. 2093, no. 2019, 2019, doi: 10.1063/1.5097116.

[4] R. Chowdhury, A. Khan, and M. H. Rashid, "Green synthesis of CuO nanoparticles using Lantana camara flower extract and their potential catalytic activity towards the aza-Michael reaction," *RSC Adv.*, vol. 10, no. 24, pp. 14374-14385, 2020, doi: 10.1039/d0ra01479f.

[5] M. P. Ravele, O. A. Oyewo, S. Ramaila, L. Mavuru, and D. C. Onwudiwe, "Facile synthesis of copper oxide nanoparticles and their applications in the photocatalytic degradation of acyclovir," *Results Eng.*, vol. 14, pp. 100479, 2022, doi: 10.1016/j.rineng.2022.100479.

[6] A. V Feradrick Samson, M. K. Racik, S. Prathap, J. Madhavan, and M. Victor Antony Raj, "Investigations of Structural, Optical and dielectric studies of Copper Oxide nanoparticles," *Materials Today: Proceedings,* vol. 8, pp. 386–392, 2019, https://doi.org/10.1016/j.matpr.2019.02.127.

[7] W. J. Stepniowski and W. Z. Misiolek, “Review of Fabrication Methods, Physical Properties, and Applications of Nanostructured Copper Oxides Formed via Electrochemical Oxidation,” *Nanomaterials*, vol. 8, no. 6, pp. 379, 2018, https://doi.org/10.3390/nano8060379.

[8] N. Syed, J. Huang, Y. Feng, X. Wang, and L. Cao, “Carbon-Based Nanomaterials via Heterojunction Serving as Photocatalyst,” *Front. Chem.*, vol. 7, pp. 1–7, 2019, doi: 10.3389/fchem.2019.00713.

[9] M. B. Tahir, A. M. Asiri, and T. Nawaz, “A perspective on the fabrication of heterogeneous photocatalysts for enhanced hydrogen production,” *Int. J. Hydrogen Energy*, vol. 45, no. 46, pp. 24544–24557, 2020, doi: 10.1016/j.ijhydene.2020.06.301.

[10] A. Umar *et al.*, “Selective ethanol gas sensing performance of flower-shaped CuO composed of thin nanoplates,” *J. Mater. Sci. Mater. Electron.*, vol. 32, no. 14, pp. 18565–18579, 2021, doi: 10.1007/s10854-021-06249-y.

[11] Z. Li *et al.*, “Hydrothermal synthesis of hierarchically flower-like CuO nanostructures with porous nanosheets for excellent H_2S sensing,” *J. Alloys Compd.*, vol. 725, pp. 1136–1143, 2017, doi: 10.1016/j.jallcom.2017.07.218.

[12] Z. Amani-Beni and A. Nezamzadeh-Ejhieh, “A novel non-enzymatic glucose sensor based on the modification of carbon paste electrode with CuO nanoflower: Designing the experiments by response surface methodology (RSM),” *J. Colloid Interface Sci.*, vol. 504, pp. 186–196, 2017, doi: 10.1016/j.jcis.2017.05.049.

[13] L. Sun, C. X. Wu, X. T. Zhou, Y. A. Zhang, and T. L. Guo, “Improving field emission properties of CuO nanowires by coating with ZnO nanoparticles,” *Materials Technology,* Vol. 30, No. 3, May 2015, doi: 10.1179/1753555714Y.0000000232.

[14] M. Ponnar, C. Thangamani, P. Monisha, S. S. Gomathi, and K. Pushpanathan, "Influence of Ce doping on CuO nanoparticles synthesized by microwave irradiation method," *Appl. Surf. Sci.*, vol. 449, pp. 132–143, Aug. 2018, doi: 10.1016/j.apsusc.2018.01.126.

[15] J. Singh and M. Rawat, "A Brief Review on Synthesis and Characterization of Copper Oxide Nanoparticles and its Applications," *J. Bioelectron. Nanotechnol.*, vol. 1, no. 1, 2016, doi: 10.13188/2475-224x.1000003.

[16] M. Y. Al Shdaifat, R. Zulkifli, K. Sopian, and A. A. Salih, "Thermal and hydraulic performance of CuO/water nanofluids: A review," *Micromachines*, vol. 11, no. 4, 2020. doi: 10.3390/MI11040416.

[17] B. T. Sone, A. Diallo, X. G. Fuku, A. Gurib-Fakim, and M. Maaza, "Biosynthesized CuO nano-platelets: Physical properties & enhanced thermal conductivity nanofluidics," *Arab. J. Chem.*, vol. 13, no. 1, pp. 160–170, Jan. 2020, doi: 10.1016/j.arabjc.2017.03.004.

[18] E. W. Marcelino, D. D. O. Silva, and R. R. Riehl, "A REVIEW ON THE INFLUENCE OF NANOPARTICLE SIZE IN THERMAL ENHANCEMENT OF CuO-WATER NANOFLUIDS AND THEIR CHARACTERISTICS." ITherm 2016, Las Vegas, NV USA, May 31 - June 3, 2016, https://www.researchgate.net/publication/322775565.

[19] K. Phiwdang, S. Suphankij, W. Mekprasart, and W. Pecharapa, "Synthesis of CuO nanoparticles by precipitation method using different precursors," *Energy Procedia*, vol. 34, pp. 740–745, 2013, doi: 10.1016/j.egypro.2013.06.808.

[20] N. Silva, S. Ramírez, I. Díaz, A. Garcia, and N. Hassan, "Easy, quick, and reproducible sonochemical synthesis of CuO nanoparticles," *Materials*, vol. 12, no. 5, pp. 1–13,

2019, doi: 10.3390/MA12050804.

[21] G. Bhanjana, N. Dilbaghi, K. H. Kim, and S. Kumar, “Low temperature synthesis of copper oxide nanoflowers for lead removal using sonochemical route,” *J. Mol. Liq.*, vol. 244, pp. 506–511, 2017, doi: 10.1016/j.molliq.2017.09.034.

[22] N. R. Dhineshbabu, V. Rajendran, N. Nithyavathy, and R. Vetumperumal, “Study of structural and optical properties of cupric oxide nanoparticles,” *Appl. Nanosci.*, vol. 6, no. 6, pp. 933–939, 2016, doi: 10.1007/s13204-015-0499-2.

[23] J. Iqbal *et al.*, “Potential antimicrobial, antidiabetic, catalytic, antioxidant and ROS/RNS inhibitory activities of Silybum marianum mediated biosynthesized copper oxide nanoparticles,” *RSC Adv.*, vol. 12, no. 22, pp. 14069–14083, 2022, doi: 10.1039/d2ra01929a.

[24] P. Bhattacharya, S. Swarnakar, S. Ghosh, S. Majumdar, and S. Banerjee, “Disinfection of drinking water via algae mediated green synthesized copper oxide nanoparticles and its toxicity evaluation,” *J. Environ. Chem. Eng.*, vol. 7, no. 1, 2019, doi: 10.1016/j.jece.2018.102867.

[25] A. C. Nwanya *et al.*, “Industrial textile effluent treatment and antibacterial effectiveness of Zea mays L. Dry husk mediated bio-synthesized copper oxide nanoparticles,” *J. Hazard. Mater.*, vol. 375, no. 5, pp. 281–289, 2019, doi: 10.1016/j.jhazmat.2019.05.004.

[26] F. Ijaz, S. Shahid, S. A. Khan, W. Ahmad, and S. Zaman, “Green synthesis of copper oxide nanoparticles using abutilon indicum leaf extract: Antimicrobial, antioxidant and photocatalytic dye degradation activities,” *Trop. J. Pharm. Res.*, vol. 16, no. 4, pp. 743–753, 2017, doi: 10.4314/tjpr.v16i4.2.

[27] L. D. Jadhav, S. P. Patil, A. U. Chavan, A. P. Jamale, and V. R. Puri, “Solution combustion synthesis of Cu nanoparticles: A role of oxidant-to-fuel ratio,” *Micro Nano Lett.*, vol. 6, no. 9, pp. 812–815, 2011, doi: 10.1049/mnl.2011.0372.

[28] J. C. Yu, A. Xu, L. Zhang, R. Song, and L. Wu, “Synthesis and characterization of porous magnesium hydroxide and oxide nanoplates,” *J. Phys. Chem. B*, vol. 108, no. 1, pp. 64–70, 2004, doi: 10.1021/jp035340w.

[29] L. Caixin, Z. Lei, D. Jiguang, M. Qing, D. Hongxing, and H. Hong, “Surfactant-aided hydrothermal synthesis and carbon dioxide adsorption behavior of three-dimensionally mesoporous calcium oxide single-crystallites with tri-, tetra-, and hexagonal morphologies,” *J. Phys. Chem. C*, vol. 112, no. 49, pp. 19248–19256, 2008, doi: 10.1021/jp8064568.

[30] Z. N. Kayani, M. Umer, S. Riaz, and S. Naseem, “Characterization of Copper Oxide Nanoparticles Fabricated by the Sol–Gel Method,” *J. Electron. Mater.*, vol. 44, no. 10, pp. 3704–3709, Oct. 2015, doi: 10.1007/s11664-015-3867-5.

[31] J. Zhu, H. Bi, Y. Wang, X. Wang, X. Yang, and L. Lu, “Synthesis of flower-like CuO nanostructures via a simple hydrolysis route,” *Mater. Lett.*, vol. 61, no. 30, pp. 5236–5238, 2007, doi: 10.1016/j.matlet.2007.04.037.

[32] S. A. Manafi and S. H. Badiee, “Production of Carbon nanofibers using a CVD method with lithium fluoride as a supported cobalt catalyst,” *Adv. Mater. Sci. Eng.*, vol. 2008, 2008, doi: 10.1155/2008/850975.

[33] D. Yadav, F. Amini, and A. Ehrmann, “Recent advances in carbon nanofibers and their applications – A review,” *Eur. Polym. J.*, vol. 138, 2020, doi: 10.1016/j.europolymj.2020.109963.

[34] C. Ma *et al.*, “Lignin-based hierarchical porous carbon nanofiber films with superior performance in supercapacitors,” *Appl. Surf. Sci.*, vol. 456, pp. 568–576, 2018, doi: 10.1016/j.apsusc.2018.06.189.

[35] B. Nahar, S. B. Chaity, M. A. Gafur, and M. Z. Hossain, “Synthesis of Spherical Copper Oxide Nanoparticles by Chemical Precipitation Method and Investigation of Their Photocatalytic and Antibacterial Activities,” *J. Nanomater.*, vol. 2023, 2023, doi: 10.1155/2023/2892081.

[36] H. Narayan, H. Alemu, H. Alemu, L. F. Maxakaza, and S. Jaybhaye, “Copper Oxide Nanoparticles : Synthesis and Characterization,” Advanced Analytical Tools for Materials Characterization (AATMC-2018) vol. 4, no. 5, pp. 43–47, 2018, https://www.researchgate.net/publication/327423519.

[37] C. Gherasim *et al.*, “Copper oxide nanostructures: Preparation, structural, dielectric and catalytic properties,” *Ceram. Int.*, vol. 48, no. 17, pp. 25556–25568, 2022, doi: 10.1016/j.ceramint.2022.05.235.

[38] A. A. Bhat *et al.*, “Synthesis and Characterization of Copper Oxide Nanoparticles by Coprecipitation Method: Electronic and Antimicrobial Properties,” *Chem. Sci. Eng. Res.*, vol. 3, no. 6, 2021, doi: 10.36686/ariviyal.cser.2021.03.06.031.

[39] K. Ali, M. Sajid, S. Abu Bakar, A. Younus, H. Ali, and M. Zahid Rashid, “Synthesis of copper oxide (CuO) via coprecipitation method: Tailoring structural and optical properties of CuO nanoparticles for optoelectronic device applications,” *Hybrid Adv.*, vol. 6, 2024, doi: 10.1016/j.hybadv.2024.100250.

[40] A. Muthuvel, M. Jothibas, and C. Manoharan, “Synthesis of copper oxide nanoparticles by chemical and biogenic methods: photocatalytic degradation and in vitro antioxidant activity,” *Nanotechnol. Environ. Eng.*, vol. 5, no. 2, pp. 1–19, 2020,

doi: 10.1007/s41204-020-00078-w.

[41] S. Thamaraiselvi and G. Thenmozhi, “Synthesis of CuO nanoparticles by using simple precipitation method,” *Int. J. Sci. Res.*, vol. 11, no. 4, pp. 1300–1302, 2022, doi: 10.21275/SR22425202059.

[42] M. H. Saleem, U. Ejaz, M. Vithanage, N. Bolan, and K. H. M. Siddique, “Synthesis, characterization, and advanced sustainable applications of copper oxide nanoparticles: a review,” *Clean Technol. Environ. Policy*, 2024, doi: 10.1007/s10098-024-02774-6.

[43] A. S. Lanje, S. J. Sharma, R. B. Pode, and R. S. Ningthoujam, “Synthesis and optical characterization of copper oxide nanoparticles,” *Adv. Appl. Sci. Res.,* vol. 1, no. 2 pp. 36-40, 2010, www.pelagiaresearchlibrary.com.

[44] L. Lu, C. Kong, V. Sahajwalla, and D. Harris, “Char structural ordering during pyrolysis and combustion and its influence on char reactivity,” *Fuel*, vol. 81, no. 9, pp. 1215–1225, 2002, doi: 10.1016/S0016-2361(02)00035-2.

[45] I. Mansuri, R. Farzana, R. Rajarao, and V. Sahajwalla, “Carbon dissolution using waste biomass—A sustainable approach for iron-carbon alloy production,” *Metals*, vol. 8, no. 4, 2018, doi: 10.3390/met8040290.

[46] M. R. Cuervo *et al.*, “Effect of carbon nanofiber functionalization on the adsorption properties of volatile organic compounds,” *J. Chromatogr. A.*, vol. 1188, no. 2, pp. 264–273, 2008, doi: 10.1016/j.chroma.2008.02.061.

[47] R. Anjabin and H. Khosravi, “Property improvement of a fibrous composite using functionalized carbon nanofibers,” *Polym. Compos.*, vol. 40, no. 11, pp. 4281–4288, 2019, doi: 10.1002/pc.25289.

[48] M. Inagaki, F. Kojin, B. Tryba, and M. Toyoda, “Carbon-coated anatase: The role of

the carbon layer for photocatalytic performance," *Carbon,* vol. 43, no. 8, pp. 1652–1659, 2005, doi: 10.1016/j.carbon.2005.01.043.

[49] A. Rita, A. Sivakumar, and S. A. Martin Britto Dhas, "Influence of shock waves on structural and morphological properties of copper oxide NPs for aerospace applications," *J. Nanostructure Chem.*, vol. 9, no. 3, pp. 225–230, 2019, doi: 10.1007/s40097-019-00313-0.

[50] M. Shafiey Dehaj and M. Zamani Mohiabadi, "Experimental study of water-based CuO nanofluid flow in heat pipe solar collector," *J. Therm. Anal. Calorim.*, vol. 137, no. 6, pp. 2061–2072, 2019, doi: 10.1007/s10973-019-08046-6.

[51] M. A. El-atawy and K. D. Khalil, "Chitosan Capped Copper Oxide Nanocomposite: Efficient, Recyclable, Heterogeneous Base Catalyst for Synthesis of Nitroolefins", *Catalysts*, vol. 12, no. 9, pp. 964, 2022, doi:10.3390/catal12090964.

[52] Y. Liu, C. Pan, and J. Wang, "Raman spectra of carbon nanotubes and nanofibers prepared by ethanol flames," *J. Mater. Sci.*, vol. 39, no. 3, pp. 1091–1094, 2004, doi: 10.1023/B:JMSC.0000012952.20840.09.

[53] J. Hodkiewicz, "Characterizing Carbon Materials with Raman Spectroscopy - application note," *Thermo Fish. Sci.*, pp. 1–5, 2010, http://thermo.com.

[54] M. Llorens-Gámez and Á. Serrano-Aroca, "Low-cost advanced hydrogels of calcium alginate/carbon nanofibers with enhancedwater diffusion and compression properties," *Polymers*, vol. 10, no. 4, 2018, doi: 10.3390/polym10040405.

[55] N. Baylan, T. Dedecan, İ. İlalan, and İ. İnci, "Preparation of Copper Oxide Nanoparticles as a Novel Adsorbent for the Isolation of Tartaric Acid," *Anal. Lett.*, vol. 54, no. 13, pp. 2113–2125, 2021, doi: 10.1080/00032719.2020.1842434.

[56] J. Singh, G. Kaur, and M. Rawat, “A Brief Review on Synthesis and Characterization of Copper Oxide Nanoparticles and its Applications,” *J. Bioelectron. Nanotechnol.*, vol. 1, no. 1, pp. 1–9, 2016, doi: 10.13188/2475-224x.1000003.

[57] N. Verma and N. Kumar, “Synthesis and Biomedical Applications of Copper Oxide Nanoparticles: An Expanding Horizon,” *ACS Biomater. Sci. Eng.*, vol. 5, no. 3, pp. 1170–1188, 2019, doi: 10.1021/acsbiomaterials.8b01092.

[58] R. Wu, Z. Ma, Z. Gu, and Y. Yang, “Preparation and characterization of CuO nanoparticles with different morphology through a simple quick-precipitation method in DMAC-water mixed solvent,” *J. Alloys Compd.*, vol. 504, no. 1, pp. 45–49, 2010, doi: 10.1016/j.jallcom.2010.05.062.

[59] S. A. Azzam *et al.*, “Effects of Morphology and Surface Properties of Copper Oxide on the Removal of Hydrogen Sulfide from Gaseous Streams,” *Ind. Eng. Chem. Res.*, vol. 58, no. 40, pp. 18836–18847, 2019, doi: 10.1021/acs.iecr.9b03975.

[60] L. Feng, N. Xie, and J. Zhong, “Carbon nanofibers and their composites: A review of synthesizing, properties and applications,” *Materials*, vol. 7, no. 5, pp. 3919–3945, 2014, doi: 10.3390/ma7053919.

CHAPTER FOUR

Efficiency of TiO_2 composited with carbon nanofibers for Hydrogen production from water

Molecular Sciences Institute, School of Chemistry, University of the Witwatersrand, Johannesburg 2050, South Africa

Abstract

The dissociation of H_2O on TiO_2 capped with metal, non-metal nitrides, and metal oxides to produce hydrogen and oxygen is a long standing research as a prospective channel to renewable, neat, extensive production. However, the rate of hydrogen production reported in these studies are low to meet the global hydrogen demands. To intensify the generation of hydrogen by light-activated catalysts using water, its implementation was examined using TiO_2 composited with carbon nano fibers (CNFs) in this study. The catalytic accomplishment of TiO_2 coated on CNFs, TiO_2 – A (anatase) and TiO_2 – P25 (P25) for hydrogen production was investigated. The CNFs were synthesized by chemical vapour deposition and purified by 55% HNO_3. The CNFs were coated with TiO_2 – A at different loadings of 0, 10%, 20% by hydrothermal method and used in hydrogen production from water using UV irradiation at room temperature (25ºC). The synthesized TiO_2 – anatase had granular nanoparticles with average particle size of 9.5 nm. All the CNFs were totally covered with TiO_2 nanoparticles. The SEM- EDS Scanning confirmed the existence of Ti, C and O in the samples, while BET surface area of the TiO_2/CNFs, TiO_2 and CNFs was 126, 73 and 32 m^2/g respectively. The 20% _TiO_2 /F_CNFs had the highest photocatalytic efficiency of 7203.50 μmol g^{-1} h^{-1} while TiO_2 -P25 and TiO_2 – A, were 126.39 and 119.39 μmol g^{-1} h^{-1} respectively.

Keywords: TiO_2; carbon nanofibers; CH_3OH; Hydrogen production; water splitting.

4.1 Introduction

There is increasing energy demands globally. Regardless of the needs, present-day point sources are shrinking and predicted to exhaust faster than envisaged. Consequently, environmentalists and researchers are presently advocating for sustainable energy to eradicate the problem. Energy systems that are sustainable are being instituted to encounter the increasing intercontinental power challenges and minimize dependence on petroleum that degrade the environment [1]. Discovering an alternative replacement of non-renewable energy for daily consumption, the power saving of the alternatives has to be greater also, ecologically friendly particularly on carbon emissions as compared to the fossil fuels which are currently in use [2]. A renewable, and neat power for innumerable applications like heating, automobile power, fuel cells, and many more which have minimal ecological deterioration influence is hydrogen [3]–[6]. Additionally, hydrogen application as a substitute fuel has been a long-term replacement to reduction of global carbon dioxide production via hydrogenation processes [3]–[5], [7], [8]. Photocatalytic hydrogen generation occurring in water splitting is a potential technique for sustainable energy and resolving, environmental degradation which is an issue to the world [9]–[13]. Naturally, water is free and can offer energy security for the future. The known commercial processes for hydrogen production are photocatalytic, electrochemical and thermochemical. These have been broadly studied methods, and are still being advanced for better results. In photocatalysis, a semi-conductor is used as a catalyst. The electronic configuration of the substance is important in determining optical energy gap (Eg), which is the difference between lower occupied energy level (valence band: VB) and higher unoccupied energy level (conductive band: CB). The semiconductor should have an ideal band gap of about 1.23 eV though a band gap range

between 1.5 to 2.5 eV may still work as some energy losses may occur [14]. In water splitting operations, water is split into gaseous H_2 and O_2 in reduction-oxidation processes (proton reduction and $4e^-$ water oxidation) [15].

The photocatalytic surface has to be irradiated with power higher than or equal to its band width for a photon absorption to take place. The process induces the formation of electron-hole pair. The light-induced electron (e^-) is lodged in CB giving rise to a vacancy/hole (h^+) in the VB. The electron- hole pairs normally referred to as charge carriers generated relocate to the facet of the photocatalyst and react with water molecules adsorbed on its surface whereby reduction and oxidation reactions take place producing H_2 and O_2 [10], [16]–[20].

The environmental friendliness of hydrogen (a zero-emitter of greenhouse gases) has triggered a lot of interest in research related to its production through water splitting, accelerated by a diversity of photocatalysts and sacrificial reagents in the production processes. Admitting the role of the photocatalysts together with the use of electron/hole separators, sacrificial electron donors and acceptor, achieving absolute water splitting is still unfeasible [10], [13], [21]–[28]. However, sacrificial reagents are used in the production of hydrogen in cases where there is need for enhancement of the yields (hydrogen and oxygen yields) under such states. The success of the use of sacrificial reagents relies on photocatalyst and the sacrificial reagent used [29], [30]

During photocatalysis, the charge carriers are abundantly produced as a result of the photon absorption as the irradiation is employed on the photocatalyst. The generated electron-hole pairs migrate to the reaction centers which are on the facet of the photocatalysts. On the photocatalyst surface, water molecules are reduced to H_2 while oxidation occurs to form O_2 [10], [31]–[33]. Different opinions have emerged concerning the benefits derived from the use of sacrificial reagents. This however has made TiO_2-based catalysts when used together

with sacrificial reagents an emerging area of interest to researchers as divided hypotheses have come up. Most research indicate that information gained in one research is not transferable to another [34]–[37]. Hence, the type of sacrificial reagent to be used in water splitting together with photocatalysts such as TiO_2 need to be investigated further. To this moment, there is no correlation between the photocatalyst ability to split water and the presence of sacrificial reagents [2], [21], [29], [31], [38]–[42].

Currently, researchers are targeting the use of carbon-based nanomaterials like helices (CNFs), CNTs and fullerenes (C_{60}) doped with semiconductor photocatalysts to enhance the effectiveness of the composite materials in water splitting [43]–[46]. The importance of this technique is perceived to be associated with the delocalization processes of the combined structure present in the carbon allotropes that act as electron reservoirs that will necessitate the transfer and splitting of the photogenerated electrons. Additionally, there is improvement of the adsorptive properties of the photocatalysts and this gives rise to catalytic sites on the photocatalyst surfaces [18], [47]. Other methods have been used to extend TiO_2 photocatalytic properties to electromagnetic radiation regions by capping it with carbon. This technique of doping TiO_2 with CNFs has combined effect thereby improving the efficiency of the photocatalyst and proposed various mechanisms which still require justification [13], [15], [16], [22], [31].

Despite the uncertainty, (this technique of doping TiO_2 with CNFs has combined effect thereby improving the efficiency of the photocatalyst and proposed various mechanisms which still require justification [13], [15], [16], [22], [31]) the enhanced compositing of CNFs with TiO_2 (TiO_2/CNFs) materials helps to advance the catalytic effect of TiO_2. Studies have shown that CNFs/CNTs have the potential to act as an electron reservoir to separate electron-hole pairs successfully [47]. Moreover, similar studies have suggested the photosensitizing

properties of CNFs/CNTs in which they directly inject electrons into the TiO_2 conductive band, CB [10], [22], [25], [45], [48], [49].

This study evaluated the efficiency of compositing TiO_2 with CNFs. The work included the preparation, identification, and utilization of TiO_2-doped CNFs as a photocatalyst for water splitting. The synthesized catalysts were also compared with TiO_2 – P25 (P25) and TiO_2 – anatase (TiO_2 – A). The parameters investigated included: loading percentage, duration of exposure of the photocatalyst to the UV radiation on the rate of hydrogen production. To ascertain best reaction conditions, sacrificial reagent, methanol (<10 %) at low concentration (negligible or no CO_2 emissions) was also studied. Since the dissociation of H_2O on TiO_2 capped with metal and non-metal nitrides, metal oxides to produce hydrogen and oxygen is a long standing research as a prospective channel to the production of hydrogen, it has been realized that the rate of hydrogen production reported in these studies are low to meet the global hydrogen demands. To intensify the generation of hydrogen by light-activated catalysts using water, TiO_2 composited with carbon nano fibers (CNFs) was used in this study. The catalytic accomplishment of TiO_2 coated on CNFs, TiO_2 – A (anatase) and TiO_2 – P25 (P25) for hydrogen production was investigated. The CNFs were synthesized by chemical vapour deposition and purified by 55% HNO_3. The CNFs were coated with TiO_2 – A at different loadings (0, 10%, 20% TiO_2 loadings) by hydrothermal method and used in hydrogen production from water using UV irradiation at room temperature (25ºC). The synthesized TiO_2 – anatase had granular nanoparticles with average particle size of 9.5 nm and all the CNFs were totally embedded with TiO_2 nanoparticles. The 20% _TiO_2 /F_CNFs had the highest photocatalytic efficiency of 7203.50 μmol g^{-1} h^{-1} as compared to the rest. TiO_2 -P25, 126.39 μmol g^{-1} h^{-1} and TiO_2 – A, 119.39 μmol g^{-1} h^{-1} recorded the lowest quantity of H_2.

4.2 Experimental

4.2.1 Materials

Methanol (analytical grade), ethanol (analytical grade), ammonia solution (25%), copper (II) nitrate trihydrate, potassium hydroxide, anhydrous, KOH, ≥ 99.95% trace metal basis, nitric acid, HNO_3 (55%), titanium butoxide and butanol were purchased from Sigma – Aldrich. Hydrogen, argon and acetylene gases were purchased from Afrox. Deionized and distilled water were employed in the procedures.

4.2.2 Preparation of CuO NPs

The CuO NPs were prepared using copper nitrate. The metal salt was dispersed in 200 mL deionized water forming 0.05M. 200 mL of 0.05M potassium hydroxide was added and vigorously stirred for 12 h. Black precipitates were obtained, repeatedly cleaned with deionized water to neutrality and dried in the oven overnight at 80 ℃. The dried CuO NPs were characterized using PXRD, Raman, HR-SEM, and FTIR.

4.2.3 Synthesis and purification of CNFs

The carbon nanofibers were prepared by the synthesized CuO NPs at 300 ℃ in a tube heating system using chemical vapour deposition, CVD technique[50]. The synthesis method of CNFs employs the fragmentation of acetylene, in a quartz tube heater, positioned horizontally. The heating system was automatically monitored by setting the thermal flux, reaction temperature, and gas flow rates. The catalyst, about 0.1g was filled into a quartz apparatus, 120 mm by 15 mm at 25℃, and positioned at the middle of the quartz tube. The heating system temperature was then raised at 10 ℃ min^{-1} with hydrogen gas, H_2 flowing over the catalyst at 50 mL min^{-1}. Upon attaining 300 ℃, the H_2 flow was retained for 30

minutes before introducing C_2H_2 at a constant flow rate of 50 $mLmin^{-1}$. Afterwards, approximately 30 minutes, the C_2H_2 flow was stopped and the furnace allowed to cool down to 25℃, under continuous H_2 flow. The quartz apparatus was later removed from the heating system, carbon deposit formed together with the catalyst measured. The CNFs (as-synthesized CNFs) were washed with concentrated nitric acid, to eliminate the remnants of the CuO NPs and to functionalize them. A 55% HNO_3 was introduced to the CNFs in a round bottom flask. The mixture was then refluxed at 110 ℃ for 2 h. The resulting suspension was allowed to cool to 25 ℃, filtered before washing with distilled water to neutrality. The washed /functionalized CNFs (F_ CNFs) were filtered and dried for 12 h in an oven at 80 ℃.

4.2.4 Synthesis of TiO_2/F_CNFs composite and TiO_2 - anatase

The TiO_2/F_CNFs was prepared by a hydrothermal method which was modified from a surfactant wrapping sol-gel approach formerly outlined by Deng et al [51], and Hamid et al [52]. In this study, a fixed amount of the purified CNFs (F_CNFs) was discharged in 25 ml butanol and homogenized for 30 minutes in a sonicator. A known amount of titanium butoxide which had been previously dispersed separately for 30 minutes in 5 ml butanol was added in drops to the F_CNFs suspension with vigorous stirring. Ammonia solution (25%, 1 ml) was introduced in drops to the F_CNFs mixture to completely hydrolyse the titanium butoxide. The mixture was then changed to a Teflon cup. The sample was then treated in an autoclave at 120ºC for 24 h. The sample was centrifuged and washed with ethanol, deionized water and dried in an oven at 80ºC for 24 h. Calcination was carried out at 400ºC for 4 h. The samples loadings were 10% and 20% loadings of TiO_2 on F_CNFs, identified as 10% TiO_2/F_CNFs and 20% TiO_2/F_CNFs respectively. The same approach was replicated without F_CNFs to prepare TiO_2 – anatase, identified as TiO_2 – A in this study.

4.2.5 Catalyst characterization

The synthesized samples were identified by different methods. Morphologies of TiO_2, CNFs, F_CNFs, TiO_2/F_CNFs composites were analysed by HRSEM analysis (ZEISS Sigma 300 VP from M/S ZEISS 'Smart SEM' OXFORD INSTRUMENTS x-act PentaFET Precision and 'Oxford INCA', United Kingdom. The same samples were analysed by X-ray diffraction (XRD) using a Brucker D2 phaser fitted with Cu – Kα radiation (λ = 1.5405 Å), operating at 30 kV (Voltage) and 10 mA, (Current). A Perkin Elmer TA TGA Q500 was employed to explore the thermogravimetric analysis. At least 10 mg sample was heated up to 900 ℃ at a heating rate of 10 ℃ min^{-1} under air. In probing the size and shape of the samples, Transmission Electron Microscopy utilizing a FEI Technai G2 Spirit electron microscope, 120 kV was used. Particles size distribution was investigated by ImageJ software in which at least 100 particles were computed for each sample. Fourier Transform Infrared spectroscopy, mounted with a Bruker Tensor 27 FT – IR spectrometer (4000 – 500 cm^{-1}) was employed to identify the functional groups present in the samples. The identification of TiO_2 and the graphicity of the F_CNFs in the composites was achieved by laser Raman spectroscopy at an excitation wavelength of 517 nm recorded by a Jobin-Yvon T64000 Raman spectrometer equipped with Olympus BX40 microscope. The optical attributes of the samples were analysed by a Varian Cary Eclipse EL0410 3870 photoluminescence/ fluorescence Spectrophotometer and SPECORD 210 plus UV – Vis Spectrophotometer. For the determination of the specific surface, Brunauer – Emmett – Teller, N_2 physisorption (Micromeritics ASAP – 2000 Tri - star analyser) was used. Prior to the analysis of the samples, 0.2 g was degassed for 6 h at 150 ℃ concealed by a N_2 flow using a Micromeritics flow Prep 060. The GC used was a HP 5890A Gas Chromatograph.

4.2.6 Photocatalytic studies

The catalytic studies were tested in a photo-chemical reactor (Lelesil Innovative Systems, 1 litre) as reported by *Walls et al* [53] using a 450 W UV Xe lamp, figure 1. In this work, 1g of the photocatalyst was dispersed in 1 L of distilled water and mixed by stirring for 15 min at room temperature, 25ºC before radiating the sample with the UV lamp for 6 h under argon and with stirring. For the sacrificial reagent study, methanol was added and the sample mixed at 1000 rpm from the start of the experiment to the end of the reaction, 6 h. The system was purged with argon until no peaks were detected on the online GC (thermal conductivity detector, TCD) from the start of the reaction and was held throughout the reaction under a flow rate of 80 ml min^{-1}.

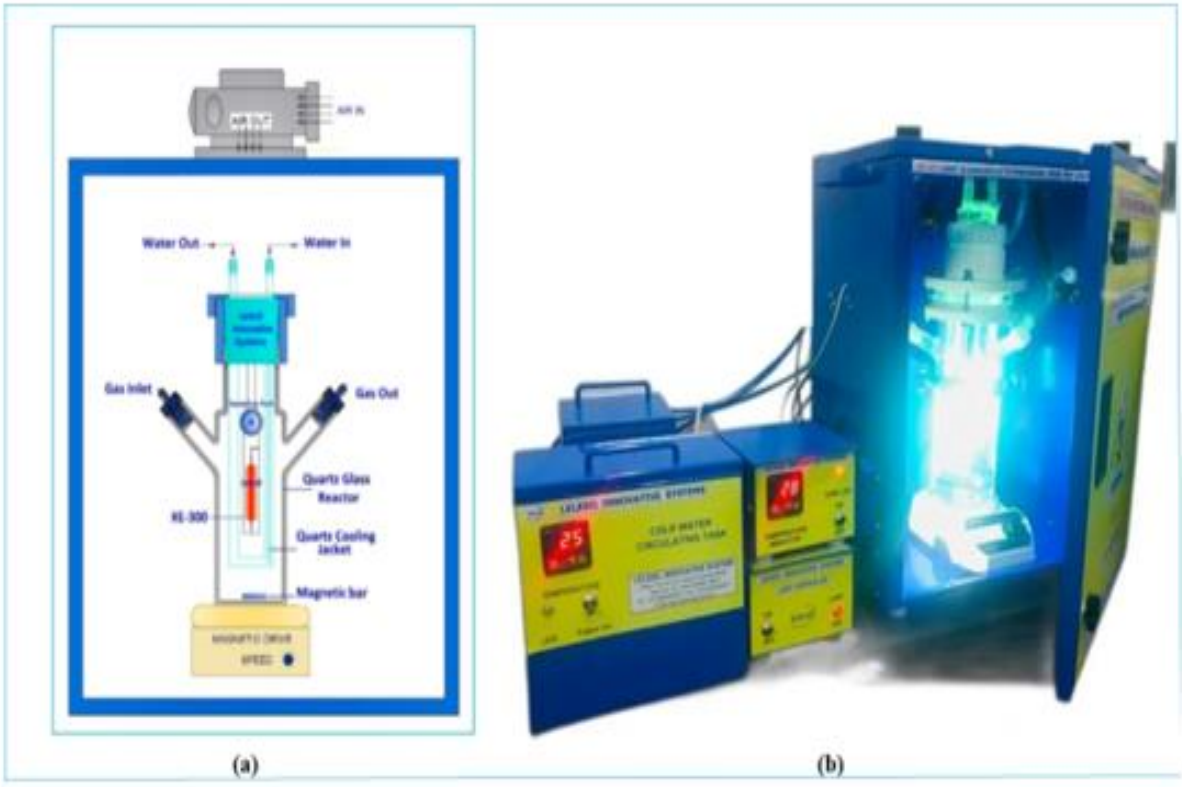

Fig. 1. (a) Representational (b) Photographic Reactor used for photocatalysis.

4.3 Results and Discussions

4.3.1 Materials characterization

The 3D morphological and structural properties of TiO_2 – anatase (TiO_2 – A), CNFs, F_CNFs and TiO_2/F_CNFs composites were studied using Field Emission Scanning Electron Microscopy, FESEM and TEM, figures 2 and 3. The CNFs, and F_CNFs were examined to be fiber-like while TiO_2 – anatase (TiO_2 – A) was granular (consisting of small particles) and the F_CNFs/TiO_2 composites were feathery in morphology, figures 2 and 3.

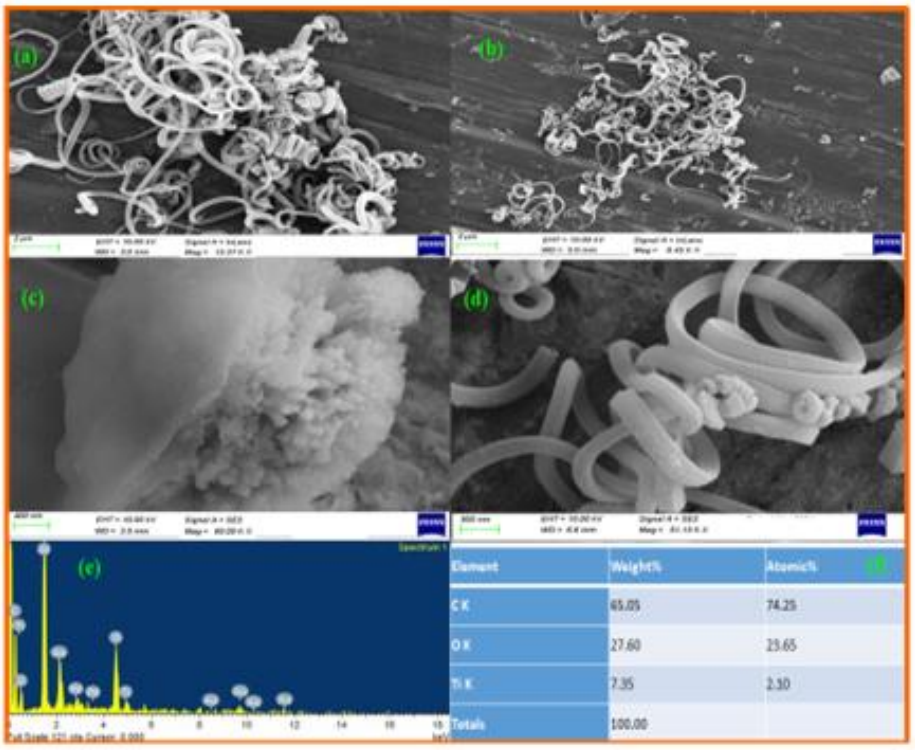

Fig. 2. Field Emission scanning electron microscopy, FESEM investigation of; as-prepared CNFs (a), Functionalized CNFs, F_CNFs (b), TiO_2 – anatase (TiO_2 – A) (c), F_CNFs/20% _TiO_2 composite (d), Energy-dispersive x-ray spectroscopy, EDS spectrum of the F_CNFs/20% _TiO_2 (e), configuration of the elements, F_CNFs/20% _TiO_2 (f).

The CNFs (as-synthesized) were purified to remove impurities and any remaining CuONPs. This step was important because the presence of CuONPs could affect the carbon nanofibers catalytic behaviour on TiO_2 under study. The FESEM pictures of the as-prepared/synthesized

CNFs and functionalized CNFs (F_CNFs), figures 2 and 3 show that the presence of traces of CuONPs were reduced to below observable limits. This shows that the CuONPs were effectively removed from the F_CNFs structures and that they are soluble in 55% HNO_3. The purified (functionalized) F_CNFs were fibrous in nature and the fibers were helical as shown by the TEM image figure 3.

It was also the same observation with CNFs and F_CNFs morphologies, FESEM, figure 2. The F_CNFs were slender in diameter averaging 81.59 nm, but varying between 14 and 134 nm.

TiO_2 – anatase which was synthesized had granular nanoparticles, figure 3(c). The average particle size was 7.2 nm and varied amid 3.0 – 13.4 nm. All the F_CNFs were totally covered with TiO_2 nanoparticles, figures 2. FESEM image clearly revealed TiO_2 nanoparticles lodged onto the surface of the F_CNFs, figure 2. *Gao et al* indicated that doping TiO_2 and CNFs by surfactant wrapping sol-gel method produced evenly covered CNTs with TiO_2 nanoparticles[54]. In this study, when the surfactant wrapping sol-gel method was modified hydrothermally, a fully coated F_CNFs were obtained.

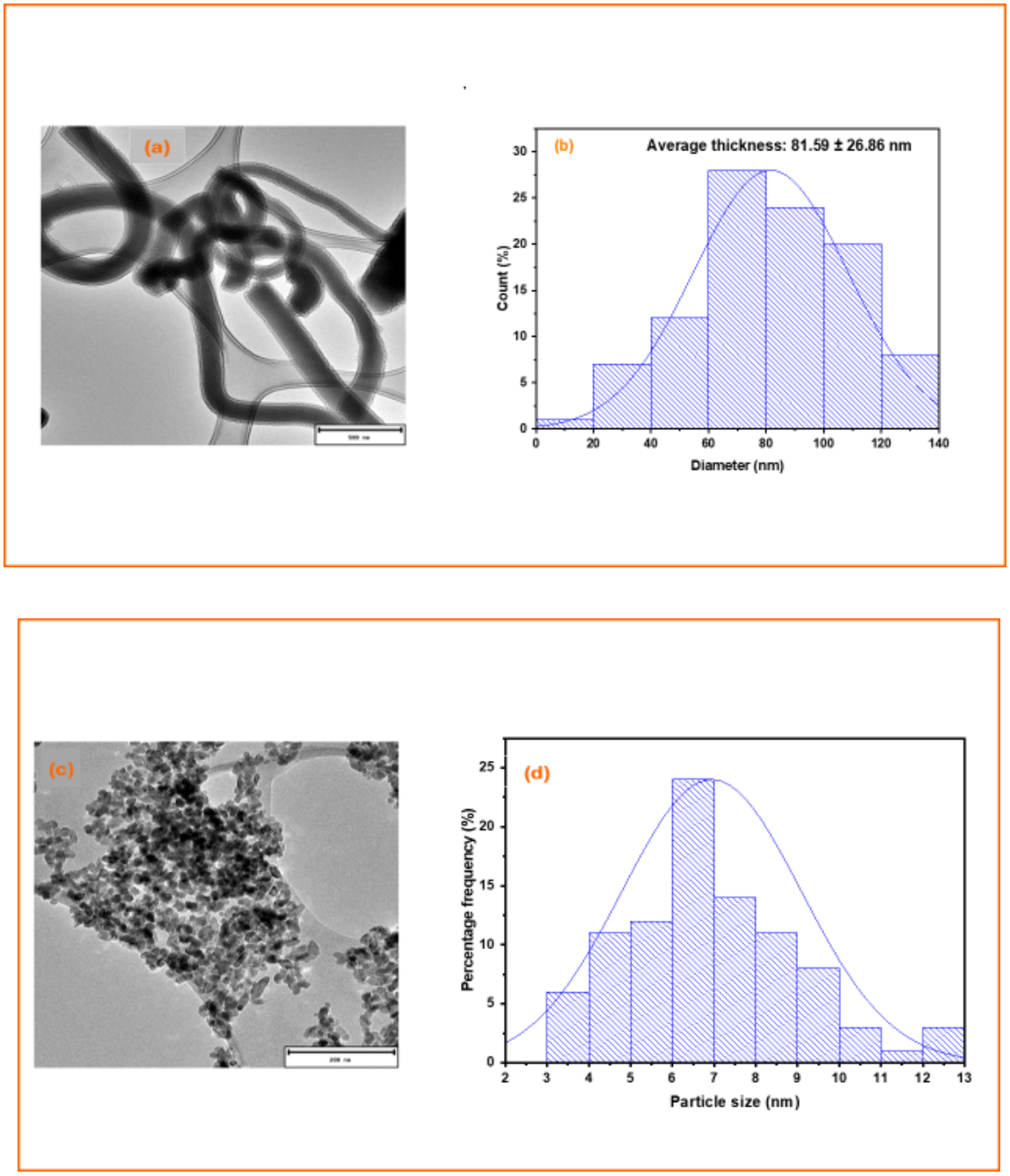

Fig. 3. TEM images: (a) Functionalized carbon nanofibers (F_CNFs), (b) The distribution diagram of the diameter of the F_CNFs (c) TiO_2 – anatase, (d) Particle size graph of TiO_2 – anatase.

The total covering of F_CNFs indicates that chemical interactions existed between the TiO_2 and F_CNFs. Adjacent closeness contact, resulting from chemical processes on F_CNFs/TiO_2 composites was identified as the source of electron transfer of similar structures thus giving rise to separation of the charges (electron-hole separation) [55]–[57].

Most of the physicochemical attributes of F_CNFs/TiO_2 composites are based on the interaction between F_CNFs and TiO_2 which successively rely upon the preparation procedures[54]. Moreover, clustering of TiO_2 nanoparticles on the surface of the functionalized carbon nanofibers (F_CNFs) provided proof that the F_CNFs contributed in the accumulation of the TiO_2 during the hydrolysis process [54].

The FESEM image, figure 2 and EDS scanning confirmed the existence of Ti, C and O in the structures. This is a confirmation that the CuONPs that was used in the preparation of the CNFs was effectively removed. Other studies have also shown that FESEM/SEM-EDS can be used to show the elemental distribution in the samples [58], [59].

The thermogravimetric analysis (TGA and DTA thermograms) plots presented in figure 4 was used in investigating the purity as well as the thermal stability of the CNFs together with F_CNFs/TiO_2 composites. The TGA of the as-synthesized CNFs are shown in figure 4. It is eminent from figure 4 that the use of 55% HNO_3 in purifying the as-synthesized CNFs effectively removed the residual CuONPs (catalyst) which could have been trapped in the CNFs during their synthesis. TGA graphs of the CuO Nanoparticles, CNFs and the functionalized CNFs at heating rates of 10ºC to 900ºC are shown in figure 4. The three mass-loss sections in the TGA spectra in figure 4 are the weight loss of 23% which occurred between 175ºC and 230ºC which resulted from thermal dehydration of the CuO Nanoparticles because water was the only solvent used in the synthesis. The as- synthesized CNFs had thermal decomposition at 185ºC to 530ºC corresponding to weight loss of 93%.

And the functionalized CNFs thermally decomposed in the range of 42ºC to 577ºC generating weight loss of 99%. However, functionalized CNFs had a higher thermal stability of 577ºC as compared to thermal stability of 530ºC for the as-synthesized CNFs. The difference in thermal stability of as-prepared carbon nanofibers and the functionalized carbon nanofibers indicates the presence of CuO Nanoparticles in trace amounts in the as-synthesized CNFs thus resulting in the low thermal stability of the CNFs as contrasted to the functionalized CNFs. It has been reported that the incorporation of functional groups during functionalization increases the thermal stability. This is because the functionalization process using acids introduces functional groups onto the surface of the CNFs hence deforming their graphicity [60]–[62]. The enhancement in thermal stability of the F_CNFs/TiO_2 composites was attributed to the covering of carbon from oxidation by the coated TiO_2 nanoparticles. Additionally, thermogravimetric analysis was used to estimate the weight fractions of TiO_2 in the composites. TiO_2 did not combust in air at temperatures below 900 ℃, Fig. 4(b).

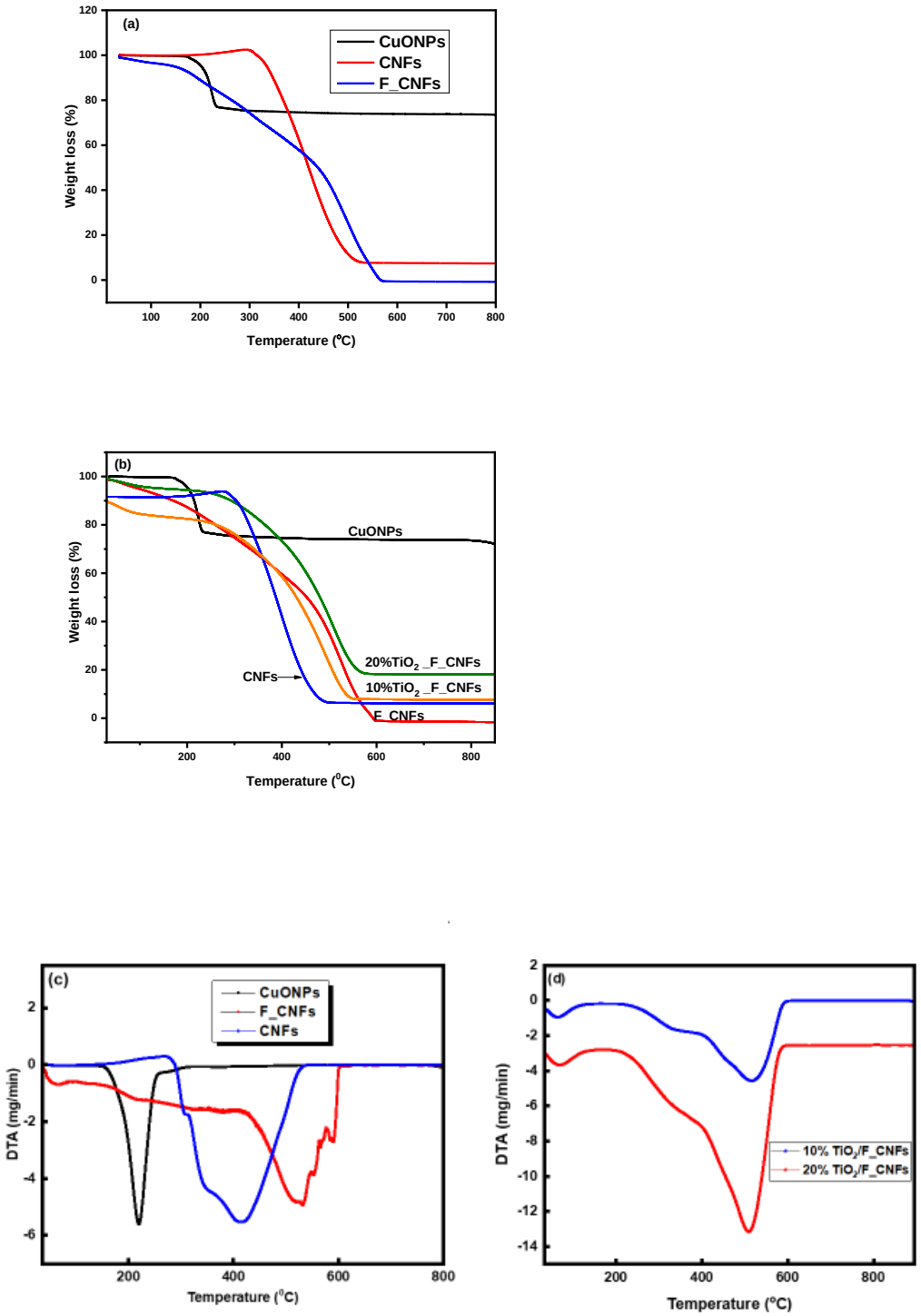

Fig. 4. TGA and DTA thermograms: (a) as-prepared CuO Nanoparticles, CNFs (as-synthesized CNFs) and functionalized CNFs (F_CNFs) (b) synthesized materials and the F_CNFs/TiO_2 composites (c) DTA of CuONPs, CNFs and F_CNFs (d) DTA of F_CNFs/TiO_2 composites.

Table 1. BET surface area, pore volume, pore diameter and $1_D/1_G$ ratio of the materials.

Sample	S_{BET} (m^2g^{-1})	PV (cm^3g^{-1})	PD (nm)	I_D/I_G	Reference
F_CNFs	32	0.091	22.6	0.87	Current study
TiO_2 - anatase	73	0.079	5.1		Current study
F_CNFs/20%TiO_2	126	0.273	10.7		Current study
TiO_2 - Dandelion	81	0.071	3.2		[63]
Degussa P25	49	_	_		[Sigma- Aldrich]

S_{BET}, PV, PD, 1_D /1_G: BET surface area, pore volume, and pore diameter, 1_D /1_G ratio respectively.

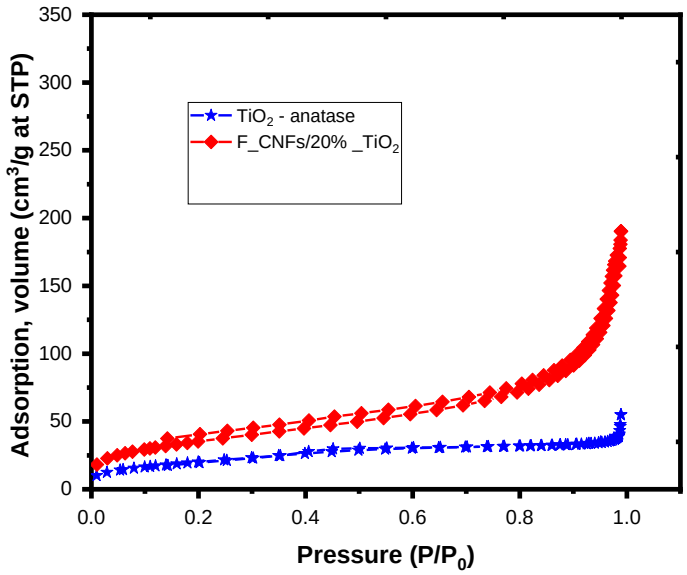

Fig. 5. (a) N_2 – adsorption – desorption isotherms of TiO_2-anatase, F_ CNFs/20%_TiO_2.

Therefore, the material that was combusted was the F_CNFs while the thermal stable residues were TiO_2. The obtained values were close to the predetermined ones indicating that about 20% of the F_CNFs/20%TiO_2 and 10% of the F_CNFs/10%TiO_2 samples consisted of 20%TiO_2 and 10%TiO_2 respectively[64].

4.3.2 Nitrogen adsorption analysis

The Brunaauer – Emmett – Teller (BET) surface area, pore volume and pore diameter (porous structure) for the materials were studied using the nitrogen adsorption method[65]. When the F_CNFs (surface area, 32 m^2/g) were composited with TiO_2 (surface area, 73 m^2/g), the specific surface of F_CNFs/TiO_2 composite (126 m^2/g) was higher than the individual entities. This is because the specific surface of the composite increased with compositing TiO_2 with F_CNFs. This observation suggests that the presence of F_CNFs during the hydrolysis of TiO_2 lowered the agglomeration of TiO_2 nanoparticles thus the increased surface area[66]. Also, the pore volume of the F_CNFs/TiO_2 composite was higher than the pore volume of TiO_2 – anatase and TiO_2 – Dandelion (Table 1). This resulted from doping of TiO_2 with F_CNFs and the functionalization of the CNFs [50]. TiO_2 – A (surface area, 73 m^2/g) which was prepared by the surfactant wrapping sol-gel/hydrothermal procedure compared well with other previous studies [66], [67].

One of the benefits of incorporating CNFs intoTiO_2 matrix is the improvement of the surface area. Thus, BET investigation was conducted to analyse the surface area of the materials as presented in Table 1 and Fig. 5. The increase in linearity of the adsorption isotherms profiles was identified in the corresponding pressure (P/P^o) range 0.30 to 0.85. This correlates with the mesoporous structure of the nanostructures [68]. The process lag curves profiles in the isotherms were categorized as type IV which is in conformity with the International Union of Pure and Applied Chemistry (IUPAC) classification characterizing the nanostructures as mesopores [69].

Raman spectroscopy was employed to investigate the graphiticity of the F_CNFs. The D-band at 1384 cm^{-1} is a defects identification on the F_CNFs, and G-band, 1590 $cm^{-1}$is C-C stretching of the F_CNFs. Also, it was used in confirming the TiO_2 – A presence in the

F_CNFs/TiO_2 composites and to study the effect of doping TiO_2 with F_CNFs in relation to crystallinity. The Raman spectrum in figure 6 has four well defined peaks at Raman shift 144, 397, 514, also 643 cm^{-1} and indexed (E_g), (B_{1g}), (A_{1g}), together with (E_g), accordingly [70], [71].

The four modes were also obtained on the spectra of the composites in smaller amounts thereby confirming the presence of TiO_2 – A in the composites, figure 6 (b).

Another important observation was that the most intense TiO_2 peak (E_g) for all the composites was blue shifted besides being broader as compared to the TiO_2 – anatase (unbound) (142 to 147 cm^{-1}). The positions and broadening of Raman peaks is a characteristic of the nanomaterials and studies show that it's associated with the size and defects in the structure, the experimental conditions and the laser – induced local heating effect upon material under investigation [70]–[72]. Since all the laser Raman analyses in this work were carried out under similar conditions, then the blue shifting and broadening of the peaks resulted from phonon confinement or surface pressure [58]. Besides, other related studies have reported similar observations such as composites of titanium nanotubes and graphene oxide. The effect was proposed to suggest the existence of strong chemical interactions between TiO_2 and F_CNFs[73]. Chemical interaction between TiO_2 and F_CNFs was expected because it helps in increasing charge separation in the F_CNFs/TiO_2 composites, thus this effect is an indication that the composites photocatalytic ability was enhanced.

(a)

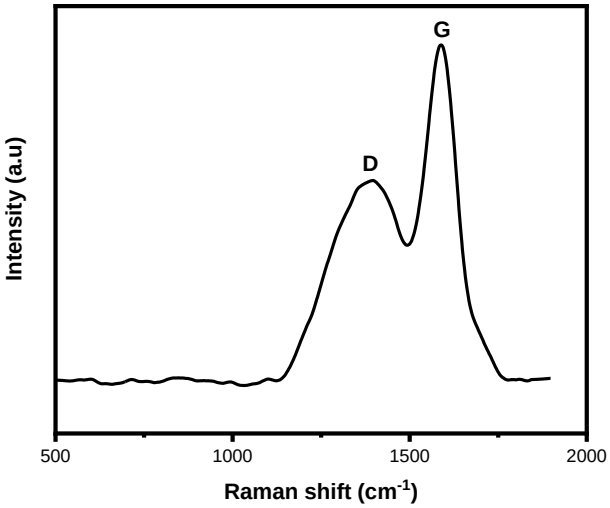

(b)

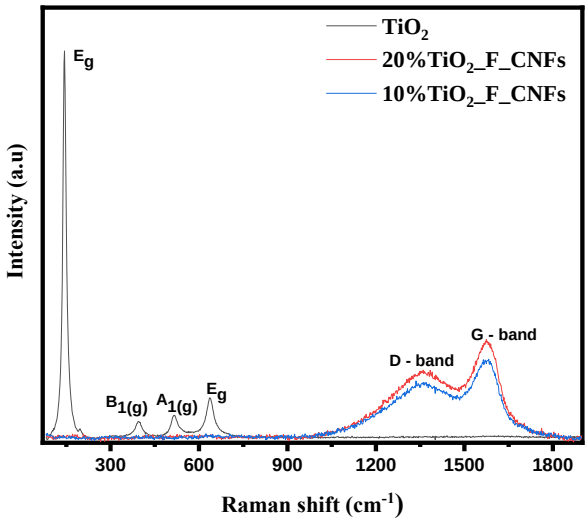

Fig. 6. Raman spectra of (a) F_CNFs (b) TiO_2 – A and TiO_2/F_CNFs composites.

TiO_2 – anatase and F_CNFs/TiO_2 composite were analysed by XRD. The characteristic peaks of TiO_2 – A (TiO_2 – anatase) also F_CNFs/TiO_2 composite are shown in Fig. 7. Some of the

peaks of the F_CNFs were not noticed clearly on the PXRD patterns of the F_CNFs/TiO_2 sample because of an extention of the intense (101) TiO_2 – anatase absoption with (002) absorption of the F_CNFs, substantial dispersion from TiO_2 – anatase and the considerable distinction in the mass of TiO_2 – anatase in relation to the mass of F_CNFs in the F_CNFs/TiO_2 material [74], [75]. After achieving clean conditions and water resources, the photocatalytic production of hydrogen is feasible. Similar studies show that the crystallinity of the catalysts affects their photonic qualities [76].

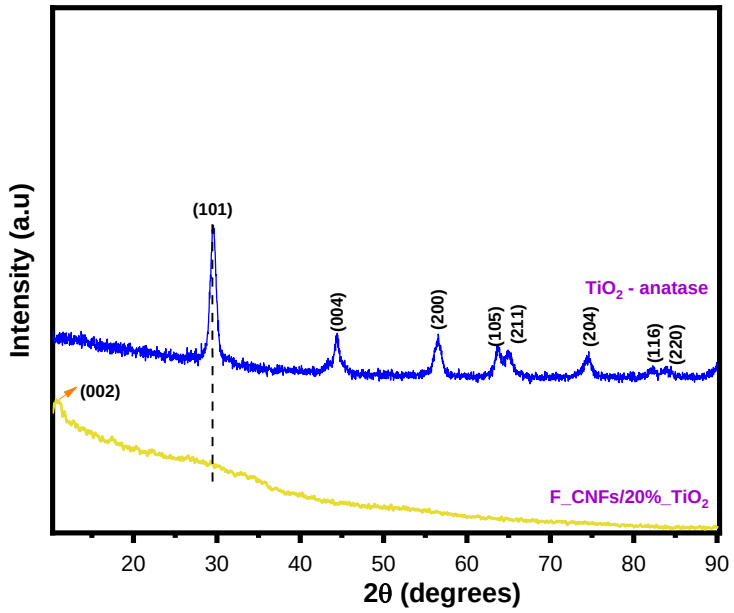

Fig. 7. PXRD spectra of TiO_2 – anatase, and F_CNFs/20%_TiO_2 composite.

The FTIR spectra of TiO_2 – anatase, F_CNFs and the composites are presented in figure 8. The FTIR spectra of the F_CNFs and the composites have a strong band at 1100 cm^{-1} which is associated with C–O stretching vibrations. The IR peak at 3438 cm^{-1} is the O-H stretching vibrations. The remainder of the peaks could be the vibrations of aliphatic C-H groups in the range of 3000-2800 cm^{-1}, 2000-1800 cm^{-1}, 1410-1395 cm^{-1}, and 820-790 cm^{-1}. The peak at

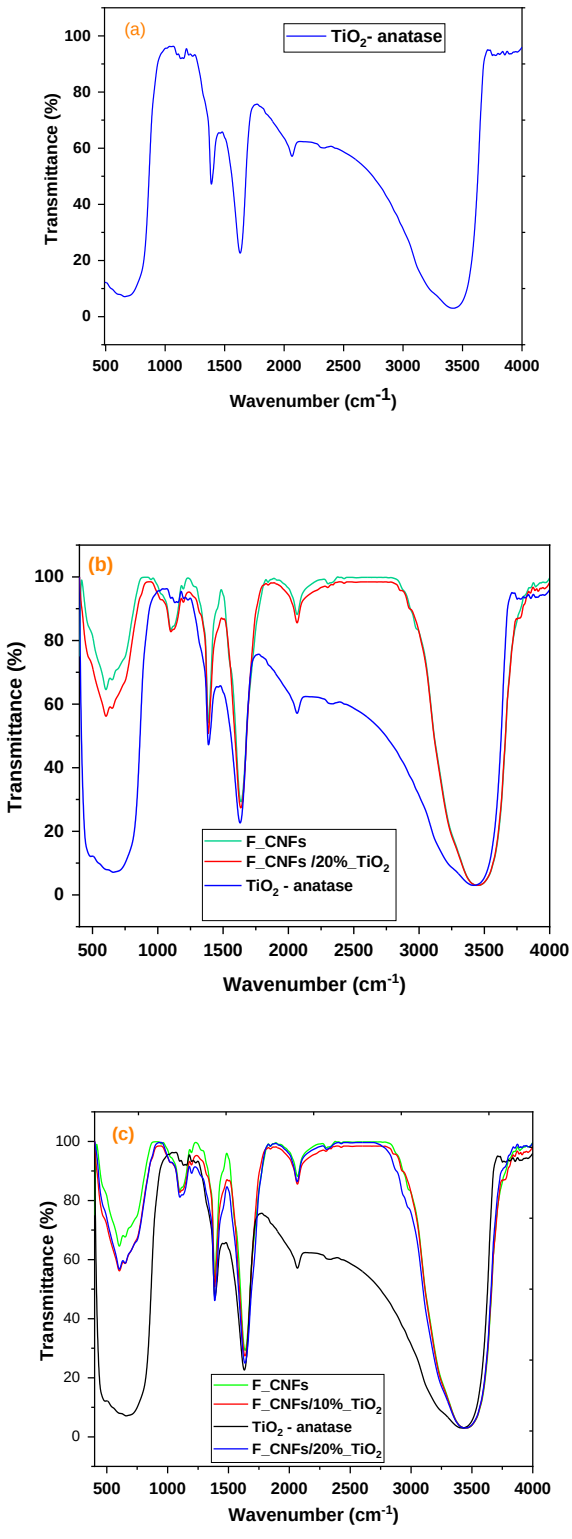

Fig. 8. The FTIR spectra of (a) TiO_2 – anatase, (b- c) F_CNFs, TiO_2 – anatase, and F_CNFs/TiO_2 composites.

3400 cm^{-1} is as a result of adsorbed water molecules. TiO_2 characteristic peak is normally in the range of 690 to 800 cm^{-1} and the broad peak which appears below 1000 cm^{-1} is as a result of two peaks [77]. The peaks from the F_CNFs and the composites at 3230, 2920, 1720, 1636, and 1330 correspond to the existence of O-H, C-H, C=O, C=C and C-O-C accordingly.

The peak at 1104 cm^{-1} for TiO_2 is Ti – O – C indicating the conjugation effect of F_CNFs and TiO_2 [78].

To explore the confinement, movement and transfer properties of the photo induced charge carriers (electron – hole pair), it was imperative to study photoluminescence of the TiO_2 – anatase and F_CNFs/TiO_2 composites. Photoluminescence studies based on photocatalysts have been reported and employed in the study of charge carriers [56], [79]. The excitation wavelengths between 350 nm to 500 nm was used and the characteristic features of charge carrier recombination rate of TiO_2 – anatase are shown in figure 9. The results from this study conform to other related studies [79].

TiO_2 – anatase had higher emission peak than the F_CNFs and F_CNFs/TiO_2 composites. The reduced intensity of the F_CNFs and the composites is as a result of limited recombination of electron – hole pairs showing that the F_CNFs had enhanced the lifetime of the charge carriers (electron – hole pair) [54], [71], [75], [79], [80]. Therefore, the higher the loading of TiO_2 on F_CNFs the better the charge separation.

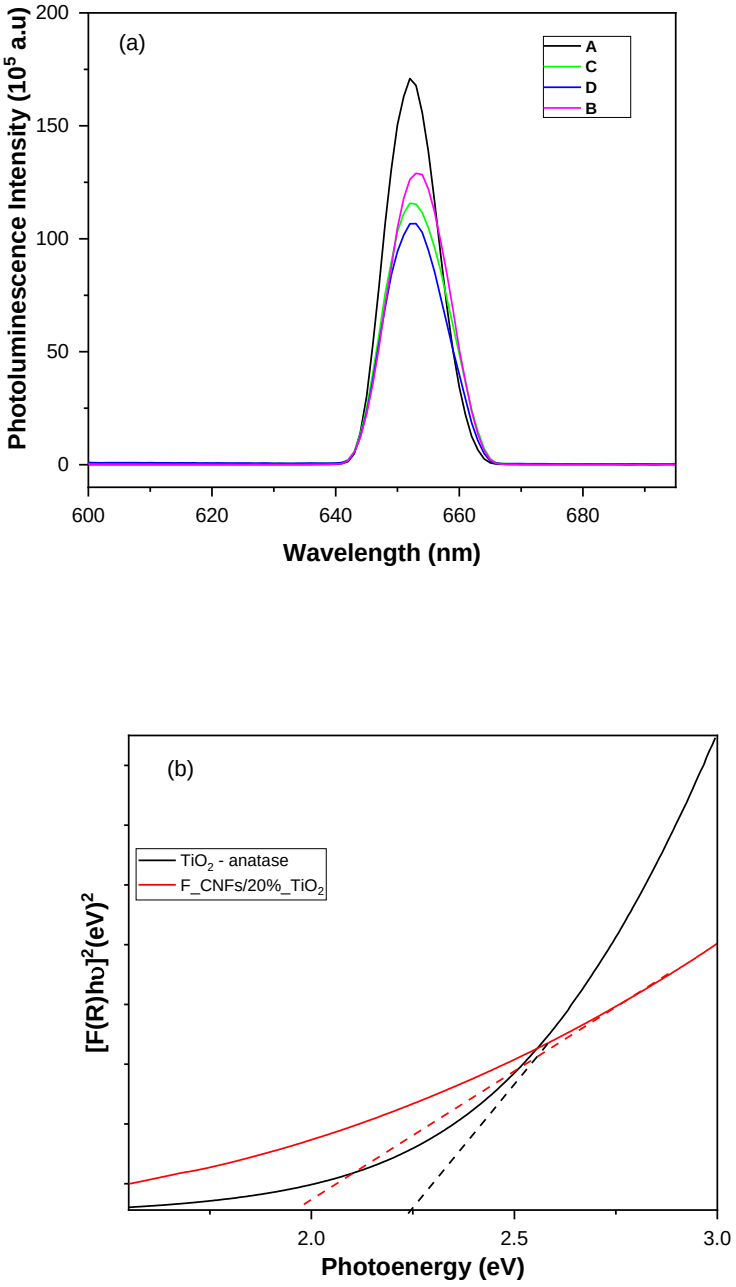

Fig. 9. (a) Photoluminescence spectra of TiO_2 – anatase and F_CNFs/TiO_2 composites; TiO_2– anatase (A), F_CNFs (B), 10% _TiO_2/F_CNFs (C), 20% _TiO_2/F_CNFs (D), and (b) The Band gap (E_g) energies (eV) of TiO_2 – anatase and F_CNFs/20%_TiO_2 composite.

Table 2. Summary of the Band gap (E_g) energies (eV) of TiO_2 phases and composite.

Sample	Energy (eV)	Reference
TiO_2 – Degussa P25	3.15	[81]
TiO_2 – Anatase	3.2	[82]
TiO_2 – Anatase	2.25	Current work and [83]
F_CNFs/20%_TiO_2	1.97	Current work

After verifying that doping of TiO_2 with F_CNFs reduced the recombination frequency of the electron-hole pairs induced during photoluminescence studies, figure 9, UV-vis DRS studies were performed to enlighten the behaviour of the composites towards visible light. The Tauc's plot obtained from UV-Visible Diffuse Reflectance Spectroscopy, UV-Vis DRS spectrum of the F_CNFs/20%_TiO_2 composite (1.97 eV) was not the same as that of TiO_2 – anatase (2.25 eV) signifying that F_CNFs had positive impact on the band gap of the F_CNFs/20%_TiO_2 composite (1.97 eV), Table 2 and figure 9 (b). This shows that the band gap energy of the F_CNFs/20%_TiO_2 composite was significantly reduced suggesting that the composite will have better photocatalytic activity as compared to TiO_2 – Anatase (3.2 eV), Table 2 [81], [82]. Also, the methods of preparation of TiO_2 – anatase can be used to get TiO_2 – anatase of different band gap energies [83].

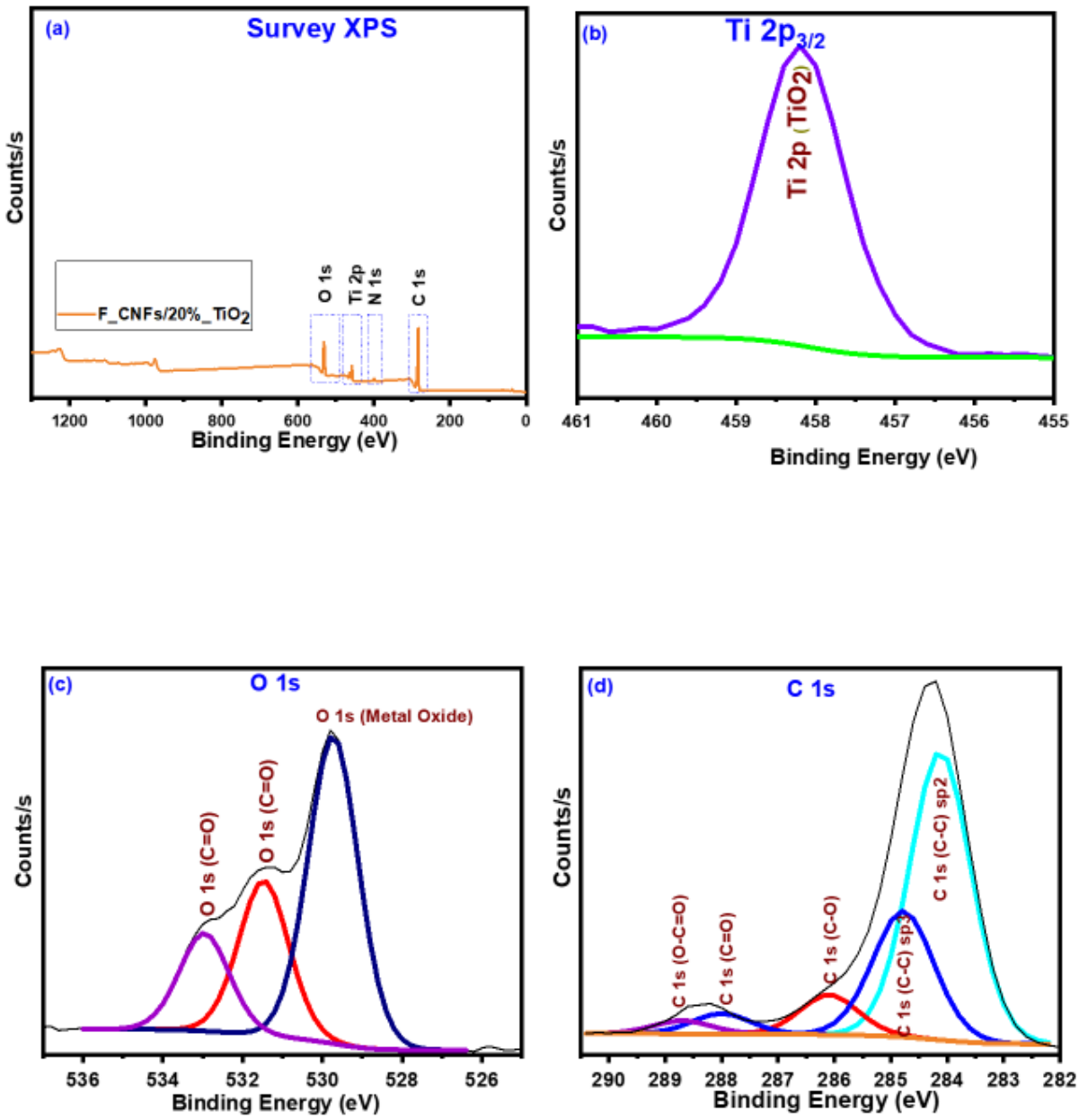

Fig. 10. X – ray photoelectron spectroscopy, XPS examination of F_CNFs/TiO_2.

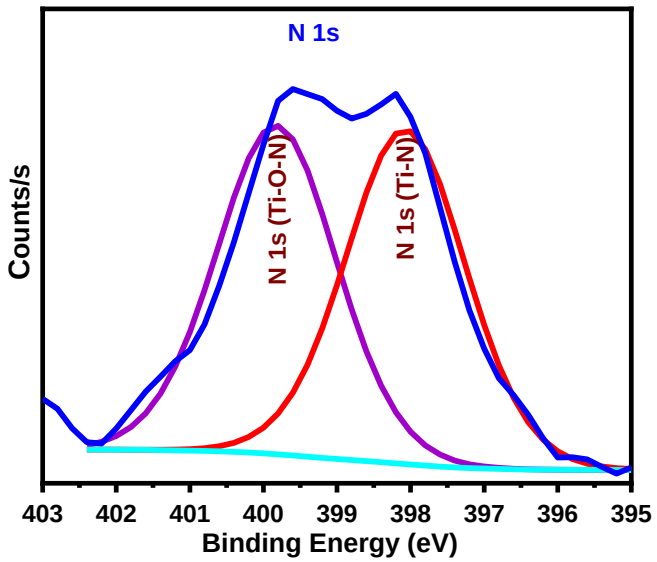

Fig. 11. XPS spectrum of nitrogen.

The electronic configurations of the elements in F_CNFs/TiO_2, were investigated by X – ray photoelectron spectroscopy, XPS and the results are shown in figure 10, and figure 11. Clearly, the XPS analysis graph in Fig. 10 (a) presents four elements, C, Ti, O, and N. In figure 10 (b), Ti 2p spectrum of binding energy, 458.20 eV for $2p_{3/2}$ is as a result of the titanium TiO_2 presence [84]. The presence of N, lower intensity of N 1s peak in Fig. 11 could be as a result of a small contamination of ammonia solution used in the synthesis of F_CNFs/20% _TiO_2, and TiO_2 – anatase. In figure 10(c), the O 1s peaks positioned at 531.6 eV, 533.1 eV, and 529.7 eV are consistent with the adsorbed oxygen [85] whereas figure 11 displays the binding energy of N 1s with the peaks at 398.1 eV and 399.8 eV. At 398.1 eV, we find a weaker peak which can be assigned to Ti – N bond signifying some absorption of nitrogen atoms into the F_CNFs/TiO_2 matrix [86], [87]. The peaks located at 398.1 eV and 399.8 eV are N 1s. They hint to the presence of small quantities of –NH and $–NH_3^+$ respectively as illustrated in XPS analysis spectrum, Fig. 10 (a) and the XPS spectrum of nitrogen Fig. 11 [88], [89]. The XPS analysis Fig. 10 (a) identifies carbon as one of the

elements present in the materials. The XPS peak, conforming to C 1s is clarified into 5 peaks, Fig. 10 (d). The bonds, C=C which are positioned around 284.7 eV point to the existence of C in the CNFs or graphene materials [90], [91]. The peaks positioned at 286.1 eV, 2.88 eV, and 288.7 eV are associated with C-O, C=O and O-C=O accordingly and moreover validates the efficient blending of the F_CNFs into the F_CNFs/20% _TiO_2 composite, Fig. 10 (d) [88].

4.3.3 Photocatalytic studies

All the photocatalysts were assessed in the H_2 production reaction using water. The cumulative hydrogen production analysis of the photocatalysts is in Fig. 12. The assessment of the catalysts was based on the materials (support), loading (efficiency) and sacrificial agent used in the study. The first category consists of TiO_2 (TiO_2 - anatase and TiO_2 – P25). The second category is the loading of TiO_2 on the functionalized CNFs (F_CNFs) thereby attaining F_CNFs/10% _TiO_2 and F_CNFs/20% _TiO_2. In the third category of photocatalysts, we have the support; F_CNFs/TiO_2 – composited with CH_3OH (methanol) and a repeat of CH_3OH - (R). In general, F_CNFs/20% _TiO_2/10%_CH_3OH – (R) was identified as the most active photocatalyst. It generated more H_2 as compared to the second group of photocatalysts in this study, F_CNFs/20% _TiO_2. Moreover, F_CNFs/20% _TiO_2/10%_CH_3OH - (R) produced more H_2 than the commercial TiO_2 (TiO_2 – P25), Table 3 and Fig. 12.

The most active photocatalyst, F_CNFs/20% _TiO_2/10%_CH_3OH – (R), had a loading of 20% by weight of TiO_2 - anatase coated on the F_CNFs as verified by the Field emission scanning electron microscopy, FESEM Fig. 2, and the Transmission electron microscopy, TEM images in Fig. 3. Further, the catalyst was evaluated in a reaction for 6 h, and produced no signs of deactivation but increased H_2 production as shown in Fig. 13.

Table 3. Outline of the photocatalytic activity of photocatalysts for water splitting.

Photocatalyst	Reactant solution & sacrificial reagents	Light source	Activity	Reference
Cu/TiO_2 nanorods	Methanol, 20 vol %	300 W Xe lamp	1023.8 μmol g^{-1} h^{-1}	[92]
Rh-Nb/TiO_2 NRs	Methanol, 10 vol %	300 W Xe lamp	7850 μmol g^{-1} h^{-1}	[93]
rGO/TiO_2	Methanol	300 W Xe lamp	149 μmol g^{-1} h^{-1}	[94]
3 wt% Ni-TiO_2/CdS	Ethanol, 25 wt%	300 W Xe lamp, 420 cut off filter	33.63 μmol /g-cat^{-1} h^{-1}	[95]
Ru/CdS-ZnS	Formic acid, methanol	300 W Xe lamp	266 mmol/m^2 h	[96]

Au/TiO_2	Ethanol	4 UV-LED lights, 12 W each	15.8 µmol /min g-cat.	[97]
SiFe co doped TiO_2	540 ml distilled H_2O, 60 ml ethanol	500 W (Xe lamp)	320 µmol g^{-1} h^{-1}	[98]
BN/1.5% Cs_2CO_3/TiO_2	Methanol	500 W halogen lamp	2638 µmol g^{-1} h^{-1}	[99]
1.5% Cs_2CO_3/TiO_2	Methanol	500 W halogen lamp	1642 µmol g^{-1} h^{-1}	[99]
BCET2	Methanol	500 W linear halogen lamp	850 µmol g^{-1} h^{-1}	[100]
CET2	Methanol	500 W linear halogen lamp	313 µmol g^{-1} h^{-1}	[100]

(0D)CT-25		(Xe lamp)	68000 μmol g^{-1} h^{-1}	[101]
GaN:ZnO /Mn_3O_4.Rh/Cr_2O_3	Distilled H_2O NaI	(Xe lamp)	20 μmol g^{-1} h^{-1}	[98]
F_CNFs/20%_TiO_2	Distilled H_2O	450 W (Xe lamp)	7203.5 μmol g^{-1} h^{-1}	Current work
TiO_2	Distilled H_2O 10% methanol	300 W (Xe lamp)	42.00 μmol g^{-1} h^{-1}	[98][102]
Mesoporous CNTs/TiO_2	Methanol	200 W super pressure Hg lamp	TiO_2 nanofibers 880 μmol g^{-1} h^{-1} TiO_2 88.2 μmol g^{-1} h^{-1} CNT/TiO_2 1218 μmol g^{-1} h^{-1} Pt/CNT/TiO_2 2940 μmol g^{-1} h^{-1}	[103]

CNT/TiO_2NPs	Methanol	UV light (365 nm LED)	TiO_2/FSWCNTs 254 μmol g^{-1} h^{-1} Pt-TiO_2/FSWCNTs 355 μmol g^{-1} h^{-1}	[104]
F_CNFs/20%_TiO_2/10%_CH_3OH	Distilled H_2O 10% methanol	450 W	50912 μmol g^{-1} h^{-1}	Current work
TiO_2 - P25	Distilled H_2O	450 W	126.39 μmol g^{-1} h^{-1}	Current work
TiO_2 - anatase	Distilled H_2O	450 W	119.39 μmol g^{-1} h^{-1}	Current work

The increament produced by TiO_2 – carbon structures when compared to pure TiO_2 (TiO_2 – anatase and TiO_2 – P25) has come about because of the increase in the surface area and reduction in the recombination rate of the charged pairs, the electron – hole recombination [105]. Leary and Westwood research and others also compared TiO_2 – carbon materials used as photocatalysts to a pure TiO_2 photocatalyst under similar experimental environment such as mass [105] as it was also done in this research. Table 3, further confirms the findings.

Several studies have been performed on TiO_2/C composites for the production of hydrogen [106]–[109]. However, comparison of the results has been a challenge because factors such as the quantity of TiO_2, the sacrificial agents (organic and/or inorganic) used and their

concentrations, the source and intensity of power used among others are hindering the comparison of the results [34]–[36]. Thus, its conceivably more appropriate to compare the results simultaneously with the experimental conditions and further incorporate a standard catalyst, such as commercial TiO_2 (TiO_2 – P25), as a reference catalyst [37]. In this research, the hydrogen produced by the most active photocatalyst (methanol – (R) was more than 100 fold the amount produced by TiO_2 - P25. Another observation was that the as-synthesized TiO_2 – anatase, F_CNFs/10% _TiO_2, and P25 produced more or less the same amount of hydrogen, Fig. 12 (a). These results and the comparisons evidence the importance of incorporating appropriate controls in the synthesis and photocatalysis for better interpretation of the results.

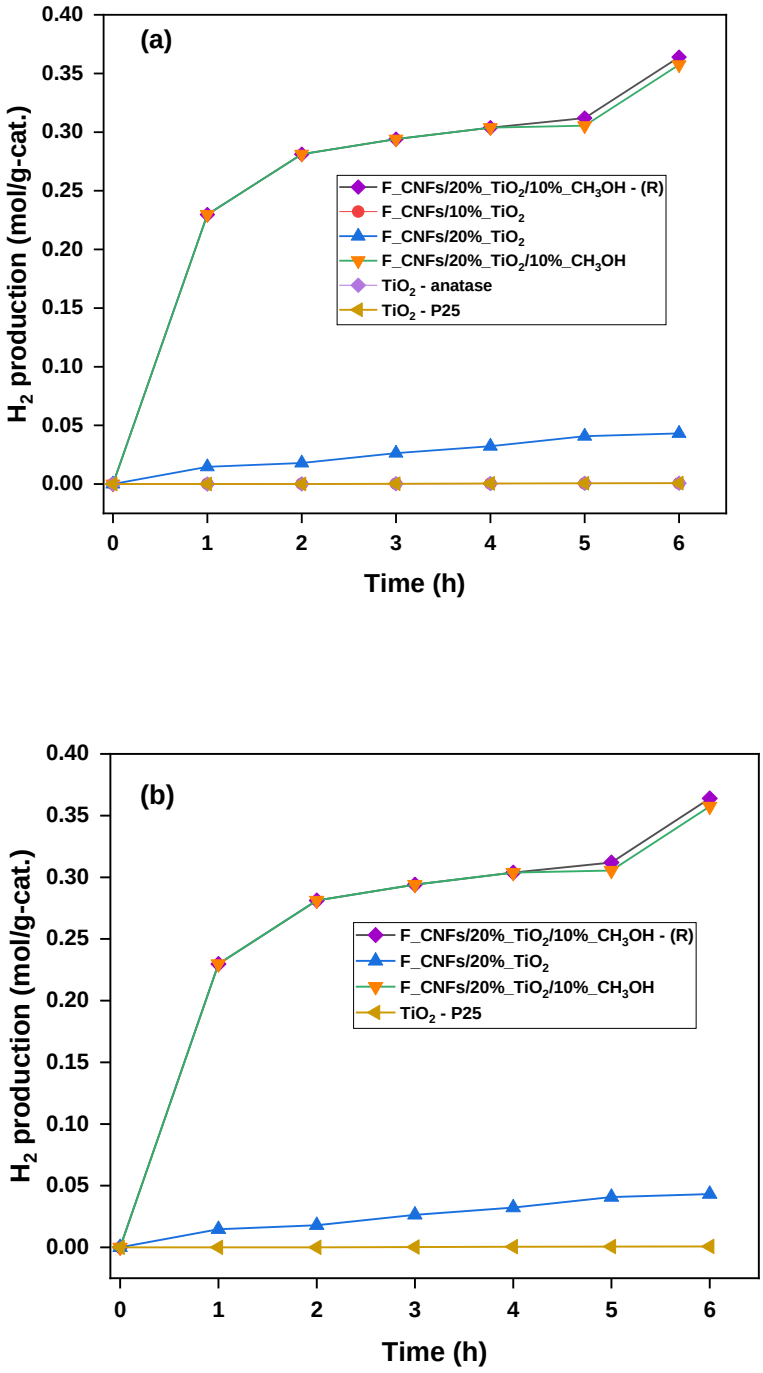

Fig. 12. The H_2 production in 6 h of reaction for the photocatalysts; (a) TiO_2 - P25 (Commercial TiO_2), TiO_2 – anatase, F_CNFs/20%_TiO_2/10%_CH_3OH, F_CNFs/20% _TiO_2, F_CNFs/10%_TiO_2, F_CNFs/20%_TiO_2/10%_CH_3OH (Repeat - R), (b) The comparison of the most active photocatalysts; F_CNFs/20%_TiO_2/10%_CH_3OH - (R), F_CNFs/20% _TiO_2, F_CNFs/20%_TiO_2/10%_CH_3OH, TiO_2 - P25.

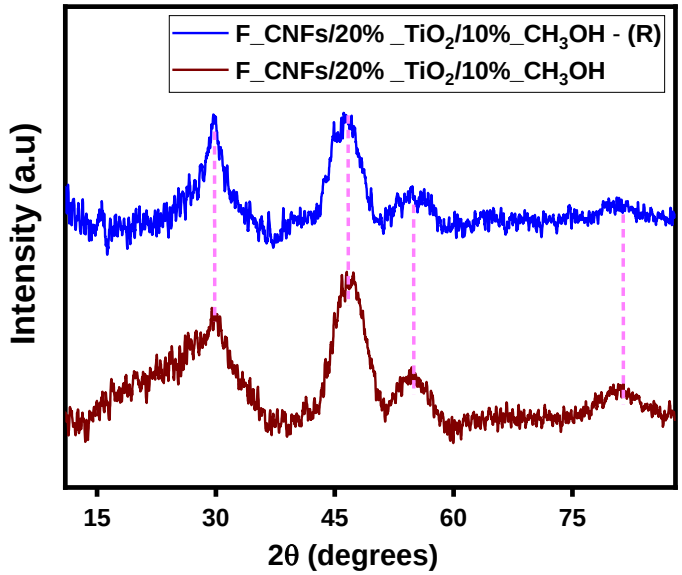

Fig. 13. The effect of stability of the most active photocatalyst, F_CNFs/20%_TiO_2/10%_CH_3OH, before analysis, and F_CNFs/20%_TiO_2/10%_CH_3OH – (R) – after analysis, XRD spectra.

4.4 Conclusion

The synthesis and the characterization of TiO_2 – anatase, F_CNFs, and the F_CNFs/TiO_2 composites have been achieved in this study. The incorporation of the F_CNFs into the titania structure increased the BET surface area of the TiO_2 – anatase from 73 m^2g^{-1} to 126 m^2g^{-1}, F_CNFs/20% _TiO_2. The pore volume of the materials further increased but the pore diameter of the composites lessened. This observation indicates that the F_CNFs can effectively tune the morphology of TiO_2 for greater surface area, larger pore volume, and lower pore diameters and therefore increase the photocatalytic properties of the F_CNFs/TiO_2 photocatalysts. The Raman, FTIR, FESEM techniques revealed a very homogeneous distribution of TiO_2 nanoparticles on the F_CNFs. The XPS analysis verified the existence of all the elements as Ti, O, C, N, and their corresponding electronic configurations (chemical

states). This was important for understanding the principles of photocatalytic water splitting with particular interest on the use of sacrificial agent, methanol. This is of importance to this study because the chemical structures, surface area, quantities, chemical states, morphology, particle sizes, functional groups play pivotal roles in photocatalytic water splitting processes. All the carbon containing samples had a change in wavelengths after UV-Vis light absorption to the visible region of the electromagnetic spectrum (TiO_2 – 3.20 eV to 1.97 eV – F_CNFs/20% _TiO_2).

The photocatalysts were tested for hydrogen evolution using water, and the most active photocatalyst, F_CNFs/20% _TiO_2/10%_CH_3OH – (R) had greater hydrogen production of 0.36 mol/g-catalyst after 6 hours as compared to TiO_2 – P25, the commercial TiO_2, 0.00076 mol/g-catalyst after 6 hours. In addition, the photocatalyst, F_CNFs/20% _TiO_2/10%_CH_3OH – (R) was stable even after 6 h use and therefore can be used for longer periods or recycled for economic purposes. The outcome of this study evidence the important role of compositing titania with F_CNFs and the use of sacrificial agent, methanol under mild conditions for effective photocatalytic water splitting. Thus, this study prefers the use of catalysts as substantive results were obtained from the use of the synthesized photocatalysts with distilled water. The incorporation of sacrificial reagents such as methanol in water splitting may be a threat to the environment.

Acknowledgement

We are grateful to the University of the Witwatersrand for financial support.

Conflicts of interest

We, the authors have no conflicts of interest to declare.

APPENDIX A

XPS data

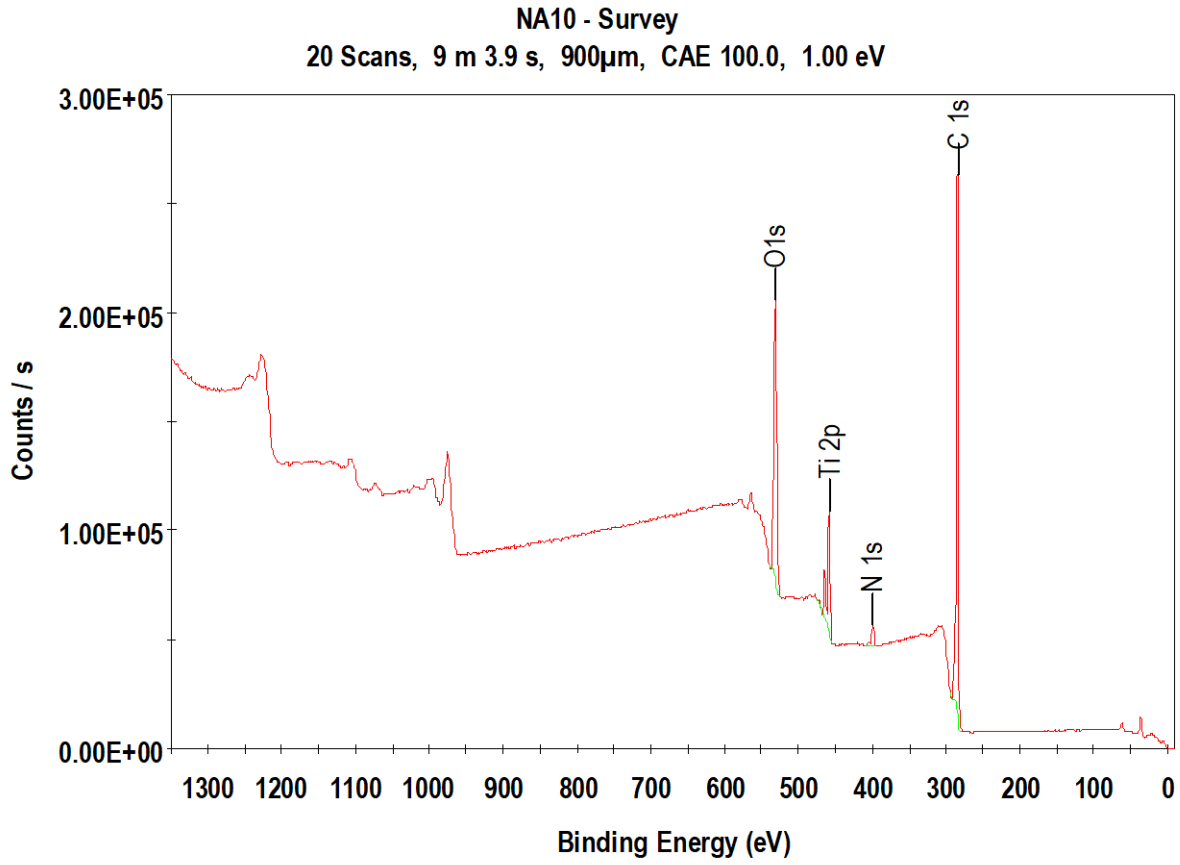

NA10

Elemental ID and Quantification

Name	*Peak BE*	*Atomic %*
C 1s	284.4	74.6
O 1s	531.4	20.3
Ti 2p	458.2	3.2
N 1s	399.2	2.0

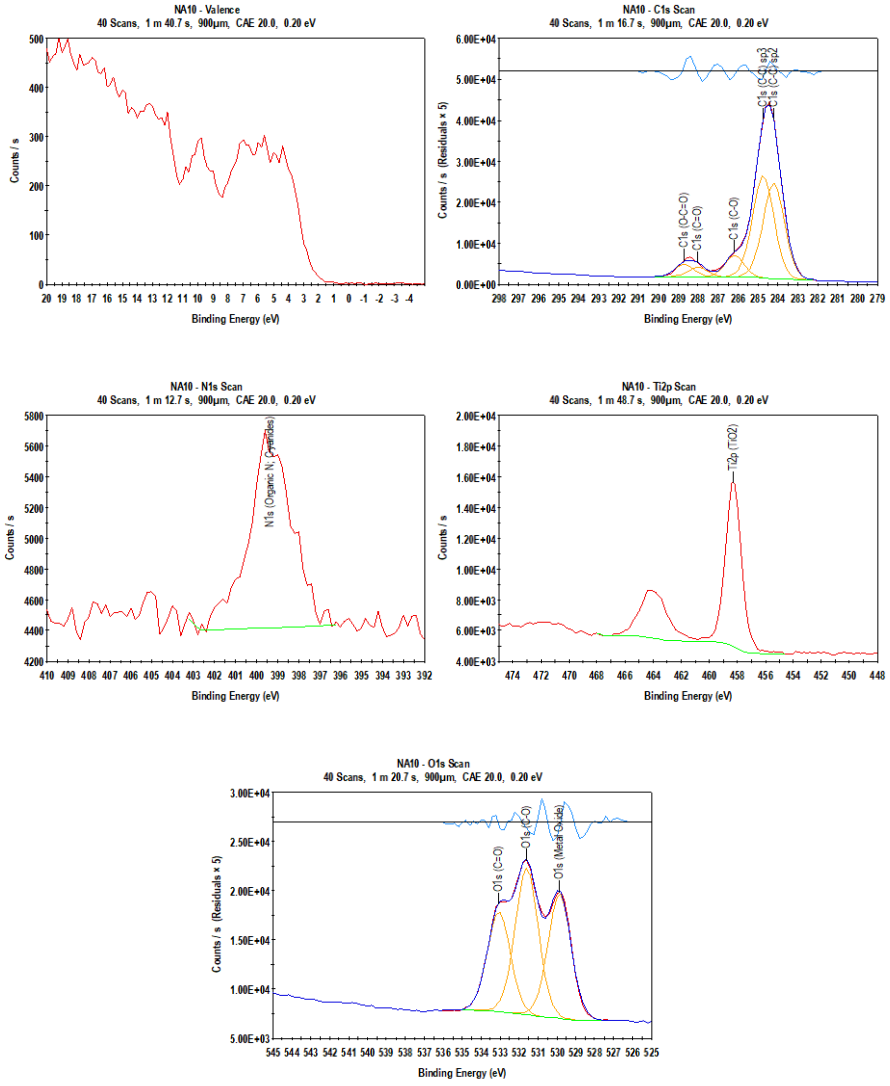

NA10

Chemical ID and Quantification

Name	*Peak BE*	*FWHM eV*	*Atomic %*
C1s (C-C) sp2	284.2	1.2	30.0
C1s (C-C) sp3	284.7	1.2	32.1
C1s (C-O)	286.2	1.1	6.1
C1s (C=O)	288.0	1.1	2.7
C1s (O-C=O)	288.7	1.1	3.4
N1s (Organic N; Cyanides)	399.4	2.0	1.8
Ti2p (TiO2)	458.3	1.3	3.5
O1s (Metal Oxide)	529.9	1.4	6.9
O1s (C-O)	531.6	1.4	8.1
O1s (C=O)	533.1	1.4	5.5

The survey spectrum shows that O 1s peaks which are located at 531.6 eV, 533.1 eV, and 529.9 eV correspond to the adsorbed oxygen while the weaker peak positioned at 399.4 eV can be assigned to the Ti – N bond which shows that nitrogen atoms have been absorbed into the lattice of F_CNFs/TiO_2 composite. The N 1s peak, 399.4 eV point to the presence of – NH_3^+ in all the composite since ammonia solution was used in the synthesis as seen in the XPS survey spectrum.

One of the elements shown in XPS survey is carbon, C 1s. The C=C bonds located in the region 284.7 eV correspond to C in F_CNFs or graphene structures.

H_2 production data

Sample ID: P25

Signal,Signal,Peak,Reten.,Area,Height,Area,Height,W05
No.,Name,No.,time,[mV.s],[mV],[%],[%],[min.]
1,INT9 - 1,1,0.876,58.15,3.59,26.6,28.1,0.244
1,INT9 - 1,2,9.19,45.63,2.9,20.9,22.7,0.24
1,INT9 - 1,3,14.8,37.54,2.19,17.2,17.1,0.264
1,INT9 - 1,4,20.4,25.95,1.62,11.9,12.7,0.248
1,INT9 - 1,5,37.4,27.35,1.41,12.5,11.1,0.284
1,INT9 - 1,6,38.8,23.84,1.07,10.9,8.4,0.336
1,INT9 - 1,,Total,218.5,12.8,100,100

Signal,Signal,Peak,Reten.,W05,Asymmetry,Capacity,Efficiency,Eff./l,Resolution,Reten.Index
No.,Name,No.,time,[min.],[-],[-],[th. pl.],[t.p./m],[-],[-]
1,INT9 - 1,1,0.876,0.244,2.47,0,7e+001,1e+003,-,0
1,INT9 - 1,2,9.19,0.24,2.56,0,8e+003,2e+005,20.3,0
1,INT9 - 1,3,14.8,0.264,2.38,0,2e+004,3e+005,13.2,0

1,INT9 - 1,4,20.4,0.248,2.79,0,4e+004,7e+005,12.8,0

1,INT9 - 1,5,37.4,0.284,2.68,0,1e+005,2e+006,37.9,0

1,INT9 - 1,6,38.8,0.336,2.64,0,7e+004,1e+006,2.51,0

,,Sample ID,Sample,Sample Amount,Sample Dilution,Injection Volume,ISTD Amount,Chromatogram Amount,Unretained Peak Time,Column Length,Noise,ASTM Noise,6-Sigma Noise,Drift,,,,,,

,,,,,,,,,,,,,,,Reten. Time,Response,Amount,Amount,Peak,Compound,

,,,,,,,,,,,,,,,[min],,[N/A],[%],Type,Name,

Thermogravimetric Analysis data

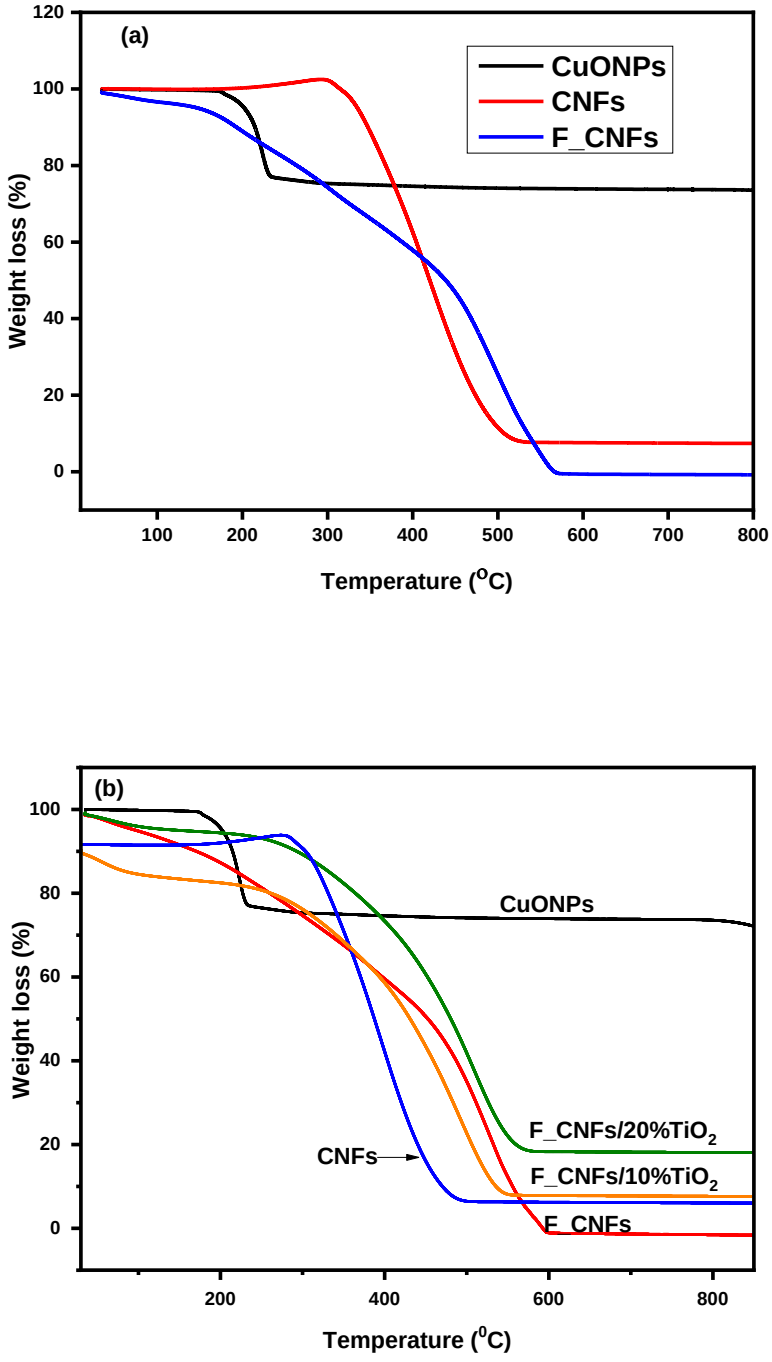

Fig. 1. TGA (a) as-prepared CuO Nanoparticles, CNFs (as-synthesized) and functionalized CNFs (F_CNFs) (b) synthesized materials and the TiO_2/F_CNFs composites.

Field Emission Scanning Electron Microscopy, FESEM

(a)

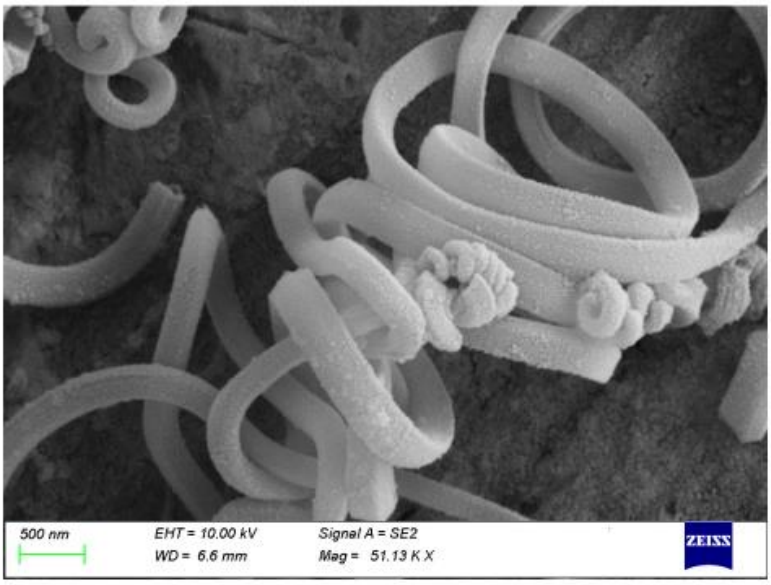

(b)

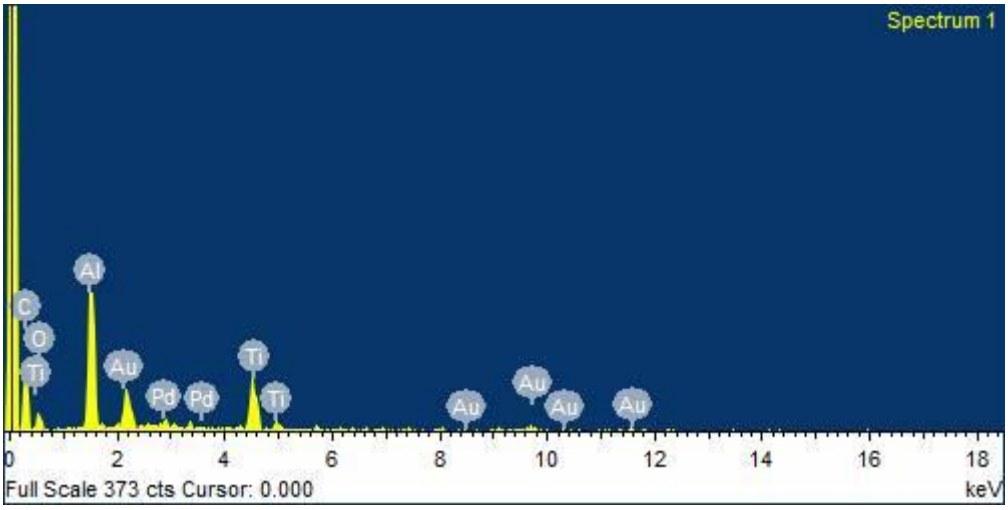

Fig. 2. Field Emission Scanning Electron Microscopy, FESEM investigation of; F_CNFs/20% _TiO_2 composite (a), EDS spectrum of the F_CNFs/20% _TiO_2 (b).

EDS scanning was performed from the SEM image, Fig. 2 (a) and it was detected that the sample consisted of Ti, C, O, Au, Al and Pd, Fig. 2 (b). The Al, Au and Pd, peaks were a result of mounting the sample on an aluminium pin stub and the coating of the sample with a single layer of Au-Pd. Therefore, the sample consisted mostly of Ti, C and O.

References

[1] N. Radenahmad *et al.*, "A review on biomass derived syngas for SOFC based combined heat and power application," *Renew. Sustain. Energy Rev.*, vol. 119, 2020, doi: 10.1016/j.rser.2019.109560.

[2] M. Ni, M. K. H. Leung, D. Y. C. Leung, and K. Sumathy, "A review and recent developments in photocatalytic water-splitting using TiO_2 for hydrogen production," *Renew. Sustain. Energy Rev.*, vol. 11, no. 3, pp. 401–425, 2007, doi: 10.1016/j.rser.2005.01.009.

[3] M. S. Reza *et al.*, "Thermochemical characterization of invasive Axonopus compressus grass as a renewable energy source," *IOP Conf. Ser. Mater. Sci. Eng.*, vol. 991, no. 1, 2020, doi: 10.1088/1757-899X/991/1/012074.

[4] M. S. Reza *et al.*, "Preparation of activated carbon from biomass and its' applications in water and gas purification, a review," *Arab J. Basic Appl. Sci.*, vol. 27, no. 1, pp. 208–238, 2020, doi: 10.1080/25765299.2020.1766799.

[5] M. S. Reza *et al.*, "Acacia holosericea: An invasive species for bio-char, bio-oil, and biogas production," *Bioengineering*, vol. 6, no. 2, 2019, doi: 10.3390/bioengineering6020033.

[6] S. Afroze, A. H. Karim, Q. Cheok, S. Eriksson, and A. K. Azad, "Latest development of double perovskite electrode materials for solid oxide fuel cells: a review," *Front. Energy*, vol. 13, no. 4, pp. 770–797, 2019, doi: 10.1007/s11708-019-0651-x.

[7] P. M. Rajaitha *et al.*, "Multifunctional materials for photo-electrochemical water splitting," *J. Mater. Chem. A*, vol. 10, no. 30, pp. 15906–15931, 2022, doi: 10.1039/d2ta01869a.

[8] M. F. Sanakousar *et al.*, “Efficient photocatalytic degradation of crystal violet dye and electrochemical performance of modified MWCNTs/Cd-ZnO nanoparticles with quantum chemical calculations,” *J. Hazard. Mater. Adv.*, vol. 2, 2021, doi: 10.1016/j.hazadv.2021.100004.

[9] A. Gupta, B. Likozar, R. Jana, W. C. Chanu, and M. K. Singh, “A review of hydrogen production processes by photocatalytic water splitting – From atomistic catalysis design to optimal reactor engineering,” *Int. J. Hydrogen Energy*, vol. 7, 2022, doi: 10.1016/j.ijhydene.2022.07.210.

[10] A. Bratovcic, “A Recent Developments in Photocatalytic Water Splitting by TiO_2 Modified Photocatalysts,” *Res. Dev. Mater. Sci.*, vol. 14, no. 1, pp. 1491–1498, 2020, doi: 10.31031/rdms.2020.14.000827.

[11] Y. Zhao *et al.*, “Classification and catalytic mechanisms of heterojunction photocatalysts and the application of titanium dioxide (TiO_2)-based heterojunctions in environmental remediation,” *J. Environ. Chem. Eng.*, vol. 10, no. 3, 2022, doi: 10.1016/j.jece.2022.108077.

[12] M. A. Aziz Aljar, M. Zulqarnain, A. Shah, M. S. Akhter, and F. J. Iftikhar, “A review of renewable energy generation using modified titania for photocatalytic water splitting,” *AIP Adv.*, vol. 10, no. 7, 2020, doi: 10.1063/5.0006196.

[13] M. B. Tahir, A. M. Asiri, and T. Nawaz, “A perspective on the fabrication of heterogeneous photocatalysts for enhanced hydrogen production,” *Int. J. Hydrogen Energy*, vol. 45, no. 46, pp. 24544–24557, 2020, doi: 10.1016/j.ijhydene.2020.06.301.

[14] P. Ganguly *et al.*, “2D Nanomaterials for Photocatalytic Hydrogen Production,” *ACS Energy Lett.*, VOL. 4, 1687−1709, 2019, doi: 10.1021/acsenergylett.9b00940.

[15] K. C. Christoforidis and P. Fornasiero, “Photocatalytic Hydrogen Production: A Rift into the Future Energy Supply,” *Chem.Cat. Chem.*, vol. 9, no. 9, pp. 1523–1544, 2017, doi: 10.1002/cctc.201601659.

[16] H. M. Moustafa, M. S. Mahmoud, and M. M. Nassar, “Photon-induced water splitting experimental and kinetic studies with a hydrothermally prepared TiO_2-doped rGO photocatalyst,” *Inorg. Chem. Commun.,* vol. 141, 2022, doi: 10.1016/j.inoche.2022.109546.

[17] Y. Zhang, F. Fu, F. Zhou, X. Yang, D. Zhang, and Y. Chen, “Synergistic effect of RGO/TiO_2 nanosheets with exposed (0 0 1) facets for boosting visible light photocatalytic activity,” *Appl. Surf. Sci.*, vol. 510, 2020, doi: 10.1016/j.apsusc.2020.145451.

[18] H. Esmaili, E. Kowsari, S. Sarabadani Tafreshi, S. Ramakrishna, N. H. de Leeuw, and M. Abdouss, “TiO_2 nanoarrays modification by a novel Cobalt-heteroatom doped graphene complex for photoelectrochemical water splitting: An experimental and theoretical study,” *J. Mol. Liq.*, vol. 356, 2022, doi: 10.1016/j.molliq.2022.118960.

[19] K. H. Ng, S. Y. Lai, C. K. Cheng, Y. W. Cheng, and C. C. Chong, “Photocatalytic water splitting for solving energy crisis: Myth, Fact or Busted?,” *Chem. Eng. J.*, vol. 417, no. 2020, 2021, doi: 10.1016/j.cej.2021.128847.

[20] P. Arunachalam, K. Nagai, M. S. Amer, M. A. Ghanem, R. J. Ramalingam, and A. M. Al-Mayouf, “Recent developments in the use of heterogeneous semiconductor photocatalyst based materials for a visible-light-inducedwater-splitting system-a brief review,” *Catalysts*, vol. 11, no. 2, pp. 1–27, 2021, doi: 10.3390/catal11020160.

[21] H. Husin *et al.*, “Efficient hydrogen production by microwave-assisted catalysis for glycerol-water solutions via NiO/zeolite-CaO catalyst,” *South African J. Chem. Eng.*,

vol. 41, 2021, pp. 43–50, 2022, doi: 10.1016/j.sajce.2022.04.004.

[22] Y. Li and S. C. E. Tsang, “Recent progress and strategies for enhancing photocatalytic water splitting,” *Mater. Today Sustain.*, vol. 9, 2020, doi: 10.1016/j.mtsust.2020.100032.

[23] F. Costantino and P. V. Kamat, “Do Sacrificial Donors Donate H_2 in Photocatalysis?,” *ACS Energy Lett.*, vol. 7, no. 1, pp. 242–246, 2022, doi: 10.1021/acsenergylett.1c02487.

[24] M. Wang, S. Shen, L. Li, Z. Tang, and J. Yang, “Effects of sacrificial reagents on photocatalytic hydrogen evolution over different photocatalysts,” *J. Mater. Sci.*, vol. 52, no. 9, pp. 5155–5164, 2017, doi: 10.1007/s10853-017-0752-z.

[25] L. Z. Wu, B. Chen, Z. J. Li, and C. H. Tung, “Enhancement of the efficiency of photocatalytic reduction of protons to hydrogen via molecular assembly,” *Acc. Chem. Res.*, vol. 47, no. 7, pp. 2177–2185, 2014, doi: 10.1021/ar500140r.

[26] A. Galińska and J. Walendziewski, “Photocatalytic water splitting over Pt-TiO_2 in the presence of sacrificial reagents,” *Energy and Fuels*, vol. 19, no. 3, pp. 1143–1147, 2005, doi: 10.1021/ef0400619.

[27] P. Chowdhury, H. Gomaa, and A. K. Ray, “Sacrificial hydrogen generation from aqueous triethanolamine with Eosin Y-sensitized Pt/TiO_2 photocatalyst in UV, visible and solar light irradiation,” *Chemosphere*, vol. 121, pp. 54–61, 2015, doi: 10.1016/j.chemosphere.2014.10.076.

[28] Y. Shen *et al.*, “Hydrogen Generation from Catalytic Reforming of Paraformaldehyde and Water by Polymeric Bifunctional Catalysts Comprising Ruthenium and Sulfonic Acid Units,” *Chem. Plus. Chem.*, vol. 85, 2020, doi: 10.1002/cplu.202000394.

[29] A. S. Hainer, J. S. Hodgins, V. Sandre, M. Vallieres, A. E. Lanterna, and J. C. Scaiano, "Photocatalytic Hydrogen Generation Using Metal-Decorated TiO_2: Sacrificial Donors vs True Water Splitting," *ACS Energy Lett.*, vol. 3, no. 3, pp. 542–545, 2018, doi: 10.1021/acsenergylett.8b00152.

[30] V. Kumaravel *et al.*, "Photocatalytic hydrogen production: Role of sacrificial reagents on the activity of oxide, carbon, and sulfide catalysts," *Catalysts*, vol. 9, no. 3, Mar. 2019, doi: 10.3390/catal9030276.

[31] T. Jafari, E. Moharreri, A. S. Amin, R. Miao, W. Song, and S. L. Suib, "Photocatalytic water splitting - The untamed dream: A review of recent advances," *Molecules*, vol. 21, no. 7, 2016, doi: 10.3390/molecules21070900.

[32] M. Ijaz and M. Zafar, "Titanium dioxide nanostructures as efficient photocatalyst: Progress, challenges and perspective," *Int. J. Energy Res.*, vol. 45, no. 3, pp. 3569–3589, 2021, doi: 10.1002/er.6079.

[33] M. A. Nadeem, M. A. Khan, A. A. Ziani, and H. Idriss, "An overview of the photocatalytic water splitting over suspended particles," *Catalysts*, vol. 11, no. 1, pp. 1–25, 2021, doi: 10.3390/catal11010060.

[34] W.-T. Chen, Y. Dong, P. Yadav, R. D. Aughterson, D. Sun-Waterhouse, and G. I. N. Waterhouse, "Effect of alcohol sacrificial agent on the performance of Cu/TiO_2 photocatalysts for UV-driven hydrogen production," *Appl. Catal. A Gen.*, vol. 602, 2020, doi: https://doi.org/10.1016/j.apcata.2020.117703.

[35] I. Rossetti, "Hydrogen Production by Photoreforming of Renewable Substrates," *Chem. Eng.*, vol. 2012, pp. 1–21, 2012, doi: 10.5402/2012/964936.

[36] F. Varas-Concha, D. Guzmán, M. Isaacs, and C. Sáez-Navarrete, "Operational

Conditions Affecting Hydrogen Production by the Photoreforming of Organic Compounds using Titania Nanoparticles with Gold," *Energy Technol.*, vol. 6, no. 2, pp. 416–431, 2018, doi: 10.1002/ente.201700546.

[37] M. Hakamizadeh, S. Afshar, A. Tadjarodi, R. Khajavian, M. R. Fadaie, and B. Bozorgi, "Improving hydrogen production via water splitting over Pt/TiO_2/activated carbon nanocomposite," *Int. J. Hydrogen Energy*, vol. 39, no. 14, pp. 7262–7269, 2014, doi: https://doi.org/10.1016/j.ijhydene.2014.03.048.

[38] W. Zhao, K. Maeda, F. Zhang, T. Hisatomi, and K. Domen, "Effect of post-treatments on the photocatalytic activity of $Sm_2Ti_2S_2O_5$ for the hydrogen evolution reaction," *Phys. Chem. Chem. Phys.*, vol. 16, no. 24, pp. 12051–12056, 2014, doi: 10.1039/c3cp54668c.

[39] S. H. Kim *et al.*, "Photophysical and photocatalytic water splitting performance of stibiotantalite type-structure compounds, $SbMO_4$ (M = Nb, Ta)," *Int. J. Hydrogen Energy*, vol. 37, no. 22, pp. 16895–16902, 2012, doi: 10.1016/j.ijhydene.2012.08.123.

[40] R. Yang, K. Song, J. He, Y. Fan, and R. Zhu, "Photocatalytic Hydrogen Production by RGO/$ZnIn_2S_4$ under Visible Light with Simultaneous Organic Amine Degradation," *ACS Omega*, vol. 4, no. 6, pp. 11135–11140, 2019, doi: 10.1021/acsomega.9b01034.

[41] J. O. M. Bockris, "Would methanol formed from CO_2 from the atmosphere give the advantage of hydrogen at lesser cost?," *Int. J. Hydrogen Energy*, vol. 35, no. 11, pp. 5165–5172, 2010, doi: 10.1016/j.ijhydene.2010.03.060.

[42] C. C. Hu and H. Teng, "Structural features of p-type semiconducting NiO as a co-catalyst for photocatalytic water splitting," *J. Catal.*, vol. 272, no. 1, pp. 1–8, 2010, doi: 10.1016/j.jcat.2010.03.020.

[43] L. S. Salah, N. Ouslimani, D. Bousba, I. Huynen, Y. Danleé, and H. Aksas, “Carbon Nanotubes (CNTs) from Synthesis to Functionalized (CNTs) Using Conventional and New Chemical Approaches,” *J. Nanomater.*, vol. 2021, 2021, doi: 10.1155/2021/4972770.

[44] M. M. Sabzehmeidani, S. Mahnaee, M. Ghaedi, H. Heidari, and V. A. L. Roy, “Carbon based materials: A review of adsorbents for inorganic and organic compounds,” *Mater. Adv.*, vol. 2, no. 2, pp. 598–627, 2021, doi: 10.1039/d0ma00087f.

[45] M. S. Nasir, G. Yang, I. Ayub, A. Nasir, and W. Yan, “Higher hydrogen production by photocatalytic water splitting using a hollow tubular graphitic carbon nitride-zinc telluride composite,” *Environ. Chem. Lett.*, vol. 20, no. 1, pp. 19–26, 2022, doi: 10.1007/s10311-021-01301-z.

[46] S. Kundu, K. Bramhaiah, and S. Bhattacharyya, “Carbon-based nanomaterials: In the quest of alternative metal-free photocatalysts for solar water splitting,” *Nanoscale Adv.*, vol. 2, no. 11, pp. 5130–5151, 2020, doi: 10.1039/d0na00569j.

[47] L. K. Putri, W. J. Ong, W. S. Chang, and S. P. Chai, “Heteroatom doped graphene in photocatalysis: A review,” *Appl. Surf. Sci.*, vol. 358, pp. 2–14, 2015, doi: 10.1016/j.apsusc.2015.08.177.

[48] H. Wang, S. Dong, Y. Chang, and J. L. Faria, “Enhancing the photocatalytic properties of TiO_2 by coupling with carbon nanotubes and supporting gold,” *J. Hazard. Mater.*, vol. 235, pp. 230–236, 2012, doi: 10.1016/j.jhazmat.2012.07.050.

[49] I. Dincer and C. Acar, “Review and evaluation of hydrogen production methods for better sustainability,” *Int. J. Hydrogen Energy*, vol. 40, no. 34, pp. 11094–11111, 2014, doi: 10.1016/j.ijhydene.2014.12.035.

[50] S. D. Mhlanga and N. J. Coville, “Iron-cobalt catalysts synthesized by a reverse micelle impregnation method for controlled growth of carbon nanotubes,” *Diam. Relat. Mater.*, vol. 17, no. 7, pp. 1489–1493, 2008, doi: 10.1016/j.diamond.2008.01.049.

[51] Y. Yan, J. Lu, C. Deng, and X. Zhang, “Facile synthesis of titania nanoparticles coated carbon nanotubes for selective enrichment of phosphopeptides for mass spectrometry analysis,” *Talanta*, vol. 107, pp. 30–35, 2013, doi: 10.1016/j.talanta.2012.12.026.

[52] S. B. A. Hamid, T. L. Tan, C. W. Lai, and E. M. Samsudin, “Multiwalled carbon nanotube/TiO_2 nanocomposite as a highly active photocatalyst for photodegradation of Reactive Black 5 dye,” *Cuihua Xuebao/Chinese J. Catal.*, vol. 35, no. 12, pp. 2014–2019, 2014, doi: 10.1016/S1872-2067(14)60210-2.

[53] J. M. Walls, J. S. Sagu, and K. G. Upul Wijayantha, “Microwave synthesised Pd-TiO_2 for photocatalytic ammonia production,” *RSC Adv.*, vol. 9, no. 11, pp. 6387–6394, 2019, doi: 10.1039/c8ra09762c.

[54] B. Gao, G. Z. Chen, and G. Li Puma, “Carbon nanotubes/titanium dioxide (CNTs/TiO_2) nanocomposites prepared by conventional and novel surfactant wrapping sol-gel methods exhibiting enhanced photocatalytic activity,” *Appl. Catal. B Environ.*, vol. 89, no. 3, pp. 503–509, 2009, doi: 10.1016/j.apcatb.2009.01.009.

[55] K. Dai, T. Peng, D. Ke, and B. Wei, “Photocatalytic hydrogen generation using a nanocomposite of multi-walled carbon nanotubes and TiO_2 nanoparticles under visible light irradiation,” *Nanotechnology*, vol. 20, no. 12, 2009, doi: 10.1088/0957-4484/20/12/125603.

[56] J. Liu, J. Li, A. Sedhain, J. Lin, and H. Jiang, “Structure and photoluminescence study of TiO_2 nanoneedle texture along vertically aligned carbon nanofiber arrays,” *J. Phys.*

Chem. C, vol. 112, no. 44, pp. 17127–17132, 2008, doi: 10.1021/jp8060653.

[57] S. Liu, H. Sun, S. Liu, and S. Wang, "Graphene facilitated visible light photodegradation of methylene blue over titanium dioxide photocatalysts," *Chem. Eng. J.*, vol. 214, pp. 298–303, 2013, doi: 10.1016/j.cej.2012.10.058.

[58] W. Wang, D. Xu, B. Cheng, J. Yu, and C. Jiang, "Hybrid carbon@TiO_2 hollow spheres with enhanced photocatalytic CO_2 reduction activity," *J. Mater. Chem. A*, vol. 5, no. 10, pp. 5020–5029, 2017, doi: 10.1039/c6ta11121a.

[59] Y. Wang, K. Hu, Y. Zhang, and X. Ding, "Dendritic fibrous nano-silica & titania (DFNST) spheres as novel cataluminescence sensing materials for the detection of diethyl ether," *RSC Adv.*, vol. 9, no. 68, pp. 39622–39630, 2019, doi: 10.1039/c9ra08152f.

[60] L. Feng, N. Xie, and J. Zhong, "Carbon nanofibers and their composites: A review of synthesizing, properties and applications," *Materials*, vol. 7, no. 5, pp. 3919–3945, 2014, doi: 10.3390/ma7053919.

[61] J. M. Muñoz-Ávila *et al.*, "Influence of carbon nanofiber functionalization and compatibilizer on the physical properties of carbon nanofiber reinforced polypropylene nanocomposites," *Polym. Compos.*, vol. 39, no. 10, pp. 3575–3585, 2018, doi: 10.1002/pc.24380.

[62] L. Ravindran, M. S. Sreekala, S. Anilkumar, and S. Thomas," Effect of MWCNT carboxylation on mechanical, thermal and morphological behaviour of phenol formaldehyde nanocomposites," *J. Compos. Mater.*, vol. 55, no. 9, pp. 1151–1166, 2021, doi: 10.1177/0021998320964263.

[63] J. Baloyi, T. Seadira, M. Raphulu, and A. Ochieng, "Preparation, Characterization and

Growth Mechanism of Dandelion-like TiO_2 Nanostructures and their Application in Photocatalysis towards Reduction of Cr(VI)," *Mater. Today Proc.*, vol. 2, no. 7, pp. 3973–3987, 2015, doi: 10.1016/j.matpr.2015.08.027.

[64] B. J. Landi, C. D. Cress, C. M. Evans, and R. P. Raffaelle, "Thermal oxidation profiling of single-walled carbon nanotubes," *Chem. Mater.*, vol. 17, no. 26, pp. 6819–6834, 2005, doi: 10.1021/cm052002u.

[65] G. Leofanti, M. Padovan, G. Tozzola, and B. Venturelli, "Surface area and pore texture of catalysts," *Catal. Today*, vol. 41, no. 1–3, pp. 207–219, 1998, doi: 10.1016/S0920-5861(98)00050-9.

[66] J. Shi, J. Chen, G. Li, T. An, and H. Yamashita, "Fabrication of Au/TiO_2 nanowires@carbon fiber paper ternary composite for visible-light photocatalytic degradation of gaseous styrene," *Catal. Today*, vol. 281, pp. 621–629, 2017, doi: 10.1016/j.cattod.2016.06.026.

[67] N. S. Babu, N. Lingaiah, N. Pasha, J. V. Kumar, and P. S. S. Prasad, "Influence of particle size and nature of Pd species on the hydrodechlorination of chloroaromatics: Studies on Pd/TiO_2 catalysts in chlorobenzene conversion," *Catal. Today*, vol. 141, no. 1, pp. 120–124, 2009, doi: 10.1016/j.cattod.2008.03.018.

[68] S. Brunauer, P. H. Emmet, and E. Teller, "Adsorption of gases in multilayer's.," *J. Am. Chem. Soc.*, vol. 60, no. 35, pp. 309–319, 1938.

[69] K. Kinashi, Y. Kambe, M. Misaki, Y. Koshiba, K. Ishida, and Y. Ueda, "Synthesis, characterization, photo-induced alignment, and surface orientation of poly(9,9-dioctylfluorene-alt-azobenzene)s," *J. Polym. Sci. Part A Polym. Chem.*, vol. 50, no. 24, pp. 5107–5114, 2012, doi: 10.1002/pola.26338.

[70] H. Berger, H. Tang, and F. Lévy, “Growth and Raman spectroscopic characterization of TiO_2 anatase single crystals,” *J. Cryst. Growth*, vol. 130, no. 1, pp. 108–112, 1993, doi: 10.1016/0022-0248(93)90842-K.

[71] S. Santangelo *et al.*, “Micro-Raman analysis of titanium oxide/carbon nanotubes-based nanocomposites for hydrogen sensing applications,” *J. Solid State Chem.*, vol. 183, no. 10, pp. 2451–2455, 2010, doi: 10.1016/j.jssc.2010.08.018.

[72] 3 Zlatko Meić Mladen Žini ć Snežzana Miljanić, Leo Frkanec, Tomislav Biljan, “Recent Advances in linear and nonlinear Raman spectroscopy I,” *J. Raman Spectrosc.*, vol. 38, pp. 1538–1553, 2007, doi: 10.1002/jrs.

[73] D. A. Solís-Casados, E. Vigueras-Santiago, S. Hernández-López, A. Gómez-Cortés, M. Aguilar-Franco, and M. A. Camacho-López, “Textural, structural and electrical properties of TiO_2 nanoparticles using Brij 35 and P123 as surfactants,” *Sci. Technol. Adv. Mater.*, vol. 9, no. 2, 2008, doi: 10.1088/1468-6996/9/2/025003.

[74] W. K. Sun, R. Khan, T. J. Kim, and W. J. Kim, “Synthesis, characterization, and application of Zr,S Co-doped TiO_2 as visible-light active photocatalyst,” *Bull. Korean Chem. Soc.*, vol. 29, no. 6, pp. 1217–1223, 2008, doi: 10.5012/bkcs.2008.29.6.1217.

[75] Y. Yu *et al.*, “Enhancement of adsorption and photocatalytic activity of TiO_2 by using carbon nanotubes for the treatment of azo dye,” *Appl. Catal. B Environ.*, vol. 61, no. 1, pp. 1–11, 2005, doi: 10.1016/j.apcatb.2005.03.008.

[76] H. Y. Liu *et al.*, “A comparative study of amorphous, anatase, rutile, and mixed phase TiO_2 films by mist chemical vapor deposition and ultraviolet photodetectors applications,” *IEEE Sens. J.*, vol. 18, no. 10, pp. 4022–4029, 2018, doi: 10.1109/JSEN.2018.2819700.

[77] H. Wu *et al.*, “Hydrothermal synthesis of Graphene-TiO_2 nanowire with an enhanced photocatalytic activity,” *Russ. J. Phys. Chem. A*, vol. 89, no. 7, pp. 1189–1194, 2015, doi: 10.1134/S0036024415070134.

[78] E. T. Mombeshora, R. Simoyi, V. O. Nyamori, and P. G. Ndungu, “Multiwalled carbon nanotube-titania nanocomposites : understanding nano-structural parameters and functionality in dye-sensitized solar cells : Research article,” *South African J. Chem.*, vol. 68, no. 1, pp. 153–164, 2015, doi: 10.17159/0379-4350/2015/v68a22.

[79] N. Hintsho, L. Petrik, A. Nechaev, S. Titinchi, and P. Ndungu, “Photo-catalytic activity of titanium dioxide carbon nanotube nano-composites modified with silver and palladium nanoparticles,” *Appl. Catal. B Environ.*, vol. 156, pp. 273–283, 2014, doi: 10.1016/j.apcatb.2014.03.021.

[80] N. Sobana, M. Muruganadham, and M. Swaminathan, “Nano-Ag particles doped TiO_2 for efficient photodegradation of Direct azo dyes,” *J. Mol. Catal. A Chem.*, vol. 258, no. 1, pp. 124–132, 2006, doi: 10.1016/j.molcata.2006.05.013.

[81] J. Coutts *et al.*, “Visible-Light-Responsive Photocatalysis: Ag-Doped TiO_2 Catalyst Development and Reactor Design Testing,” *46th Int. Conf. Environ. Syst.*, 2016, https://ttu-ir.tdl.org/ttu-ir/handle/2346/67573

[82] J. Zhang, P. Zhou, J. Liu, and J. Yu, “New understanding of the difference of photocatalytic activity among anatase, rutile and brookite TiO_2,” *Phys. Chem. Chem. Phys.*, vol. 16, no. 38, pp. 20382–20386, 2014, doi: 10.1039/c4cp02201g.

[83] C. Dette *et al.*, “TiO_2 anatase with a bandgap in the visible region,” *Nano Lett.*, vol. 14, no. 11, pp. 6533–6538, 2014, doi: 10.1021/nl503131s.

[84] W. Wang, D. Zhu, Z. Shen, J. Peng, J. Luo, and X. Liu, “One-Pot Hydrothermal Route

to Synthesize the Bi-doped Anatase TiO_2 Hollow Thin Sheets with Prior Facet Exposed for Enhanced Visible-Light-Driven Photocatalytic Activity," *Ind. Eng. Chem. Res.*, vol. 55, no. 22, pp. 6373–6383, 2016, doi: 10.1021/acs.iecr.6b00618.

[85] B. H. Aw, K. K. Looh, H. S. O. Chan, K. L. Tan, and T. S. A. Hor, "X-Ray photoelectron spectroscopic characterization of [{$Pt(PPh3)_2(\mu3\text{-}S)$}2$PtCl_2$] [{$Pt_2(PPh3)_4(\mu3\text{-}S)2Cu\}_2(\mu$-dppf)][$PF6]_2$[dppf = Fe ($C_5H_4PPh2)_2$] and other heterometallic aggregates derived from [{$Pt(PPh3)_2(\mu$-S)$\}_2$]," *J. Chem. Soc. Dalt. Trans.*, no. 21, pp. 3177–3182, 1994, doi: 10.1039/DT9940003177.

[86] M. Ismael, "A review and recent advances in solar-to-hydrogen energy conversion based on photocatalytic water splitting over doped-TiO_2 nanoparticles," *Sol. Energy*, vol. 211, pp. 522–546, Nov. 2020, doi: 10.1016/J.SOLENER.2020.09.073.

[87] T. S. Natarajan, V. Mozhiarasi, and R. J. Tayade, "Nitrogen Doped Titanium Dioxide (N-TiO_2): Synopsis of Synthesis Methodologies, Doping Mechanisms, Property Evaluation and Visible Light Photocatalytic Applications," *Photochem*, vol. 1, no. 3, pp. 371–410, 2021, doi: 10.3390/photochem1030024.

[88] C. Wang, L. Ling, Y. Yao, and Q. Song, "One-step synthesis of fluorescent smart thermo-responsive copper clusters: A potential nanothermometer in living cells," *Nano Res.*, vol. 8, no. 6, pp. 1975–1986, 2015, doi: 10.1007/s12274-015-0707-0.

[89] E. S. Shibu and T. Pradeep, "Quantum clusters in cavities: Trapped Au15 in cyclodextrins," *Chem. Mater.*, vol. 23, no. 4, pp. 989–999, 2011, doi: 10.1021/cm102743y.

[90] Q. Ye, Z. Z. Yin, H. Wu, D. Wu, Y. Tao, and Y. Kong, "Decoration of glutathione with copper-platinum nanoparticles for chirality sensing of tyrosine enantiomers," *Electrochem. commun.*, vol. 110, no. 2019, 2020, doi: 10.1016/j.elecom.2019.106638.

[91] T. Rahimi-Aghdam, Z. Shariatinia, M. Hakkarainen, and V. Haddadi-Asl, “Nitrogen and phosphorous doped graphene quantum dots: Excellent flame retardants and smoke suppressants for polyacrylonitrile nanocomposites,” *J. Hazard. Mater.*, vol. 381, Jan. 2020, doi: 10.1016/J.JHAZMAT.2019.121013.

[92] W. Chen *et al.*, “Non-noble metal Cu as a cocatalyst on TiO_2 nanorod for highly efficient photocatalytic hydrogen production,” *Appl. Surf. Sci.*, vol. 445, pp. 527–534, 2018, doi: 10.1016/j.apsusc.2018.03.209.

[93] J. Huang *et al.*, “Efficient photocatalytic hydrogen production over Rh and Nb codoped TiO_2 nanorods,” *Chem. Eng. J.*, vol. 337, no. 2017, pp. 282–289, 2018, doi: 10.1016/j.cej.2017.12.088.

[94] D. Xu, L. Li, R. He, L. Qi, L. Zhang, and B. Cheng, “Noble metal-free RGO/TiO_2 composite nanofiber with enhanced photocatalytic H_2 -production performance,” *Appl. Surf. Sci.*, vol. 434, pp. 620–625, 2018, doi: 10.1016/j.apsusc.2017.10.192.

[95] T. T. D. Vu, F. Mighri, A. Ajji, and T. O. Do, “Synthesis of titanium dioxide/cadmium sulfide nanosphere particles for photocatalyst applications,” *Ind. Eng. Chem. Res.*, vol. 53, no. 10, pp. 3888–3897, 2014, doi: 10.1021/ie403718n.

[96] X. Wang, W. C. Peng, and X. Y. Li, “Photocatalytic hydrogen generation with simultaneous organic degradation by composite CdS-ZnS nanoparticles under visible light,” *Int. J. Hydrogen Energy*, vol. 39, no. 25, pp. 13454–13461, 2014, doi: 10.1016/j.ijhydene.2014.04.034.

[97] E. Taboada, I. Angurell, and J. Llorca, “Dynamic photocatalytic hydrogen production from ethanol-water mixtures in an optical fiber honeycomb reactor loaded with Au/TiO_2,” *J. Catal.*, vol. 309, pp. 460–467, 2014, doi: 10.1016/j.jcat.2013.10.025.

[98] R. D. Tentu and S. Basu, “Photocatalytic water splitting for hydrogen production,” *Curr. Opin. Electrochem.*, vol. 5, no. 1, pp. 56–62, 2017, doi: 10.1016/j.coelec.2017.10.019.

[99] M. Ghorbanloo *et al.*, “BN/Cs_2CO_3/TiO_2 composite nanofibers to improve hydrogen generation,” *J. Alloys Compd.*, vol. 945, 2023, doi: 10.1016/j.jallcom.2023.169218.

[100] M. Ghorbanloo *et al.*, “Superior efficiency of BN/Ce_2O_3/TiO_2 nanofibers for photocatalytic hydrogen generation reactions,” *Appl. Surf. Sci.*, vol. 594, 2022, doi: 10.1016/j.apsusc.2022.153438.

[101] H. H. El-Maghrabi *et al.*, “Synthesis of mesoporous core-shell CdS@TiO_2 (0D and 1D) photocatalysts for solar-driven hydrogen fuel production,” *J. Photochem. Photobiol. A Chem.*, vol. 351, pp. 261–270, 2018, doi: 10.1016/j.jphotochem.2017.10.048.

[102] C. Huang, M. Wu, and V. Nguyen, “Preparation and Characterization of Nanocrystalline TiO_2 on Microsericite for High-Efficiency Photo-Energy Conversion of Methanol to Hydrogen,” *Crystals*, vol. 9, no. 380, 2019, doi: 10.3390/cryst9080380.

[103] A. Moya *et al.*, “Oxygen vacancies and interfaces enhancing photocatalytic hydrogen production in mesoporous CNT/TiO_2 hybrids,” *Appl. Catal. B Environ.*, vol. 179, pp. 574–582, 2015, doi: 10.1016/j.apcatb.2015.05.052.

[104] F. H. Abdulrazzak, F. H. Hussein, A. F. Alkaim, I. Ivanova, A. V. Emeline, and D. W. Bahnemann, “Sonochemical/hydration-dehydration synthesis of Pt-TiO_2 NPs/decorated carbon nanotubes with enhanced photocatalytic hydrogen production activity,” *Photochem. Photobiol. Sci.*, vol. 15, no. 11, pp. 1347–1357, 2016, doi: 10.1039/c6pp00240d.

[105] R. Leary and A. Westwood, “Carbonaceous nanomaterials for the enhancement of TiO_2 photocatalysis,” *Carbon,* vol. 49, no. 3, pp. 741–772, 2011, doi: https://doi.org/10.1016/j.carbon.2010.10.010.

[106] M. Hakamizadeh, S. Afshar, A. Tadjarodi, R. Khajavian, M. R. Fadaie, and B. Bozorgi, “Improving hydrogen production via water splitting over Pt/TiO_2/activated carbon nanocomposite,” *Int. J. Hydrogen Energy*, vol. 39, no. 14, pp. 7262–7269, 2014, doi: 10.1016/j.ijhydene.2014.03.048.

[107] N. Lakshminarasimhan, E. Bae, and W. Choi, “Enhanced photocatalytic production of H_2 on mesoporous TiO_2 prepared by template-free method: Role of interparticle charge transfer,” *J. Phys. Chem. C*, vol. 111, no. 42, pp. 15244–15250, 2007, doi: 10.1021/jp0752724.

[108] J. Jitputti, S. Pavasupree, Y. Suzuki, and S. Yoshikawa, “Synthesis and photocatalytic activity for water-splitting reaction of nanocrystalline mesoporous titania prepared by hydrothermal method,” *J. Solid State Chem.*, vol. 180, no. 5, pp. 1743–1749, 2007, doi: https://doi.org/10.1016/j.jssc.2007.03.018.

[109] H. Yi, T. Peng, D. Ke, D. Ke, L. Zan, and C. Yan, “Photocatalytic H_2 production from methanol aqueous solution over titania nanoparticles with mesostructures,” *Int. J. Hydrogen Energy*, vol. 33, no. 2, pp. 672–678, 2008, doi: https://doi.org/10.1016/j.ijhydene.2007.10.034.

CHAPTER FIVE

Highly enhanced photocatalytic hydrogen production of TiO_2/CNFs doped with Pt, Au and Ir nanoparticles

Molecular Sciences Institute, School of Chemistry, University of the Witwatersrand, Johannesburg 2050, South Africa

Abstract

The use of semiconductor photocatalysts with sunlight in hydrogen production has long-standing consideration as a favourable technique to large scale production of H_2 from inexhaustible reserves. Typically, the reaction is realizable upon reconstructing a photocatalyst with appropriate cocatalyst that successfully boosts the reduction of water. Thus, it is a prerequisite to establish both photocatalysts and cocatalysts in conformity. Titanium is one of the most attractive d-block transition metals in use as water splitting photocatalyst. It is preferred because of its low density, high strength, corrosion resistance, availability and cost effectiveness. However, efficient water splitting using visible light and TO_2 has been a challenge. TO_2 has a setback of wide bandgap, 3.0 – 3.2 eV, which lowers its prospective for visible light absorption. This study outlines the development and the testing of TiO_2/CNFs composites together with cocatalysts, Pt, Au and Ir for overall water splitting. The photocatalysts were tested for hydrogen production using water, and the most active photocatalyst, F_CNFs/20% _TiO_2/6%Pt exhibited an activity of 0.45 mol g^{-1} h^{-1}. This was followed by F_CNFs/10%_TiO_2/5%Au and F_CNFs/20%_TiO_2/1%Ir with activities of 0.28 mol g^{-1} h^{-1}, and 0.21 mol g^{-1} h^{-1} respectively. The study identifies the important role of nanocarbons and cocatalysts in improving the photocatalytic activity of TiO_2 for hydrogen production from water.

Keywords: TiO_2/CNFs, Au, Pt, Ir nanoparticles, water splitting.

5.1 Introduction

The diminishing of fossil fuels, coal, natural gas and oil, and the serious ecological deterioration resulting from their combustion, has led to the promotion of the production of hydrogen, H_2 from water and sunlight using particulate photocatalysts as a favourable technology to tackle the power and the ecological problems [1]–[4]. Despite the fact that, indisputable attempts have been dedicated, the level of H_2 evolution is still below par to be used commercially [5]. Obtaining a substitution for the dependence on fossil fuels for everyday operations, the energy efficiency of the substitutes must be greater and their environmental impact, particularly on carbon emissions, has to be lower than the fractional process of combusting fossil fuels [6].

By evaluating the semiconductors that are suitable for photocatalysis, TiO_2 has been widely used because of its many advantages namely non-toxicity, high photochemical stability, abundance, low cost and high stability against photo corrosion [7], [8]. Nevertheless, TO_2 also has a setback of wide bandgap, 3.0 – 3.2 eV, which lowers its prospective for visible light absorption [9]–[11]. Owing to the structural and chemical properties of TiO_2, it is feasible to construct the bandgap, recombination rate, and light absorption properties by controlling and improving the electrical properties [12]–[16]. There are different polymorphs of TiO_2 with dissimilar behaviours. The common and most important ones are anatase, rutile and brookite, Fig. 1. Anatase and rutile TiO_2 polymorphs are primarily used for photocatalytic water splitting; though some research have been done with amorphous TiO_2 [17], [18].

Since there is need for clean, renewable and ecologically friendly energy, photocatalytic water splitting to produce H_2 using renewable energy is a promising technique. Photocatalytic water splitting can be viewed as a photochemical process in which a catalyst reacts and

harnesses solar power in the form of chemical energy upon irradiation. Looney [19], [20], reported that the sun energy reaching the earth's surface is about 9600 times of the global energy consumption [20]. The advantage of solar energy has been used as an environmentally friendly method for fuel generation and waste water treatment (H_2 production from water splitting and CH_4 production through CO_2 reduction. It is acknowledged that photocatalytic water splitting is a multidisciplinary study area which requires advanced knowledge of chemistry, chemical engineering, nanoscience, material science, nanotechnology and physics.

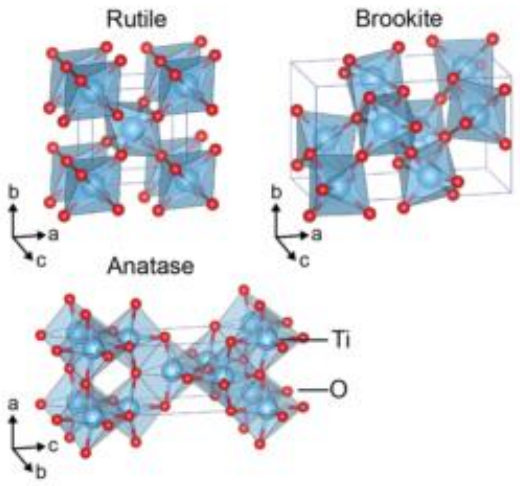

Fig. 1. Different polymorphs of TiO_2; rutile, brookite, and anatase [18][21].

Basically, photocatalytic overall water splitting (POWS) takes place in three main steps. In step one, the electron- hole pairs are initiated by irradiation. This is achieved by employing the semiconducting characteristics of the photocatalysts to promote electrons from the valence band (VB) to the conduction band (CB). This step occurs when the photocatalyst absorbs electromagnetic radiation with energy greater than its bandgap energy. The aforementioned electrons and holes are referred to as photogenerated carriers or simply photogenerated

(electron – hole) pairs. Considering that photon generation of electron–holes depends on excitation of the semiconductor with radiation, photocatalysts with a broad- spectrum of light responses and sufficient light absorption coefficient have to be produced, which could be acquired by pursuing mitigation of photocatalysts by doping or solid solution fabrication [22]. Step two involves charge separation and relocation of the photogenerated charge carriers. In the course of relocation of the electron – hole pairs to the exterior of the photocatalyst, some recombination of the electrons and holes may occur, and only the charge carriers that eventually reach the redox-active sites can take part in the redox-reaction processes. Fundamentally, accelerated charge separation must be enhanced (charge separation must be accelerated or enhanced) by fabricating hetero/homo-junctions to maximize the photocatalytic efficiency [23], [24]. The final step comprises the electrons, which migrate from the CB to the photocatalyst surface to take part in a reduction reaction and produce hydrogen, while the holes move from the VB to the surface of the catalyst to be involved in oxidation reaction forming oxygen. As a result of the high activation energy of water splitting [25], [26], only a few of the photogenerated electron- hole pairs reaching the photocatalyst facet can be involved in the water splitting reaction in good time, hence surface recombination occurs thereby greatly reducing the photocatalytic overall water splitting efficiency [25], [26]. Thus, several strategies, as well as loading cocatalysts which are mainly metals or metal oxides for instance Pt, NiO, and RuO_2, which are capable of acting as the sites of action by promoting electron movement that can be used to enhance the surface redox reaction.

The reduction and oxidation (redox) processes on the surface of the catalysts are shown as follows [27];

Photo - reduction: $2H_2O + 2e^- \rightarrow H_2 + 2OH^-$ (1)

Photo - oxidation: $2H_2O \rightarrow O_2 + 4H^+ + 4e^-$ (2)

Overall reaction: $H_2O + 1.23eV\ (h\nu) \rightarrow H_2 + 1/2O_2$ (3)

To accelerate the surface redox response, numerous techniques of inserting cocatalysts on the photocatalysts have been established, including impregnation [28], photodeposition [29], [30], and others [31], [32]. Suitable cocatalysts composited with photocatalysts function as active sites and catalyse the process by enhancing charge separation, together with relocation caused by the heterojunction existing in the midst of semiconductor photocatalyst and the cocatalyst [33].

Carbon from charcoal was first proposed by A. L. Lavoisier in 1789. It is one of the most available elements on earth. Besides, it is capable of forming several compounds [34]. Carbon has proved to have distinctive physicochemical and thermal properties [35]. Eminently, during photocatalytic water splitting, the material can capably play several roles, including co-catalyst, supporting material and electron acceptor [36]. The aforementioned functions of carbon basically enhance the surface reaction sites, visible light capturing as well as competently transferring the electrons to the surface reaction sites in TiO_2 [37], [38]. Additionally, carbon also promotes the segregation of the photogenerated electron-hole pairs of TiO_2 showing that carbon has gained electron storage potential [39]. Other studies by Gao et al., also reported the compositing of TiO_2 carbon for H_2 evolution upon illumination with visible light [40]. Also, it turned out that the inclusion of carbon in TiO_2 photocatalysts helps to advance the photocatalytic stability [41], [42]. Chengwu et al. [43] prepared carbon-TiO_2 composite with sheets coated on the shell type TiC (TiC/TiO_2-C) by thermal growth process. The TiC/TiO_2-C principal covering produced enhanced hydrogen evolution results than the neat TiO_2 (P-25) as a result of the principal covering structure that helped to shift the band edge of TiO_2 which

resulted from the retardation of the photogenerated electron- hole pair recombination efficiency.

In this study we report on the enhancement of photocatalytic activities and the high amount of H_2 evolved during the photocatalytic water splitting using Pt, Au or Ir supported on CNFs coated with TiO_2. Hydrothermal method was used to coat the CNFs with TiO_2 – anatase (TiO_2 – A).

5.2 Experimental procedure

5.2.1 Materials

Gold (I) chloride, 99.9% metals basis, ethanol (99.9%), ammonia solution (25%), copper (II) nitrate trihydrate, and platinum acetylacetonate, 97%, potassium hydroxide, anhydrous, KOH, ≥ 99.95% trace metals basis and nitric acid, HNO_3 (55%), titanium butoxide, butanol and Iridium (III) chloride hydrate, 99.9% trace metals basis were purchased from Sigma – Aldrich. Hydrogen, argon and acetylene gases were purchased from Afrox. Part of the experiment used deionized and distilled water.

5.2.2 The preparation of copper oxide nanoparticles, carbon nano-fibers, and the functionalization of carbon nano-fibers, F_CNFs

Copper oxide nanoparticles, CuONPs were prepared using copper nitrate which was dispersed in deionized water (0.05M). Potassium hydroxide, 0.05M was added with vigorous stirring for 12 h. Black precipitates were obtained, cleaned severally with deionized water to neutrality, dried in the oven overnight at 80 ℃ and characterized by XRD, Raman, SEM, FTIR, and thermogravimetric analysis.

The CNFs were prepared by CuONPs at 300 ℃ in a tube heating system using chemical vapour deposition, CVD technique [44]. The synthesis method of CNFs employs fragmentation of C_2H_2 in a quartz heating tube, positioned horizontally in the heating system.

The heating system was automatically monitored by programming the heating efficiency, and gas circulation rates. 0.1g was packed in a quartz apparatus, 120 mm by 15 mm at 25 ℃, and the apparatus transferred to the centre of the heating system. The heating system was then set at 10 ℃ min^{-1} with hydrogen gas, H_2 (50 mL min^{-1}). Upon attaining heating of 300 ℃, the H_2 flow was retained for 30 minutes before introducing C_2H_2 (50 $mLmin^{-1}$). 30 minutes later, the C_2H_2 flow was ceased, and the heating system temperature lowered to 25 ℃, with H_2 flow. The quartz apparatus later removed from the heater and the product quantified. CNFs were washed with concentrated nitric acid, to get rid of traces of CuO NPs as well as functionalizing them. CNFs were refluxed with 55% HNO_3 at 110 ℃ (2 h). The resultant mixture at 25 ℃, was centrifuged, cleaned with distilled water to neutrality. The washed CNFs (F_CNFs) were transferred to an oven at 80 ℃ for 12 h.

5.2.3 The preparation of F_CNFs/TiO_2 and TiO_2 nanocomposites

The TiO_2/F_CNFs was synthesized by hydrothermal process modified from a surfactant wrapping sol-gel approach formerly outlined by Deng et al [45], and Hamid et al [46]. In this investigation, fixed amount of the purified CNFs (F_CNFs) was discharged in 25 ml butanol and homogenized for 30 minutes in a sonicator. A known amount of titanium butoxide which had been previously dispersed separately for 30 minutes in 5 ml butanol was introduced drop-wise to F_CNFs suspension and vigorously mixed. The introduction of an aqueous Ammonia solution (25%, 1 ml) resulted in the complete hydrolysis of titanium butoxide (no traces of . titanium butoxide during the washing of the product). The mixture was then transferred to a Teflon cup autoclaved at 120ºC (24 h), cooled, centrifuged and washed with ethanol, deionized water and dried in an oven at 80ºC for 24 h. Calcination at 400ºC, 4 h was performed. 10% and 20% loadings of TiO_2 on F_CNFs, identified as F_CNFs/10% _TiO_2

and F_CNFs/20% _TiO_2 respectively were obtained. The above procedure was repeated without F_CNFs for the preparation of TiO_2 – anatase (TiO_2 – A), a control in this research.

5.2.4 The preparation of F_CNFs/TiO_2- Pt, F_CNFs/TiO_2/Au, and F_CNFs/TiO_2/Ir nanocomposites

The F_CNFs/TiO_2- Pt, F_CNFs/TiO_2/Au, and F_CNFs/TiO_2/Ir nanocomposites were prepared by a modified impregnation method. The method facilitated the homogeneous dispersion of the metals onto the surface of the supports, F_CNFs/TiO_2 nanocomposites [47], [48]. By having a known amount of each noble metal precursor and 1 g of the support, the mixture was then sonicated for 45 minutes and calcined at 350 ºC for 2 hours under continuous flow of Ar to eliminate any unwanted materials [49], [50].

5.2.5 The characterization processes

The synthesized CuONPs, F_CNFs, TiO_2, F_CNFs/TiO_2, together with the metal – F_CNFs/TiO_2 were identified by a variety of analytical processes. The structural properties of the F_CNFs, TiO_2, F_CNFs/TiO_2 and the metal - TiO_2/F_CNFs nanostructures were identified by High Resolution Scanning Electron Microscopy, HR-SEM analysis (ZEISS Sigma 300 VP from M/S ZEISS ‘Smart SEM’ OXFORD INSTRUMENTS x-act PentaFET Precision and ‘Oxford INCA’, United Kingdom, X-ray diffraction (XRD) using a Brucker D2 phaser fitted with Cu – Kα radiation (λ = 1.5405 Å), operating at 30 kV (Voltage) and 10 mA, (Current). A Perkin Elmer TA TGA Q500 for thermogravimetric analysis (TGA) in which 10 mg sample was heated to 900 ℃ at 10 ℃ min^{-1} under air. Additionally, the size and shape of the samples, was also achieved by the Transmission Electron Microscopy (TEM) utilizing a FEI Technai G2 Spirit electron microscope, with 120 kV. The particles size distribution analysis was done by ImageJ software whereby at least 100 particles were computed per sample. Fourier Transform Infrared, FT- IR Spectroscopy, mounted with a

Bruker Tensor 27 FT – IR spectrometer (4000 – 500 cm^{-1}) helped in the elucidation of the functional groups in the samples. The optical properties were investigated by a Varian Cary Eclipse EL0410 3870 photoluminescence/ fluorescence Spectrophotometer and a SPECORD 210 plus UV – Vis Spectrophotometer. The specific surface analysis, Brunauer – Emmett – Teller (BET), N_2 physisorption (Micromeritics ASAP – 2000 Tri - star analyser) was used. The sample preparation was performed earlier in which 0.2 g was degassed, 6 h (150 ℃) and concealed by a N_2 circulation with the help of a Micromeritics flow Prep 060. The X – ray Photoelectron Spectroscopy, XPS study was invested by a Thermo Scientific ESCALAB 250Xi spectrometer with a monochromatic Al Kα source (1486.7 eV).

5.2.6 The catalyst Activity: Hydrogen production from water

The catalytic hydrogen evolution from water was performed by submersion type reactor, Lelesil Innovative Systems, Thane, India, Fig. 2, described by *Walls et al.* [51] in which a 450 W UV lamp was used. The reactor is a tightly closed setup. The research used 1g of the sample in 1 L of distilled water, homogenized by stirring for 15 minutes then radiating the sample with the UV lamp at room temperature, 25ºC for 6 h under argon gas. The system was purged with argon until no peaks were detected on the online GC (thermal conductivity detector, TCD). The flow rate of the argon was 80 ml min^{-1} (the circulation of the argon was kept constant throughout the experiment). The rate of hydrogen formation was quantified by the GC using thermal conductivity detector (TCD).

Fig. 2. (a) Representational (b) Photographic Reactor used for photocatalysis, (1 litre).

5.3 Results and Discussions

5.3.1 The characterization of the support materials and the photocatalysts

TiO_2 – anatase and F_CNFs/TiO_2 materials were analysed by XRD. The characteristic peaks of TiO_2 – A (TiO_2 – anatase) also F_CNFs/TiO_2 composites are shown in Fig. 3. Some of the peaks of the F_CNFs were not noticed clearly on the PXRD patterns of the F_CNFs/TiO_2 samples because of an extention of the intense (101) TiO_2 – anatase absoption with (002) absorption of the F_CNFs, substantial dispersion from TiO_2 – anatase and the considerable distinction in the mass of TiO_2 – anatase in relation to the mass of F_CNFs in the F_CNFs/TiO_2 materials [52], [53]. After achieving clean conditions and water resources, the photocatalytic production of hydrogen is feasible. Similar studies show that the crystallinity of the catalysts affects their photonic qualities [54].

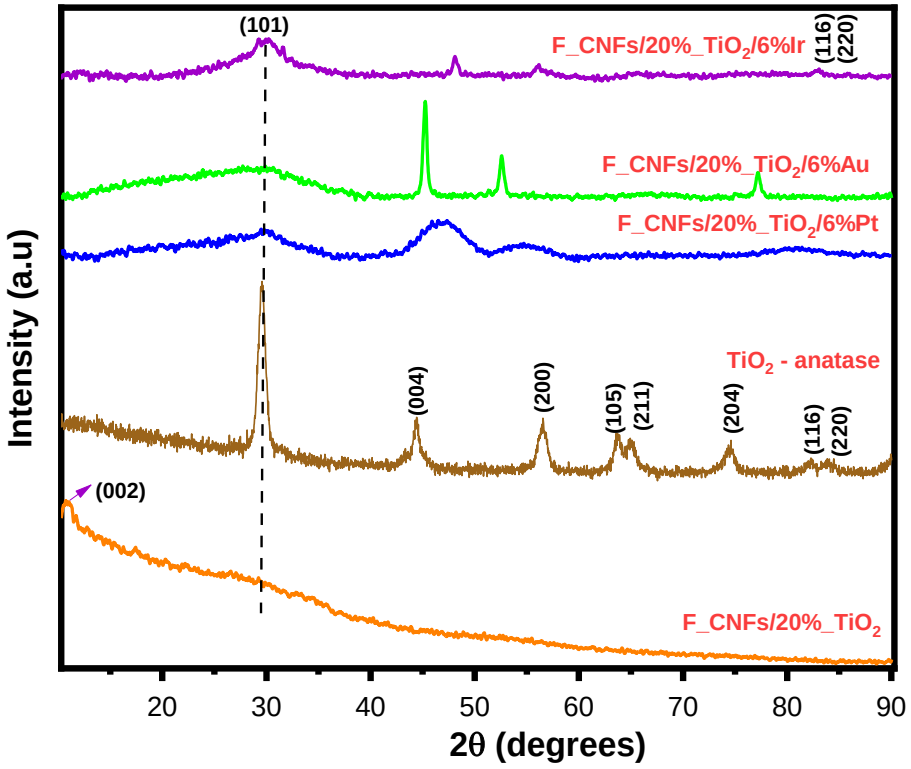

Fig. 3. XRD spectra of TiO_2 – anatase, and F_CNFs/TiO_2 composites.

Raman spectroscopy was employed in the investigation of the graphiticity of F_CNFs. The D-band at 1379 cm^{-1} identifies defects on the F_CNFs, while the G-band at 1592 $cm^{-1}$is C-C stretching of the F_CNFs, Fig. 4 (a). In addition, the D and G bands in the materials proved the existence of TiO_2 – anatase in the F_CNFs/TiO_2Pt/Au/Ir nanostructures as well as the crystallinity of the synthesized materials, Fig. 4(b). The Raman shift 144, 399, 513, and 639 cm^{-1} and are indexed (E_g), (B_{1g}), (A_{1g}), and (E_g), correspondingly [55], [56]. At least four modes were also realized on the spectra of the nanostructures, indicating the presence of TiO_2 – A in the synthesized materials.

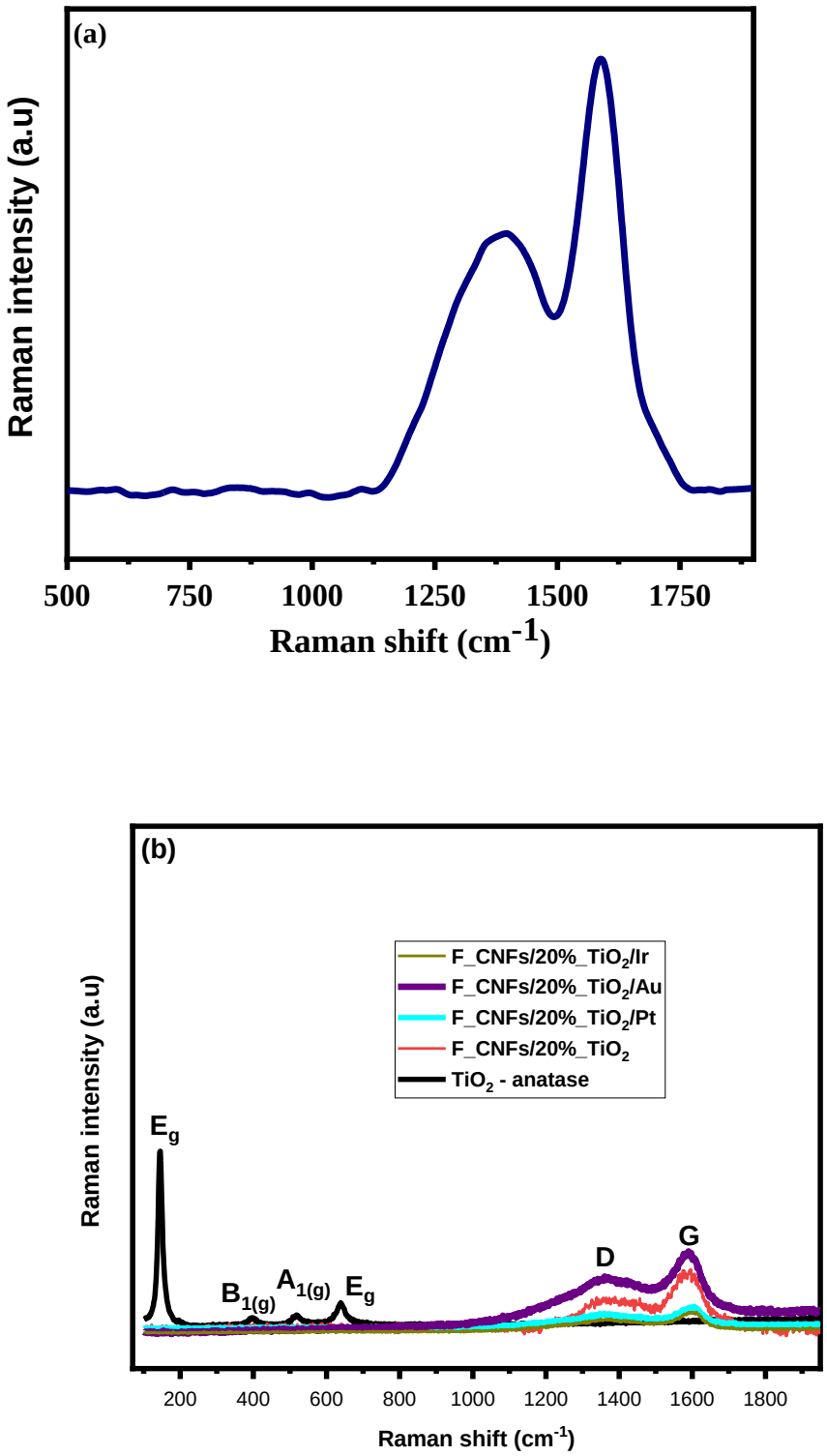

Fig. 4. Raman spectroscopy (spectra); (a) F_CNFs (b) TiO_2 – anatase as well as F_CNFs/TiO_2 composites.

The major observation was the intense TiO_2 peak (E_g) which was present in all the materials at lower wavelengths. Studies have shown that the positions and broadening of Raman peaks is a characteristic of the nanomaterials and its associated with the size and defects in the nanostructures, the conditions like temperature and the laser – induced local heating effect on the material under investigation [55]–[57]. The fact that all the laser Raman investigations in this work were carried out under identical experimental conditions, then the decrease in wavelengths (blue shifting) and broadening of the peaks resulted from phonon confinement and surface pressure [58]. Additionally, similar research have found identical observations particularly with titanium nanotubes and graphene oxide. These findings evidence the existence of higher chemical interactions in the F_CNFs/TiO_2 materials [59]. The chemical reactions in TiO_2 and F_CNFs were predicted and it suggests an increase in charge separation in the F_CNFs/TiO_2 matrix, thereby pointing to improvement in photo-catalysis. The outcome of the analysis (Raman spectroscopy) reveal the strong chemical interactions in TiO_2, F_CNFs and Pt, Au, Ir of noble metal – TiO_2 /F_CNFs interfaces.

The 3D analysis and the composition of TiO_2 – anatase, F_CNFs, F_CNFs/TiO_2 and F_CNFs/TiO_2 – noble metal heterostructures were evaluated by the Scanning Electron Microscopy, SEM and Transmission Electron Microscopy, TEM, Fig. 5 and 6. The F_CNFs were fiber-like while TiO_2 – anatase was granular (consisting of small particles). The F_CNFs/TiO_2 and F_CNFs/TiO_2- noble metal structures were fluffy in morphology, figure 5.

The synthesized carbon nanofibers were washed to remove impurities and to functionalize them. Other analyses including FESEM of the CNFs and functionalized, F_CNFs are presented in figure 5. The analyses presented in figure 5 show that the catalyst, CuONPs was completely removed from the F_CNFs. The purified (functionalized) F_CNFs were fibrous in

nature and the fibers were helical as shown by the TEM image figure 6. It was also the same observation with F_CNFs morphology, FESEM analysis, figure 5. The F_CNFs were found to be narrow in diameter averaging 81.59 nm, but varying between 14 and 134 nm. This is in order with other observations on CNFs [60].

The synthesized TiO_2 – anatase nanoparticles were grainy, and averaging closer to 7.2 nm, figure 6. The CNFs were totally coated with TiO_2, figures 5. The Field Emission Scanning Electron Microscopy disclosed the existence of TiO_2 nanoparticles on the CNFs. This is in agreement with what *Gao et al* found that blending TiO_2 and CNFs by the hydrothermal sol-gel method gives evenly covered CNTs with TiO_2 nanoparticles [61]. In this study, hydrothermal process fully coated the F_CNFs.

The complete coating of the F_CNFs suggested that chemical interactions existed between the TiO_2 and F_CNFs because proximity and chemical reactions in the F_CNFs/TiO_2 composites have been recognized as the origin of electron transfer of related complexes consequently bringing about charges separation [62]–[64].

Most of the work done by different researchers have reported that the physicochemical properties of F_CNFs/TiO_2 materials depend on the interaction between F_CNFs and TiO_2 and the synthesis methods [61]. Furthermore, clustering of TiO_2 nanoparticles over the surface of the F_CNFs verified that the F_CNFs contributed in the building up of the TiO_2 nanoparticles in the course of the synthesis [61].

In figure 5, the Field Emission Scanning Electron Microscopy and Energy - dispersive X-ray spectroscopy verified Ti, C as well as O to be present in the support materials and that photo-catalysts were composited with the noble metals, Pt, Au and Ir. Related work have proved that Field emission scanning electron microscopy and energy - dispersive x-ray spectroscopy have been used to show the composition of the samples [58], [65].

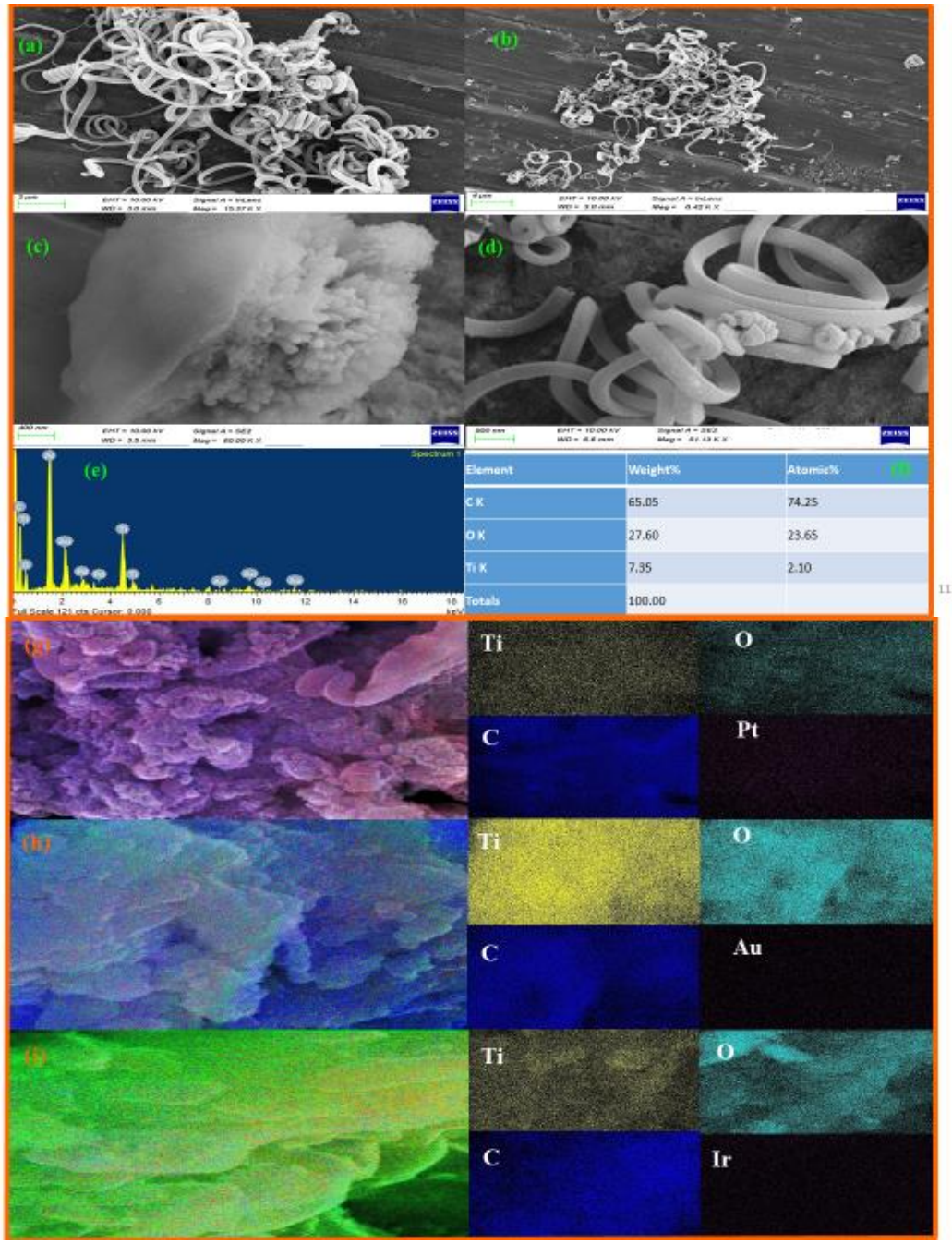

Fig. 5. Field Emission Scanning Electron Microscopy, FESEM investigation of; as-prepared CNFs (a), Functionalized CNFs, F_CNFs (b), TiO_2 – anatase (c), F_CNFs/20% _TiO_2 composite (d), EDS spectrum of the F_CNFs/20% _TiO_2 (e), configuration of the elements, F_CNFs/20% _TiO_2 (f), EDS mapping survey of F_CNFs/20% _TiO_2/6%Pt (g), EDS mapping survey of F_CNFs/20% _TiO_2/6%Au (h), and EDS mapping survey of F_CNFs/20% _TiO_2/6%Ir (i).

(a) (b)

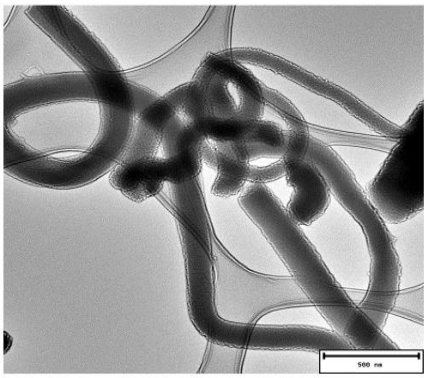

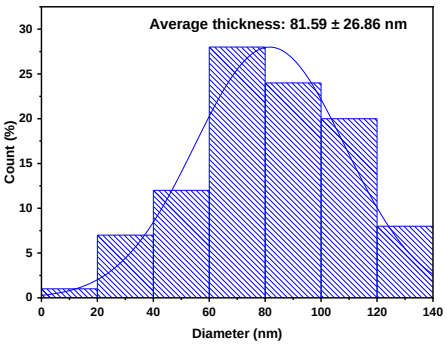

(C) (d)

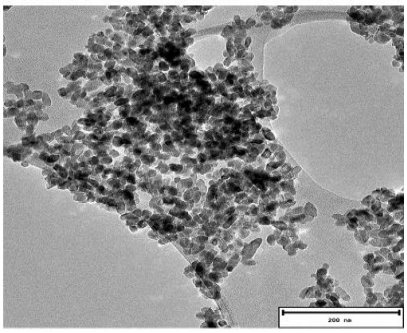

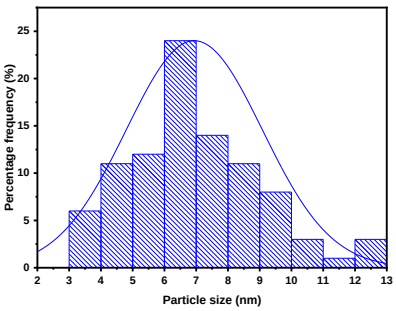

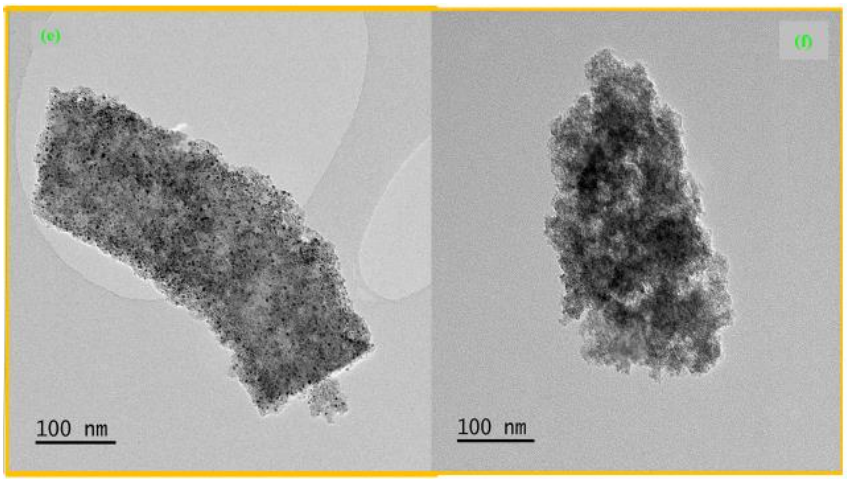

Fig. 6. The Transmission Electron Microscopy images; F_CNFs (a), the diameter of the F_CNFs (b), TiO_2 – anatase (c), the size distribution of TiO_2 – anatase (d), F_CNFs/20% _TiO_2/ 6%_Pt (e), and F_CNFs/20% _TiO_2/ 6%_Au (f).

The electronic configurations of the elements in F_CNFs/TiO_2, F_CNFs/20% _TiO_2/ 6%_Pt, and F_CNFs/20% _TiO_2/ 6%_Au photo-catalysts were investigated by X – ray photoelectron spectroscopy, XPS and the results are shown in figure 7, and figure 8. Clearly, the XPS analysis graph in Fig. 7 (a) presents six elements, C, Ti, O, N, Pt together with Au on the facial of the photo-catalysts (the presence of N, lower intensity of N 1s peak in Fig. 7 (a) and Fig. 8 (a) could be as a result of a small contamination of ammonia solution used in the synthesis of F_CNFs/20% _TiO_2, and the F_CNFs/20% _TiO_2 – noble metals composites). In figure 7(b), Ti 2p spectrum of binding energy, 458.20 eV for $2p_{3/2}$ is as a result of the titanium TiO_2 presence[66].

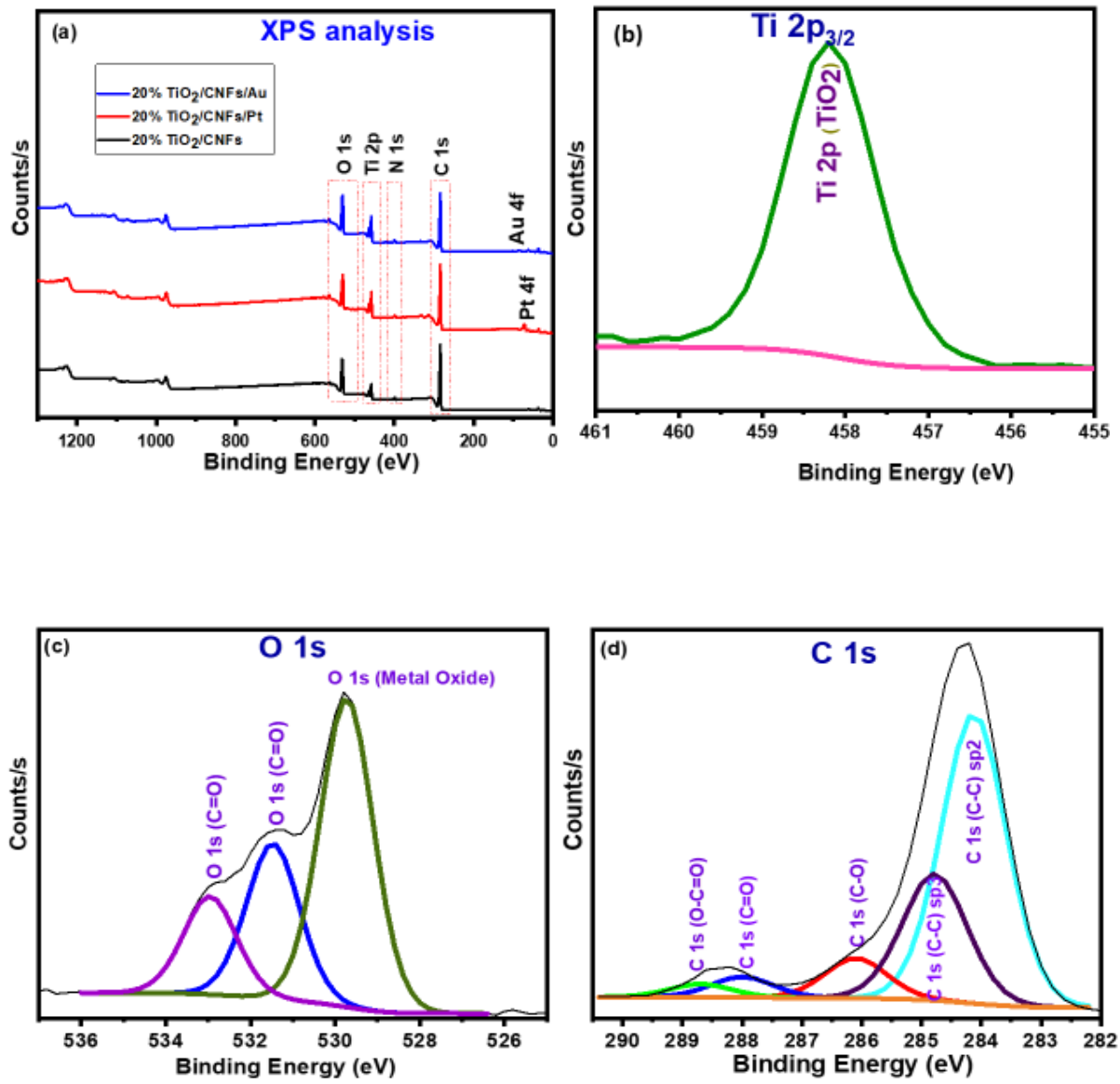

Fig. 7. X – ray photoelectron spectroscopy, XPS examination of F_CNFs/TiO_2, F_CNFs/20% _TiO_2/Pt, and F_CNFs/20% _TiO_2/Au, XPS summary spectra of the composites (a), and (b) – (d) XPS spectra of titanium, oxygen, and carbon respectively.

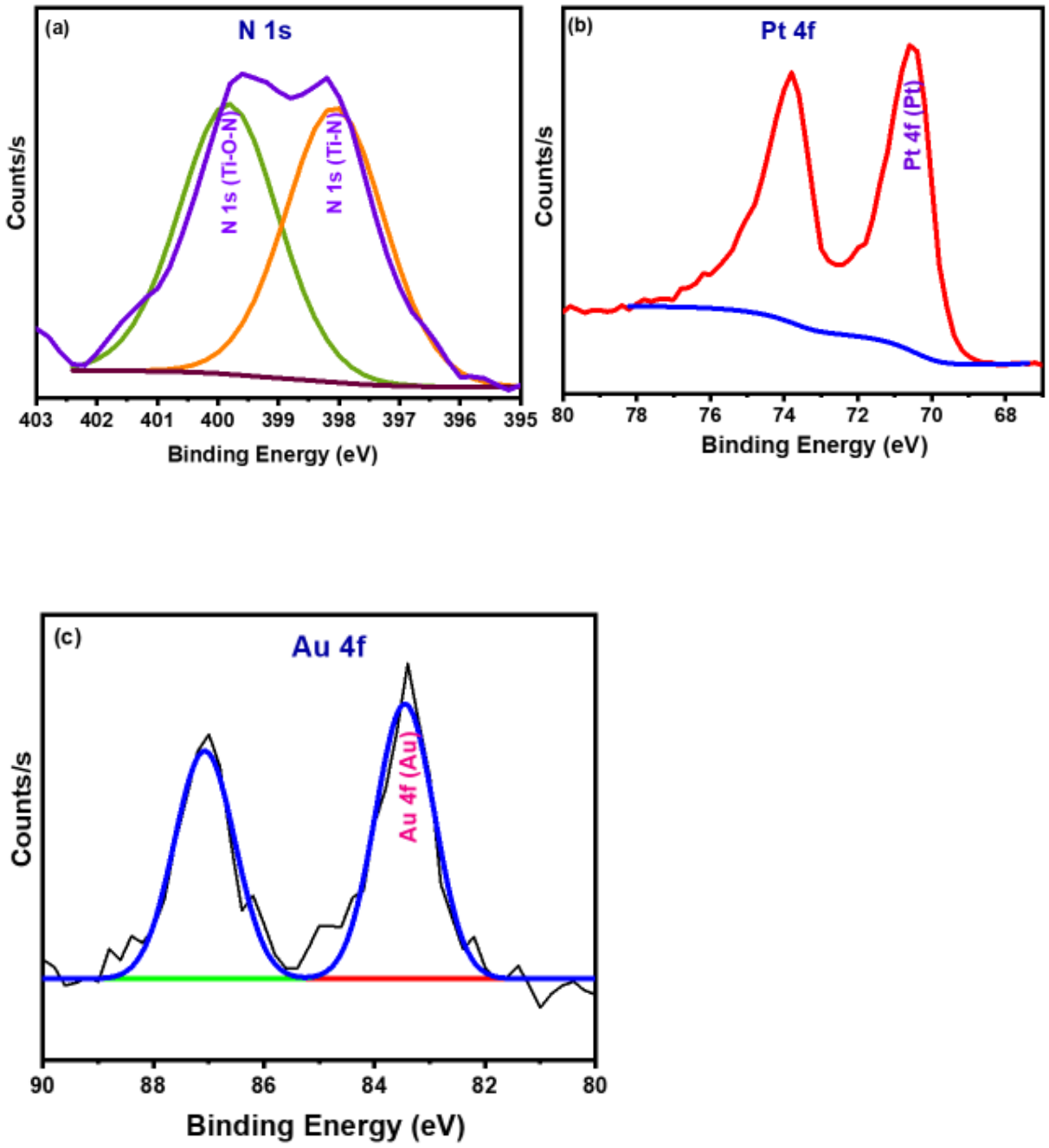

Fig. 8. X – ray photoelectron spectroscopy, XPS examination of F_CNFs/20% _TiO_2, F_CNFs/20% _TiO_2/Pt, and F_CNFs/20% _TiO_2/Au, XPS spectra of nitrogen, platinum, gold (a) – (c).

The Pt 4f spectrum of Pt particles in figure 8(b) is associated with the binding energy of Pt^o metallic nanoparticles at 70.60 eV thereby demonstrating that Pt nanoparticles were coated on the F_CNFs/20% _TiO_2 composites. Related studies also reported comparable findings [67], [68]. Further, in figure 8(b), the XPS spectrum of Pt 4f is presented. The peak which is located at 70.60 eV corresponds to Pt 4f implying that Pt in F_CNFs/20% _TiO_2 composite is in the form of Pt^o [69]. The presence of N, lower intensity of N 1s peak in Fig. 7 (a) and Fig. 8 (a) could be as a result of a small contamination of ammonia solution used in the synthesis of F_CNFs/20% _TiO_2, and the F_CNFs/20% _TiO_2 – noble metals composites.

In figure 7(c), the O 1s peaks positioned at 531.6 eV, 533.1 eV, and 529.7 eV are consistent with the adsorbed oxygen[70] whereas figure 8(a) displays the binding energy of N 1s with the peaks at 398.1 eV and 399.8 eV. At 398.1 eV, we find a weaker peak which can be assigned to Ti – N bond signifying some absorption of nitrogen atoms into the F_CNFs/TiO_2 matrix [71], [72]. The peaks located at 398.1 eV and 399.8 eV are N 1s. They hint to the presence of small quantities of –NH and $–NH_3^+$ respectively in all the structures as illustrated in XPS analysis spectra, Fig. 7(a) and the XPS spectrum of nitrogen Fig. 8(a) [73], [74]. The XPS analysis Fig. 7(a) identifies carbon as one of the elements present in the materials. The XPS peak, conforming to C 1s is clarified into 5 peaks, Fig. 7(d). The bonds, C=C which are positioned around 284.7 eV point to the existence of C in the CNFs or graphene materials [68], [75].

The peaks positioned at 286.1 eV, 2.88 eV, and 288.7 eV are associated with C-O, C=O and O-C=O accordingly and moreover validates the efficient blending of the F_CNFs into the F_CNFs/20% _TiO_2 composite and the other composite materials, Fig. 7(d) [73]. The X – ray photoelectron spectroscopy spectrum in Fig. 8(c) is of the F_CNFs/20% _TiO_2/Au. The 4f (83.4 eV) peak is of Au as was also found by other similar studies [74].

Table 1. Surface area (BET) analysis of the structures.

Materials	**Surface area (m^2g^{-1})**	**Pore volume (cm^3g^{-1})**	**Pore diameter (nm)**	**I_D/I_G**	**Reference**
TiO_2- anatase	73	0.079	5.1		Current work
TiO_2 – rutile (dandelion)	81	0.071	3.2		[76]
TiO_2-P25	49	-	-		[Sigma-Aldrich]
F_CNFs	32	0.091	22.6	0.87	Current work
F_CNFs/10% _TiO_2	89	0.120	5.4		Current work
F_CNFs/20% _TiO_2	126	0.273	10.7		Current work
F_CNFs/10% _TiO_2/5%Au	171	0.140	3.3		Current work
F-CNFs/20% -TiO_2/6%Au	79	0.103	5.3		Current work
F_CNFs/20% _TiO_2/6%Pt	341	0.302	3.6		Current work
F-CNFs 20%-TiO_2/6%Ir	336	0.309	3.7		Current work

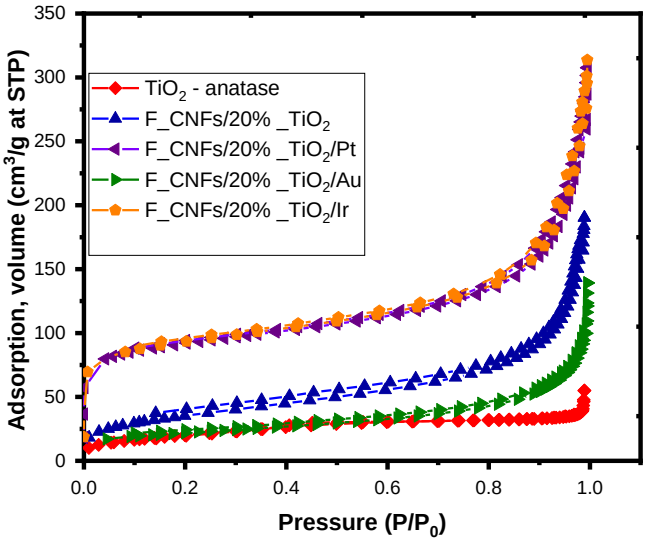

Fig. 9. (a) N_2 – adsorption – desorption isotherms of TiO_2-anatase, F_ CNFs/20%_TiO_2, F_ CNFs/20%_TiO_2/Pt, F_ CNFs/20%_TiO_2/Au, F_ CNFs/20%_TiO_2/Ir.

One of the benefits of incorporating CNFs intoTiO_2 matrix is the improvement of the surface area. Thus, BET investigation was conducted to analyse the surface area and the results are presented in Table 1 and Fig. 9.

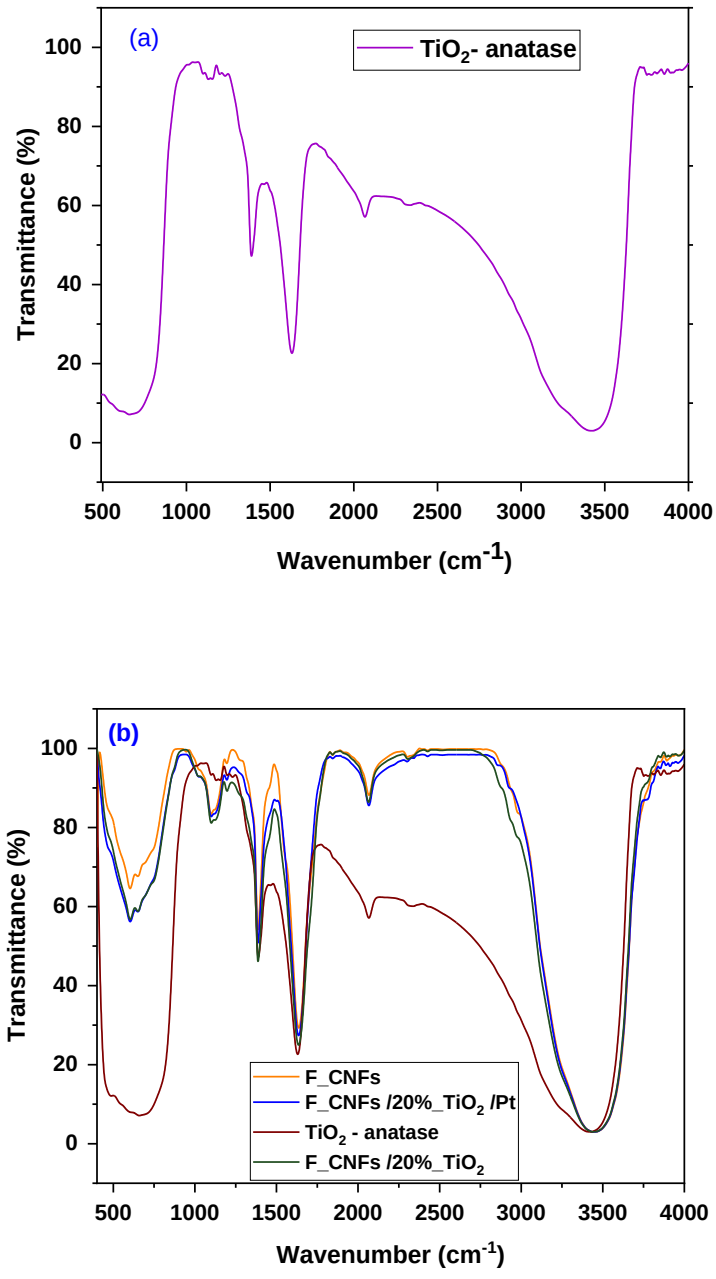

Fig. 10. The FTIR spectra; (a) TiO_2 – anatase (b) F_CNFs, TiO_2 – anatase and TiO_2 - anatase/F_CNFs/Pt composites.

The increase in linearity of the adsorption isotherms profiles was identified in the corresponding pressure (P/P^o) range 0.30 to 0.85. This correlates with the mesoporous structure of the nanostructures [77]. The BET surface area of the photo-catalysts is in Table 1. The process lag curves profiles in the isotherms were categorized as type IV which is in conformity with the International Union of Pure and Applied Chemistry (IUPAC) classification characterizing the nanostructures as mesopores [78].

The compositing of the F_CNFs of surface area, 32 m^2/g with TiO_2 of surface area, 73 m^2/g resulted in the F_CNFs/TiO_2 composite with surface area of 126 m^2/g. This finding shows that the composite formed was greater in surface area than the starting materials. Furthermore, the pore volume of the F_CNFs/TiO_2 composite was greater, Table 1. Therefore, the increase in the surface area of the F_CNFs/TiO_2 composite is as a result of doping and the functionalization of the materials [44]. The TiO_2 – anatase (surface area, 73 m^2/g) that was prepared by the modified hydrothermal process matched with the results of similar work. The addition of the precious metals also increased the surface area.

The FTIR spectra of the F_CNFs and the composites are shown in figure 10. The dominant band at 1100 cm^{-1} is correlated with C–O stretching vibrations while the peak at 3438 cm^{-1} is the O-H stretching vibrations. The other peaks are the vibrations of aliphatic C-H groups in the range of 3000-2800 cm^{-1}, 2000-1800 cm^{-1}, 1410-1395 cm^{-1}, and 820-790 cm^{-1}. The 3400 cm^{-1} peak is the adsorbed water molecules. The range of the peaks, 690 to 800 cm^{-1} and the broad peak further down than 1000 cm^{-1} are the TiO_2 characteristic peaks [79]. The 3300cm^{-1} peak was common in the F_CNFs/TiO_2 composites, figure 10. The 3230, 2920, 1720, 1636, and 1330 cm^{-1} peaks show the presence of O-H, C-H, C=O, C=C and C-O-C accordingly. The peak located at 1104 cm^{-1} for TiO_2 is Ti – O – C and is used in identifying the conjugation effect of the F_CNFs and TiO_2 [80].

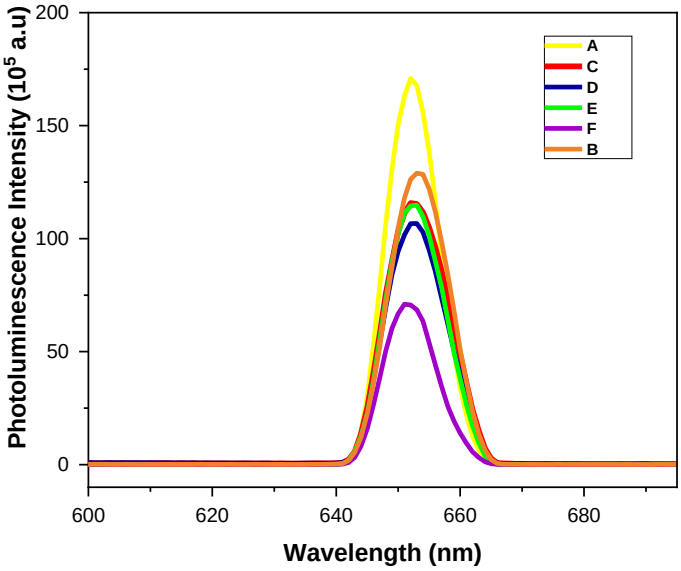

Fig. 11. The spectra of the photoluminescence study of TiO_2– anatase (A), F_CNFs (B), 10% _TiO_2/F_CNFs (C), 20% _TiO_2/F_CNFs (D), 20% _TiO_2/F_CNFs/Pt (E), and 20% _TiO_2/F_CNFs/Au (F) composites.

The investigation of the confinement, movement and transfer properties of the photo-generated electron – hole pairs of the TiO_2 – anatase and F_CNFs/TiO_2 composites was obtained by the photoluminescence study because similar studies of photocatalysts have been identified and used in the study of electron – hole pairs [63], [81]. The excitation wavelength, 350 nm was used and the obtained resultsare in figure 11. These results are in agreement with other similar studies [81].

From the results in figure 11, TiO_2 – anatase had greater emission peak than the F_CNFs/TiO_2 composites. The lower intensity of the composites was because the recombination rate of the electron – hole pairs was reduced indicating that the F_CNFs had improved the separation of electron – hole pairs [53], [56], [61], [81], [82]. Hence, the bigger the loading of TiO_2 on the F_CNFs the greater the charge separation.

Table 2: The Band gap (E_g) energies (eV) of the materials

Sample	Energy (eV)	Reference
F_CNFs/20%_TiO_2	1.97	Current work
F_CNFs/20%_TiO_2/Pt	1.71	Current work
F_CNFs/20%_TiO_2/Au	1.88	Current work
F_CNFs/20%_TiO_2/Ir	1.71	Current work
TiO_2 – Degussa P25	3.10	[83][84][85]
TiO_2 – Anatase	3.20, 2.13	[84][86]
TiO_2 – Anatase	2.25	Current work
TiO_2 – rutile	3.00	[84]

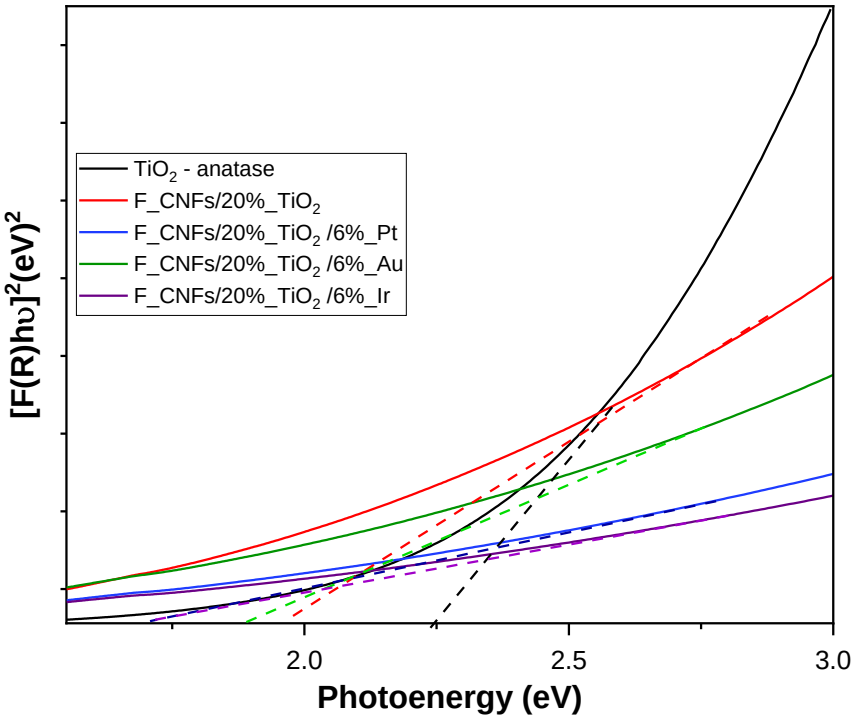

Fig. 12. The energy (eV), band gap (E_g) of TiO_2 – anatase, F_CNFs/20% _TiO_2, F_CNFs/20% _TiO_2/Pt, F_CNFs/20% _TiO_2/Au, F_CNFs/20% _TiO_2/Ir composites.

Following the verification that compositing TiO_2 with F_CNFs lowered the recombination rate of the charge carriers by the photoluminescence studies, Fig. 11, UV-vis DRS studies were conducted to investigate the response of the composites with visible light.

The Tauc's plot attained from UV-vis DRS spectra of the F_CNFs/TiO_2 composite was not comparable to that of TiO_2 – anatase indicating that the F_CNFs had positive impact on the band gap of the F_CNFs/TiO_2 composite (1.97 eV), Table 2 and Fig. 12. This shows that the band gap energies of the F_CNFs/TiO_2 were significantly lowered suggesting that the composites will have improved photocatalytic activity as compared to TiO_2 – Anatase (3.2 eV), table 2 [83], [86].

5.3.2 Photocatalytic studies

The photocatalysts were assessed in the H_2 production reaction using water. The cumulative H_2 production analysis of the photocatalysts is in Fig. 13 (a). The assessment of the catalysts was based on the materials (support), loading (efficiency) and cocatalysts used in the study. Thus, the first category consists of TiO_2 - anatase and TiO_2 – P25. The second category is the loading of TiO_2 on the functionalized CNFs (F_CNFs) thereby attaining F_CNFs/10% _TiO_2 and F_CNFs/20% _TiO_2. In the third category of photocatalysts, we have the support; F_CNFs/TiO_2 – composited with Pt, Au or Ir with the noble metal loading of 1%, 5%, and 6%. In general, F_CNFs/20% _TiO_2/6%Pt was established as the most active photocatalyst. It generated about 62 times more H_2 as compared to the second group of photocatalysts in this study, F_CNFs/20% _TiO_2. Moreover, F_CNFs/20% _TiO_2/6%Pt produced more H_2 than the commercial TiO_2 (TiO_2 – P25), Table 3 and Fig. 13.

Table 3: Outline of the photocatalytic activity of photocatalysts for water splitting

Photocatalyst	**Reactant & sacrificial agents**	**Parameter (Light source)**	**Activity (H_2 evolution)**	**Ref**
Cu/TiO_2 nanorods	Methanol, 20 vol %	300 W Xe lamp	1023.8 μmol g^{-1} h^{-1}	[87]
Rh-Nb/TiO_2 NRs	Methanol, 10 vol %	300 W Xe lamp	7850 μmol g^{-1} h^{-1}	[88]
rGO/TiO_2	Methanol	300 W Xe lamp	149 μmol g^{-1} h^{-1}	[89]
3 wt% Ni-TiO_2/CdS	Ethanol, 25 wt%	300 W Xe lamp, 420 cut off filter	33.63 μmol /g-cat^{-1} h^{-1}	[90]
Ru/CdS-ZnS	Formic acid, methanol, ethanol	300 W Xe lamp	266 mmol/m^2 h	[91]
Au/TiO_2	Ethanol	4 UV-LED lights, 12 W each	15.8 μmol /min g-cat.	[92]
SiFe co doped TiO_2	540 ml distilled H_2O, 60 ml ethanol	500 W	320 μmol g^{-1} h^{-1}	[93]

GaN:ZnO (Mn_3O_4.Rh/Cr_2O_3	Distilled H_2O NaI		20 μmol g^{-1} h^{-1}	[93]
F_CNFs/20%_TiO_2	Distilled H_2O	450 W Xe lamp	0.00720 mol g^{-1} h^{-1}	Current work
TiO_2	Distilled H_2O 10% methanol	300 W Xe lamp	42.00 μmol g^{-1} h^{-1}	[93][94]
F_CNFs/20%_TiO_2/6%Pt	Distilled H_2O	450 W Xe lamp	0.45 mol g^{-1} h^{-1}	Current work
F_CNFs/10%_TiO_2/5%Au	Distilled H_2O	450 W Xe lamp	0.28 mol g^{-1} h^{-1}	Current work
F_CNFs/20%_TiO_2/1%Ir	Distilled H_2O	450 W Xe lamp	0.21 mol g^{-1} h^{-1}	Current work
TiO_2 – P25	Distilled H_2O	450 W Xe lamp	0.000126 mol g^{-1} h^{-1}	Current work
TiO_2 - anatase	Distilled H_2O	450 W Xe lamp	0.000119 mol g^{-1} h^{-1}	Current work

(a)

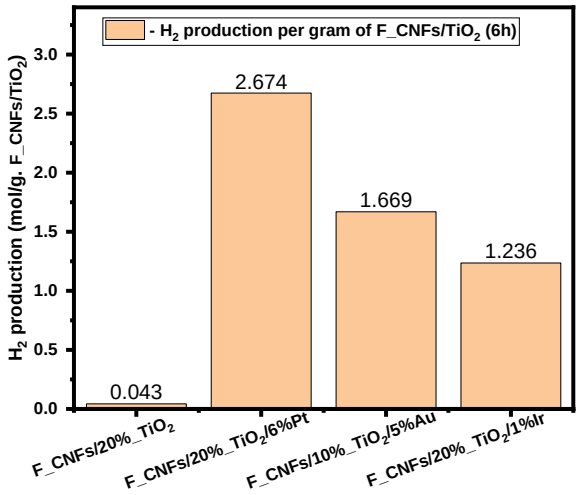

(b)

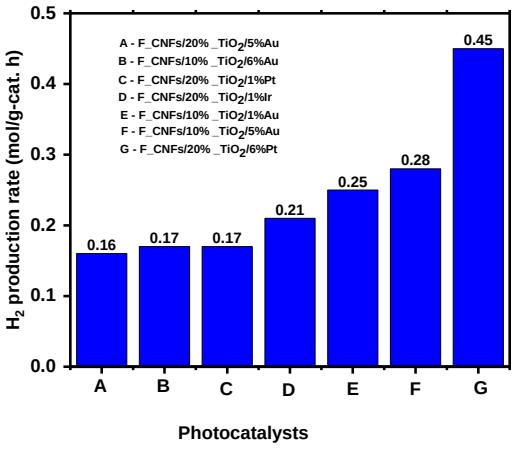

Fig. 13. The H_2 produced in 6 h of reaction (moles of H_2 per gram of the support, F_CNFs/TiO_2) for the photocatalysts, F_CNFs/20% _TiO_2, F_CNFs/20% _TiO_2/6%Pt, F_CNFs/10% _TiO_2/5%Au, F_CNFs/20% _TiO_2/1%Ir (b) The H_2 production rate (mol/g-cat.h) of the photocatalysts: F_CNFs/20% _TiO_2/5%Au, F_CNFs/10% _TiO_2/6%Au, F_CNFs/20% _TiO_2/1%Pt, F_CNFs/20% _TiO_2/1%Ir, F_CNFs/10% _TiO_2/1%Au, F_CNFs/10% _TiO_2/5%Au, and F_CNFs/20% _TiO_2/6%Pt (the arrangement of the photocatalysts is for easy interpretation of the data).

The most active structure, F_CNFs/20% _TiO_2/6%Pt, had a loading of 20% by weight of TiO_2 coated on the surface of the F_CNFs as evidenced by the Field Emission Scanning Electron Microscopy Fig. 5(d) and (g) and the Transmission Electron Microscopy image in Fig. 6(e). In addition, the catalyst was assessed in a reaction for 6 h, and produced no signs of deactivation but increased H_2 production as shown in Fig. 14.

The increament produced by TiO_2 – carbon structures when compared to pure TiO_2 (TiO_2 – anatase and TiO_2 – P25) has come about because of the increase in the surface area and reduction in the recombination rate of the charged pairs, the electron – hole recombination [95]. Leary and Westwood studies and others also compared TiO_2 – carbon structures used as photocatalysts to a pure TiO_2 photocatalyst under similar experimental environment such as mass [95] as it was also done in this research. Table 3, further confirms the findings.

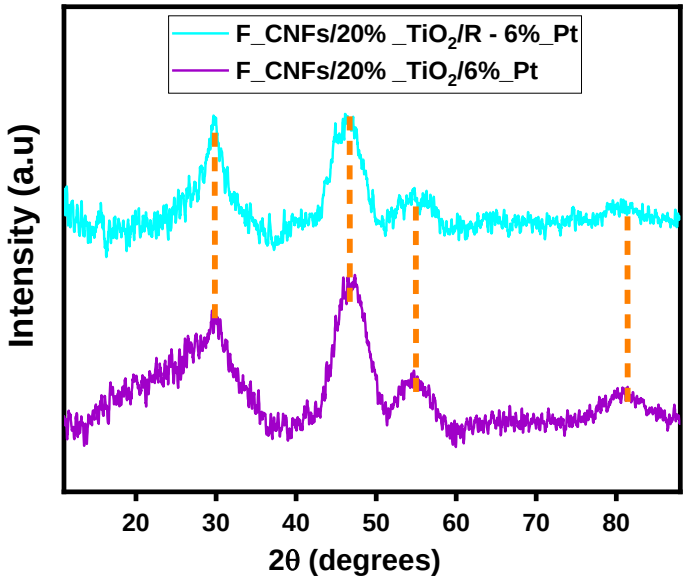

Fig. 14. Effect of stability of the photocatalyst, F_CNFs/20% _TiO_2/6%_Pt, and F_CNFs/20%_TiO_2/R - 6%_Pt, XRD spectra.

Several studies have been performed on TiO_2/C composites for the production of hydrogen [96]–[99]. However, comparison of the results has been a challenge because factors such as the quantity of TiO_2, the sacrificial agents (organic and/or inorganic) used and their concentrations, the source and intensity of power used among others are hindering the comparison of the results [100]–[102]. Thus, its conceivably more appropriate to compare the results simultaneously with the experimental conditions and further incorporate a standard catalyst, such as commercial TiO_2 (TiO_2 – P25), as a reference catalyst [96]. In this research, the hydrogen produced when F_CNFs/20% _TiO_2/6%Pt photocatalyst was used is about 100 fold the amount produced by TiO_2 - P25. Another observation was that the as-synthesized TiO_2 – anatase and P25 produced more or less the same amount of hydrogen, Fig. 13. These results and the comparisons evidence the importance of incorporating appropriate controls in the synthesis and photocatalysis.

The proposed schematic diagram of synergies of CNFs/Pt/Au/Ir nanocomposites in regard to efficient photocatalytic activity of TiO_2 for H_2 evolution is presented in Fig. 15.

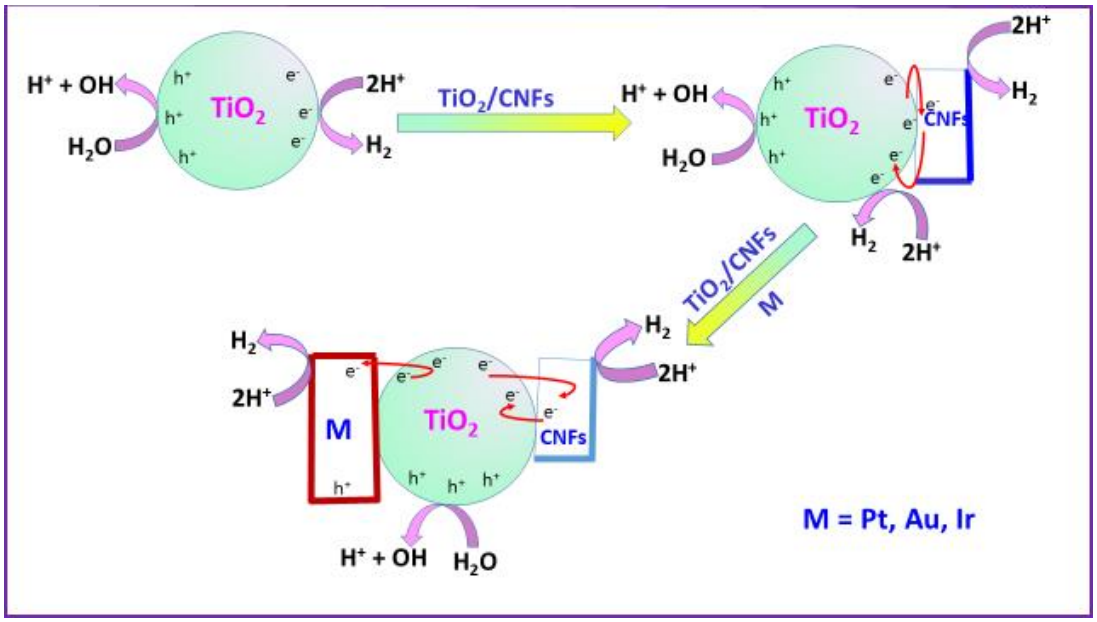

Fig. 15. The schematic illustration of synergies of F_CNFs/Pt/Au/Ir nanocomposites towards efficient photocatalytic activity of TiO_2 for H_2 evolution.

5.4 CONCLUSION

There were different F_CNFs/TiO_2 composites synthesized in this study. They included F_CNFs/10% _TiO_2, F_CNFs/20% _TiO_2, F_CNFs/20% _TiO_2 – metal composites. The incorporation of the F_CNFs into the titania structure increased the BET surface area of the TiO_2 from 73 m^2g^{-1} to 126 m^2g^{-1}, F_CNFs/20% _TiO_2. Moreover, the Brunauer – Emmett – Teller, BET surface area basically increased with the noble metal inclusion and it was confirmed that the F_CNFs/20% _TiO_2/6%Pt structure had the greatest surface area of 341 m^2g^{-1}. The pore volume of the materials further increased but the pore diameter of the composites lessened. This observation indicates that the noble metals and CNFs can effectively tune the morphology of TiO_2 for greater surface area, larger pore volume, and lower pore diameters and therefore increase the photocatalytic properties of the TiO_2/C – noble metal photocatalysts. The Raman, FTIR, FESEM techniques revealed a very homogeneous distribution of TiO_2 nanoparticles on the F_CNFs. The XPS analysis verified the existence of all the elements as Ti, O, C, N, Pt as well as Au and their corresponding electronic configurations (chemical states). This was important for understanding the mechanism of photocatalytic water splitting with particular interest on the cocatalysts (Pt and Au) as their chemical structures, surface area, quantities, chemical states, morphology, particle sizes, functional groups play important roles in photocatalytic water splitting processes. All the carbon containing samples had a change in wavelengths after UV-Vis light absorption to the visible region of the electromagnetic spectrum (TiO_2 – 3.20 eV to 1.71 eV – F_CNFs/20% _TiO_2/6%Pt, F_CNFs/20% _TiO_2/1%Ir).

The photocatalysts were tested for hydrogen evolution using water, and the most active photocatalyst, F_CNFs/20% _TiO_2/6%Pt had greater activity, 0.45 mol g^{-1} h^{-1} as compared to TiO_2 – P25, the commercial TiO_2 (0.000126 mol g^{-1} h^{-1}). Furthermore, the photocatalyst, F_CNFs/20% _TiO_2/6%Pt was stable even after 6 h use and therefore can be used for longer

periods or recycled for economic purposes. The outcome of this study evidence the important role of compositing titania with CNFs and decorating the composites with small quantities (1%, - 6%) of noble metals as cocatalysts for effective photocatalytic water splitting.

Acknowledgement

We thank the University of the Witwatersrand and Prof Rudolph Erasmus of the University of the Witwatersrand for the assistance with Raman, UV – Vis and Photoluminescence analyses, we appreciate the services.

Conflicts of interest

There are no conflicts of interest to be declared by the authors.

APPENDIX I. SUPPLEMENTARY DATA

XPS data

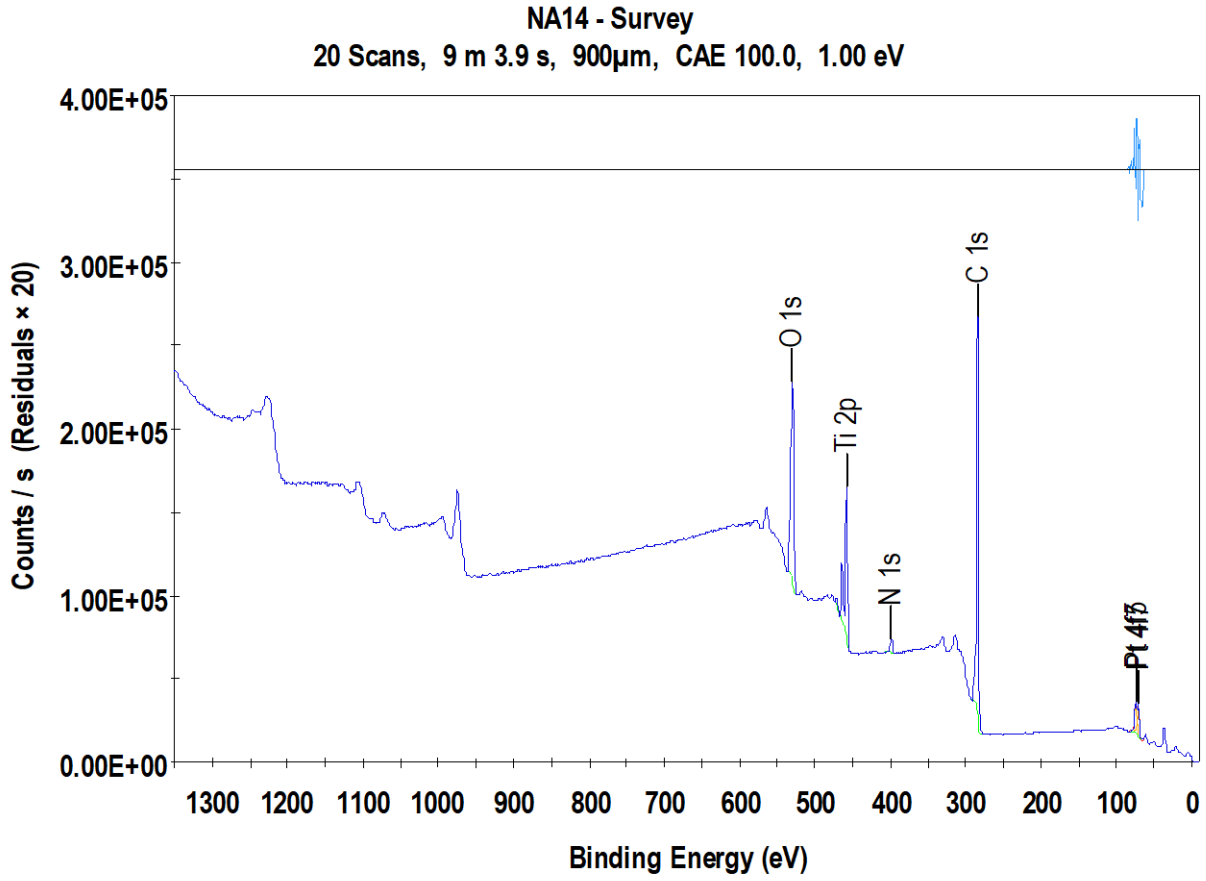

NA14

Elemental ID and Quantification

Name	*Peak BE*	*Atomic %*
C 1s	284.3	72.4
O 1s	530.3	20.0
Ti 2p	458.1	5.3
N 1s	398.9	1.7
Pt 4f7	70.7	0.6

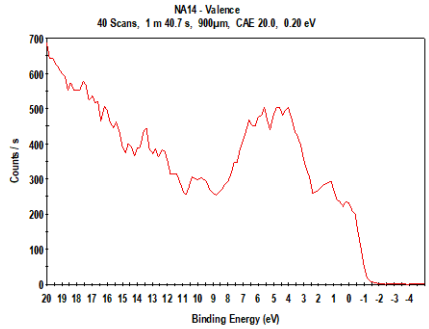
NA14 - Valence
40 Scans, 1 m 40.7 s, 900µm, CAE 20.0, 0.20 eV
Counts / s
Binding Energy (eV)

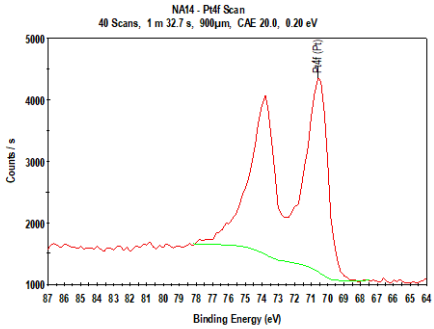
NA14 - Pt4f Scan
40 Scans, 1 m 32.7 s, 900µm, CAE 20.0, 0.20 eV
Pt4f (Pt)
Counts / s
Binding Energy (eV)

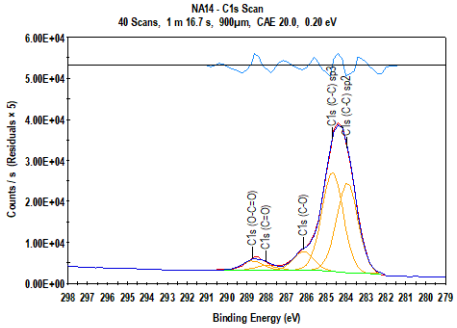
NA14 - C1s Scan
40 Scans, 1 m 16.7 s, 900µm, CAE 20.0, 0.20 eV
C1s (O-C=O)
C1s (C=O)
C1s (C-O)
C1s (C-C) sp3
C1s (C-C) sp2
Counts / s (Residuals x 5)
Binding Energy (eV)

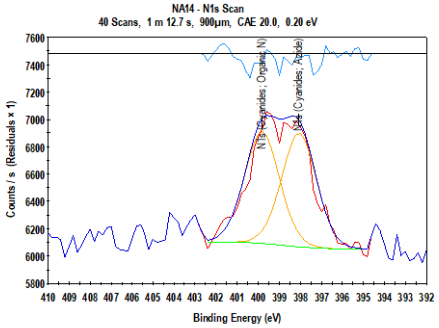
NA14 - N1s Scan
40 Scans, 1 m 12.7 s, 900µm, CAE 20.0, 0.20 eV
N1s (Organic; N)
N1s (Cyanides; Azide)
Counts / s (Residuals x 1)
Binding Energy (eV)

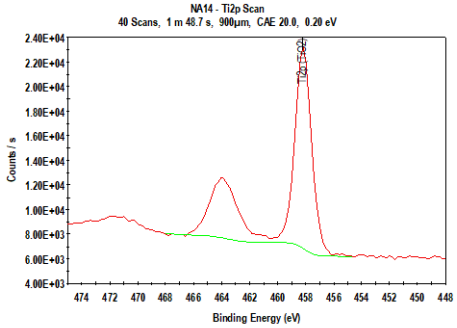
NA14 - Ti2p Scan
40 Scans, 1 m 48.7 s, 900µm, CAE 20.0, 0.20 eV
Ti2p (Ti-O)
Counts / s
Binding Energy (eV)

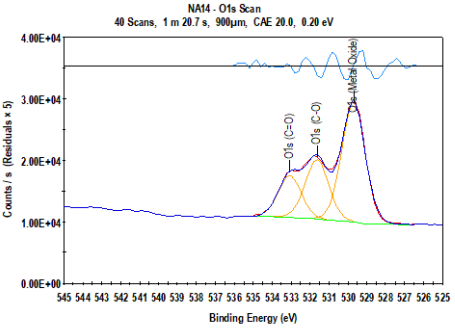
NA14 - O1s Scan
40 Scans, 1 m 20.7 s, 900µm, CAE 20.0, 0.20 eV
O1s (C=O)
O1s (C-O)
O1s (Metal Oxide)
Counts / s (Residuals x 5)
Binding Energy (eV)

NA14

Chemical ID and Quantification

Name	*Peak BE*	*FWHM eV*	*Atomic %*
Pt4f (Pt)	70.6	1.5	0.6
C1s (C-C) sp2	283.9	1.2	29.0
C1s (C-C) sp3	284.7	1.2	32.2
C1s (C-O)	286.1	1.2	5.9
C1s (C=O)	288.0	1.2	1.5
C1s (O-C=O)	288.7	1.2	2.8
N1s (Cyanides; Azide)	398.1	1.9	1.0
N1s (Cyanides; Organic N)	399.8	1.9	1.0
Ti2p (TiO2)	458.2	1.3	5.6
O1s (Metal Oxide)	529.7	1.4	11.0
O1s (C-O)	531.6	1.4	5.5
O1s (C=O)	533.1	1.4	3.8

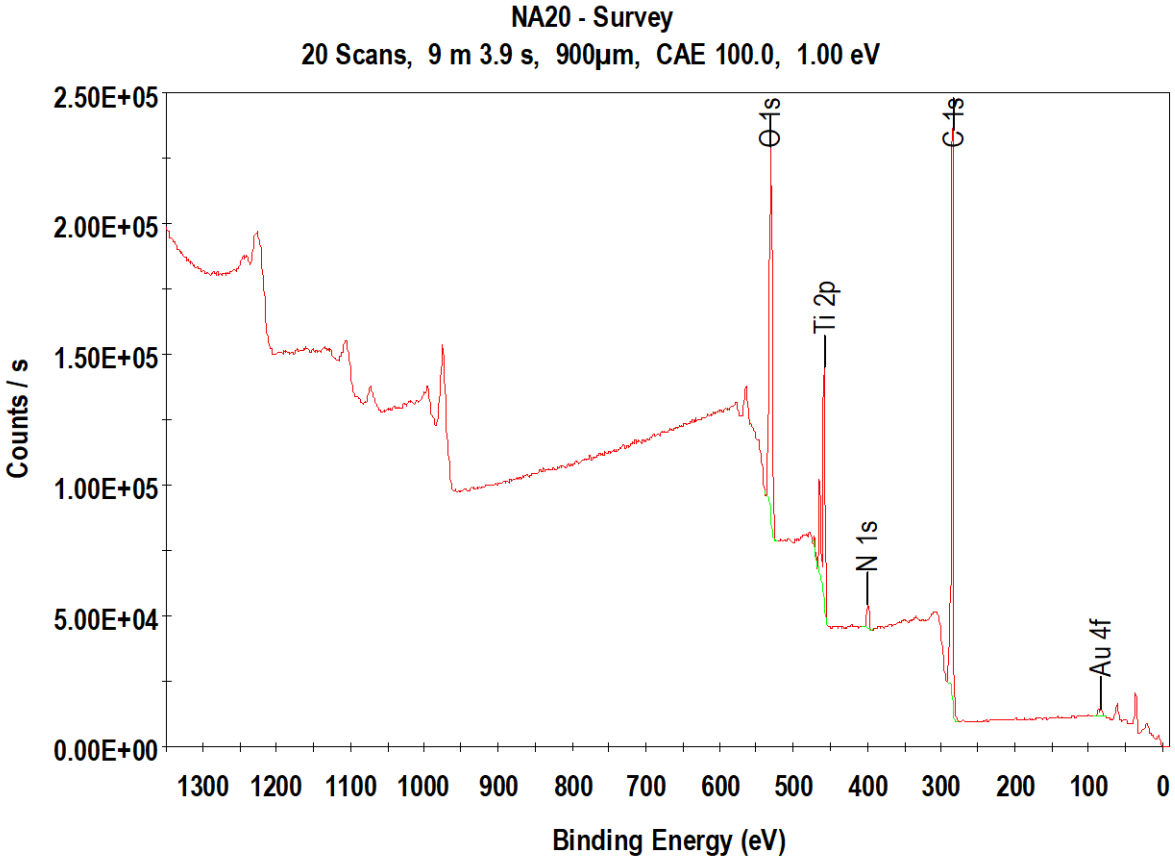

NA20

Elemental ID and Quantification

Name	*Peak BE*	*Atomic %*
C 1s	284.4	68.9
O 1s	530.8	23.7
Ti 2p	458.2	5.5
N 1s	399.2	1.9
Au 4f	84.1	0.1

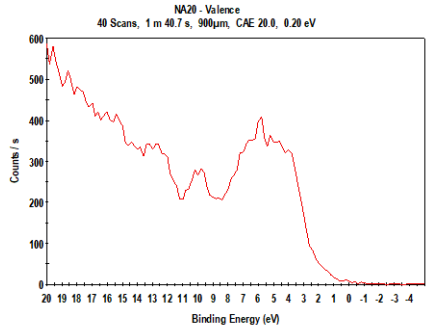
NA20 - Valence
40 Scans, 1 m 40.7 s, 900µm, CAE 20.0, 0.20 eV
Counts / s
Binding Energy (eV)

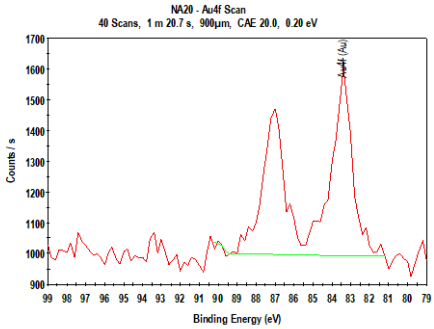
NA20 - Au4f Scan
40 Scans, 1 m 20.7 s, 900µm, CAE 20.0, 0.20 eV
Au4f (Au)
Counts / s
Binding Energy (eV)

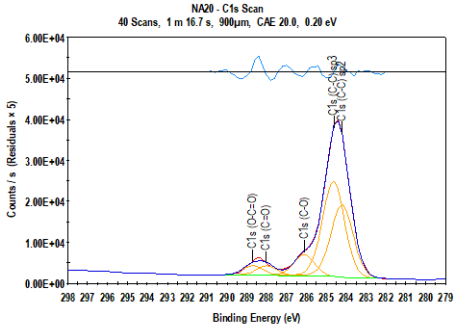
NA20 - C1s Scan
40 Scans, 1 m 16.7 s, 900µm, CAE 20.0, 0.20 eV
C1s (O-C=O)
C1s (C=O)
C1s (C-O)
C1s (C-C) Sp3
C1s (C-C) Sp2
Counts / s (Residuals x 5)
Binding Energy (eV)

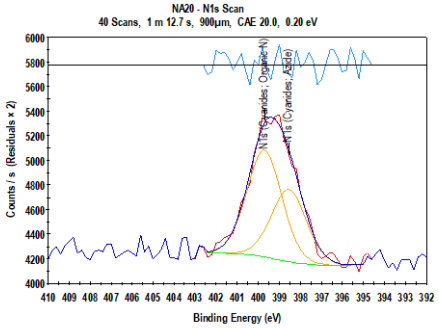
NA20 - N1s Scan
40 Scans, 1 m 12.7 s, 900µm, CAE 20.0, 0.20 eV
N1s (Cyanides; Organic-N)
N1s (Cyanides; Azide)
Counts / s (Residuals x 2)
Binding Energy (eV)

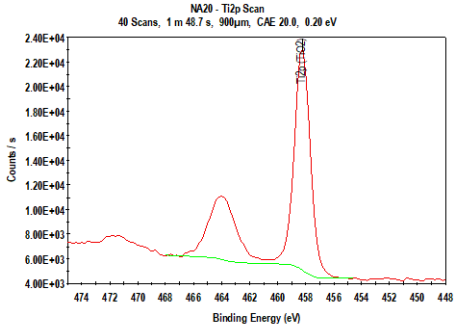
NA20 - Ti2p Scan
40 Scans, 1 m 48.7 s, 900µm, CAE 20.0, 0.20 eV
Ti2p (TiO2)
Counts / s
Binding Energy (eV)

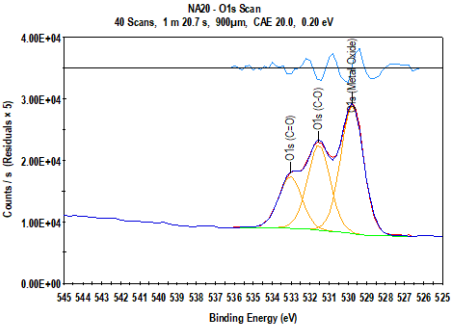
NA20 - O1s Scan
40 Scans, 1 m 20.7 s, 900µm, CAE 20.0, 0.20 eV
O1s (C=O)
O1s (C-O)
O1s (Metal Oxide)
Counts / s (Residuals x 5)
Binding Energy (eV)

NA20

Chemical ID and Quantification

Name	*Peak BE*	*FWHM eV*	*Atomic %*
Au4f (Au)	83.4	1.1	0.1
C1s (C-C) sp2	284.2	1.3	24.3
C1s (C-C) sp3	284.6	1.3	31.8
C1s (C-O)	286.1	1.2	6.4
C1s (C=O)	288.0	1.2	2.8
C1s (O-C=O)	288.7	1.2	2.9
N1s (Cyanides; Azide)	398.6	1.9	0.7
N1s (Cyanides; Organic N)	399.7	1.9	1.1
Ti2p (TiO2)	458.2	1.2	5.9
O1s (Metal Oxide)	529.8	1.4	11.6
O1s (C-O)	531.5	1.4	7.7
O1s (C=O)	533.0	1.4	4.7

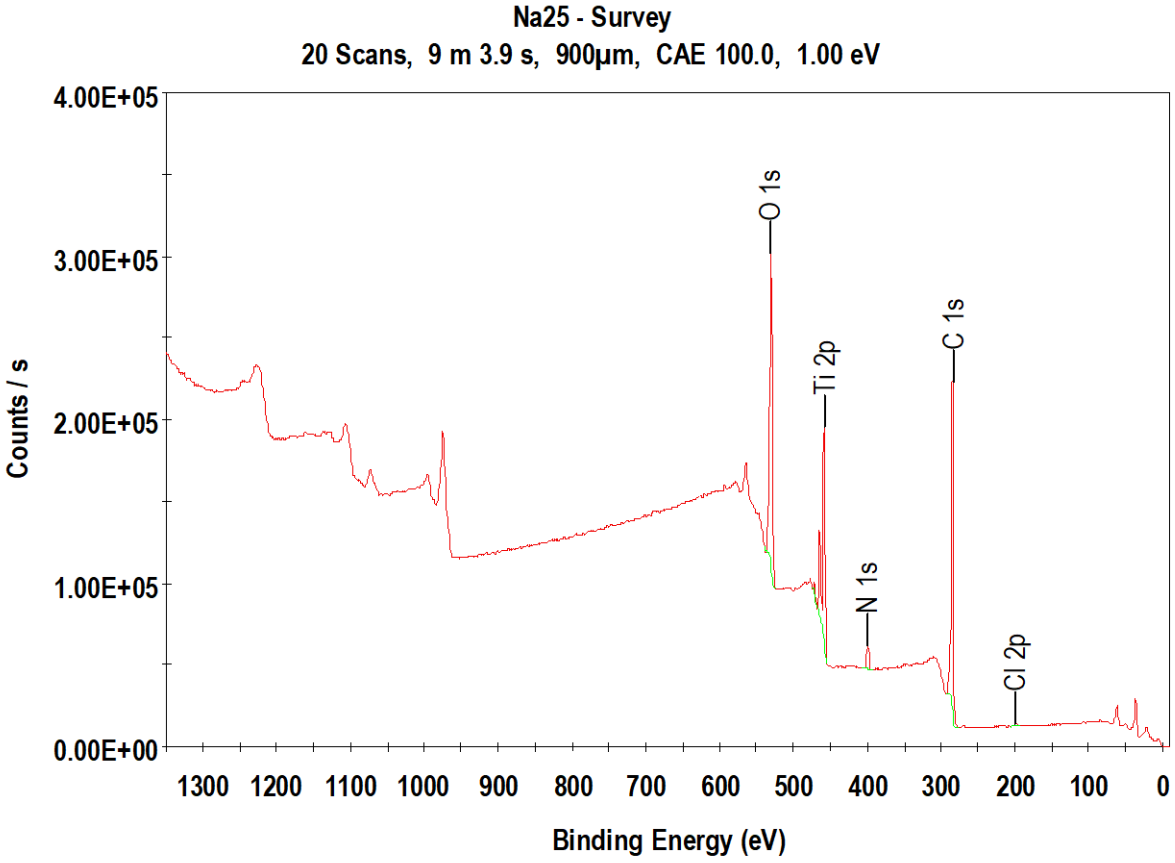

NA25

Elemental ID and Quantification

Name	*Peak BE*	*Atomic %*
C 1s	284.4	62.3
O 1s	530.4	27.0
Ti 2p	458.2	7.7
N 1s	399.2	2.7
Cl 2p	198.7	0.2

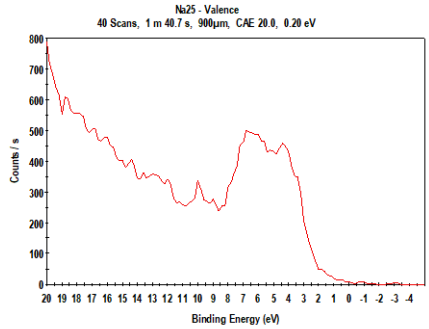
Na25 - Valence
40 Scans, 1 m 40.7 s, 900µm, CAE 20.0, 0.20 eV
Counts / s
Binding Energy (eV)

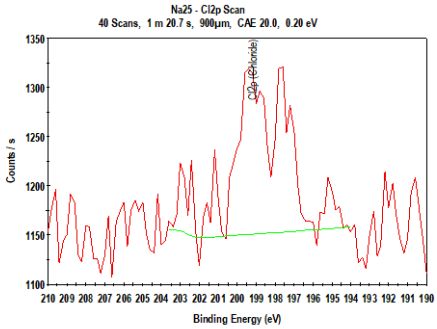
Na25 - Cl2p Scan
40 Scans, 1 m 20.7 s, 900µm, CAE 20.0, 0.20 eV
Counts / s
Binding Energy (eV)

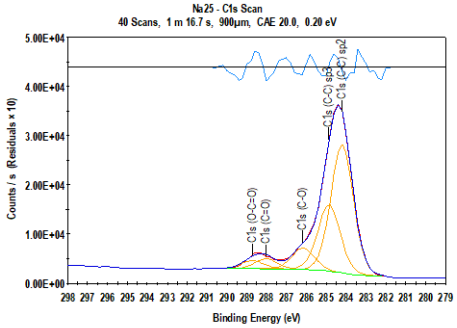
Na25 - C1s Scan
40 Scans, 1 m 16.7 s, 900µm, CAE 20.0, 0.20 eV
Counts / s (Residuals x 10)
C1s (O-C=O)
C1s (C=O)
C1s (C-O)
C1s (C-O) sat
C1s (C-C) sat2
Binding Energy (eV)

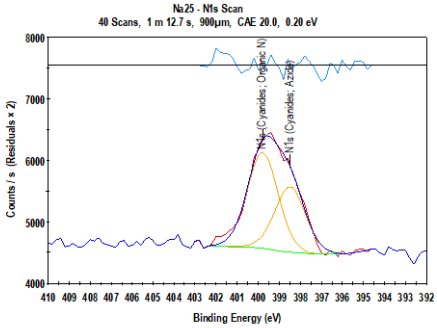
Na25 - N1s Scan
40 Scans, 1 m 12.7 s, 900µm, CAE 20.0, 0.20 eV
Counts / s (Residuals x 2)
N1s (Cyanides; Organic N)
N1s (Cyanides; Azide)
Binding Energy (eV)

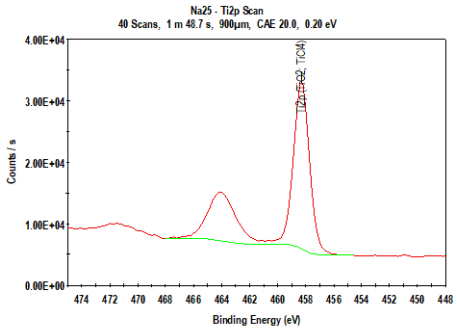
Na25 - Ti2p Scan
40 Scans, 1 m 48.7 s, 900µm, CAE 20.0, 0.20 eV
Counts / s
Ti2p (Ti-O2, TiO4)
Binding Energy (eV)

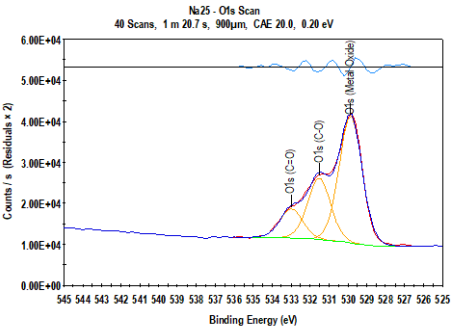
Na25 - O1s Scan
40 Scans, 1 m 20.7 s, 900µm, CAE 20.0, 0.20 eV
Counts / s (Residuals x 2)
O1s (C=O)
O1s (C-O)
O1s (Metal Oxide)
Binding Energy (eV)

NA25

Chemical ID and Quantification

Name	*Peak BE*	*FWHM eV*	*Atomic %*
Cl2p (Chloride)	199.2	1.5	0.2
C1s (C-C) sp2	284.2	1.3	33.6
C1s (C-C) sp3	284.9	1.3	17.4
C1s (C-O)	286.2	1.3	5.6
C1s (C=O)	288.0	1.3	2.7
C1s (O-C=O)	288.7	1.3	2.2
N1s (Cyanides; Azide)	398.5	1.7	1.1
N1s (Cyanides; Organic N)	399.8	1.7	1.6
Ti2p (TiO2; TiCl4)	458.3	1.2	8.3
O1s (Metal Oxide)	529.9	1.4	16.0
O1s (C-O)	531.5	1.4	7.7
O1s (C=O)	533.0	1.4	3.6

APPENDIX II. SUPPLEMENTARY DATA

EDS spectrum

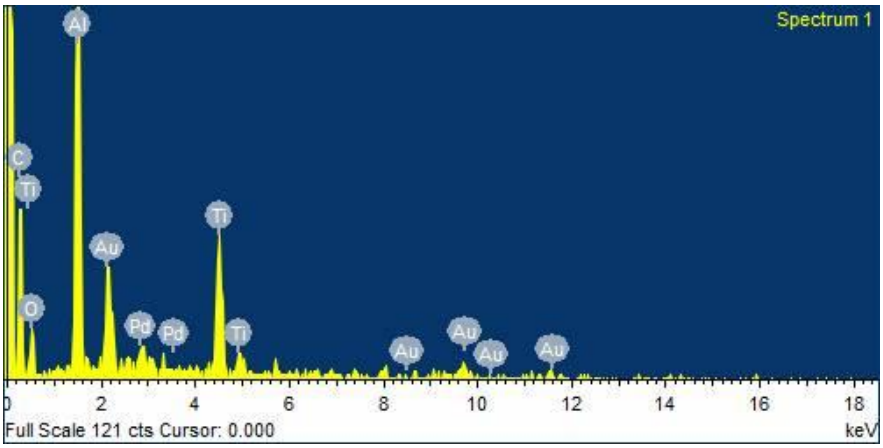

Fig. 1. EDS spectrum of the F_CNFs/20% TiO_2 composite.

EDS scanning detected that the sample consisted of Ti, C, O, Au, Al and Pd, Fig. 1. The Al, Au and Pd, peaks were a result of mounting the sample on an aluminium pin stub and the coating of the sample with a single layer of Au-Pd. Therefore, the sample consisted mostly of Ti, C and O.

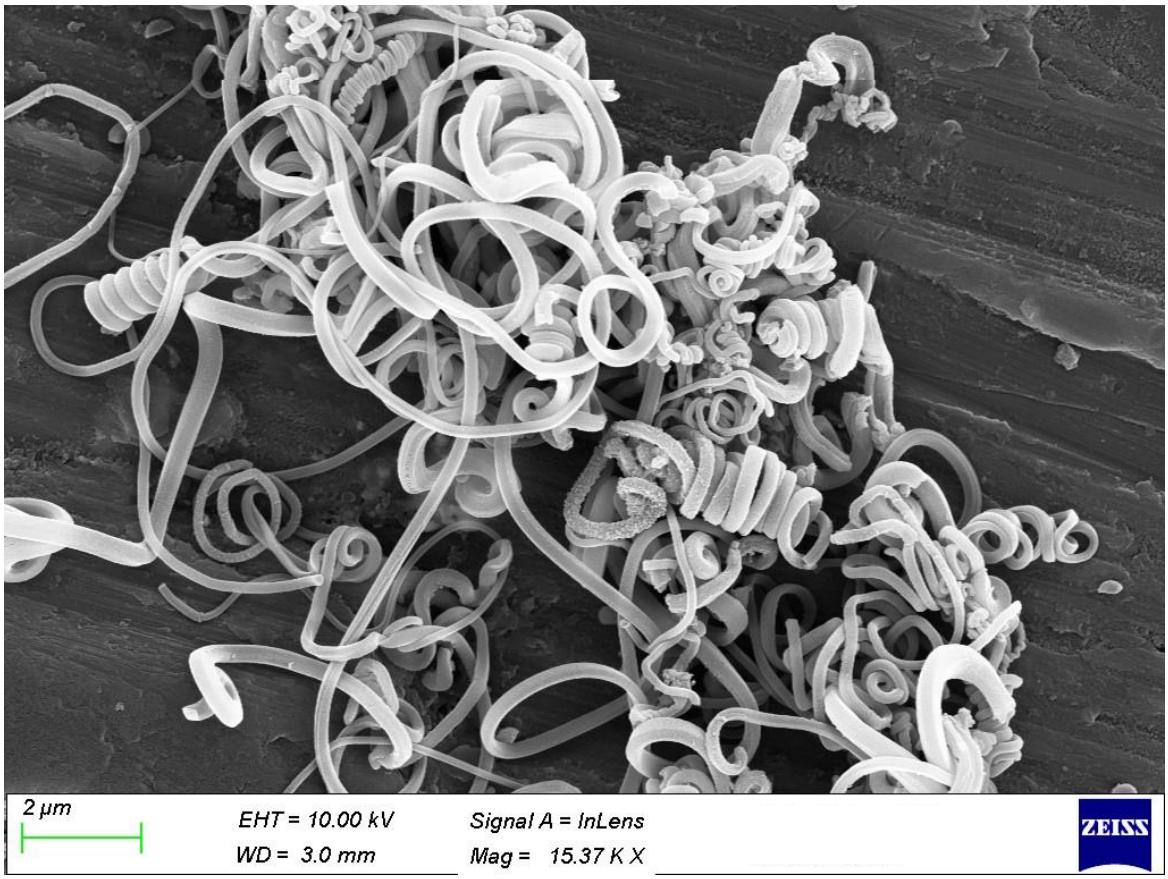

Fig. 2. Field emission scanning electron microscopy, FESEM investigation of; as-prepared CNFs

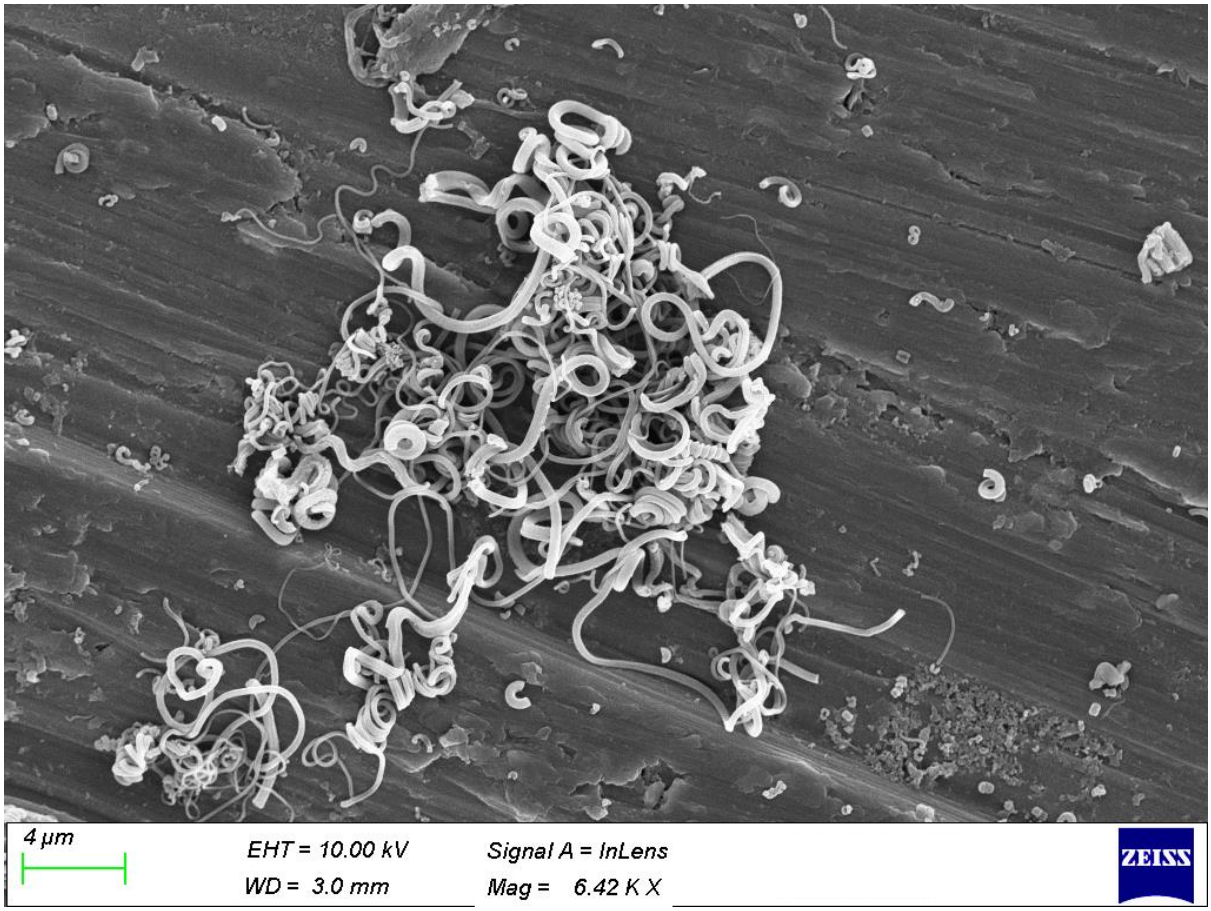

Fig. 3. Field Emission Scanning Electron Microscopy, FESEM investigation of;

Functionalized CNFs, F_CNFs

REFERENCES

[1] T. Kawawaki, Y. Kataoka, S. Ozaki, M. Kawachi, M. Hirata, and Y. Negishi, "Creation of active water-splitting photocatalysts by controlling cocatalysts using atomically precise metal nanoclusters," *Chem. Commun.*, vol. 57, no. 4, pp. 417–440, 2021, doi: 10.1039/d0cc06809h.

[2] N. Abas, A. Kalair, and N. Khan, "Review of fossil fuels and future energy technologies," *Futures*, vol. 69, pp. 31–49, 2015, doi: 10.1016/j.futures.2015.03.003.

[3] C. Zou, Q. Zhao, G. Zhang, and B. Xiong, "Energy revolution: From a fossil energy era to a new energy era," *Nat. Gas Ind. B*, vol. 3, no. 1, pp. 1–11, 2016, doi: 10.1016/j.ngib.2016.02.001.

[4] M. Momirlan and T. N. Veziroglu, "The properties of hydrogen as fuel tomorrow in sustainable energy system for a cleaner planet," *Int. J. Hydrogen Energy*, vol. 30, no. 7, pp. 795–802, 2005, doi: 10.1016/j.ijhydene.2004.10.011.

[5] N. Fajrina and M. Tahir, "A critical review in strategies to improve photocatalytic water splitting towards hydrogen production," *Int. J. Hydrogen Energy*, vol. 44, no. 2, pp. 540–577, 2019, doi: 10.1016/j.ijhydene.2018.10.200.

[6] N. Radenahmad *et al.*, "A review on biomass derived syngas for SOFC based combined heat and power application," *Renew. Sustain. Energy Rev.*, vol. 119, no. October 2019, p. 109560, 2020, doi: 10.1016/j.rser.2019.109560.

[7] W. Mulewa, M. Tahir, and N. A. S. Amin, "MMT-supported Ni/TiO_2 nanocomposite for low temperature ethanol steam reforming toward hydrogen production," *Chem. Eng. J.*, vol. 326, pp. 956–969, 2017, doi: 10.1016/j.cej.2017.06.012.

[8] M. Tahir, W. Mulewa, N. A. S. Amin, and Z. Y. Zakaria, "Thermodynamic and

experimental analysis on ethanol steam reforming for hydrogen production over Ni-modified TiO_2/MMT nanoclay catalyst," *Energy Convers. Manag.*, vol. 154, no. October, pp. 25–37, 2017, doi: 10.1016/j.enconman.2017.10.042.

[9] H. Zhao *et al.*, "Blue-edge slow photons promoting visible-light hydrogen production on gradient ternary 3DOM TiO_2-Au-CdS photonic crystals," *Nano Energy*, vol. 47, no. December 2017, pp. 266–274, 2018, doi: 10.1016/j.nanoen.2018.02.052.

[10] M. Tahir, "Ni/MMT-promoted TiO_2 nanocatalyst for dynamic photocatalytic H_2 and hydrocarbons production from ethanol-water mixture under UV-light," *Int. J. Hydrogen Energy*, vol. 42, no. 47, pp. 28309–28326, 2017, doi: 10.1016/j.ijhydene.2017.09.116.

[11] B. Wang, S. Shen, and S. S. Mao, "Black TiO_2 for solar hydrogen conversion," *J. Mater.*, vol. 3, no. 2, pp. 96–111, 2017, doi: 10.1016/j.jmat.2017.02.001.

[12] X. Chen and S. S. Mao, "Titanium dioxide nanomaterials: Synthesis, properties, modifications and applications," *Chem. Rev.*, vol. 107, no. 7, pp. 2891–2959, 2007, doi: 10.1021/cr0500535.

[13] N. M. Gupta, "Factors affecting the efficiency of a water splitting photocatalyst: A perspective," *Renewable and Sustainable Energy Reviews*, vol. 71. pp. 585–601, May 01, 2017. doi: 10.1016/j.rser.2016.12.086.

[14] M. Ijaz and M. Zafar, "Titanium dioxide nanostructures as efficient photocatalyst: Progress, challenges and perspective," *Int. J. Energy Res.*, vol. 45, no. 3, pp. 3569–3589, 2021, doi: 10.1002/er.6079.

[15] M. B. Tahir, A. M. Asiri, and T. Nawaz, "A perspective on the fabrication of heterogeneous photocatalysts for enhanced hydrogen production," *Int. J. Hydrogen Energy*, vol. 45, no. 46, pp. 24544–24557, 2020, doi: 10.1016/j.ijhydene.2020.06.301.

[16] P. V. Govardhana Reddy *et al.*, “A review on multicomponent reactions catalysed by zero-dimensional/one-dimensional titanium dioxide (TiO_2) nanomaterials: Promising green methodologies in organic chemistry,” *J. Environ. Manage.*, vol. 279, no. November 2020, p. 111603, 2021, doi: 10.1016/j.jenvman.2020.111603.

[17] K. Kaur and C. V. Singh, “Amorphous TiO_2 as a photocatalyst for hydrogen production: A DFT study of structural and electronic properties,” *Energy Procedia*, vol. 29, pp. 291–299, 2012, doi: 10.1016/j.egypro.2012.09.035.

[18] J. E. S. Haggerty *et al.*, “High-fraction brookite films from amorphous precursors,” *Sci. Rep.*, vol. 7, no. 1, pp. 1–11, 2017, doi: 10.1038/s41598-017-15364-y.

[19] A. Gupta, B. Likozar, R. Jana, W. C. Chanu, and M. K. Singh, “A review of hydrogen production processes by photocatalytic water splitting – From atomistic catalysis design to optimal reactor engineering,” *Int. J. Hydrogen Energy*, vol. 7, 2022, doi: 10.1016/j.ijhydene.2022.07.210.

[20] BP, “Statistical Review of World Energy globally consistent data on world energy markets and authoritative publications in the field of energy,” *BP Energy Outlook*, vol. 70, p. 72, 2021.

[21] J. Buckeridge *et al.*, “Polymorph Engineering of TiO_2: Demonstrating How Absolute Reference Potentials Are Determined by Local Coordination,” *Chem. Mater.*, vol. 27, no. 11, pp. 3844–3851, 2015, doi: 10.1021/acs.chemmater.5b00230.

[22] W. Zhang *et al.*, “Merging Single-Atom-Dispersed Iron and Graphitic Carbon Nitride to a Joint Electronic System for High-Efficiency Photocatalytic Hydrogen Evolution,” *Small*, vol. 15, no. 50, pp. 1–8, 2019, doi: 10.1002/smll.201905166.

[23] D. Zhao, X. Guan, and S. Shen, “Design of polymeric carbon nitride-based

heterojunctions for photocatalytic water splitting: a review," *Environ. Chem. Lett.*, vol. 20, no. 6, pp. 3505–3523, 2022, doi: 10.1007/s10311-022-01429-6.

[24] X. Guan, S. Zong, and S. Shen, "Homojunction photocatalysts for water splitting," *Nano Res.*, vol. 15, no. 12, pp. 10171–10184, 2022, doi: 10.1007/s12274-022-4704-9.

[25] A. Meng, L. Zhang, B. Cheng, and J. Yu, "Dual Cocatalysts in TiO_2 Photocatalysis," *Adv. Mater.*, vol. 31, no. 30, pp. 1–31, 2019, doi: 10.1002/adma.201807660.

[26] G. Zhao and X. Xu, "Cocatalysts from types, preparation to applications in the field of photocatalysis," *Nanoscale*, vol. 13, no. 24, pp. 10649–10667, 2021, doi: 10.1039/d1nr02464g.

[27] H. Wang, S. Dong, Y. Chang, and J. L. Faria, "Enhancing the photocatalytic properties of TiO_2 by coupling with carbon nanotubes and supporting gold," *J. Hazard. Mater.*, vol. 235–236, pp. 230–236, 2012, doi: 10.1016/j.jhazmat.2012.07.050.

[28] T. K. Townsend, N. D. Browning, and F. E. Osterloh, "Nanoscale strontium titanate photocatalysts for overall water splitting," *ACS Nano*, vol. 6, no. 8, pp. 7420–7426, 2012, doi: 10.1021/nn302647u.

[29] Q. Wang *et al.*, "Oxysulfide photocatalyst for visible-light-driven overall water splitting," *Nat. Mater.*, vol. 18, no. 8, pp. 827–832, 2019, doi: 10.1038/s41563-019-0399-z.

[30] T. Takata *et al.*, "Photocatalytic water splitting with a quantum efficiency of almost unity," *Nature*, vol. 581, no. 7809, pp. 411–414, 2020, doi: 10.1038/s41586-020-2278-9.

[31] A. Aguirre-Astrain, E. Luévano-Hipólito, and L. M. Torres-Martínez, "Integration of 2D printing technologies for AV_2O_6 (A=Ca, Sr, Ba)-MO (M=Cu, Ni, Zn) photocatalyst manufacturing to solar fuels production using seawater," *Int. J. Hydrogen Energy*, vol. 46, no. 75, pp. 37294–37310, 2021, doi: 10.1016/j.ijhydene.2021.09.007.

[32] Y. Liu, X. Zhou, Y. Zhou, and G. Chen, “Construction of Ag decorated 2D rGO/SnS_2 nanostructure towards synergistically enabling overall water splitting,” *Chem. Eng. J.*, vol. 433, no. 2, 2022, doi: 10.1016/j.cej.2021.133198.

[33] H. Zhao *et al.*, “Transition-Metal-Based Cocatalysts for Photocatalytic Water Splitting,” *Small Struct.*, vol. 3, no. 7, 2022, doi: 10.1002/sstr.202100229.

[34] D. Chen, Z. Jiang, J. Geng, Q. Wang, and D. Yang, “Carbon and nitrogen co-doped TiO_2 with enhanced visible-light photocatalytic activity,” *Ind. Eng. Chem. Res.*, vol. 46, no. 9, pp. 2741–2746, 2007, doi: 10.1021/ie061491k.

[35] J. Schneider *et al.*, “Understanding TiO_2 Photocatalysis Mechanisms and Materials,” *Chem. Rev.*, vol. 114, no. 9, pp. 9919−9986, 2014, doi:10.1021/cr5001892.

[36] J. Lu *et al.*, “Coking- and sintering-resistant palladium catalysts achieved through atomic layer deposition,” *Science*, vol. 335, no. 6073, pp. 1205–1208, 2012, doi: 10.1126/science.1212906.

[37] B. Neumann, P. Bogdanoff, H. Tributsch, S. Sakthivel, and H. Kisch, “Electrochemical mass spectroscopic and surface photovoltage studies of catalytic water photooxidation by undoped and carbon-doped titania,” *J. Phys. Chem. B*, vol. 109, no. 35, pp. 16579–16586, 2005, doi: 10.1021/jp051339g.

[38] G. Zhang *et al.*, “Preparation of carbon-TiO_2 nanocomposites by a hydrothermal method and their enhanced photocatalytic activity,” *RSC Adv.*, vol. 3, no. 46, pp. 24644–24649, 2013, doi: 10.1039/c3ra44950e.

[39] Z. He, W. Que, and Y. He, “Enhanced photocatalytic performance of sensitized mesoporous TiO_2 nanoparticles by carbon mesostructures,” *RSC Adv.*, vol. 4, no. 7, pp. 3332–3339, 2014, doi: 10.1039/c3ra46389c.

[40] S. Qiu *et al.*, “Highly selective colorimetric bacteria sensing based on protein-capped nanoparticles,” *Analyst*, vol. 140, no. 4, pp. 1149–1154, 2015, doi: 10.1039/c4an02106a.

[41] M. Inagaki, Y. Okada, H. Miura, and H. Konno, “Preparation of carbon-coated transition metal particles from mixtures of metal oxide and Polyvinylchloride,” *Carbon*, vol. 37, no. 2, pp. 329–334, 1999, doi: 10.1016/S0008-6223(98)00200-0.

[42] M. Inagaki, F. Kojin, B. Tryba, and M. Toyoda, “Carbon-coated anatase: The role of the carbon layer for photocatalytic performance,” *Carbon*, vol. 43, no. 8, pp. 1652–1659, 2005, doi: 10.1016/j.carbon.2005.01.043.

[43] C. Yang *et al.*, “Porous carbon-doped TiO_2 on TiC nanostructures for enhanced photocatalytic hydrogen production under visible light,” *J. Catal.*, vol. 347, pp. 36–44, 2017, doi: 10.1016/j.jcat.2016.11.041.

[44] S. D. Mhlanga and N. J. Coville, “Iron-cobalt catalysts synthesized by a reverse micelle impregnation method for controlled growth of carbon nanotubes,” *Diam. Relat. Mater.*, vol. 17, no. 7, pp. 1489–1493, 2008, doi: 10.1016/j.diamond.2008.01.049.

[45] Y. Yan, J. Lu, C. Deng, and X. Zhang, “Facile synthesis of titania nanoparticles coated carbon nanotubes for selective enrichment of phosphopeptides for mass spectrometry analysis,” *Talanta*, vol. 107, pp. 30–35, 2013, doi: 10.1016/j.talanta.2012.12.026.

[46] S. B. A. Hamid, T. L. Tan, C. W. Lai, and E. M. Samsudin, “Multiwalled carbon nanotube/TiO_2 nanocomposite as a highly active photocatalyst for photodegradation of Reactive Black 5 dye,” *Cuihua Xuebao/Chinese J. Catal.*, vol. 35, no. 12, pp. 2014–2019, 2014, doi: 10.1016/S1872-2067(14)60210-2.

[47] J. Restivo, O. S. G. P. Soares, J. J. M. Órfão, and M. F. R. Pereira, “Metal assessment for the catalytic reduction of bromate in water under hydrogen,” *Chem. Eng. J.*, vol. 263, pp.

119–126, 2015, doi: 10.1016/j.cej.2014.11.052.

[48] O. S. G. P. Soares, P. S. F. Ramalho, A. Fernandes, J. J. M. Órfão, and M. F. R. Pereira, “Catalytic bromate reduction in water: Influence of carbon support,” *J. Environ. Chem. Eng.*, vol. 7, no. 3, 2019, doi: 10.1016/j.jece.2019.103015.

[49] O. S. G. P. Soares, J. J. M. Órfão, and M. F. R. Pereira, “Nitrate reduction with hydrogen in the presence of physical mixtures with mono and bimetallic catalysts and ions in solution,” *Appl. Catal. B Environ.*, vol. 102, no. 3, pp. 424–432, 2011, doi: 10.1016/j.apcatb.2010.12.017.

[50] O. S. G. P. Soares, J. J. M. Órfão, J. Ruiz-Martínez, J. Silvestre-Albero, A. Sepúlveda-Escribano, and M. F. R. Pereira, “Pd-Cu/AC and Pt-Cu/AC catalysts for nitrate reduction with hydrogen: Influence of calcination and reduction temperatures,” *Chem. Eng. J.*, vol. 165, no. 1, pp. 78–88, 2010, doi: 10.1016/j.cej.2010.08.065.

[51] J. M. Walls, J. S. Sagu, and K. G. Upul Wijayantha, “Microwave synthesised Pd-TiO_2 for photocatalytic ammonia production,” *RSC Adv.*, vol. 9, no. 11, pp. 6387–6394, 2019, doi: 10.1039/c8ra09762c.

[52] W. K. Sun, R. Khan, T. J. Kim, and W. J. Kim, “Synthesis, characterization, and application of ZrS Co-doped TiO_2 as visible-light active photocatalyst,” *Bull. Korean Chem. Soc.*, vol. 29, no. 6, pp. 1217–1223, 2008, doi: 10.5012/bkcs.2008.29.6.1217.

[53] Y. Yu *et al.*, “Enhancement of adsorption and photocatalytic activity of TiO_2 by using carbon nanotubes for the treatment of azo dye,” *Appl. Catal. B Environ.*, vol. 61, no. 1, pp. 1–11, 2005, doi: 10.1016/j.apcatb.2005.03.008.

[54] H. Y. Liu *et al.*, “A comparative study of amorphous, anatase, rutile, and mixed phase TiO_2 films by mist chemical vapor deposition and ultraviolet photodetectors applications,”

IEEE Sens. J., vol. 18, no. 10, pp. 4022–4029, 2018, doi: 10.1109/JSEN.2018.2819700.

[55] H. Berger, H. Tang, and F. Lévy, "Growth and Raman spectroscopic characterization of TiO_2 anatase single crystals," *J. Cryst. Growth*, vol. 130, no. 1, pp. 108–112, 1993, doi: 10.1016/0022-0248(93)90842-K.

[56] S. Santangelo *et al.*, "Micro-Raman analysis of titanium oxide/carbon nanotubes-based nanocomposites for hydrogen sensing applications," *J. Solid State Chem.*, vol. 183, no. 10, pp. 2451–2455, 2010, doi: 10.1016/j.jssc.2010.08.018.

[57] 3 Zlatko Meić Mladen Žini ć Snežzana Miljanić, Leo Frkanec, Tomislav Biljan, "Recent Advances in linear and nonlinear Raman spectroscopy I," *J. Raman Spectrosc.*, vol. 38, pp. 1538–1553, 2007, doi: 10.1002/jrs.

[58] W. Wang, D. Xu, B. Cheng, J. Yu, and C. Jiang, "Hybrid carbon@TiO_2 hollow spheres with enhanced photocatalytic CO_2 reduction activity," *J. Mater. Chem. A*, vol. 5, no. 10, pp. 5020–5029, 2017, doi: 10.1039/c6ta11121a.

[59] D. A. Solís-Casados, E. Vigueras-Santiago, S. Hernández-López, A. Gómez-Cortés, M. Aguilar-Franco, and M. A. Camacho-López, "Textural, structural and electrical properties of TiO_2 nanoparticles using Brij 35 and P123 as surfactants," *Sci. Technol. Adv. Mater.*, vol. 9, no. 2, 2008, doi: 10.1088/1468-6996/9/2/025003.

[60] L. Feng, N. Xie, and J. Zhong, "Carbon nanofibers and their composites: A review of synthesizing, properties and applications," *Materials*, vol. 7, no. 5, pp. 3919–3945, 2014, doi: 10.3390/ma7053919.

[61] B. Gao, G. Z. Chen, and G. Li Puma, "Carbon nanotubes/titanium dioxide (CNTs/TiO_2) nanocomposites prepared by conventional and novel surfactant wrapping sol-gel methods exhibiting enhanced photocatalytic activity," *Appl. Catal. B Environ.*, vol. 89,

no. 3, pp. 503–509, 2009, doi: 10.1016/j.apcatb.2009.01.009.

[62] S. Liu, H. Sun, S. Liu, and S. Wang, “Graphene facilitated visible light photodegradation of methylene blue over titanium dioxide photocatalysts,” *Chem. Eng. J.*, vol. 214, pp. 298–303, 2013, doi: 10.1016/j.cej.2012.10.058.

[63] J. Liu, J. Li, A. Sedhain, J. Lin, and H. Jiang, “Structure and photoluminescence study of TiO_2 nanoneedle texture along vertically aligned carbon nanofiber arrays,” *J. Phys. Chem. C*, vol. 112, no. 44, pp. 17127–17132, 2008, doi: 10.1021/jp8060653.

[64] K. Dai, T. Peng, D. Ke, and B. Wei, “Photocatalytic hydrogen generation using a nanocomposite of multi-walled carbon nanotubes and TiO_2 nanoparticles under visible light irradiation,” *Nanotechnology*, vol. 20, no. 12, 2009, doi: 10.1088/0957-4484/20/12/125603.

[65] Y. Wang, K. Hu, Y. Zhang, and X. Ding, “Dendritic fibrous nano-silica & titania (DFNST) spheres as novel cataluminescence sensing materials for the detection of diethyl ether,” *RSC Adv.*, vol. 9, no. 68, pp. 39622–39630, 2019, doi: 10.1039/c9ra08152f.

[66] W. Wang, D. Zhu, Z. Shen, J. Peng, J. Luo, and X. Liu, “One-Pot Hydrothermal Route to Synthesize the Bi-doped Anatase TiO_2 Hollow Thin Sheets with Prior Facet Exposed for Enhanced Visible-Light-Driven Photocatalytic Activity,” *Ind. Eng. Chem. Res.*, vol. 55, no. 22, pp. 6373–6383, 2016, doi: 10.1021/acs.iecr.6b00618.

[67] A. Romanchenko, M. Likhatski, and Y. Mikhlin, “X-ray photoelectron spectroscopy (XPS) study of the products formed on sulfide minerals upon the interaction with aqueous platinum (IV) chloride complexes,” *Minerals*, vol. 8, no. 12, 2018, doi: 10.3390/min8120578.

[68] Q. Ye, Z. Z. Yin, H. Wu, D. Wu, Y. Tao, and Y. Kong, “Decoration of glutathione with copper-platinum nanoparticles for chirality sensing of tyrosine enantiomers,” *Electrochem. commun.*, vol. 110, no. November 2019, 2020, doi:

10.1016/j.elecom.2019.106638.

[69] P. Légaré *et al.*, “On the interaction of O_2 with Pt(111) and Pt(557) surfaces: core-level shift study using conventional and synchrotron radiation sources,” *Surf. Sci.*, vol. 198, no. 1, 1988, doi: 10.1016/0039-6028(88)90472-4.

[70] B. H. Aw, K. K. Looh, H. S. O. Chan, K. L. Tan, and T. S. A. Hor, “X-Ray photoelectron spectroscopic characterization of $[\{Pt(PPh_3)_2(\mu_3\text{-}S)\}_2PtCl_2]$ $[\{Pt_2(PPh_3)_4(\mu_3\text{-}S)_2Cu\}_2(\mu\text{-dppf})][PF_6]_2$[dppf = Fe $(C_5H_4PPh_2)_2$] and other heterometallic aggregates derived from $[\{Pt(PPh_3)_2(\mu\text{-}S)\}_2]$,” *J. Chem. Soc. Dalt. Trans.*, vol. 21, pp. 3177–3182, 1994, doi: 10.1039/DT9940003177.

[71] M. Ismael, “A review and recent advances in solar-to-hydrogen energy conversion based on photocatalytic water splitting over doped-TiO_2 nanoparticles,” *Sol. Energy*, vol. 211, pp. 522–546, Nov. 2020, doi: 10.1016/J.SOLENER.2020.09.073.

[72] T. S. Natarajan, V. Mozhiarasi, and R. J. Tayade, “Nitrogen Doped Titanium Dioxide (N-TiO_2): Synopsis of Synthesis Methodologies, Doping Mechanisms, Property Evaluation and Visible Light Photocatalytic Applications,” *Photochem*, vol. 1, no. 3, pp. 371–410, 2021, doi: 10.3390/photochem1030024.

[73] C. Wang, L. Ling, Y. Yao, and Q. Song, “One-step synthesis of fluorescent smart thermo-responsive copper clusters: A potential nanothermometer in living cells,” *Nano Res.*, vol. 8, no. 6, pp. 1975–1986, 2015, doi: 10.1007/s12274-015-0707-0.

[74] E. S. Shibu and T. Pradeep, “Quantum clusters in cavities: Trapped Au15 in cyclodextrins,” *Chem. Mater.*, vol. 23, no. 4, pp. 989–999, 2011, doi: 10.1021/cm102743y.

[75] T. Rahimi-Aghdam, Z. Shariatinia, M. Hakkarainen, and V. Haddadi-Asl, “Nitrogen and phosphorous doped graphene quantum dots: Excellent flame retardants and smoke

suppressants for polyacrylonitrile nanocomposites," *J. Hazard. Mater.*, vol. 381, Jan. 2020, doi: 10.1016/J.JHAZMAT.2019.121013.

[76] J. Baloyi, T. Seadira, M. Raphulu, and A. Ochieng, "Preparation, Characterization and Growth Mechanism of Dandelion-like TiO_2 Nanostructures and their Application in Photocatalysis towards Reduction of Cr(VI)," *Mater. Today Proc.*, vol. 2, no. 7, pp. 3973–3987, 2015, doi: 10.1016/j.matpr.2015.08.027.

[77] S. Brunauer, P. H. Emmet, and E. Teller, "Adsorption of gases in multilayer's," *J. Am. Chem. Soc.*, vol. 60, no. 35, pp. 309–319, 1938. https://doi.org/10.1007/s11356-024-34848-9

[78] K. Kinashi, Y. Kambe, M. Misaki, Y. Koshiba, K. Ishida, and Y. Ueda, "Synthesis, characterization, photo-induced alignment, and surface orientation of poly(9,9-dioctylfluorene-alt-azobenzene)s," *J. Polym. Sci. Part A Polym. Chem.*, vol. 50, no. 24, pp. 5107–5114, 2012, doi: 10.1002/pola.26338.

[79] H. Wu *et al.*, "Hydrothermal synthesis of Graphene-TiO_2 nanowire with an enhanced photocatalytic activity," *Russ. J. Phys. Chem. A*, vol. 89, no. 7, pp. 1189–1194, 2015, doi: 10.1134/S0036024415070134.

[80] E. T. Mombeshora, R. Simoyi, V. O. Nyamori, and P. G. Ndungu, "Multiwalled carbon nanotube-titania nanocomposites : understanding nano-structural parameters and functionality in dye-sensitized solar cells : Research article," *South African J. Chem.*, vol. 68, no. 1, pp. 153–164, 2015, doi: 10.17159/0379-4350/2015/v68a22.

[81] N. Hintsho, L. Petrik, A. Nechaev, S. Titinchi, and P. Ndungu, "Photo-catalytic activity of titanium dioxide carbon nanotube nano-composites modified with silver and palladium nanoparticles," *Appl. Catal. B Environ.*, vol. 156, pp. 273–283, 2014, doi: 10.1016/j.apcatb.2014.03.021.

[82] N. Sobana, M. Muruganadham, and M. Swaminathan, “Nano-Ag particles doped TiO_2 for efficient photodegradation of Direct azo dyes,” *J. Mol. Catal. A Chem.*, vol. 258, no. 1, pp. 124–132, 2006, doi: 10.1016/j.molcata.2006.05.013.

[83] J. Coutts *et al.*, “Visible-Light-Responsive Photocatalysis: Ag-Doped TiO_2 Catalyst Development and Reactor Design Testing,” *46th Int. Conf. Environ. Syst.*, ICES-2016-169, 2016, https://ttu-ir.tdl.org/ttu-ir/handle/2346/67573.

[84] M. Janczarek and E. Kowalska, “On the origin of enhanced photocatalytic activity of copper-modified titania in the oxidative reaction systems,” *Catalysts*, vol. 7, no. 11, 2017, doi: 10.3390/catal7110317.

[85] G. Wang, L. Xu, J. Zhang, T. Yin, and D. Han, “Enhanced photocatalytic activity of TiO_2 powders (P25) via calcination treatment,” *Int. J. Photoenergy*, vol. 2012, 2012, doi: 10.1155/2012/265760.

[86] J. Zhang, P. Zhou, J. Liu, and J. Yu, “New understanding of the difference of photocatalytic activity among anatase, rutile and brookite TiO_2,” *Phys. Chem. Chem. Phys.*, vol. 16, no. 38, pp. 20382–20386, 2014, doi: 10.1039/c4cp02201g.

[87] W. Chen *et al.*, “Non-noble metal Cu as a cocatalyst on TiO_2 nanorod for highly efficient photocatalytic hydrogen production,” *Appl. Surf. Sci.*, vol. 445, pp. 527–534, 2018, doi: 10.1016/j.apsusc.2018.03.209.

[88] J. Huang *et al.*, “Efficient photocatalytic hydrogen production over Rh and Nb codoped TiO_2 nanorods,” *Chem. Eng. J.*, vol. 337, no. September 2017, pp. 282–289, 2018, doi: 10.1016/j.cej.2017.12.088.

[89] D. Xu, L. Li, R. He, L. Qi, L. Zhang, and B. Cheng, “Noble metal-free RGO/TiO_2 composite nanofiber with enhanced photocatalytic H_2 -production performance,” *Appl. Surf.*

Sci., vol. 434, pp. 620–625, 2018, doi: 10.1016/j.apsusc.2017.10.192.

[90] T. T. D. Vu, F. Mighri, A. Ajji, and T. O. Do, "Synthesis of titanium dioxide/cadmium sulfide nanosphere particles for photocatalyst applications," *Ind. Eng. Chem. Res.*, vol. 53, no. 10, pp. 3888–3897, 2014, doi: 10.1021/ie403718n.

[91] X. Wang, W. C. Peng, and X. Y. Li, "Photocatalytic hydrogen generation with simultaneous organic degradation by composite CdS-ZnS nanoparticles under visible light," *Int. J. Hydrogen Energy*, vol. 39, no. 25, pp. 13454–13461, 2014, doi: 10.1016/j.ijhydene.2014.04.034.

[92] E. Taboada, I. Angurell, and J. Llorca, "Dynamic photocatalytic hydrogen production from ethanol-water mixtures in an optical fiber honeycomb reactor loaded with Au/TiO_2," *J. Catal.*, vol. 309, pp. 460–467, 2014, doi: 10.1016/j.jcat.2013.10.025.

[93] R. D. Tentu and S. Basu, "Photocatalytic water splitting for hydrogen production," *Curr. Opin. Electrochem.*, vol. 5, no. 1, pp. 56–62, 2017, doi: 10.1016/j.coelec.2017.10.019.

[94] C. Huang, M. Wu, and V. Nguyen, "Preparation and Characterization of NanocrystallineTiO_2 on Microsericite for High-Efficiency Photo-Energy Conversion of Methanol to Hydrogen," *Crystals*, vol. 9, no. 380, 2019, doi:10.3390/cryst9080380.

[95] R. Leary and A. Westwood, "Carbonaceous nanomaterials for the enhancement of TiO_2 photocatalysis," *Carbon*, vol. 49, no. 3, pp. 741–772, 2011, doi: https://doi.org/10.1016/j.carbon.2010.10.010.

[96] M. Hakamizadeh, S. Afshar, A. Tadjarodi, R. Khajavian, M. R. Fadaie, and B. Bozorgi, "Improving hydrogen production via water splitting over Pt/TiO_2/activated carbon nanocomposite," *Int. J. Hydrogen Energy*, vol. 39, no. 14, pp. 7262–7269, 2014, doi: https://doi.org/10.1016/j.ijhydene.2014.03.048.

[97] H. Yi, T. Peng, D. Ke, D. Ke, L. Zan, and C. Yan, “Photocatalytic H_2 production from methanol aqueous solution over titania nanoparticles with mesostructures,” *Int. J. Hydrogen Energy*, vol. 33, no. 2, pp. 672–678, 2008, doi: https://doi.org/10.1016/j.ijhydene.2007.10.034.

[98] N. Lakshminarasimhan, E. Bae, and W. Choi, “Enhanced photocatalytic production of H_2 on mesoporous TiO_2 prepared by template-free method: Role of interparticle charge transfer,” *J. Phys. Chem. C*, vol. 111, no. 42, pp. 15244–15250, 2007, doi: 10.1021/jp0752724.

[99] J. Jitputti, S. Pavasupree, Y. Suzuki, and S. Yoshikawa, “Synthesis and photocatalytic activity for water-splitting reaction of nanocrystalline mesoporous titania prepared by hydrothermal method,” *J. Solid State Chem.*, vol. 180, no. 5, pp. 1743–1749, 2007, doi: https://doi.org/10.1016/j.jssc.2007.03.018.

[100] W.-T. Chen, Y. Dong, P. Yadav, R. D. Aughterson, D. Sun-Waterhouse, and G. I. N. Waterhouse, “Effect of alcohol sacrificial agent on the performance of Cu/TiO_2 photocatalysts for UV-driven hydrogen production,” *Appl. Catal. A Gen.*, vol. 602, 2020, doi: https://doi.org/10.1016/j.apcata.2020.117703.

[101] I. Rossetti, “Hydrogen Production by Photoreforming of Renewable Substrates,” *Chem. Eng.*, vol. 2012, pp. 1–21, 2012, doi: 10.5402/2012/964936.

[102] F. Varas-Concha, D. Guzmán, M. Isaacs, and C. Sáez-Navarrete, “Operational Conditions Affecting Hydrogen Production by the Photoreforming of Organic Compounds using Titania Nanoparticles with Gold,” *Energy Technol.*, vol. 6, no. 2, pp. 416–431, 2018, doi: 10.1002/ente.201700546.

CHAPTER SIX

Significantly advanced hydrogen production via water splitting over Zn/TiO_2/CNFs and Cu/TiO_2/CNFs nanocomposites https://doi.org/10.1016/j.jiec.2023.12.061

Nancy Nyamai[1*], Tumelo Phaahlamohlaka[1]

[1]Molecular Sciences Institute, School of Chemistry, University of the Witwatersrand, Johannesburg 2050, South Africa

nanyamai@yahoo.com

GRAPHICAL ABSTRACT

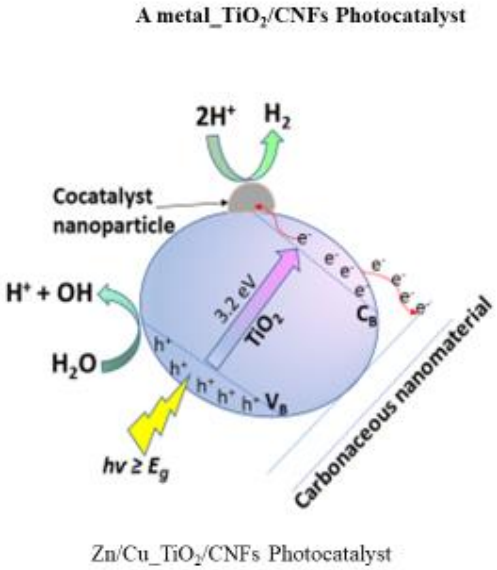

Abstract

Photocatalytic water splitting using solar radiation has drawn considerable attention for production of hydrogen because of minimal carbon emissions, however huge limitations that still exist are low light harnessing catalysts and high recombination rate of the photo-generated charge carriers. This study focuses on the fabrication of nanomaterials for advanced photocatalytic water splitting as a result, structures of TiO_2/CNFs, Cu/TiO_2/CNFs, and Zn/ TiO_2/CNFs nanocomposites of mesoporous nature were synthesized using CNFs and

surfactant wrapping sol-gel/hydrothermal method. Impregnation technique was used in copper and zinc loading while characterization of the synthesized catalysts was achieved by XRD, Raman, FESEM, TEM, UV/DRS, BET, FTIR, XPS, and PL techniques. Water splitting was performed by UV light irradiation and the effect of compositing TiO_2/CNFs-Cu/Zn evaluated. 10%_TiO_2/CNFs/5%Zn composite was the most efficient photocatalyst for hydrogen production when compared with the rest of the samples. 10%_TiO_2/CNFs/5%Zn, 0.53 mol (h g cat.)$^{-1}$, was 90-100 folds the amount generated over commercial TiO_2 - P25, and pure TiO_2 photocatalysts. The improved photo-activity of the TiO_2/CNFs, Cu/TiO_2/CNFs, and Zn/ TiO_2/CNFs composites were due to the synergistic effect between Cu, Zn and CNFs. This work gives promising route for fabricating TiO_2/CNFs/metal (Cu, Zn) composites for advanced H_2 production using UV- radiation.

Keywords: Carbon nanofibers, Zn – doped TiO_2, Cu – doped TiO_2, H_2 production, Photocatalytic water splitting.

6.1 Introduction

The principal supplier of power with vast recognition in the contemporary research advancement process is hydrogen. It has been realized that hydrogen is clean, environmentally-friendly, and can be generated from sustainable reserves via simple catalytic processes[1]. Currently, hydrogen is mostly sourced from steam reforming of fossil gas and crude oil which release carbon dioxide, CO_2 and other greenhouse gases. These processes can have irreversible or temporary detrimental impact on the environment[2], [3]. It is easy to benefit from sun energy as a sustainable power, plentiful supplies like water, and bio-degradable wastes, and a photocatalyst in water splitting photocatalysis for hydrogen production. The technology has received enormous attractions from all over the world

because it is environmentally-friendly and has renewable resources such as solar energy[2], [4]. However, even 5 decades following the achievement of Fujishima and Honda, the innovation has not achieved maximum industrial application. At present, solar hydrogen efficiency is approximately 10%[5]. Various exhaustive investigations are energy gap, effective surface, weather condition based. These factors affect the photocatalytic water splitting results[6]. Therefore, the analysis involved in the methodology and the fabrication of effective photocatalytic materials for hydrogen production is of great importance.

One of the semiconductors, TiO_2 has been broadly explored because of its many benefits like greater photo-chemical resistance, non-poisonous, availability in nature, low cost and resistance to light deterioration[7], [8]. There exist numerous techniques to improve the characteristics of TiO_2 in order to optimize its effectiveness in hydrogen production. The d-block elements used as cocatalysts appear to be the most efficient ones. Generally, its accepted that precious metals can act as electron scavengers producing a retarded re-joining rate of electron- hole pairs[9]. The drawbacks of precious metals are their values and availability. Nonetheless, one will find transition metals such as Zn, Cu and Ni which are comparatively cheaper and simultaneously efficient. For instance, compositing TiO_2 and Zn, Cu or Ni nanoparticles[10]–[12]. Lately, high hydrogen production has been reported for other photocatalysts such as two-dimensional (2D) few- layered $MoSe_2$ coated on CdS quantum rods[13]. Biochar-supported photocatalytic system[14], also, bi-functional photocatalysts have been developed such as hetero-phase Mo_2C – CoO@N – CNFs film[15]. Mostly, the existence of Ni, and other d-block elements, held steady the anatase against phase transformation, lowers the particle size and therefore increases the total area of the external surface of the photocatalyst, extends the lifetime of electrons and holes pairs, and promotes the absorption of visible light[16]. Additionally, carbon materials have attracted enormous interest as a result of their unique characteristics and as low cost compounds[17], [18].

Studies have further revealed that compositing TiO_2 with carbon nano-materials improves the photocatalytic quantum yield of TiO_2[19]–[23]. The inclusion of carbon nano- materials establishes defects on the surface that serve as active sites for electrons hence reducing the electron and hole recombination rate. This has been reported to be accurate in numerous TiO_2 and carbon nano material structures. For illustrations, Wang *et al*. reported integrating carbon into TiO_2 hollow spheres (carbon@TiO_2) and realized an improved photocatalytic activity towards the reduction of CO_2 relative to pure TiO_2[24]. In related study, He *et al*. covered carbon with mesoporous TiO_2. They realized that the structure was an effective photocatalyst in the reduction of nitrous oxide, relative to TiO_2 alone[24]. Carbon nanofibers were coated with TiO_2 nanoparticles using electro-spinning. These types of structures have been reported to have more potent photocatalysts in removal of congo red in water as compared to TiO_2 – P25[19]. Many attempts have been made to institute dopants to enhance the optical absorption of TiO_2. For instance, Zhang *et al*. established that 12.5% copper – doped anatase - TiO_2 indicated a broader absorption peak than pure TiO_2 - anatase[25].

An alternative approach to quantum yield enhancement is via the formation of a semiconductor – metal intersection; known as the a Schottky barrier which is defined as a charge separation in space[23]. At the semiconductor – metal intersection, electrons flow from the structure with a higher energy level to the structure with a lower energy level therefore achieving charge (electron – hole pair) separation. This concept is normally realized in the intersection of d-block elements, particularly the rare-earth metals and an n-type semiconductor such as TiO_2, through which an electron would transfer from the semiconductor to the metal. CNFs can be tailored to possess metallic properties like precious metals, by which the CNFs may function as sinks for electrons because of their large electron storage capacity.

Water splitting on a particulate photocatalyst is presented in Fig. 1. Step 1, the absorption of photon energy by the photocatalyst. Step 2, the photogenerated carriers (pairs) segregate and move to the surface of the photocatalyst without reunion, and step 3, the adsorbed species undergo reduction and oxidation with the photogenerated electrons and holes to produce H_2 and O_2 separately.

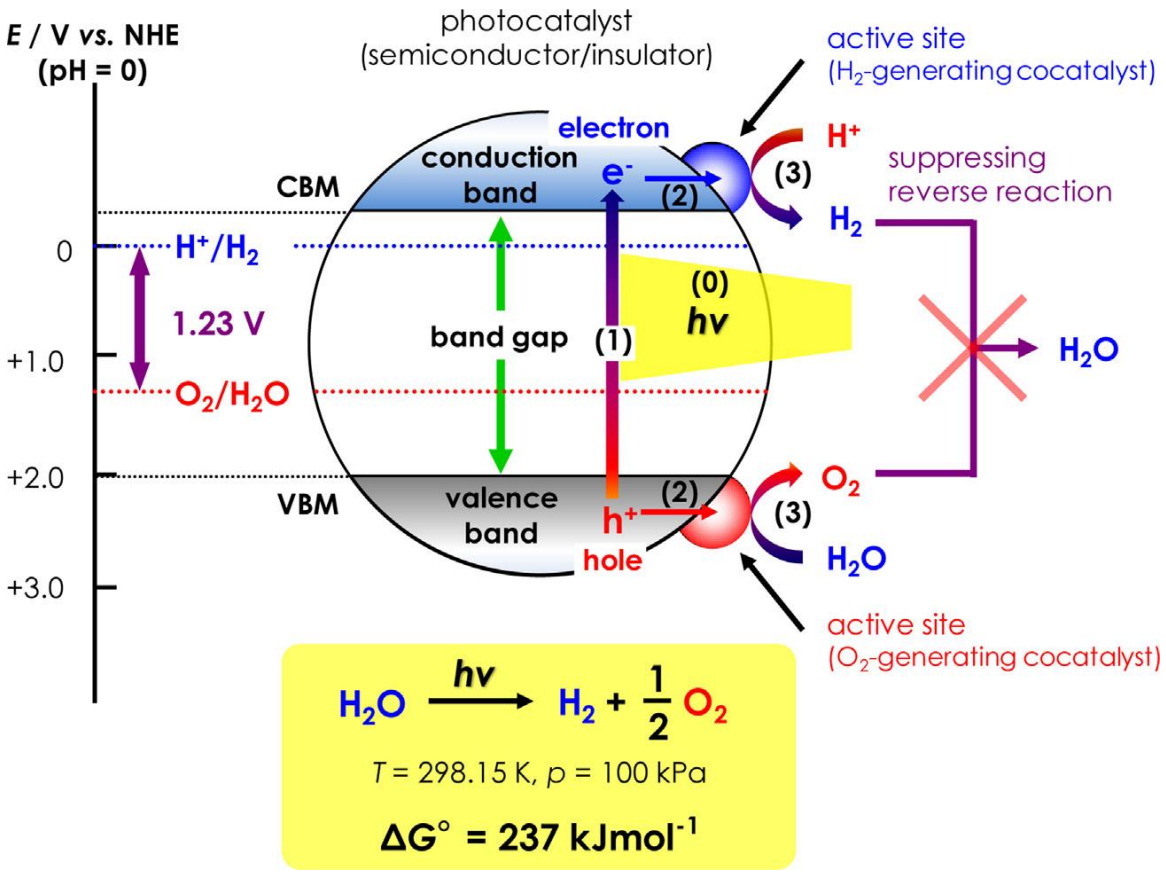

Fig. 1. Illustrative representation of the basic photocatalytic steps for a particulate photocatalyst: (1) Photon absorption and generation of the charge pairs (2) Migration of the electrons – holes to the surface; (3) The production H_2 and O_2 resulting from the photogenerated charge pairs[26].

Steps one and two are based on the structural and electronic characteristics of the particulate photocatalyst. Normally high crystallinity has a positive impact on activity, since the density

of defects, which serve as active centres between photogenerated electrons and holes decline with high crystallinity[27]–[29]. Also, the improvement in photocatalytic efficiency can be achieved by reducing the particle size of the photocatalyst, since it leads to the shortening of diffusion length of photogenerated electron – hole pairs. The reduction and oxidation reactions on the surface of the photocatalyst are reported below[30].

$$\text{Oxidation: } H_2O + 2h^+ \rightarrow 2H^+ + \frac{1}{2}O_2 \qquad (1)$$

$$\text{Reduction: } 2H^+ + 2e^- \rightarrow H_2 \qquad (2)$$

$$\text{Overall reaction: } H_2O + 1.23\ eV \rightarrow H_2 + \frac{1}{2}O_2 \qquad (3)$$

The process of water splitting is greatly energy-absorbing and needs Gibb's free energy of 1.23 eV per electron. The energy gap of 1.23 eV corresponds to light with a wavelength of 1008 nm. Therefore, the photocatalyst must have energy gap of 1.23 eV or more or-else the electrons will not have enough energy to initiate the reaction. Practically, the limit should be 1.6 eV to 1.8 eV because of some over-potentials[30].

In this study, we pay attention to the role of support, CNFs and cocatalysts, Cu and Zn in the semiconductor – based photocatalysts and illustrate the synergetic effect of the support and cocatalysts loading for reduction and oxidation reactions which lead to improved overall water splitting. A modified surfactant wrapping sol – gel / hydrothermal process was adopted to composite the TiO_2 with CNFs.

6.2 Experimental

6.2.1 Materials

Zinc chloride, Reagent grade, ≥ 98%, ethanol (99.9%), ammonium solution (25%), copper (II) nitrate trihydrate, $Cu(NO_3)_2.3H_2O$ (99%), potassium hydroxide, anhydrous, KOH, ≥

99.95% trace metals basis and nitric acid, HNO_3 (55%), titanium butoxide, butanol all were bought from Sigma – Aldrich while hydrogen, argon and acetylene gas were purchased from Afrox. Part of the experiment used distilled and deionized water.

6.2.2 Synthesis of copper oxide Nanoparticles and carbon nano-fibers, CNFs

Copper oxide nanoparticles, CuONPs were prepared from 0.05M solution of copper nitrate, $Cu(NO_3)_2.3H_2O$ with the addition of 0.05M potassium hydroxide that was followed by a 12 h vigorous stirring. Black particles formed, and deionized water was used to clean them to neutrality, dried in the oven overnight at 80 ℃ and characterized by PXRD, Raman, HR-SEM, FTIR, and TGA.

CuONPs were used to synthesize CNFs at 300 ℃ in a tube heater using chemical vapour deposition, CVD technique[31]. The synthesis method of CNFs employs the breaking down of acetylene, C_2H_2 in a tubular quartz reactor, placed horizontally in a heater. The heater was electronically controlled by setting the heating rate, reaction temperature, and gas flow rates. 0.1g of CuONPs was packed into a quartz boat, 120 mm by 15 mm at room temperature and the boat placed at the centre of the quartz tube. The heating was at 10 ℃ min^{-1} with hydrogen gas, H_2 flowing over the CuONPs at 50 mL min^{-1}. Upon attaining heating of 300 ℃, the H_2 flow was retained for 30 minutes before introducing C_2H_2 at a constant flow rate of 50 mL/min. 30 minutes later, the C_2H_2 flow was ceased, and the furnace was allowed to cool down to room temperature under H_2 gas flow. The quartz boat was later removed from the reactor and the product, carbon deposit formed along with the catalyst weighed. The CNFs were washed with concentrated nitric acid, HNO_3 to remove the residues of the CuO NPs and to functionalize them. 55% HNO_3 was added to the CNFs in a flask before refluxing for 2 h

at 110 ℃. The resultant suspension was cooled to 25 ℃, filtered and cleaned to neutrality with distilled water. The cleaned CNFs were filtered before drying for 12 h in an oven at 80 ℃.

6.2.3 Preparation of the support materials, TiO_2 and TiO_2/CNFs composite

The composite of the particulate photocatalyst, titanium dioxide-anatase and carbon nanofibers was prepared by a surfactant wrapping sol-gel/hydrothermal process which was modified from a surfactant wrapping sol-gel approach formerly outlined by Deng et al[32], and Hamid et al[33]. In this study, a fixed amount of the purified CNFs was discharged in 25 ml butanol and homogenized for 30 minutes in a sonicator. A known amount of titanium butoxide which had been previously dispersed separately for 30 minutes in butanol (5 mL) was introduced in drops and with vigorous stirring to the CNFs suspension. For complete hydrolysis of the titanium butoxide, ammonium solution (25%, 1 ml) was introduced to the mixture, set up in an autoclave, treated at 120ºC as shown in Fig. 2. The obtained product centrifuged and cleaned with ethanol, deionized water and finally dried at 80ºC, 24 h in an oven. Calcination conditions were 400ºC and 4 h. Loadings; 10% and 20% of TiO_2 on CNFs, identified as 10% TiO_2/CNFs and 20% TiO_2/CNFs respectively. The same approach was replicated without CNFs to prepare TiO_2 – anatase which was one of the controls in this study and identified as TiO_2 – A.

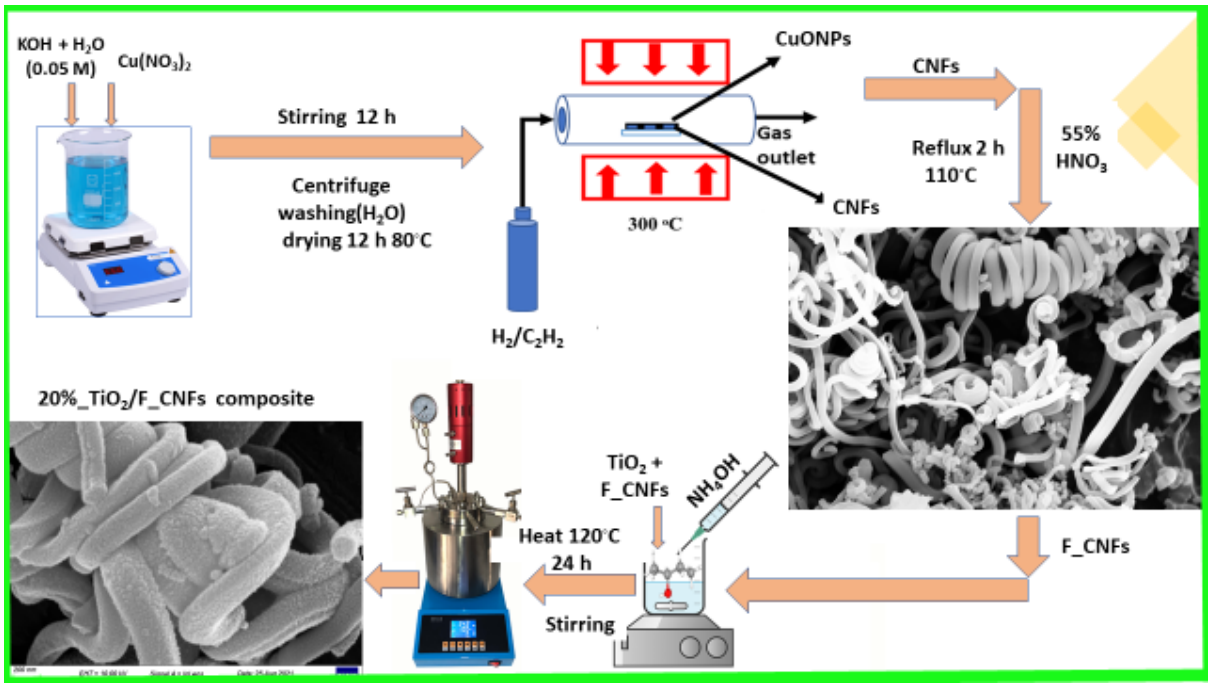

Fig. 2. Simplified route used in the synthesis of TiO_2/CNFs structures.

6.2.4 Preparation of Cu, and Zn -TiO_2/CNFs composites by impregnation method

Impregnation method with modification was used for Cu, and Zn incorporation in the TiO_2-A/CNFs composites supports. This method enabled the metals to be dispersed on the surface of the supports (10% TiO_2-A/CNFs, 20% TiO_2-A/CNFs)[34], [35]. In the first place, a known amount of each non - precious metal precursor and 10% TiO_2-A/CNFs, 20% TiO_2-A/CNFs were sonicated for 45 minutes. The mixture was then calcined under Ar at 350 ºC for 2 hours to remove undesirable residues[36], [37].

6.2.5 Catalyst characterization

Different technologies were used to identify the synthesized CuONPs, CNFs, TiO_2-A, TiO_2-A/CNFs, the metal - TiO_2-A/CNFs structures. Morphologies of the TiO_2-A, CNFs, TiO_2-A/CNFs and the metal - TiO_2-A/CNFs composites were investigated by HRSEM analysis (ZEISS Sigma 300 VP from M/S ZEISS 'Smart SEM' OXFORD INSTRUMENTS x-act PentaFET Precision and 'Oxford INCA', United Kingdom. The same samples were analysed by X-ray diffraction (XRD) using a Brucker D2 phaser fitted with Cu – Kα radiation (λ = 1.5405 Å), operating at 30 kV (Voltage) and 10 mA, (Current). A Perkin Elmer TA TGA Q500 was used to explore the thermal stability of the samples, thermogravimetric analysis (TGA). At least 10 mg of the sample was heated up to 900 ℃ at a heating rate of 10 ℃ min^{-1} under air. In probing the size and shape of the samples, Transmission Electron Microscopy (TEM) utilizing a FEI Technai G2 Spirit electron microscope, 120 kV was used. Particles size distribution was investigated by ImageJ software in which at least 100 particles were computed for each sample. Fourier Transform Infrared, FT- IR Spectroscopy, mounted with a Bruker Tensor 27 FT – IR spectrometer (4000 – 500 cm^{-1}) was used to identify the functional groups present in the samples. The optical attributes of the samples were analysed by a Varian Cary Eclipse EL0410 3870 photoluminescence/ fluorescence Spectrophotometer and a SPECORD 210 plus UV – Vis Spectrophotometer. For the determination of the specific surface, N_2 physisorption (Micromeritics – 2000 Tri - star analyser) was used. Prior to the analysis of the samples, 0.2 g was degassed for 6 h at 150 ℃ concealed by a N_2 flow using a Micromeritics flow Prep 060. Measurements of XPS were carried out by a Thermo Scientific ESCALAB 250Xi spectrometer with a monochromatic Al Kα source (1486.7 eV).

6.2.6 Catalytic activity using particulate photocatalysts in water splitting

The hydrogen evolution experiments were conducted in a submersion type reactor, Lelesil Innovative Systems, Thane, India, Fig. 3, reported by *Walls et al*[38] using a 450 W UV lamp.

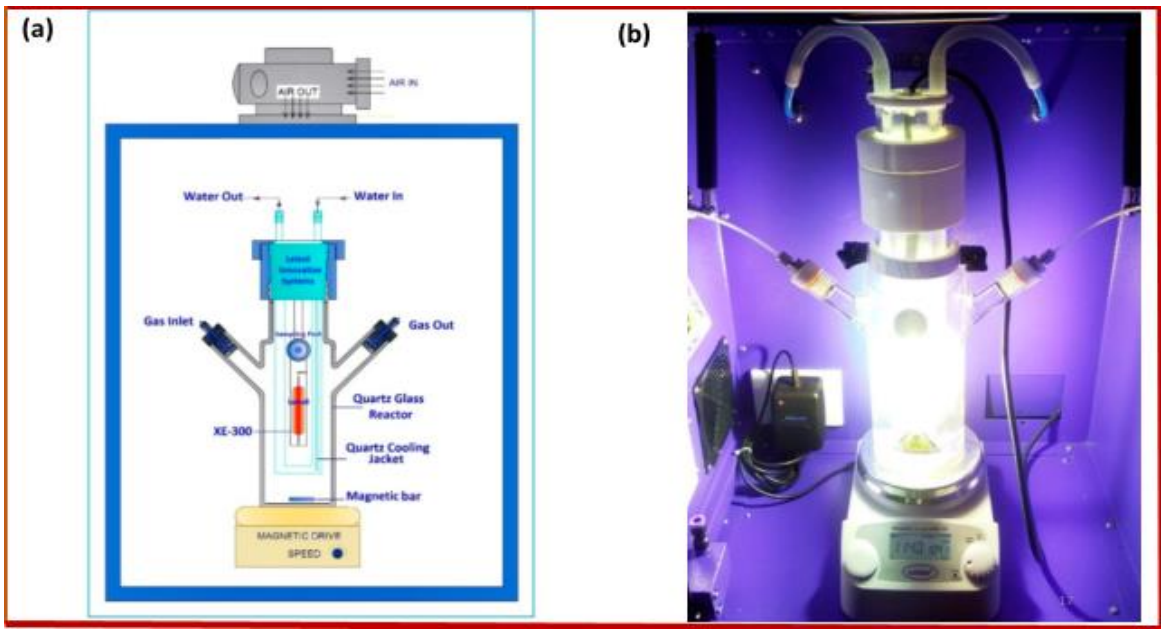

Fig. 3. (a) Diagrammatic (b) Pictorial; water splitting reactor.

In this work, 1g of the photocatalyst, was stirred in 1 L of water (15 minutes) before radiating the sample with the UV lamp at room temperature, 25ºC for 6 h under argon gas and with stirring. The system was stirred at 1000 rpm from the start of the experiment to the end of the reaction, 6 h. The system was flushed with argon until no peaks were detected on the online GC (thermal conductivity detector, TCD) from the start of the reaction and was held throughout the reaction under a flow rate of 80 ml min^{-1}.

6.3 Results and Discussions

6.3.1 Materials characterization

TiO_2 – anatase and TiO_2/CNFs composites were analysed by PXRD. Fig. 4. Indicates the characteristic peaks. The characteristic peaks of the CNFs were not observed clearly on the

PXRD patterns of the TiO_2/CNFs composites in the studied range due to (i) overlap of the intense (101) TiO_2 – anatase reflection with (002) reflection of the CNFs, (ii) greater scattering from TiO_2 – anatase, and (iii) the large difference in mass of TiO_2 – anatase as compared to the mass of CNFs in the TiO_2/CNFs composites[39], [40]. Having pure photocatalyst and water, photocatalytic hydrogen evolution is possible because the photoelectrical characteristics of the photocatalyst are influenced by their crystallinity[41].

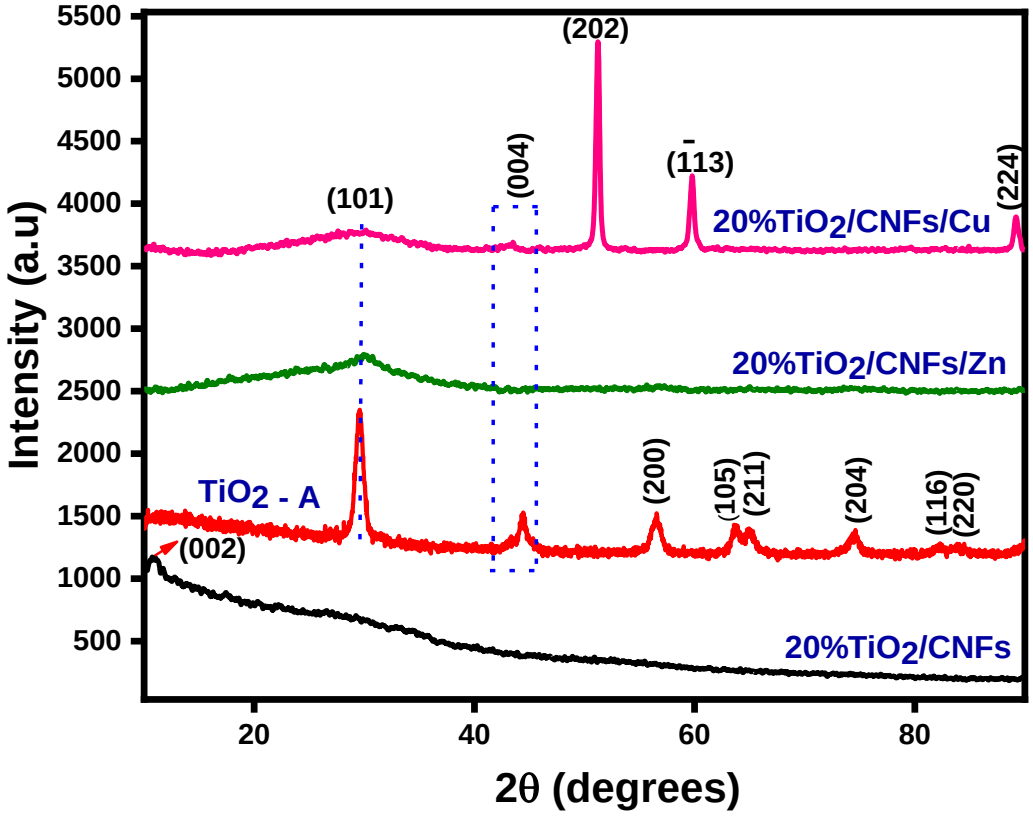

Fig. 4. PXRD range of titanium dioxide (anatase) and the composites.

Raman scattering effect was used to study the graphiticity of the CNFs. The D-band at 1384 cm^{-1} is a defects identification on the F_CNFs, and at 1590 $cm^{-}1$ (G-band) is C-C stretching of the F_CNFs, Fig. 5 (a).

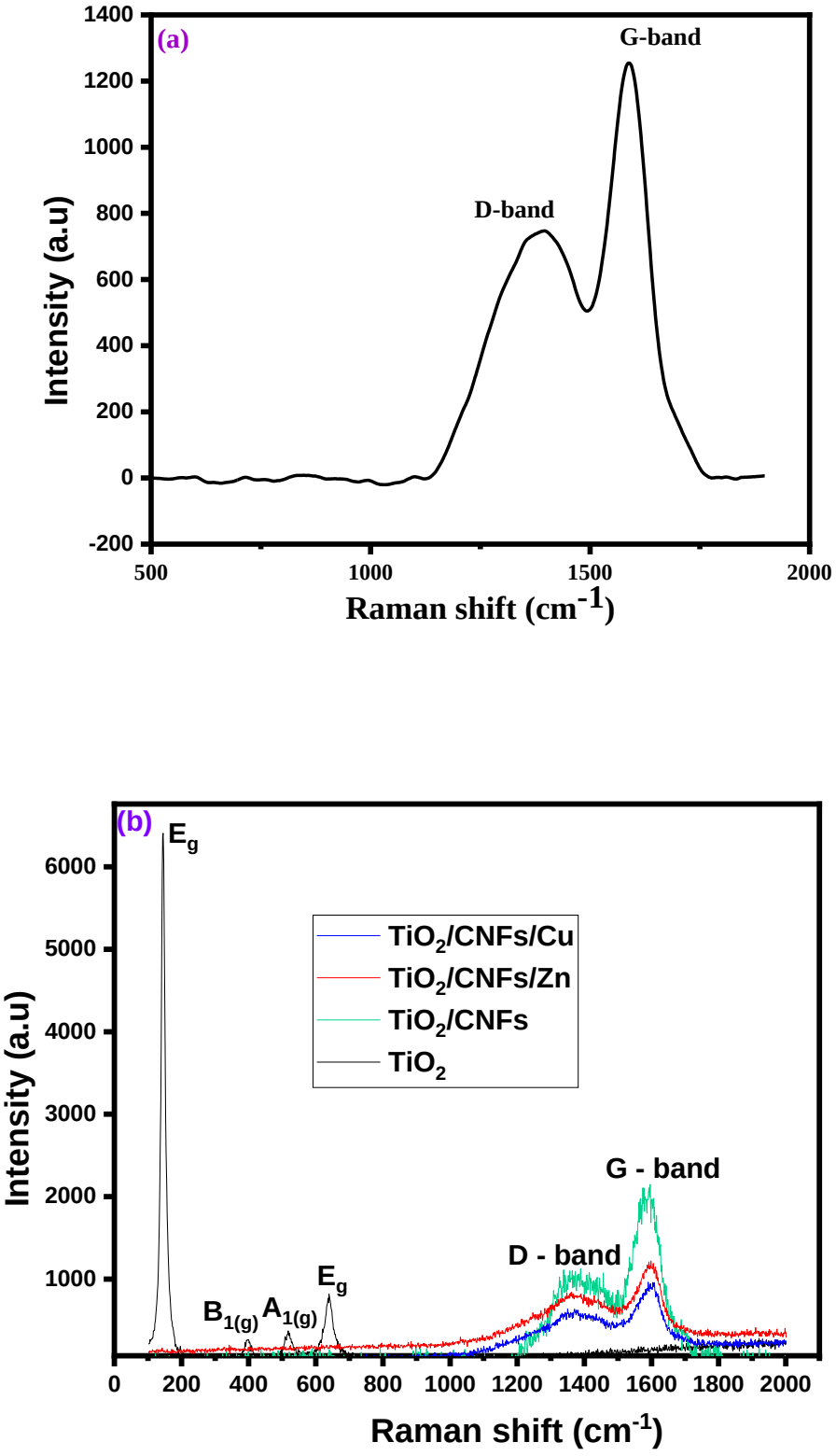

Fig. 5. Raman spectra of (a) F_CNFs (b) TiO_2 – A and TiO_2/F_CNFs composites.

Also, it was used in confirming the TiO_2 – A presence in the TiO_2/CNFs composites and to study the effect of doping TiO_2 with CNFs and non - precious metals, Cu and Zn in relation to crystallinity, Fig. 5(b). The Raman spectrum in Fig. 5 has four well defined peaks at Raman shift 144, 397, 517, and 640 cm^{-1} and are listed (E_g), (B_{1g}), (A_{1g}), and (E_g), accordingly[42], [43].

The four modes were also obtained on the spectra of the composites, thereby confirming the presence of TiO_2 – A in the composites.

One of the significant observation was that the most intense TiO_2 peak (E_g) for all the composites was blue shifted besides being broader as compared to the TiO_2 – anatase (unbound) (142 to 144 cm^{-1}). The positions and broadening of Raman peaks is a characteristic of the nanomaterials and studies show that its associated with the size and defects in the nanomaterial, the experimental conditions such as temperature and the laser – induced local heating effect on the material under investigation[42]–[44]. Considering that all the laser Raman analyses in this work were carried out under the same experimental conditions, then the blue shifting and broadening of the peaks resulted from phonon confinement or surface pressure[24]. Furthermore, other related studies have reported similar observations, composites of titanium nanotubes and graphene oxide. The effect was proposed to be an indicative of the existence of strong chemical interactions between TiO_2 and CNFs[45]. Chemical interactions between TiO_2 and CNFs was expected as it helps in increasing charge separation in the TiO_2/CNFs composites, thus this effect is an indication that the composites photocatalytic ability was enhanced. The results of Raman spectroscopy signify the successful chemical interaction between TiO_2, CNFs and Cu, Zn in the non - precious metal – TiO_2 /CNFs heterojunctions.

The 3D morphological and structural properties of TiO_2 – A, CNFs, TiO_2/CNFs and TiO_2/CNFs – noble metal composites were studied using SEM and TEM, Fig. 5 and 6. The CNFs were examined to be fiber-like while TiO_2 – A was granular (consisting of small particles), TiO_2/CNFs and TiO_2/CNFs- noble metal composites were feathery in morphology, figures 5.

The CNFs were purified to eliminate the effect that the CuONPs (used in the synthesis of the CNFs) would feasibly have on the impact of the CNFs on the photocatalytic properties of TiO_2 which is under study. The FESEM analysis of the as-synthesized and purified CNFs, Fig. 5 show that the presence of traces of CuONPs were reduced to below observable limits. This shows that the CuONPs were effectively removed from the CNFs structures and that they are soluble in 55% HNO_3. The purified (functionalized) CNFs were fibrous in nature and the fibers were helical as shown by the TEM image Fig. 7. It was also the same observation with CNFs morphology, FESEM analysis, Fig 6. The CNFs were slender in diameter averaging 132 nm, but varying between 115 and 140 nm and conforms to similar studies on CNFs[46].

TiO_2 – anatase which was synthesized had granular nanoparticles Fig. 7(c) and Fig. 6 (c - d). The average particle size was 9.5 nm and ranged between 2.0 - 20 nm. All the CNFs were uniformly and totally covered with TiO_2 nanoparticles Fig. 6. The FESEM analysis further revealed that the TiO_2 nanoparticles were lodged onto the surface of the CNFs. In other studies, where TiO_2 are composited with CNFs, *Gao et al* also found out that doping TiO_2 and

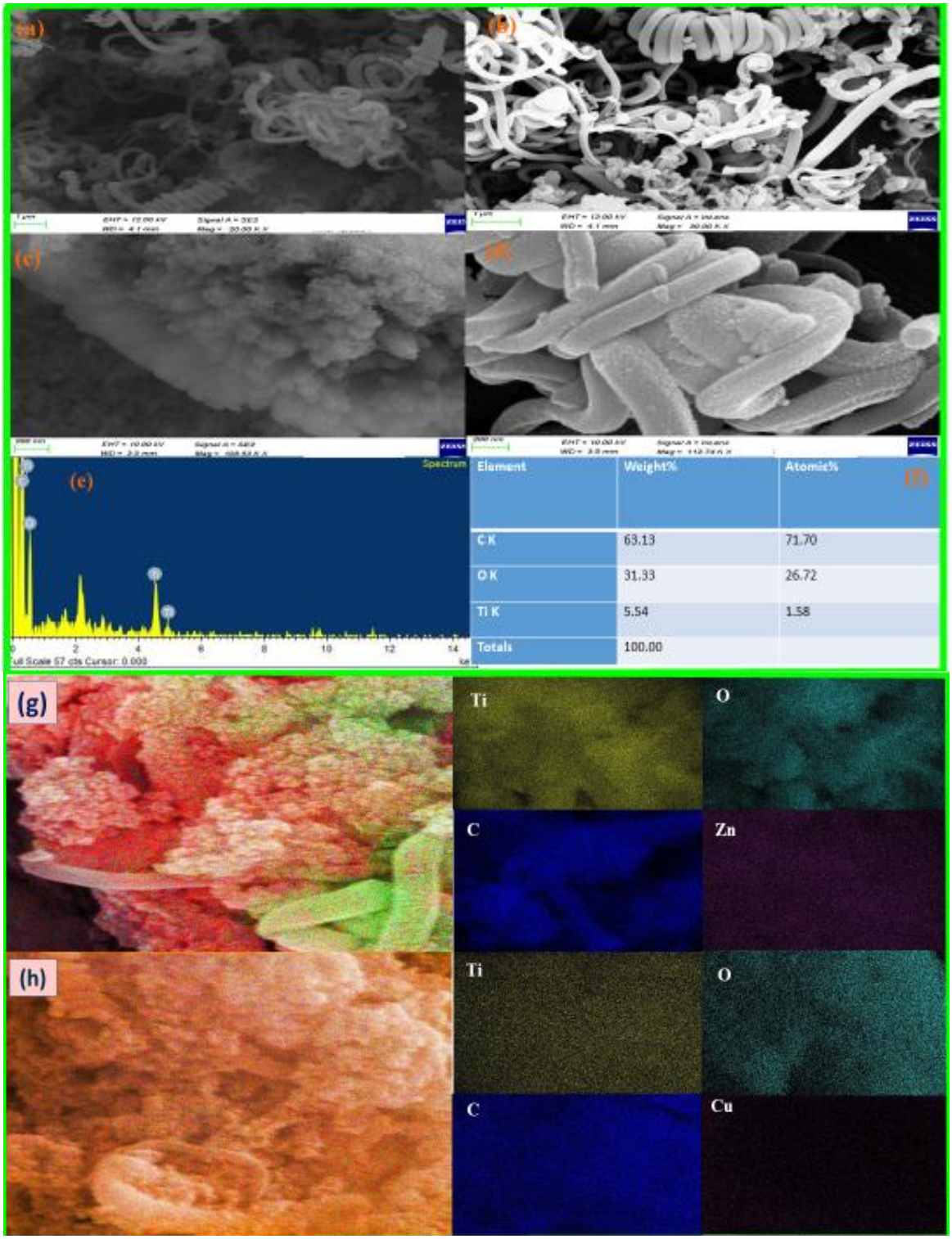

Fig. 6. FESEM analysis of (a) as-synthesized CNFs (b) Purified CNFs (c) TiO_2 – A (d) 20% TiO_2/CNFs composite (e) EDX spectrum of 20% TiO_2/CNFs composite (f) Composition of the elements (20%TiO_2/CNFs) (g) EDX mapping analysis of Zn – 20%TiO_2/CNFs composite (h) EDX mapping analysis of Cu – 20%TiO_2/CNFs composite.

(b) (b)

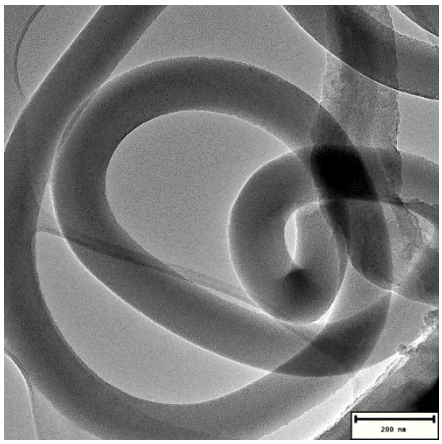

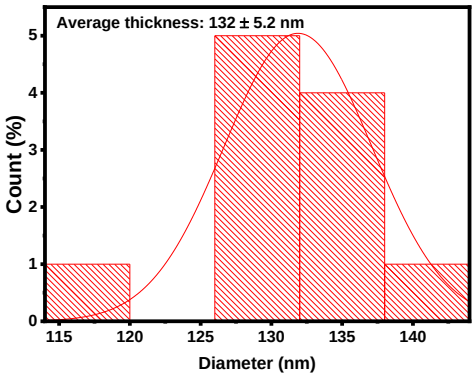

(c) (d)

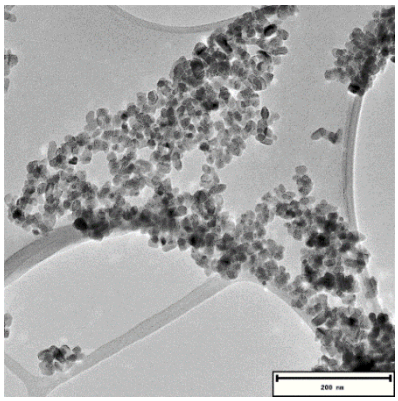

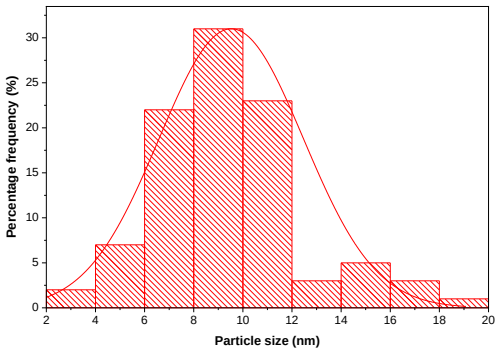

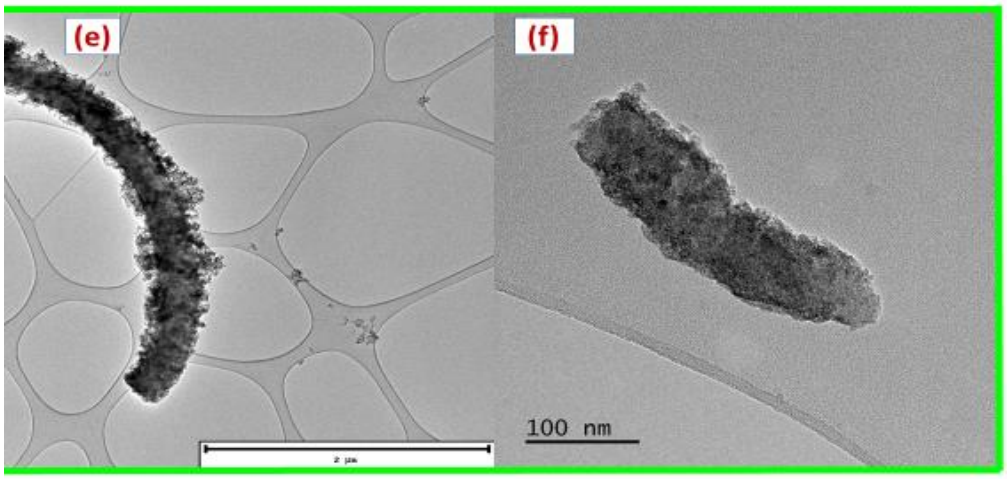

Fig. 7. TEM images of (a) CNFs (b) The distribution diagram of the diameter of the CNFs (c) TiO_2 – A (d) Particle size distribution of TiO_2 – A (e) 6%_Zn (2µm) - (f) 6%_Cu (HR-TEM) - 20%_TiO_2/CNFs.

CNFs by surfactant wrapping sol-gel method produced homogeneously covered CNTs with TiO_2 nanoparticles[47].

In this study, when the surfactant wrapping sol-gel method was modified hydrothermally, a fully coated CNFs were obtained.

The total covering of CNFs presented an impression that chemical interactions existed between the TiO_2 and CNFs. Adjacent closeness contact, resulting in chemical interaction between TiO_2 and CNFs had been identified to be the source of electron transfer in similar composites thus giving rise to separation of the charges (electron-hole separation)[48]–[50].

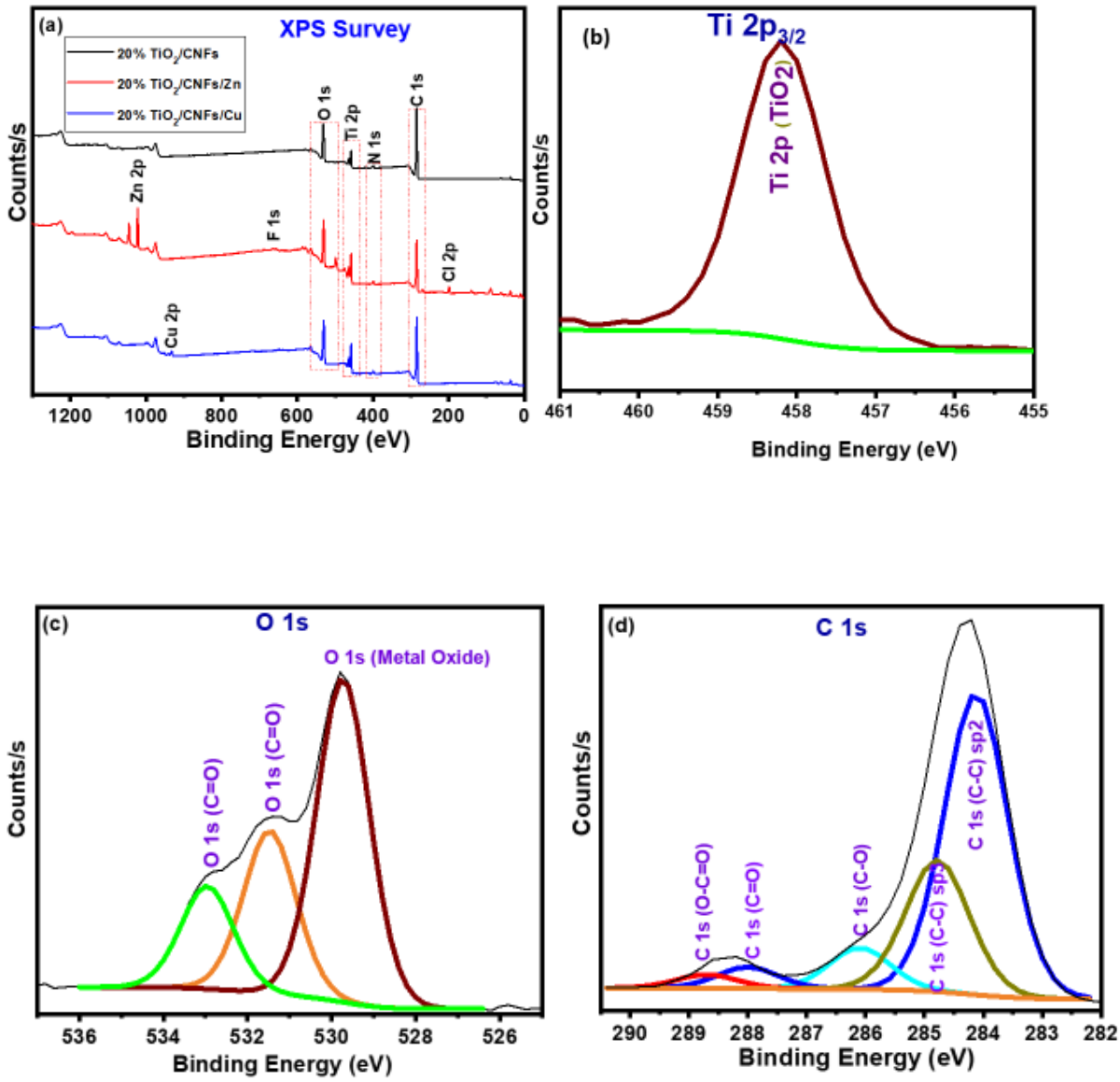

Fig. 8. XPS analysis of TiO_2/CNFs, 20%TiO_2/CNFs/Pt, and 20%TiO_2/CNFs/Au (a) XPS survey spectra of the composites (b) XPS spectrum of titanium, (c) XPS spectrum of oxygen, (d) XPS spectrum of carbon.

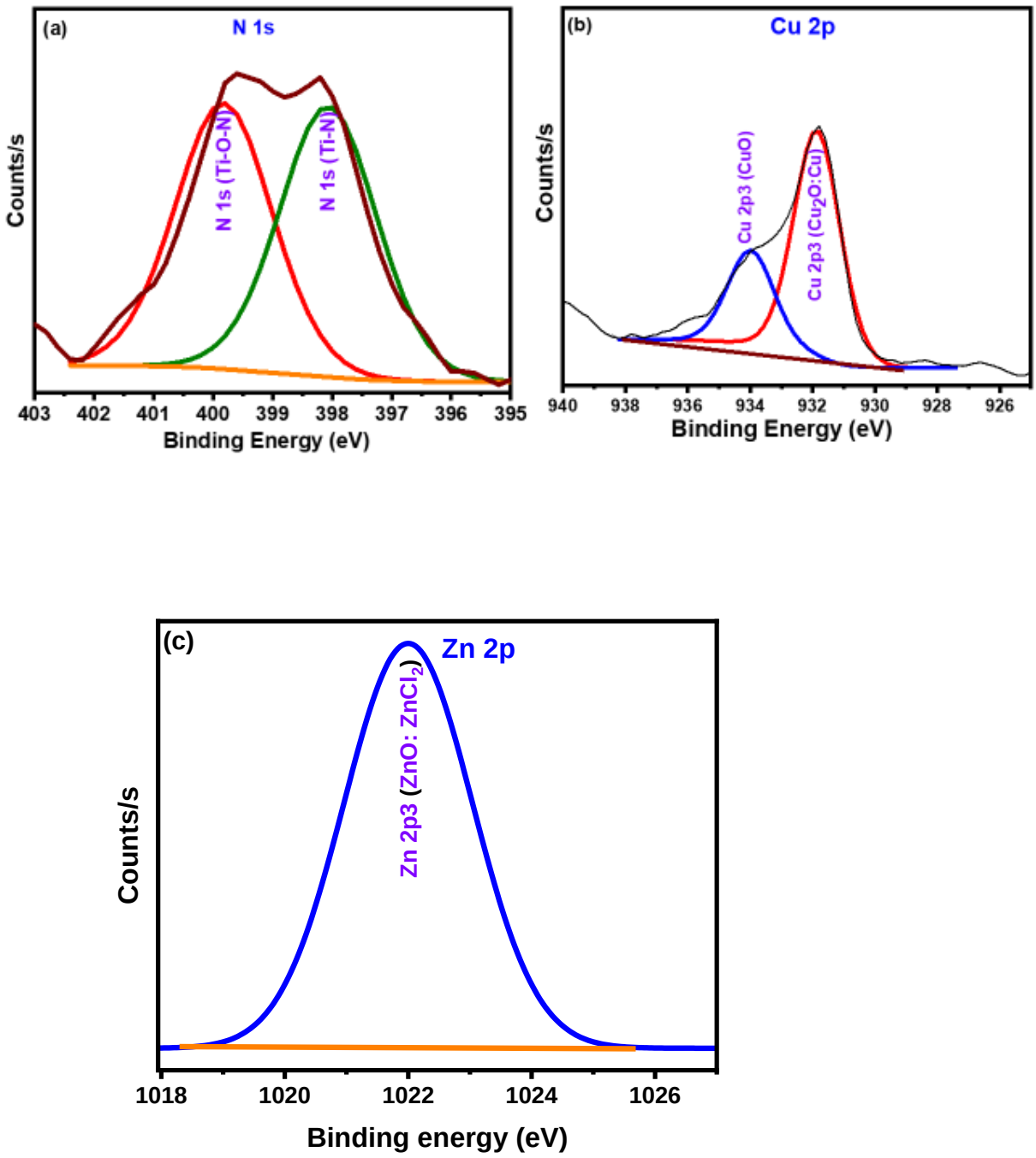

Fig. 9. XPS analysis of 20%TiO_2/CNFs, 20%TiO_2/CNFs/Pt, and 20%TiO_2/CNFs/Au (a) XPS spectrum of nitrogen, (b) XPS spectrum of copper, and (c) XPS spectrum of zinc.

Related studies have noted that most of the physical and chemical properties of TiO_2/CNFs composites are based on the interaction between CNFs and TiO_2 which successively rely upon preparation processes [47]. Additionally, clustering metal-particles provided proof that the CNFs contributed in the accumulation of the TiO_2 during the hydrolysis process[47].

The FESEM analysis, Fig. 6 and EDS scanning confirmed that the samples consisted of Ti, C and O (support materials) and the photocatalysts were doped with the non -precious metals, Zn and Cu. This is a confirmation that the CuONPs that was used in the preparation of the CNFs was effectively removed. Other studies have also shown that SEM-EDS can be used to show the elemental distribution in the samples[24], [51].

The chemical states of the elements in TiO_2/CNFs, Zn - doped TiO_2/CNFs, and Cu – doped TiO_2/CNFs catalysts were analysed using X – ray photoelectron spectroscopy, XPS and the results are presented in Fig. 8 and Fig. 9. It is visible from the XPS survey graph in Fig. 8(a) that there are six elements, Ti, O, C, N, F, Cl, Zn, and Cu on the surface of the catalysts. The Ti 2p spectrum in Fig. 8(b) with binding energy, 458.20 eV for $2p_{3/2}$ attributes to the existence of titanium TiO_2[52].

The XPS spectrum in Fig. 9 is for Zn 2p. The XPS peak in Zn 2p at 1022 eV is similar to what has been reported for Zn $2p_{3/2}$, ZnO hence it is associated with Zn^{2+}[53]–[56]. This illustrates that Zn nanoparticles were deposited on the 20% TiO_2/CNFs composites. The results signal little impurities of F 1s and Cl 2p (possible impurities from the $ZnCl_2$, 98% – reagent grade not analytical used in the synthesis) in Fig. 8(a). Also, a little contaminant of ammonium solution (lower intensity of N 1s peak in Fig. 8(a)) and Fig. 9(a) used in the synthesis of 20% TiO_2/CNFs and the 20% TiO_2/CNFs – non precious metals composites.

Fig. 8(c) shows that O 1s peaks which are located at 531.6 eV, 533.1 eV, and 529.7 eV correspond to the adsorbed oxygen[57] while Fig. 9(a) displays the binding energy of N 1s which is located at 398.1 eV and 399.8 eV. The weaker peak positioned at 398.1 eV can be assigned to the Ti – N bond which shows that nitrogen atoms have been absorbed into the lattice of TiO_2/CNFs composites[58], [59]. The N 1s peaks 398.1 eV and 399.8 eV point to the presence of –NH and $–NH_3^+$ respectively in all the composites as shown in the XPS survey spectra in Fig. 8(a) and Fig. 9(a)[60], [61].

One of the elements shown in XPS survey Fig. 8(a) is carbon. In Fig. 8(d) the XPS peak corresponding to C 1s is simplified into 5 peaks. The C=C bonds located in the region 284.7 eV correspond to C in CNFs or graphene structures[62], [63]. The peaks 286.1 eV, 2.88 eV, and 288.7 eV are related to C-O, C=O and O-C=O respectively. This further confirms the successful incorporation of the CNFs in the 20% TiO_2/CNFs and other composite materials as shown in Fig. 8(d)[60]. The XPS spectrum of the 20% TiO_2/CNFs/Cu in the Cu 2p (931.9 eV and 934 eV) regions are presented in Fig. 9(b). The results are consistent with related studies[64].

The advantage of compositing TiO_2 with CNFs is to increase the surface area of the composite materials. Hence, Brunauer – Emmett – Teller (BET) surface area (S_{BET}) analysis was performed to explore the benefits. Fig. 10 shows the nitrogen adsorption – desorption isotherms while the associated specific surface area, pore diameter and pore volume are given in Table 1.

A linear increase of the adsorption isotherms profiles was detected in the relative pressure (P/P_0) range from about 0.23 to 0.85 which corresponds to the mesoporous structure of the nanomaterials[65]. The obtained BET surface areas of the catalysts are presented in Table 1.

Table 1. BET surface area, pore volume, pore diameter and 1_D /1_G ratio of the materials.

Sample	**S_{BET} (m^2g^{-1})**	**PV (cm^3g^{-1})**	**PD (nm)**	**I_D/I_G**	**Reference**
TiO_2-A	73	0.079	5.1		This study
TiO_2 – Dandelion	81	0.071	3.2		[66]
Degussa (TiO_2-P25)	49	-	-		[Sigma-Aldrich]
CNFs	32	0.091	22.6	0.87	This study
10% _TiO_2-CNFs	89	0.120	5.4		This study
20% _TiO_2-CNFs	126	0.273	10.7		This study
20%_ TiO_2-CNFs_6%Zn	239	0.259	4.3		This study
20%_ TiO_2-CNFs_6%Cu	297	0.303	4.1		This study

S_{BET}, PV, PD, 1_D /1_G: BET surface area, pore volume, and pore diameter, 1_D /1_G ratio.

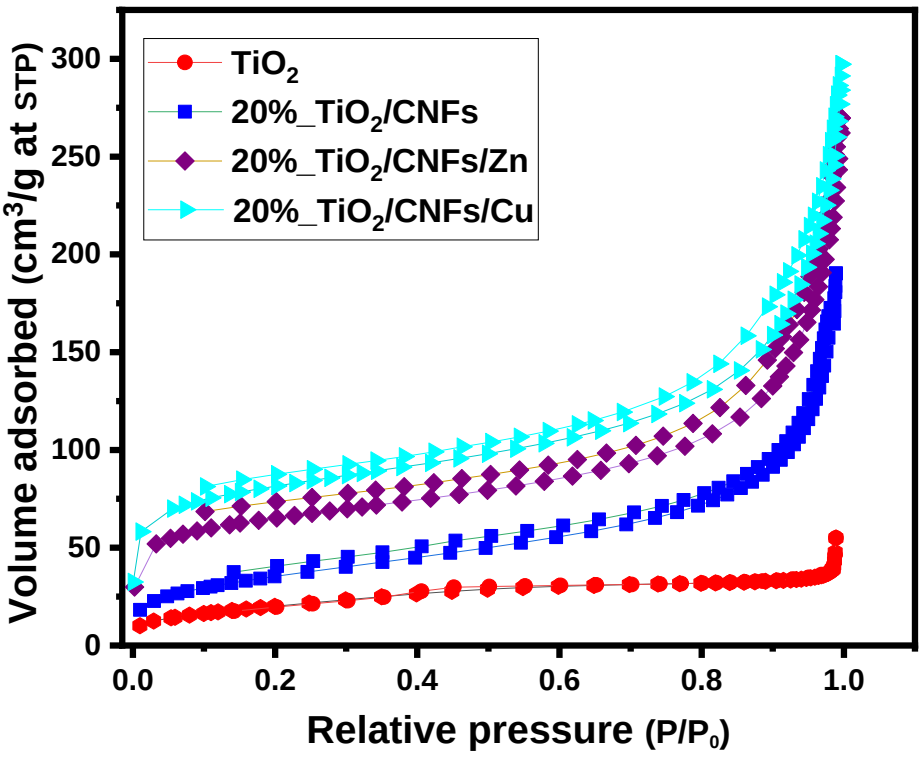

Fig. 10. (a) N_2 – BET graphs; 20%_TiO_2/CNFs, 20%_TiO_2/CNFs/Zn, and 20%_TiO_2/CNFs/Cu.

The hysteresis loops profiles in the isotherm was classified as type IV in accordance with the International Union of Pure and Applied Chemistry (IUPAC) categorization depicting the presence of mesopores[67].

When the CNFs (surface area, 32 m^2/g) were composited with TiO_2 (surface area, 73 m^2/g), the surface area of the TiO_2/CNFs composite (126 m^2/g) was higher than the individual entities. Also, the pore volume of the TiO_2/CNFs composite was higher (Table 1). This resulted from doping and functionalization of the materials[31]. TiO_2 – A (surface area, 73m^2/g) compared well with other previous studies.

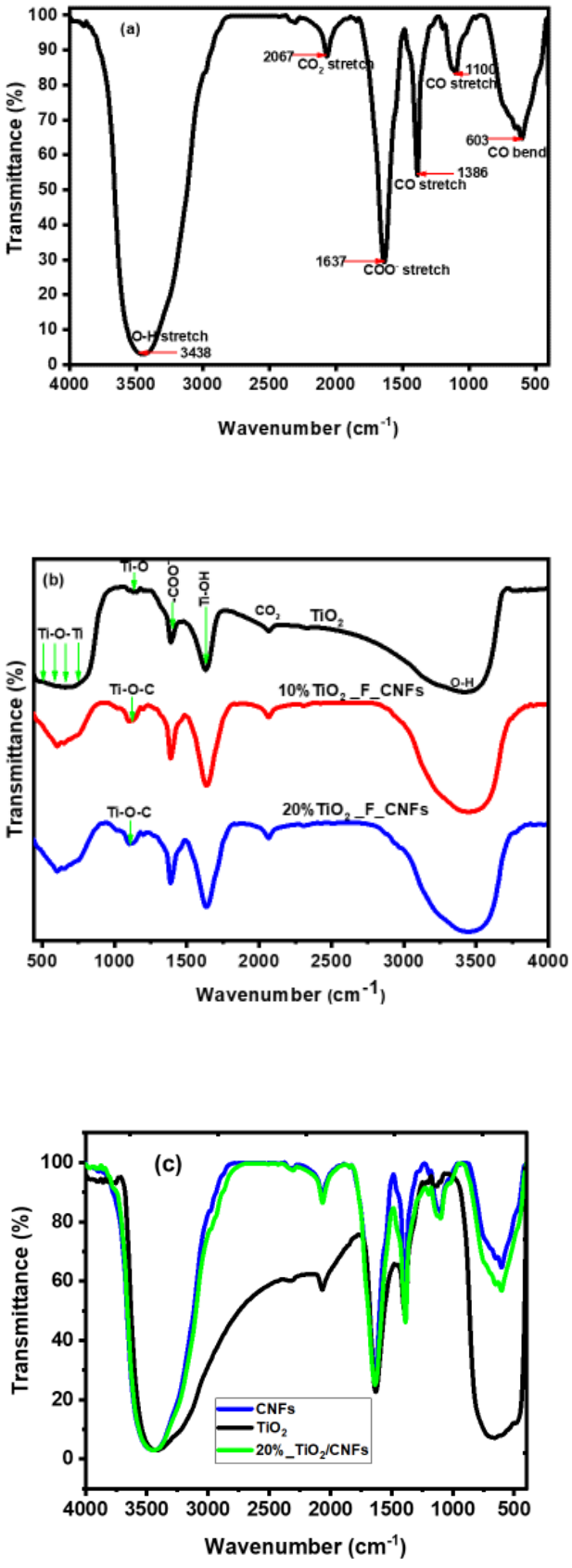

Fig. 11. The FTIR spectra for the composites.

Moreover, the BET surface area generally increased with the non – precious metal addition whereby the 20% TiO_2/CNFs – 6%Cu composite was the greatest, 297 m^2/g. Pore volumes of the composites also increased in this order 0.303 > 0.259 cm^3/g while the pore diameters of the composites decreased, 4.1 < 4.3 nm. This suggests that the non - precious metals and CNFs can effectively tune the morphology of TiO_2 for higher surface area, larger pore volume, and lower pore diameters thus enhancing the catalytic properties (non - precious metal photocatalysts).

Fig. 11 shows the FTIR of the samples. The strong band at 1100 cm^{-1} was associated with C–O stretching vibrations. The IR peak at 3438 cm^{-1} was O-H stretching vibrations. The remainder of the peaks could be the vibrations of aliphatic C-H groups in the range of 3000-2800 cm^{-1}, 2000-1800 cm^{-1}, 1410-1395 cm^{-1}, and 820-790 cm^{-1}. The peak at 3400 cm^{-1} was as a result of adsorbed water molecules. TiO_2 characteristic peak is normally in the range of 690 to 800 cm^{-1} and the broad peak which appears below 1000 cm^{-1} is as a result of two peaks[68]. The peak at 3300cm^{-1} was also present in the TiO_2/CNFs composites and other peaks, Fig. 11. The peaks from the composites at 3230, 2920, 1720, 1636, and 1330 correspond to the presence of O-H, C-H, C=O, C=C and C-O-C respectively. The peak at 1104 cm^{-1} for TiO_2 is Ti – O – C indicating the conjugation effect of CNFs and TiO_2[69].

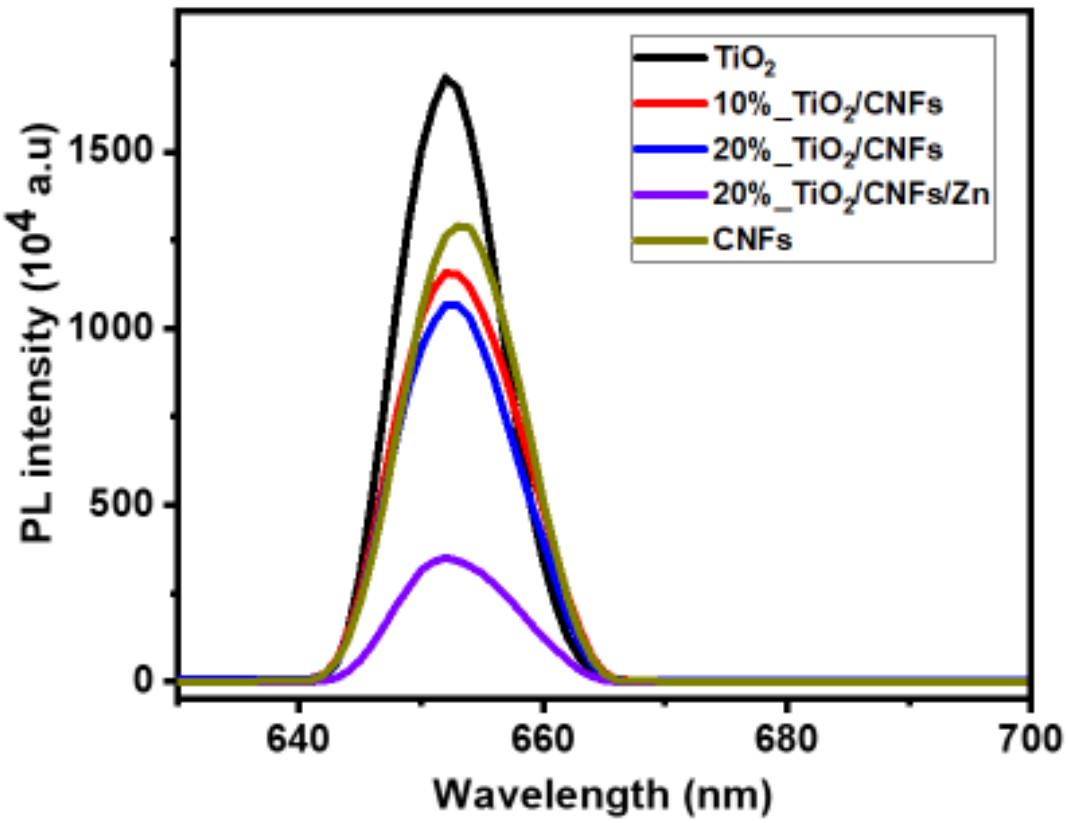

Fig. 12. Photoluminescence spectra of TiO_2, CNFs, 10% _TiO_2/CNFs, 20% _TiO_2/CNFs and 20% _TiO_2/CNFs/Zn composites.

To examine the confinement, and movement of electron – hole pairs, it was imperative to study photoluminescence of the TiO_2 – anatase and TiO_2/CNFs composites. Photoluminescence studies based on photocatalysts have been reported and employed in the study of charge carriers[49], [70]. The excitation wavelength 350 nm was used and the characteristic features of charge carrier recombination rate of TiO_2 – anatase are shown in Fig. 12. The results from this study conform to other related studies[70].

TiO_2 (anatase) had higher emission peak than the TiO_2/CNFs composites. The reduced intensity of the composites was as a result of limited recombination of electron – hole pairs showing that the CNFs had enhanced the lifetime of the charge carriers (electron – hole

pair)[40], [43], [47], [70], [71]. Therefore, the higher the loading of TiO_2 on CNFs the greater the charge separation.

After verifying that doping was effective by photoluminescence studies, Fig. 12, UV-vis DRS studies were performed to elucidate the behaviour of the composites towards visible light. Tauc's plot obtained from UV-vis DRS spectra of the TiO_2/CNFs composite was not the same as that of TiO_2 – A signifying that CNFs had positive impact Table 2 and Fig. 13.

Table 2. Summary of the Band gap (E_g) energies (eV) of TiO_2 phases and composite.

Sample	**Energy (eV)**	**Reference**
TiO_2 – Degussa P25	3.15	[72]
TiO_2 – Anatase	3.20	[73]
TiO_2 – Anatase	2.22	This study
20%_TiO_2/CNFs	1.96	This study
20%_TiO_2/CNFs/Zn	1.67	This study
20%_TiO_2/CNFs/Cu	1.72	This study

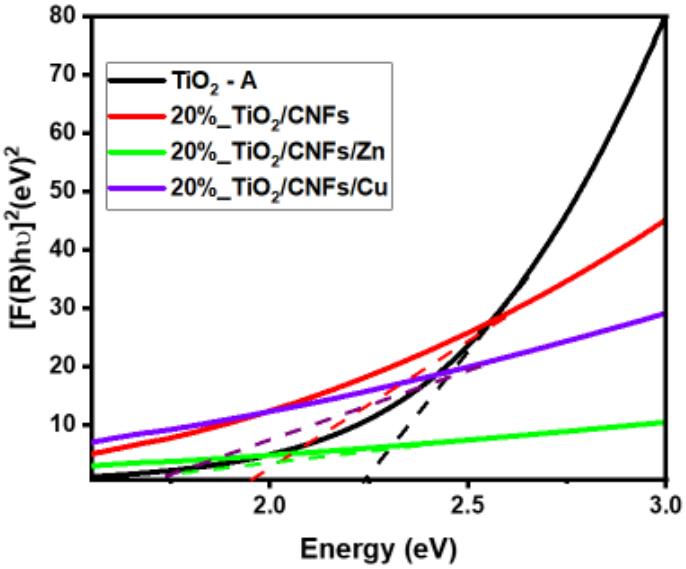

Fig. 13. The Band gap (E_g) energy (eV) of TiO_2 – A, 20% _TiO_2/CNFs, 20% _TiO_2/CNFs/Zn, and 20% _TiO_2/CNFs/Cu composites.

This shows that energy gaps (1.96, 1.72 and 1.67 eV) are smaller as compared to the energy gap of TiO_2 Table 2[72], [73].

6.3.2 Photocatalytic studies

All as-synthesized photocatalysts were tested in the H_2 production reaction using water. The accumulated H_2 production outline of the catalysts is presented in Fig. 14 (a). The photocatalysts tested were analysed according to the support material, loading efficiency and cocatalysts used in the experiments.

The first group consists of commercial photocatalyst P25 (TiO_2) and pure TiO_2. The second group is the loading of TiO_2 on the functionalized CNFs obtaining 10% TiO_2/CNFs or 20% TiO_2/CNFs, third group-photocatalysts are the support (TiO_2/CNFs) – doped with Zn or Cu (1, 5, and 6% by weight). 10%_ TiO_2/CNFs/5% Zn was found to be the most active photocatalyst with activity of 0.53 mol g^{-1} h^{-1}.

Table 3. Comparison of the photocatalytic activities of the synthesized catalysts and others from similar studies used in water splitting.

Photocatalyst	**Reactant & sacrificial agents**	**Light source**	**Activity**	**Ref.**
SiFe co doped TiO_2	540 ml distilled H_2O, 60 ml ethanol	500 W	320 μmol g^{-1} h^{-1}	[74]
GaN:ZnO (Mn_3O_4.Rh/Cr_2O_3	Distilled H_2O NaI	450 W **(**Xe lamp)	20 μmol g^{-1} h^{-1}	[74]
20%_TiO_2/CNFs	Distilled H_2O	450 W **(**Xe lamp)	0.00720 **(**mol g^{-1} h^{-1})	Current work
TiO_2	Distilled H_2O 10% methanol	300 W	42.00 μmol g^{-1} h^{-1}	[74][75]
10%_TiO_2/CNFs/5%Zn	Distilled H_2O	450 W **(**Xe lamp)	0.53 **(**mol g^{-1} h^{-1})	Current work
20%_TiO_2/CNFs/6%Zn	Distilled H_2O	450 W **(**Xe lamp)	0.43 **(**mol g^{-1} h^{-1})	Current work
10%_TiO_2/CNFs/6%Zn	Distilled H_2O	450 W **(**Xe lamp)	0.42 **(**mol g^{-1} h^{-1})	Current work
20%_TiO_2/CNFs/5%Zn	Distilled H_2O	450 W **(**Xe lamp)	0.37 **(**mol g^{-1} h^{-1})	Current work
20%_TiO_2/CNFs/5%Cu	Distilled H_2O	450 W **(**Xe lamp)	0.32 **(**mol g^{-1} h^{-1})	Current work
TiO_2 – P25	Distilled H_2O	450 W **(**Xe lamp)	1.26 (10^{-4}) **(**mol g^{-1} h^{-1})	Current work
TiO_2 - anatase	Distilled H_2O	450 W **(**Xe lamp)	1.19 (10^{-4}) **(**mol g^{-1} h^{-1})	Current work

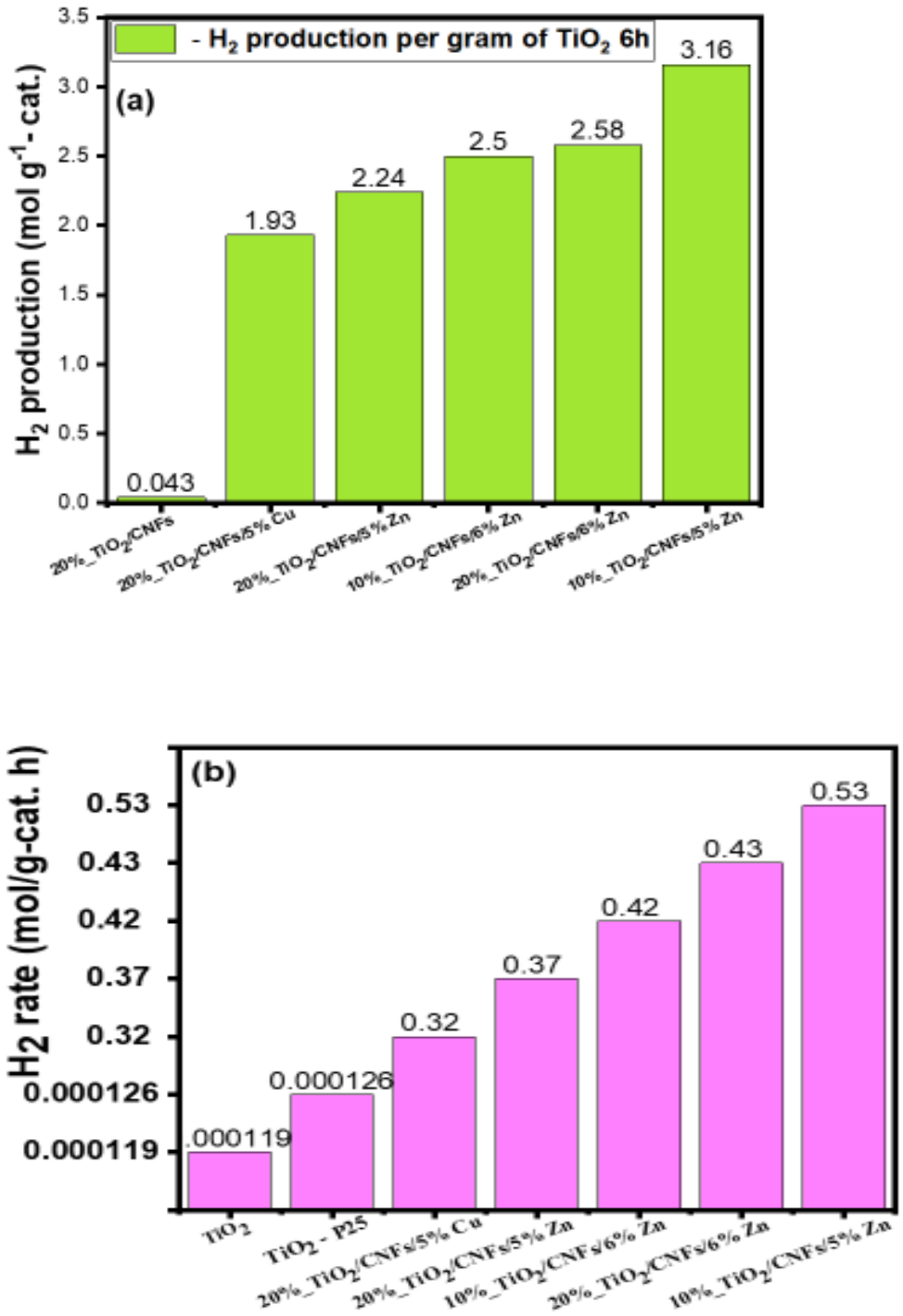

Fig. 14. **(a)** The H_2 produced during the process (moles-6 h 1 g) **(b)** The activity of the photocatalysts: TiO_2, TiO_2 – P25, 20%_TiO_2/CNFs/5% Cu, 20%_TiO_2/CNFs/5% Zn, 10%_TiO_2/CNFs/6% Zn, 20%_TiO_2/CNFs/6% Zn, and 10%_TiO_2/CNFs/5% Zn.

It generated H_2 more than 100 times as compared to the commercial photocatalyst P25 (TiO_2) and the as-synthesized TiO_2 (pure TiO_2) catalysts, Fig. 14 (a). It was followed by

20%_TiO_2/CNFs/6% Zn, 10%_TiO_2/CNFs/6% Zn, 20%_TiO_2/CNFs/5% Zn and 20%_TiO_2/CNFs/5%Cu with activities of 0.43, 0.42, 0.37, and 0.32 mol g^{-1} h^{-1} respectively (Table 3, Fig. 14).

Additionally, the results were compared with the results obtained from similar studies as indicated in Table 3 and it was realized that the results of this study were better than what had been previously reported.

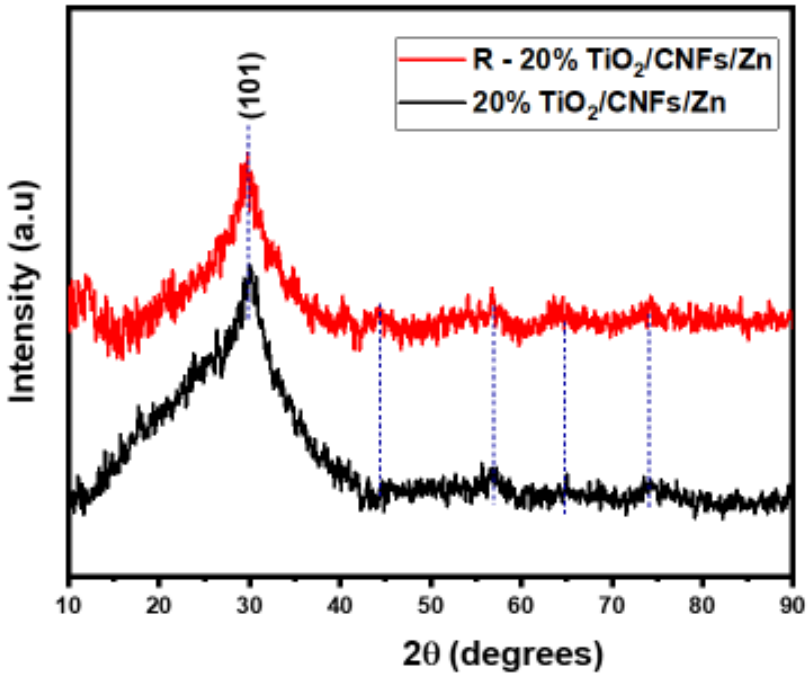

Fig. 15. Effect of stability of the photocatalyst, 20% TiO_2/CNFs/6% Zn, and R - 20% TiO_2/CNFs/ 6%/ Zn, XRD spectra.

The most active photocatalyst, had TiO_2 loading of 20% by weight, optimally embedded on the surface of CNFs as evidenced by the FESEM analysis Fig. 5(d) and (g) and TEM image

in Fig. 6(e). Furthermore, the photocatalyst was tested in a reaction for 6 h, and showed no signs of deactivation but enhanced H_2 production, Fig. 14.

The enhancement observed for TiO_2 – carbon composites compared to pure TiO_2 (TiO_2 – anatase and TiO_2 – P25) is attributed to an increase in the surface area and delay/ elimination of the electron – hole recombination[76][77]. Indications by Leary and Westwood of studies conducted by others comparing TiO_2 – carbon composites catalysts to a pure TiO_2 photocatalyst under the same experimental conditions such as mass[76] as in this study, Table 3.

It has been realized that several similar studies have been conducted [78]–[81]. However, comparing results has been a challenge as factors such as the TiO_2 content, the organic or inorganic sacrificial agents used and their concentrations, the type and intensity of radiation used among others are the hindrance[82]–[84]. Consequently, its perhaps more convenient to compare the results obtained together with the experimental conditions and also incorporate a standard catalyst, such as TiO_2 – P25, as a reference[85]. In this study, hydrogen production with 10% TiO_2/CNFs – 5% Zn was more than 100 times greater than the commercial TiO_2 (P25) measured in per gram of catalyst and per hour.

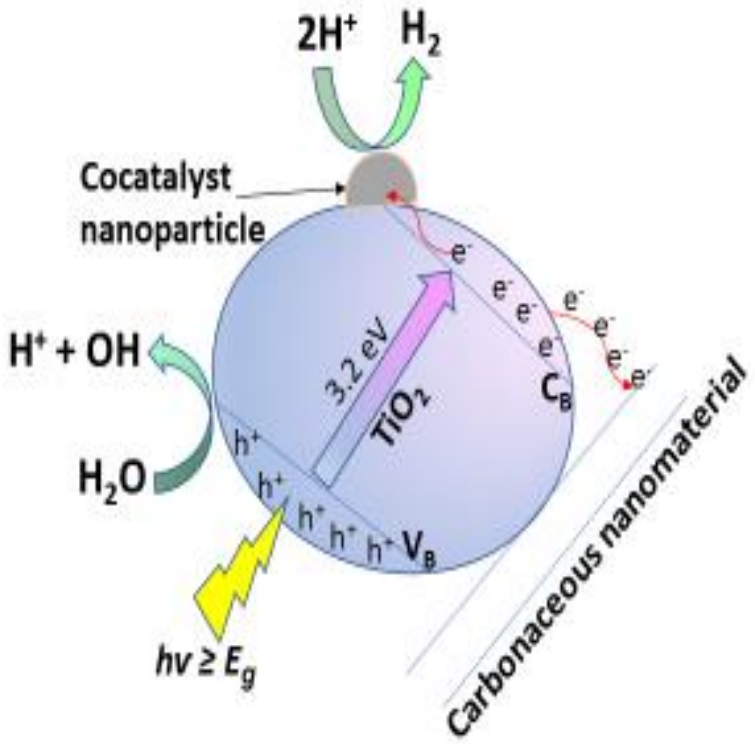

Fig. 16. Photocatalytic mechanism for photocatalytic hydrogen production from water using metal- TiO_2/CNFs photocatalyst.

Furthermore, hydrogen produced by as-synthesized TiO_2 – anatase and commercial TiO_2 are nearly the same, Fig. 14 (b). These results and the comparisons evidence the importance of incorporating appropriate controls in the synthesis and photocatalysis. Fig. 15 is the PXRD spectra of the photocatalyst, 20% TiO_2/CNFs/6% Zn, prior to photocatalysis and after recovery processes. The spectra show that there is no sintering or dispersion of the photocatalysts during the water splitting process and therefore the photocatalysts can be used for longer hours more than 6 h and later recovered by filtration and re-used. The recovery of the photocatalyst was above 95%.

The proposed mechanism of this work is presented in Fig. 16. The proposed mechanism is not exclusive to this study. Similar proposals have been suggested in various other reports[24], [33], [47].

6.4 Conclusions

Cu, Zn – TiO_2/CNFs nanostructures were efficiently synthesized and investigated for H_2 production from water using UV – light irradiations. The assembly of the photocatalysts significantly advanced the H_2 production rate and the greatest production of H_2 of 0.53 mol (h g cat.)$^{-1}$ was achieved using 10%_TiO_2/CNFs/5%Zn, 90-100 folds greater than using commercial TiO_2 - P25, and pure TiO_2 photocatalysts.

All the samples including, 10%TiO_2/CNFs, 20% TiO_2/CNFs, 20% TiO_2/CNFs – non precious metals composites were tested for stability by longer performances of over 6 h of irradiation period and XRD and found to efficiently improve the photocatalytic evolution of H_2 using UV – light irradiation beyond 6 h. The compositing of CNFs with titania increased the BET surface area of the TiO_2 from 73 m^2g^{-1} to 126 m^2g^{-1} 20% TiO_2/CNFs. Further, the BET surface area generally increased with the non – precious metal addition whereby the 20% TiO_2/CNFs – 6% Cu composite had the highest surface area of 297 m^2g^{-1}. The pore volume of the composites also increased in this order while the pore diameter of the composites decreased. This suggests that the non - precious metals and CNFs can efficiently modify the structure of TiO_2 for higher surface area, larger pore volume, and smaller pore diameters thus increasing the photocatalytic properties of the TiO_2/C – non - precious metal photocatalysts. Raman, FTIR, FESEM characterization techniques show a very homogeneous distribution of TiO_2 nanoparticles on the CNFs. The XPS analysis confirmed the presence of all the elements as Ti, O, C, N, F, Cl, Zn and Cu and their respective chemical states. This was important for understanding the mechanism of water splitting with particular interest on Ti, O, C and the

cocatalysts (Zn and Cu) as their quantities, chemical states, and morphology play important roles in water splitting processes. In all the carbon containing samples, there was a shift of light absorption to the visible range (TiO_2 – 3.20 eV to 1.67 eV - 20% _TiO_2/CNFs/6% Zn). Basically, Cu, Zn - TiO_2/CNFs has significant prospects because of its considerable stability and high photocatalytic activity for water splitting.

Acknowledgement

We are thankful to the University of the Witwatersrand for the support. We acknowledge Prof Rudolph Erasmus of the University of the Witwatersrand for the assistance with Raman, UV – Vis and Photoluminescence analyses.

Conflicts of interest

There are no conflicts of interest to be declared by the authors.

APPENDIX A. SUPPLEMENTARY MATERIAL

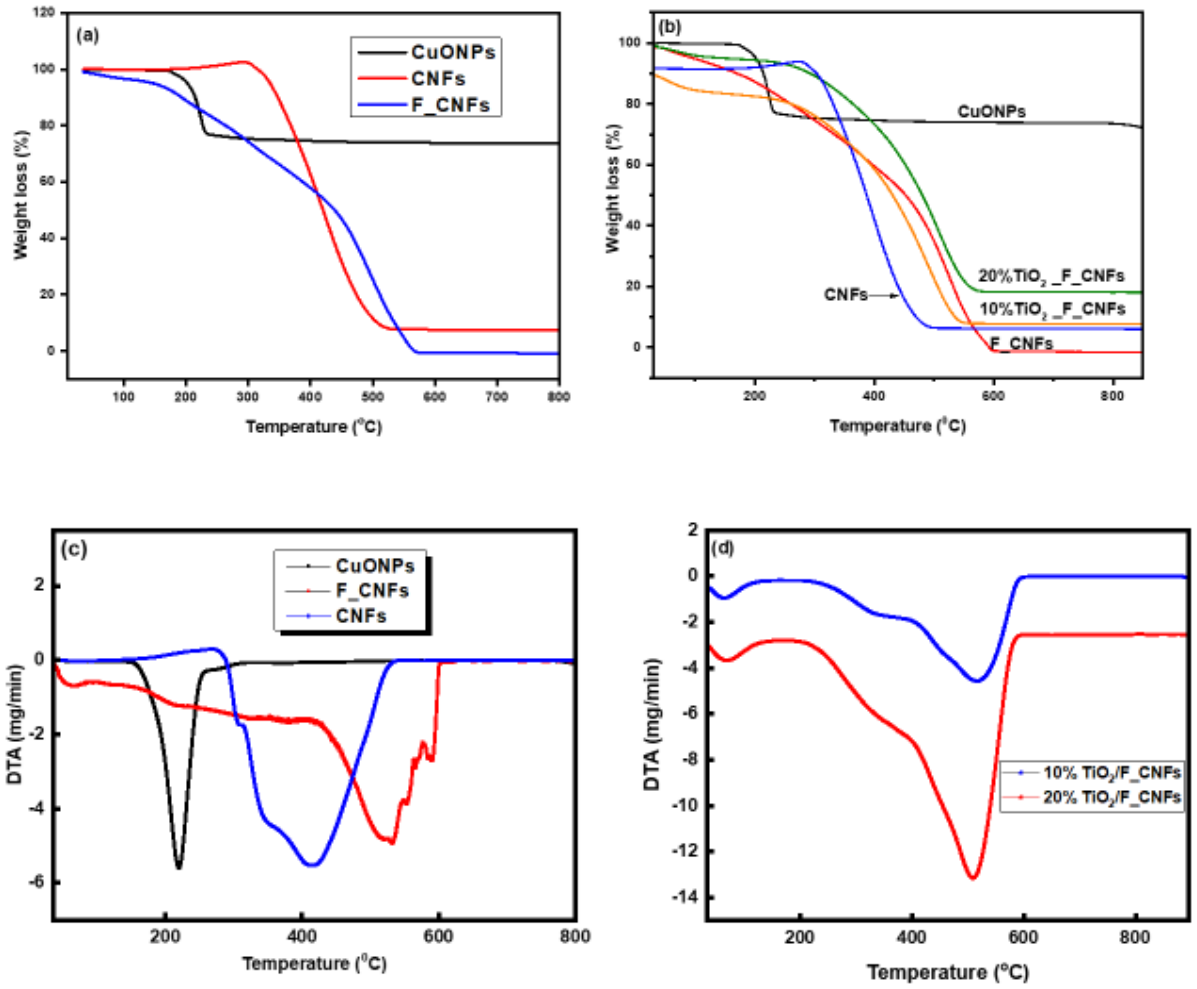

Fig. 17. The Thermogravimetric Analysis (TGA) and the Differential Thermal Analysis (DTA) thermograms: (a) as-synthesized CuO Nanoparticles, CNFs and functionalized CNFs (b) synthesized materials and the TiO_2/CNFs composites (c) DTA of CuONPs, CNFs and F_CNFs (d) DTA of TiO_2/CNFs composites.

XPS data

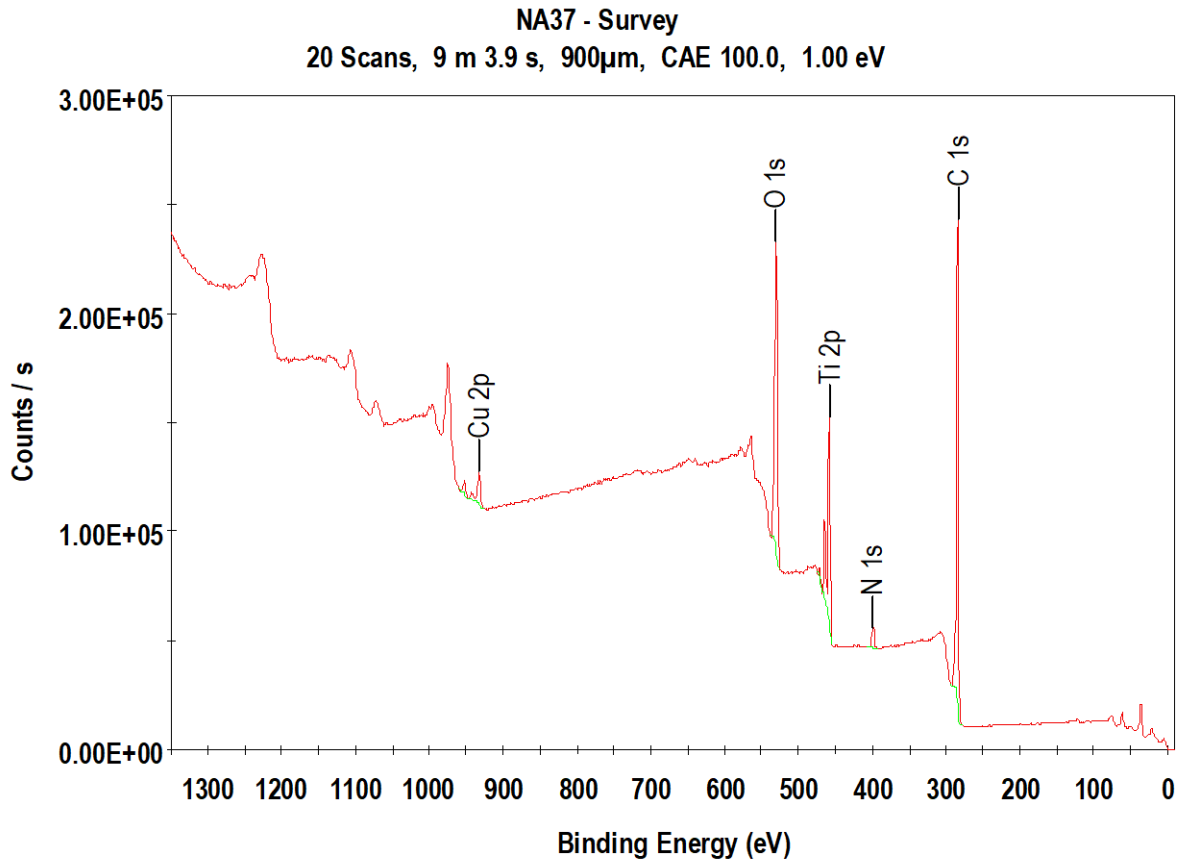

NA37

Elemental ID and Quantification

Name	*Peak BE*	*Atomic %*
C 1s	284.2	68.7
O 1s	530.4	22.8
Ti 2p	458.1	5.8
N 1s	399.0	2.1
Cu 2p	932.7	0.6

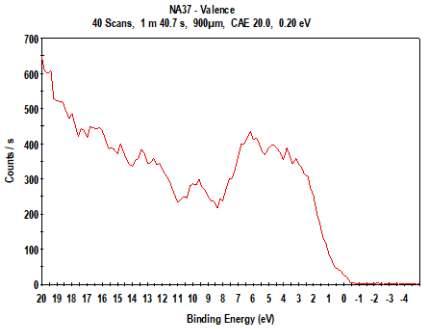

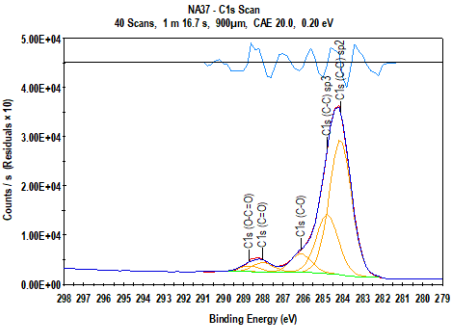

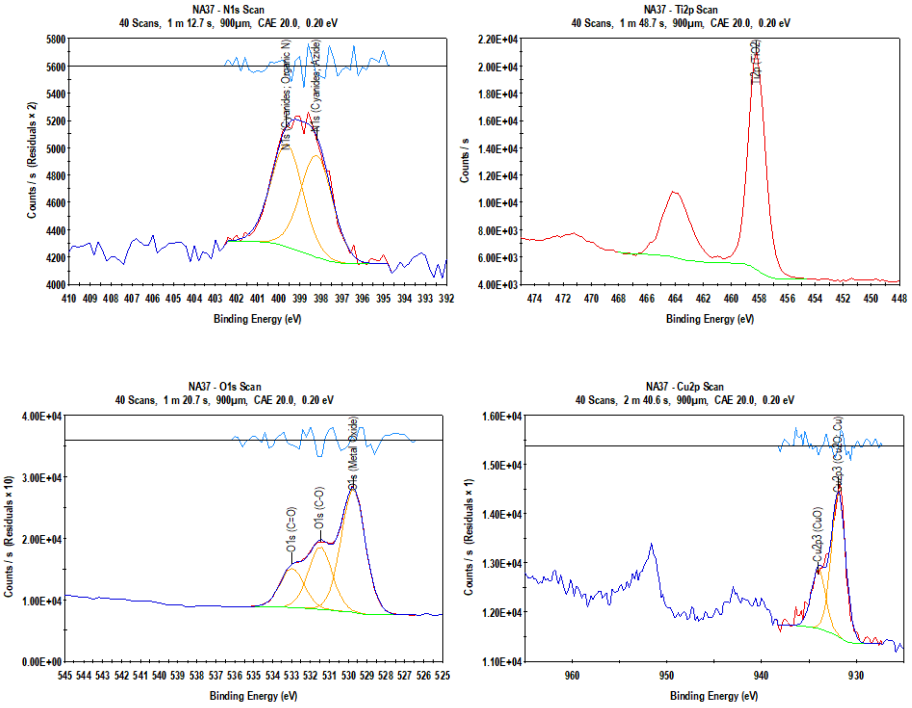
NA37 - N1s Scan
40 Scans, 1 m 12.7 s, 900µm, CAE 20.0, 0.20 eV
Counts / s (Residuals x 2)
Binding Energy (eV)
N1s (Cyanides - Organic N)
N1s (Cyanides - N2Ge)
NA37 - Ti2p Scan
40 Scans, 1 m 48.7 s, 900µm, CAE 20.0, 0.20 eV
Counts / s
Binding Energy (eV)
Ti2p (TiO2)
NA37 - O1s Scan
40 Scans, 1 m 20.7 s, 900µm, CAE 20.0, 0.20 eV
Counts / s (Residuals x 10)
Binding Energy (eV)
O1s (C=O)
O1s (C-O)
O1s (Metal Oxide)
NA37 - Cu2p Scan
40 Scans, 2 m 40.6 s, 900µm, CAE 20.0, 0.20 eV
Counts / s (Residuals x 1)
Binding Energy (eV)
Cu2p3 (CuO)

NA37

Chemical ID and Quantification

Name	*Peak BE*	*FWHM eV*	*Atomic %*
C1s (C-C) sp2	284.1	1.3	40.6
C1s (C-C) sp3	284.8	1.3	17.7
C1s (C-O)	286.1	1.2	5.4
C1s (C=O)	288.0	1.2	2.8
C1s (O-C=O)	288.7	1.2	1.8
N1s (Cyanides; Azide)	398.2	1.8	0.9
N1s (Cyanides; Organic N)	399.6	1.8	0.9
Ti2p (TiO2)	458.2	1.4	6.2
O1s (Metal Oxide)	529.7	1.5	12.7
O1s (C-O)	531.5	1.5	6.4
O1s (C=O)	533.0	1.5	4.0
Cu2p3 (Cu2O; Cu)	931.9	1.7	0.4
Cu2p3 (CuO)	934.0	1.7	0.2

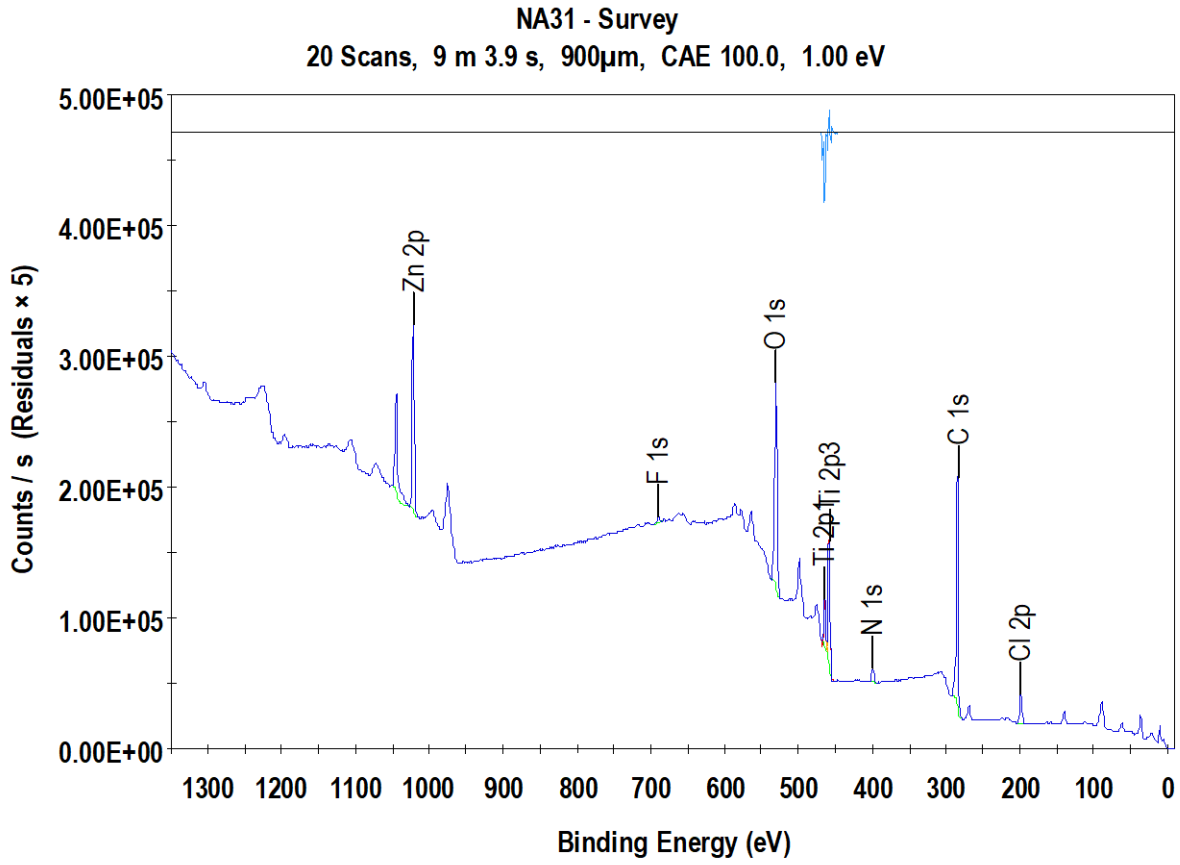

NA31

Elemental ID and Quantification

Name	*Peak BE*	*Atomic %*
C 1s	284.4	59.5
O 1s	530.7	24.5
Ti 2p3	458.4	6.6
Zn 2p	1022.1	4.0
Cl 2p	198.8	2.7
N 1s	399.2	2.3
F 1s	689.0	0.4

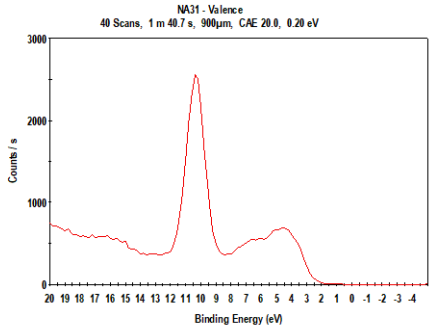
NA31 - Valence
40 Scans, 1 m 40.7 s, 900µm, CAE 20.0, 0.20 eV
Counts / s
Binding Energy (eV)

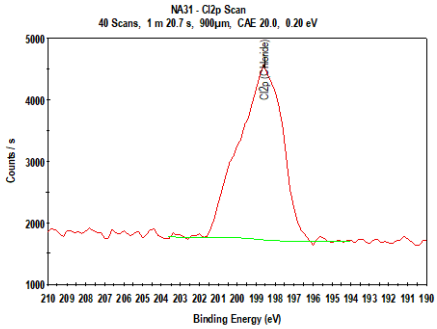
NA31 - Cl2p Scan
40 Scans, 1 m 20.7 s, 900µm, CAE 20.0, 0.20 eV
Cl2p (Chloride)
Counts / s
Binding Energy (eV)

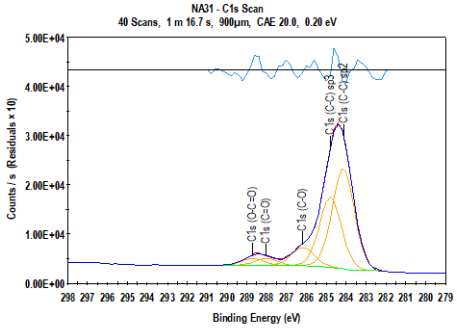
NA31 - C1s Scan
40 Scans, 1 m 16.7 s, 900µm, CAE 20.0, 0.20 eV
C1s (C-C) sp3
C1s (C-C) sp2
C1s (C=O)
C1s (O-C=O)
C1s (C-O)
Counts / s (Residuals x 10)
Binding Energy (eV)

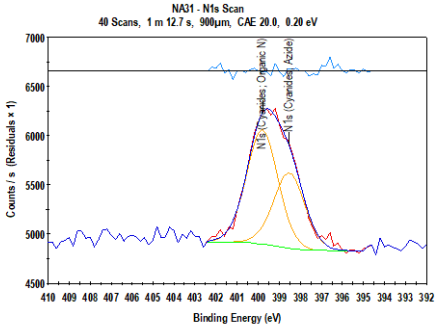
NA31 - N1s Scan
40 Scans, 1 m 12.7 s, 900µm, CAE 20.0, 0.20 eV
N1s (Cyanides, Organic N)
N1s (Cyanides, Azide)
Counts / s (Residuals x 1)
Binding Energy (eV)

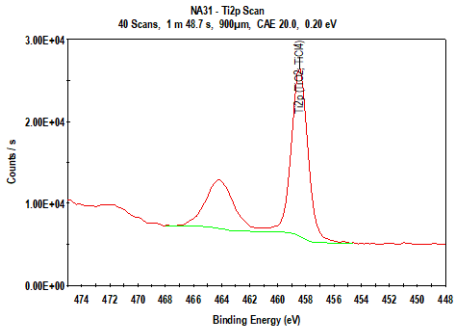
NA31 - Ti2p Scan
40 Scans, 1 m 48.7 s, 900µm, CAE 20.0, 0.20 eV
Ti2p (TiO2 - TiO4)
Counts / s
Binding Energy (eV)

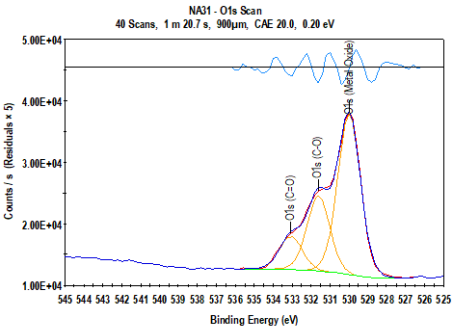
NA31 - O1s Scan
40 Scans, 1 m 20.7 s, 900µm, CAE 20.0, 0.20 eV
O1s (Metal Oxide)
O1s (C-O)
O1s (C=O)
Counts / s (Residuals x 5)
Binding Energy (eV)

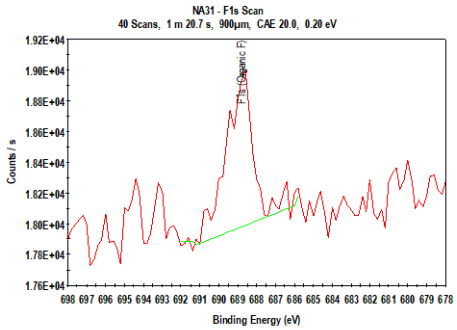
NA31 - F1s Scan
40 Scans, 1 m 20.7 s, 900µm, CAE 20.0, 0.20 eV
F1s (Organic F)
Counts / s
Binding Energy (eV)

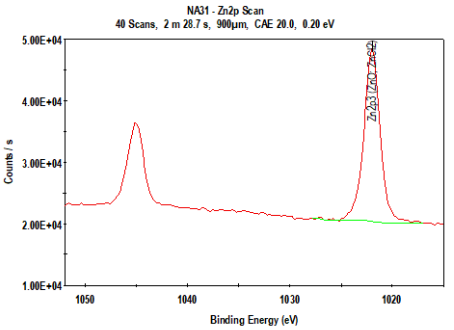
NA31 - Zn2p Scan
40 Scans, 2 m 28.7 s, 900µm, CAE 20.0, 0.20 eV
Zn2p3 (ZnO, ZnAl2)
Counts / s
Binding Energy (eV)

NA31

Chemical ID and Quantification

Name	*Peak BE*	*FWHM eV*	*Atomic %*
Cl2p (Chloride)	198.5	2.7	2.8
C1s (C-C) sp2	284.1	1.3	28.9
C1s (C-C) sp3	284.8	1.3	20.2
C1s (C-O)	286.2	1.3	5.6
C1s (C=O)	288.0	1.3	2.1
C1s (O-C=O)	288.7	1.3	2.1
N1s (Cyanides; Azide)	398.5	1.7	0.9
N1s (Cyanides; Organic N)	399.8	1.7	1.4
Ti2p (TiO2; TiCl4)	458.4	1.2	7.1
O1s (Metal Oxide)	530.0	1.4	15.0
O1s (C-O)	531.6	1.4	7.0
O1s (C=O)	533.1	1.4	3.1
F1s (Organic F)	688.7	1.4	0.5
Zn2p3 (ZnO; ZnCl2)	1022.0	1.6	3.5

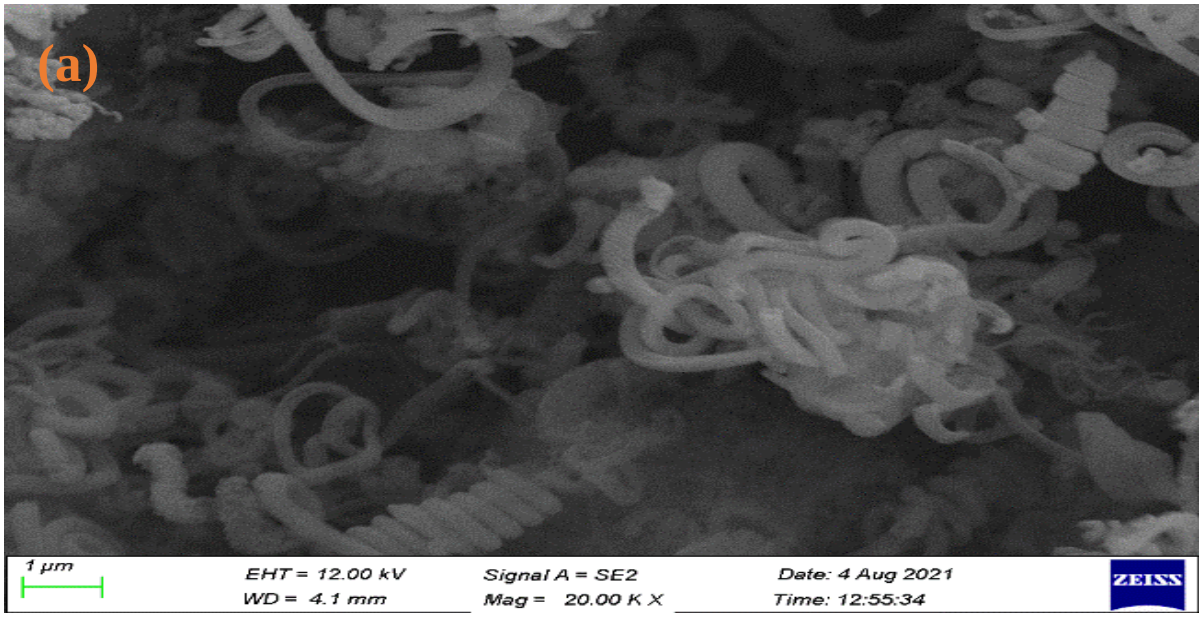
(a)
1 µm
EHT = 12.00 kV
WD = 4.1 mm
Signal A = SE2
Mag = 20.00 K X
Date: 4 Aug 2021
Time: 12:55:34
ZEISS

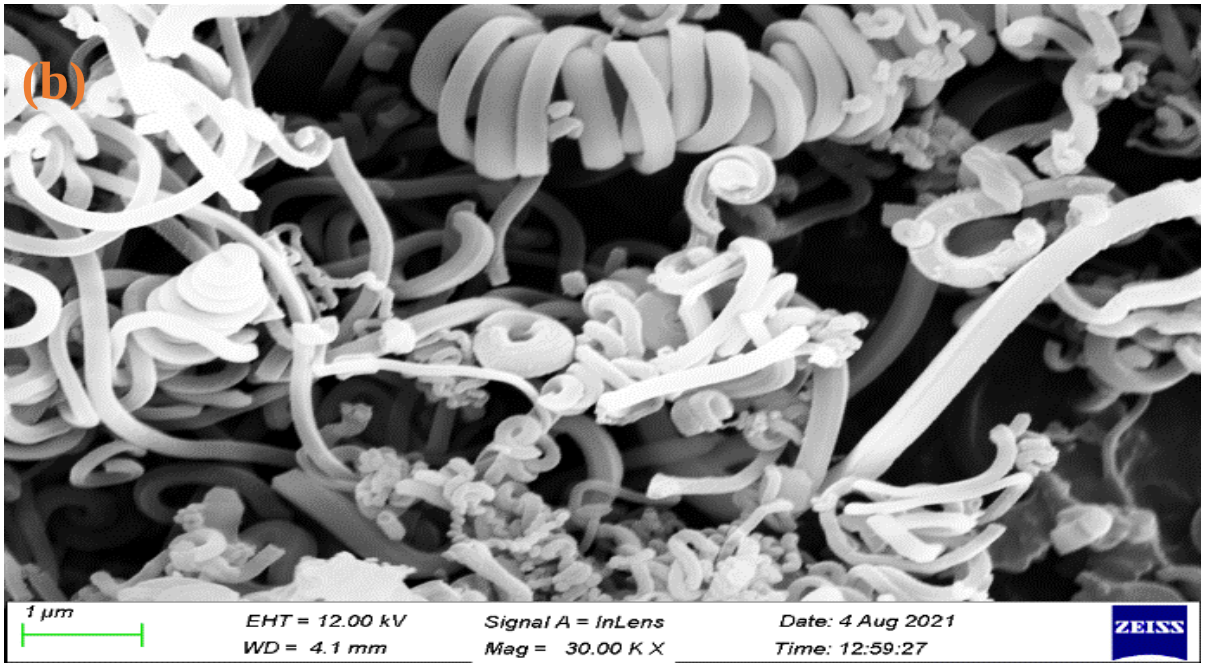
(b)
1 µm
EHT = 12.00 kV
WD = 4.1 mm
Signal A = InLens
Mag = 30.00 K X
Date: 4 Aug 2021
Time: 12:59:27
ZEISS

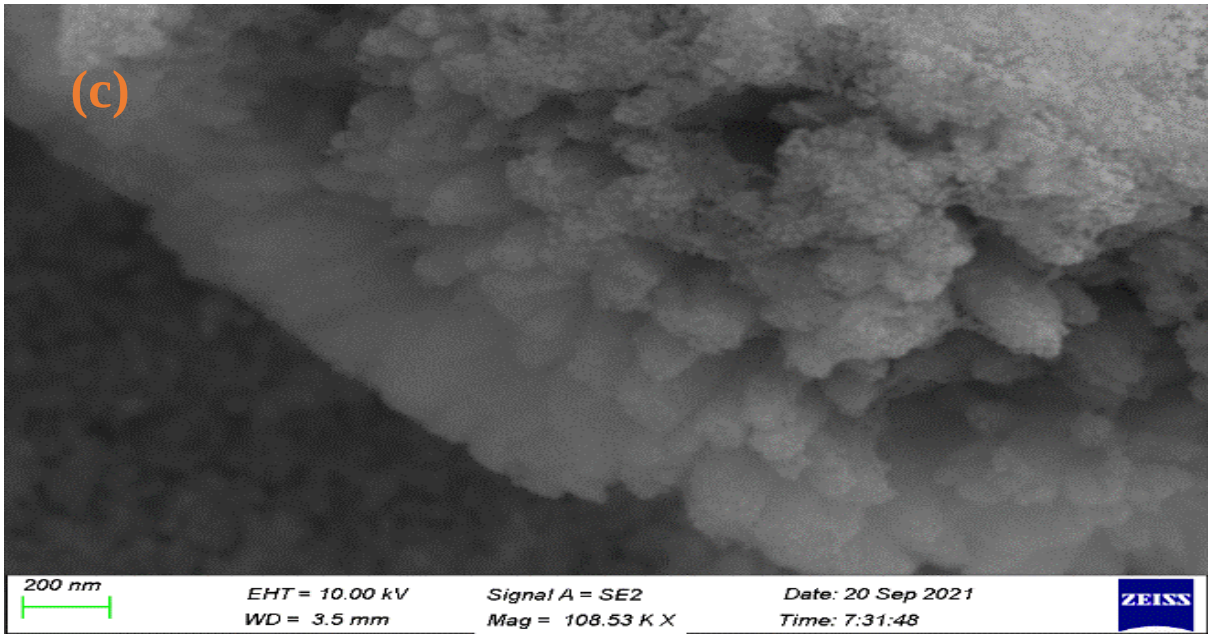
(c)
200 nm
EHT = 10.00 kV
WD = 3.5 mm
Signal A = SE2
Mag = 108.53 K X
Date: 20 Sep 2021
Time: 7:31:48
ZEISS

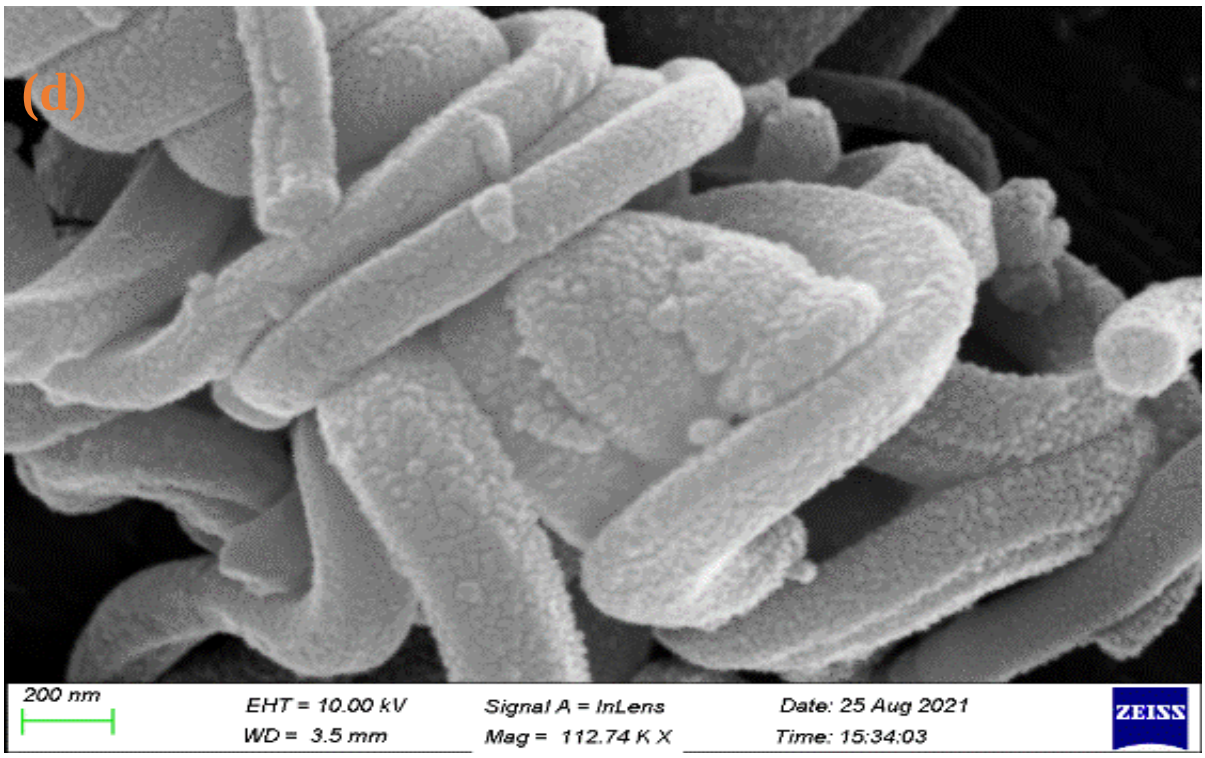
(d)
200 nm
EHT = 10.00 kV
WD = 3.5 mm
Signal A = InLens
Mag = 112.74 K X
Date: 25 Aug 2021
Time: 15:34:03
ZEISS

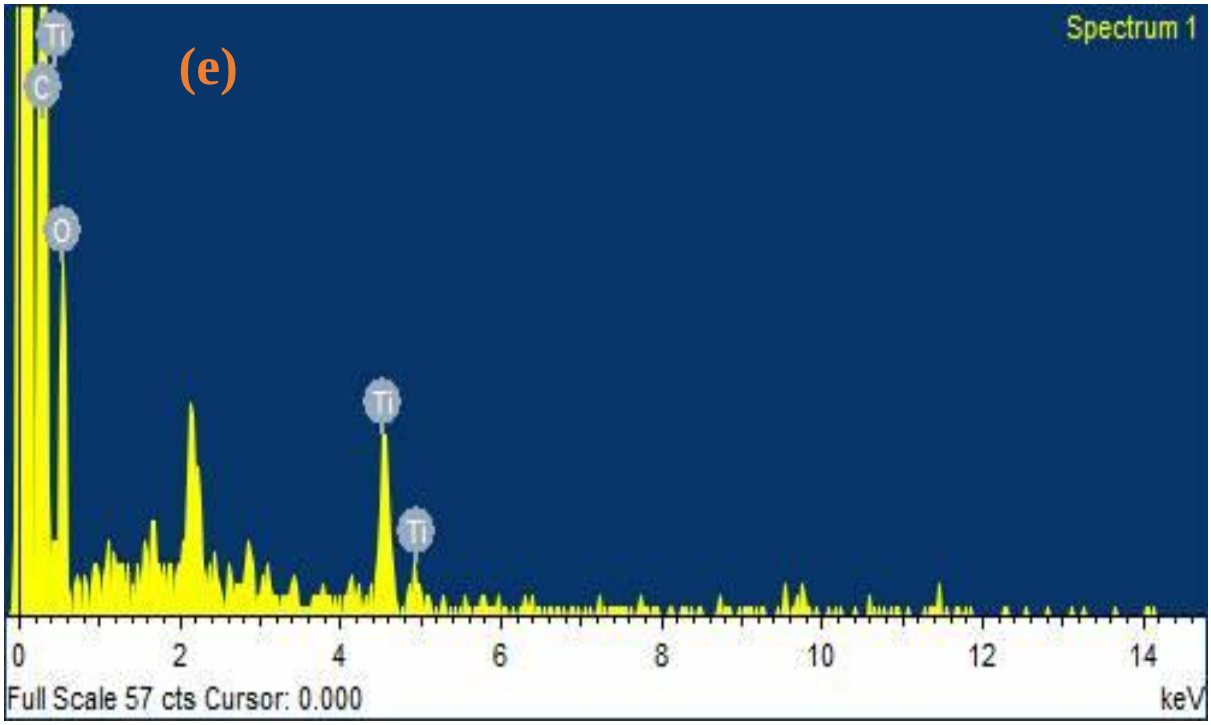

Fig. 6. SEM analysis of (a) as-synthesized CNFs (b) Purified CNFs (c) TiO_2 – A (d) 20% TiO_2/CNFs composite (e) EDXss spectrum of 20% TiO_2/CNFs .

References

[1] L. Liu, D. Hong, N. Wang, and X. Guo, "High purity H2 production from sorption enhanced bio-ethanol reforming via sol-gel-derived Ni–CaO–Al2O3 bi-functional materials," *Int. J. Hydrogen Energy*, vol. 45, no. 59, pp. 34449–34460, 2020, doi: 10.1016/j.ijhydene.2020.02.158.

[2] C. Zou, Q. Zhao, G. Zhang, and B. Xiong, "Energy revolution: From a fossil energy era to a new energy era," *Nat. Gas Ind. B*, vol. 3, no. 1, pp. 1–11, 2016, doi: 10.1016/j.ngib.2016.02.001.

[3] J. G. Wang, L. Y. Yang, H. Liu, and C. Y. Li, "Intrinsic kinetics of methane steam reforming over a Ni/α-Al2O3 catalyst," *Beijing Huagong Daxue Xuebao (Ziran Kexueban)/Journal Beijing Univ. Chem. Technol. (Natural Sci. Ed.*, vol. 32, no. 1, pp. 10–15, 2005.

[4] T. Chen *et al.*, "Room temperature synthesized BaTiO3 for photocatalytic hydrogen evolution," *J. Alloys Compd.*, vol. 754, pp. 184–189, 2018, doi: 10.1016/j.jallcom.2018.04.300.

[5] Y. Liu, Z. Sun, and Y. H. Hu, "Bimetallic cocatalysts for photocatalytic hydrogen production from water," *Chem. Eng. J.*, vol. 409, no. December 2020, p. 128250, 2021, doi: 10.1016/j.cej.2020.128250.

[6] M. A. Aziz Aljar, M. Zulqarnain, A. Shah, M. S. Akhter, and F. J. Iftikhar, "A review of renewable energy generation using modified titania for photocatalytic water splitting," *AIP Adv.*, vol. 10, no. 7, 2020, doi: 10.1063/5.0006196.

[7] W. Mulewa, M. Tahir, and N. A. S. Amin, "MMT-supported Ni/TiO2 nanocomposite for low temperature ethanol steam reforming toward hydrogen production," *Chem.*

Eng. J., vol. 326, pp. 956–969, 2017, doi: 10.1016/j.cej.2017.06.012.

[8] M. Tahir, W. Mulewa, N. A. S. Amin, and Z. Y. Zakaria, "Thermodynamic and experimental analysis on ethanol steam reforming for hydrogen production over Ni-modified TiO2/MMT nanoclay catalyst," *Energy Convers. Manag.*, vol. 154, no. November, pp. 25–37, 2017, doi: 10.1016/j.enconman.2017.10.042.

[9] J. Yang, D. Wang, H. Han, and C. Li, "Roles of cocatalysts in photocatalysis and photoelectrocatalysis," *Acc. Chem. Res.*, vol. 46, no. 8, pp. 1900–1909, 2013, doi: 10.1021/ar300227e.

[10] M. T. Uddin *et al.*, "Band alignment investigations of heterostructure NiO/TiO2 nanomaterials used as efficient heterojunction earth-abundant metal oxide photocatalysts for hydrogen production," *Phys. Chem. Chem. Phys.*, vol. 19, no. 29, pp. 19279–19288, 2017, doi: 10.1039/c7cp01300k.

[11] W. T. Chen, A. Chan, D. Sun-Waterhouse, J. Llorca, H. Idriss, and G. I. N. Waterhouse, "Performance comparison of Ni/TiO2 and Au/TiO2 photocatalysts for H2 production in different alcohol-water mixtures," *J. Catal.*, vol. 367, pp. 27–42, 2018, doi: 10.1016/j.jcat.2018.08.015.

[12] X. Chen, J. Xiong, J. Shi, S. Xia, S. Gui, and W. Shangguan, "Roles of various Ni species on TiO2 in enhancing photocatalytic H2 evolution," *Front. Energy*, vol. 13, no. 4, pp. 684–690, 2019, doi: 10.1007/s11708-018-0585-8.

[13] P. Bhavani, D. Praveen Kumar, M. Hussain, W. H. Chen, S. S. Lam, and Y. K. Park, "Surface ligand functionalized Few-layered MoSe2 nanosheets decorated CdS nanorods for spectacular rate of H2 production," *Fuel*, vol. 334, no. P1, p. 126551, 2023, doi: 10.1016/j.fuel.2022.126551.

[14] P. Bhavani, M. Hussain, and Y. K. Park, “Recent advancements on the sustainable biochar based semiconducting materials for photocatalytic applications: A state of the art review,” *J. Clean. Prod.*, vol. 330, no. August 2021, p. 129899, 2022, doi: 10.1016/j.jclepro.2021.129899.

[15] T. Gong, J. Zhang, Y. Liu, L. Hou, J. Deng, and C. Yuan, “Construction of hetero-phase Mo2C-CoO@N-CNFs film as a self-supported Bi-functional catalyst towards overall water splitting,” *Chem. Eng. J.*, vol. 451, no. P4, p. 139025, 2023, doi: 10.1016/j.cej.2022.139025.

[16] M. Alijani and N. N. Ilkhechi, “Effect of Ni Doping on the Structural and Optical Properties of TiO2 Nanoparticles at Various Concentration and Temperature,” *Silicon*, vol. 10, no. 6, pp. 2569–2575, 2018, doi: 10.1007/s12633-018-9792-5.

[17] D. Xu, L. Li, R. He, L. Qi, L. Zhang, and B. Cheng, “Noble metal-free RGO/TiO 2 composite nanofiber with enhanced photocatalytic H 2 -production performance,” *Appl. Surf. Sci.*, vol. 434, pp. 620–625, 2018, doi: 10.1016/j.apsusc.2017.10.192.

[18] H. Y. Hafeez, S. K. Lakhera, P. Karthik, M. Anpo, and B. Neppolian, “Facile construction of ternary CuFe 2 O 4 -TiO 2 nanocomposite supported reduced graphene oxide (rGO) photocatalysts for the efficient hydrogen production,” *Appl. Surf. Sci.*, vol. 449, pp. 772–779, 2018, doi: 10.1016/j.apsusc.2018.01.282.

[19] X. Li *et al.*, “Fabrication of TiO2/porous carbon nanofibers with superior visible photocatalytic activity,” *New J. Chem.*, vol. 39, no. 10, pp. 7863–7872, 2015, doi: 10.1039/c5nj01189b.

[20] Y. Lian *et al.*, “A biomass carbon mass coated with modified TiO2 nanotube/graphene for photocatalysis,” *New J. Chem.*, vol. 41, no. 10, pp. 4212–4219, 2017, doi: 10.1039/c6nj04005e.

[21] J. Yu, T. Ma, and S. Liu, “Enhanced photocatalytic activity of mesoporous TiO2 aggregates by embedding carbon nanotubes as electron-transfer channel,” *Phys. Chem. Chem. Phys.*, vol. 13, no. 8, pp. 3491–3501, 2011, doi: 10.1039/c0cp01139h.

[22] D. Hazarika and N. Karak, “Photocatalytic degradation of organic contaminants under solar light using carbon dot/titanium dioxide nanohybrid, obtained through a facile approach,” *Appl. Surf. Sci.*, vol. 376, pp. 276–285, 2016, doi: 10.1016/j.apsusc.2016.03.165.

[23] K. Woan, G. Pyrgiotakis, and W. Sigmund, “Photocatalytic carbon-nanotube-Ti02 composites,” *Adv. Mater.*, vol. 21, no. 21, pp. 2233–2239, 2009, doi: 10.1002/adma.200802738.

[24] W. Wang, D. Xu, B. Cheng, J. Yu, and C. Jiang, “Hybrid carbon@TiO2 hollow spheres with enhanced photocatalytic CO2 reduction activity,” *J. Mater. Chem. A*, vol. 5, no. 10, pp. 5020–5029, 2017, doi: 10.1039/c6ta11121a.

[25] W. Zhang, J. R. Yin, X. Q. Tang, P. Zhang, and Y. H. Ding, “Density functional theory studies on the structural and physical properties of Cu-doped anatase TiO2(101) surface,” *Phys. E Low-Dimensional Syst. Nanostructures*, vol. 85, pp. 259–263, 2017, doi: 10.1016/j.physe.2016.09.008.

[26] Y. Moriya, T. Takata, and K. Domen, “Recent progress in the development of (oxy)nitride photocatalysts for water splitting under visible-light irradiation,” *Coord. Chem. Rev.*, vol. 257, no. 13–14, pp. 1957–1969, 2013, doi: 10.1016/j.ccr.2013.01.021.

[27] K. Maeda, “Photocatalytic water splitting using semiconductor particles: History and recent developments,” *J. Photochem. Photobiol. C Photochem. Rev.*, vol. 12, no. 4, pp. 237–268, 2011, doi: 10.1016/j.jphotochemrev.2011.07.001.

[28] K. Maeda and K. Domen, “Photocatalytic water splitting: Recent progress and future challenges,” *J. Phys. Chem. Lett.*, vol. 1, no. 18, pp. 2655–2661, 2010, doi: 10.1021/jz1007966.

[29] K. Maeda and K. Domen, “Chapter 12 Nano-particulate photocatalysts for overall water splitting under visible light,” *Theor. Comput. Chem.*, vol. 18, pp. 301–315, 2007, doi: 10.1016/S1380-7323(06)80014-2.

[30] J. S. Jang, H. G. Kim, and J. S. Lee, “Heterojunction semiconductors: A strategy to develop efficient photocatalytic materials for visible light water splitting,” *Catal. Today*, vol. 185, no. 1, pp. 270–277, 2012, doi: 10.1016/j.cattod.2011.07.008.

[31] S. D. Mhlanga and N. J. Coville, “Iron-cobalt catalysts synthesized by a reverse micelle impregnation method for controlled growth of carbon nanotubes,” *Diam. Relat. Mater.*, vol. 17, no. 7–10, pp. 1489–1493, 2008, doi: 10.1016/j.diamond.2008.01.049.

[32] Y. Yan, J. Lu, C. Deng, and X. Zhang, “Facile synthesis of titania nanoparticles coated carbon nanotubes for selective enrichment of phosphopeptides for mass spectrometry analysis,” *Talanta*, vol. 107, pp. 30–35, 2013, doi: 10.1016/j.talanta.2012.12.026.

[33] S. B. A. Hamid, T. L. Tan, C. W. Lai, and E. M. Samsudin, “Multiwalled carbon nanotube/TiO2 nanocomposite as a highly active photocatalyst for photodegradation of Reactive Black 5 dye,” *Cuihua Xuebao/Chinese J. Catal.*, vol. 35, no. 12, pp. 2014–2019, 2014, doi: 10.1016/S1872-2067(14)60210-2.

[34] J. Restivo, O. S. G. P. Soares, J. J. M. Órfão, and M. F. R. Pereira, “Metal assessment for the catalytic reduction of bromate in water under hydrogen,” *Chem. Eng. J.*, vol. 263, pp. 119–126, 2015, doi: 10.1016/j.cej.2014.11.052.

[35] O. S. G. P. Soares, P. S. F. Ramalho, A. Fernandes, J. J. M. Órfão, and M. F. R. Pereira, "Catalytic bromate reduction in water: Influence of carbon support," *J. Environ. Chem. Eng.*, vol. 7, no. 3, p. 103015, 2019, doi: 10.1016/j.jece.2019.103015.

[36] O. S. G. P. Soares, J. J. M. Órfão, and M. F. R. Pereira, "Nitrate reduction with hydrogen in the presence of physical mixtures with mono and bimetallic catalysts and ions in solution," *Appl. Catal. B Environ.*, vol. 102, no. 3–4, pp. 424–432, 2011, doi: 10.1016/j.apcatb.2010.12.017.

[37] O. S. G. P. Soares, J. J. M. Órfão, J. Ruiz-Martínez, J. Silvestre-Albero, A. Sepúlveda-Escribano, and M. F. R. Pereira, "Pd-Cu/AC and Pt-Cu/AC catalysts for nitrate reduction with hydrogen: Influence of calcination and reduction temperatures," *Chem. Eng. J.*, vol. 165, no. 1, pp. 78–88, 2010, doi: 10.1016/j.cej.2010.08.065.

[38] J. M. Walls, J. S. Sagu, and K. G. Upul Wijayantha, "Microwave synthesised Pd-TiO 2 for photocatalytic ammonia production," *RSC Adv.*, vol. 9, no. 11, pp. 6387–6394, 2019, doi: 10.1039/c8ra09762c.

[39] W. K. Sun, R. Khan, T. J. Kim, and W. J. Kim, "Synthesis, characterization, and application of Zr,S Co-doped TiO 2 as visible-light active photocatalyst," *Bull. Korean Chem. Soc.*, vol. 29, no. 6, pp. 1217–1223, 2008, doi: 10.5012/bkcs.2008.29.6.1217.

[40] Y. Yu *et al.*, "Enhancement of adsorption and photocatalytic activity of TiO2 by using carbon nanotubes for the treatment of azo dye," *Appl. Catal. B Environ.*, vol. 61, no. 1–2, pp. 1–11, 2005, doi: 10.1016/j.apcatb.2005.03.008.

[41] H. Y. Liu *et al.*, "A comparative study of amorphous, anatase, rutile, and mixed phase TiO2 films by mist chemical vapor deposition and ultraviolet photodetectors applications," *IEEE Sens. J.*, vol. 18, no. 10, pp. 4022–4029, 2018, doi: 10.1109/JSEN.2018.2819700.

[42] H. Berger, H. Tang, and F. Lévy, “Growth and Raman spectroscopic characterization of TiO2 anatase single crystals,” *J. Cryst. Growth*, vol. 130, no. 1–2, pp. 108–112, 1993, doi: 10.1016/0022-0248(93)90842-K.

[43] S. Santangelo *et al.*, “Micro-Raman analysis of titanium oxide/carbon nanotubes-based nanocomposites for hydrogen sensing applications,” *J. Solid State Chem.*, vol. 183, no. 10, pp. 2451–2455, 2010, doi: 10.1016/j.jssc.2010.08.018.

[44] 3 Zlatko Meić Mladen Žini ć Snežzana Miljanić, Leo Frkanec, Tomislav Biljan, “Recent Advances in linear and nonlinear Raman spectroscopy I,” *J. Raman Spectrosc.*, vol. 38, no. April, pp. 1538–1553, 2007, doi: 10.1002/jrs.

[45] D. A. Solís-Casados, E. Vigueras-Santiago, S. Hernández-López, A. Gómez-Cortés, M. Aguilar-Franco, and M. A. Camacho-López, “Textural, structural and electrical properties of TiO2nanoparticles using Brij 35 and P123 as surfactants,” *Sci. Technol. Adv. Mater.*, vol. 9, no. 2, 2008, doi: 10.1088/1468-6996/9/2/025003.

[46] L. Feng, N. Xie, and J. Zhong, “Carbon nanofibers and their composites: A review of synthesizing, properties and applications,” *Materials (Basel).*, vol. 7, no. 5, pp. 3919–3945, 2014, doi: 10.3390/ma7053919.

[47] B. Gao, G. Z. Chen, and G. Li Puma, “Carbon nanotubes/titanium dioxide (CNTs/TiO2) nanocomposites prepared by conventional and novel surfactant wrapping sol-gel methods exhibiting enhanced photocatalytic activity,” *Appl. Catal. B Environ.*, vol. 89, no. 3–4, pp. 503–509, 2009, doi: 10.1016/j.apcatb.2009.01.009.

[48] S. Liu, H. Sun, S. Liu, and S. Wang, “Graphene facilitated visible light photodegradation of methylene blue over titanium dioxide photocatalysts,” *Chem. Eng. J.*, vol. 214, pp. 298–303, 2013, doi: 10.1016/j.cej.2012.10.058.

[49] J. Liu, J. Li, A. Sedhain, J. Lin, and H. Jiang, “Structure and photoluminescence study of TiO2 nanoneedle texture along vertically aligned carbon nanofiber arrays,” *J. Phys. Chem. C*, vol. 112, no. 44, pp. 17127–17132, 2008, doi: 10.1021/jp8060653.

[50] K. Dai, T. Peng, D. Ke, and B. Wei, “Photocatalytic hydrogen generation using a nanocomposite of multi-walled carbon nanotubes and TiO2 nanoparticles under visible light irradiation,” *Nanotechnology*, vol. 20, no. 12, 2009, doi: 10.1088/0957-4484/20/12/125603.

[51] Y. Wang, K. Hu, Y. Zhang, and X. Ding, “Dendritic fibrous nano-silica & titania (DFNST) spheres as novel cataluminescence sensing materials for the detection of diethyl ether,” *RSC Adv.*, vol. 9, no. 68, pp. 39622–39630, 2019, doi: 10.1039/c9ra08152f.

[52] W. Wang, D. Zhu, Z. Shen, J. Peng, J. Luo, and X. Liu, “One-Pot Hydrothermal Route to Synthesize the Bi-doped Anatase TiO2 Hollow Thin Sheets with Prior Facet Exposed for Enhanced Visible-Light-Driven Photocatalytic Activity,” *Ind. Eng. Chem. Res.*, vol. 55, no. 22, pp. 6373–6383, 2016, doi: 10.1021/acs.iecr.6b00618.

[53] N. T. Mai, T. T. Thuy, D. M. Mott, and S. Maenosono, “Chemical synthesis of blue-emitting metallic zinc nano-hexagons,” *CrystEngComm*, vol. 15, no. 33, pp. 6606–6610, 2013, doi: 10.1039/c3ce40801a.

[54] M. Wang, L. Jiang, E. J. Kim, and S. H. Hahn, “Electronic structure and optical properties of Zn(OH)2: LDA+U calculations and intense yellow luminescence,” *RSC Adv.*, vol. 5, no. 106, pp. 87496–87503, 2015, doi: 10.1039/c5ra17024a.

[55] S. Sepulveda-Guzman, B. Reeja-Jayan, E. de la Rosa, A. Torres-Castro, V. Gonzalez-Gonzalez, and M. Jose-Yacaman, “Synthesis of assembled ZnO structures by precipitation method in aqueous media,” *Mater. Chem. Phys.*, vol. 115, no. 1, pp. 172–

178, 2009, doi: 10.1016/j.matchemphys.2008.11.030.

[56] S. Bai *et al.*, “Reverse microemulsion in situ crystallizing growth of ZnO nanorods and application for NO2 sensor,” *Sensors Actuators, B Chem.*, vol. 190, pp. 760–767, 2014, doi: 10.1016/j.snb.2013.09.032.

[57] B. H. Aw, K. K. Looh, H. S. O. Chan, K. L. Tan, and T. S. A. Hor, “X-Ray photoelectron spectroscopic characterization of [{Pt(PPh3)2(μ3-S)}2PtCl2]{,} [{Pt2(PPh3)4(μ3-S)2Cu}2(μ-dppf)][PF6]2[dppf = Fe (C5H4PPh2)2] and other heterometallic aggregates derived from [{Pt(PPh3)2(μ-S)}2],” *J. Chem. Soc.{,} Dalt. Trans.*, no. 21, pp. 3177–3182, 1994, doi: 10.1039/DT9940003177.

[58] M. Ismael, “A review and recent advances in solar-to-hydrogen energy conversion based on photocatalytic water splitting over doped-TiO2 nanoparticles,” *Sol. Energy*, vol. 211, pp. 522–546, Nov. 2020, doi: 10.1016/J.SOLENER.2020.09.073.

[59] T. S. Natarajan, V. Mozhiarasi, and R. J. Tayade, “Nitrogen Doped Titanium Dioxide (N-TiO2): Synopsis of Synthesis Methodologies, Doping Mechanisms, Property Evaluation and Visible Light Photocatalytic Applications,” *Photochem*, vol. 1, no. 3, pp. 371–410, 2021, doi: 10.3390/photochem1030024.

[60] C. Wang, L. Ling, Y. Yao, and Q. Song, “One-step synthesis of fluorescent smart thermo-responsive copper clusters: A potential nanothermometer in living cells,” *Nano Res.*, vol. 8, no. 6, pp. 1975–1986, 2015, doi: 10.1007/s12274-015-0707-0.

[61] E. S. Shibu and T. Pradeep, “Quantum clusters in cavities: Trapped Au15 in cyclodextrins,” *Chem. Mater.*, vol. 23, no. 4, pp. 989–999, 2011, doi: 10.1021/cm102743y.

[62] Q. Ye, Z. Z. Yin, H. Wu, D. Wu, Y. Tao, and Y. Kong, “Decoration of glutathione with

copper-platinum nanoparticles for chirality sensing of tyrosine enantiomers," *Electrochem. commun.*, vol. 110, no. November 2019, p. 106638, 2020, doi: 10.1016/j.elecom.2019.106638.

[63] T. Rahimi-Aghdam, Z. Shariatinia, M. Hakkarainen, and V. Haddadi-Asl, "Nitrogen and phosphorous doped graphene quantum dots: Excellent flame retardants and smoke suppressants for polyacrylonitrile nanocomposites," *J. Hazard. Mater.*, vol. 381, p. 121013, Jan. 2020, doi: 10.1016/J.JHAZMAT.2019.121013.

[64] R. A. D. Pattrick *et al.*, "The structure of amorphous copper sulfide precipitates: An X-ray absorption study," *Geochim. Cosmochim. Acta*, vol. 61, no. 10, pp. 2023–2036, 1997, doi: https://doi.org/10.1016/S0016-7037(97)00061-6.

[65] S. Brunauer, P. H. Emmet, and E. Teller, "Adsorption of gases in multilayer's.," *J. Am. Chem. Soc.*, vol. 60, no. 35, pp. 309–319, 1938.

[66] J. Baloyi, T. Seadira, M. Raphulu, and A. Ochieng, "Preparation, Characterization and Growth Mechanism of Dandelion-like TiO2 Nanostructures and their Application in Photocatalysis towards Reduction of Cr(VI)," *Mater. Today Proc.*, vol. 2, no. 7, pp. 3973–3987, 2015, doi: 10.1016/j.matpr.2015.08.027.

[67] K. Kinashi, Y. Kambe, M. Misaki, Y. Koshiba, K. Ishida, and Y. Ueda, "Synthesis, characterization, photo-induced alignment, and surface orientation of poly(9,9-dioctylfluorene-alt-azobenzene)s," *J. Polym. Sci. Part A Polym. Chem.*, vol. 50, no. 24, pp. 5107–5114, 2012, doi: 10.1002/pola.26338.

[68] H. Wu *et al.*, "Hydrothermal synthesis of Graphene-TiO2 nanowire with an enhanced photocatalytic activity," *Russ. J. Phys. Chem. A*, vol. 89, no. 7, pp. 1189–1194, 2015, doi: 10.1134/S0036024415070134.

[69] E. T. Mombeshora, R. Simoyi, V. O. Nyamori, and P. G. Ndungu, “Multiwalled carbon nanotube-titania nanocomposites : understanding nano-structural parameters and functionality in dye-sensitized solar cells : Research article,” *South African J. Chem.*, vol. 68, no. 1, pp. 153–164, 2015, doi: 10.17159/0379-4350/2015/v68a22.

[70] N. Hintsho, L. Petrik, A. Nechaev, S. Titinchi, and P. Ndungu, “Photo-catalytic activity of titanium dioxide carbon nanotube nano-composites modified with silver and palladium nanoparticles,” *Appl. Catal. B Environ.*, vol. 156–157, pp. 273–283, 2014, doi: 10.1016/j.apcatb.2014.03.021.

[71] N. Sobana, M. Muruganadham, and M. Swaminathan, “Nano-Ag particles doped TiO2 for efficient photodegradation of Direct azo dyes,” *J. Mol. Catal. A Chem.*, vol. 258, no. 1–2, pp. 124–132, 2006, doi: 10.1016/j.molcata.2006.05.013.

[72] J. Coutts *et al.*, “Visible-Light-Responsive Photocatalysis: Ag-Doped TiO2 Catalyst Development and Reactor Design Testing,” *46th Int. Conf. Environ. Syst.*, no. July, p. ICES-2016-169, 2016, [Online]. Available: https://ttu-ir.tdl.org/ttu-ir/handle/2346/67573

[73] J. Zhang, P. Zhou, J. Liu, and J. Yu, “New understanding of the difference of photocatalytic activity among anatase, rutile and brookite TiO2,” *Phys. Chem. Chem. Phys.*, vol. 16, no. 38, pp. 20382–20386, 2014, doi: 10.1039/c4cp02201g.

[74] R. D. Tentu and S. Basu, “Photocatalytic water splitting for hydrogen production,” *Curr. Opin. Electrochem.*, vol. 5, no. 1, pp. 56–62, 2017, doi: 10.1016/j.coelec.2017.10.019.

[75] C. Huang, M. Wu, and V. Nguyen, “TiO 2 on Microsericite for High-E ffi ciency”.

[76] R. Leary and A. Westwood, “Carbonaceous nanomaterials for the enhancement of

TiO2 photocatalysis," *Carbon N. Y.*, vol. 49, no. 3, pp. 741–772, 2011, doi: https://doi.org/10.1016/j.carbon.2010.10.010.

[77] L. Yu *et al.*, "One-pot microwave synthesized high-performance BiVO4/InVO4 heterojunction for photocatalytic reduction of Cr6+," *Sep. Purif. Technol.*, vol. 310, no. December 2022, pp. 1–9, 2023, doi: 10.1016/j.seppur.2023.123143.

[78] M. Hakamizadeh, S. Afshar, A. Tadjarodi, R. Khajavian, M. R. Fadaie, and B. Bozorgi, "Improving hydrogen production via water splitting over Pt/TiO2/activated carbon nanocomposite," *Int. J. Hydrogen Energy*, vol. 39, no. 14, pp. 7262–7269, 2014, doi: https://doi.org/10.1016/j.ijhydene.2014.03.048.

[79] H. Yi, T. Peng, D. Ke, D. Ke, L. Zan, and C. Yan, "Photocatalytic H2 production from methanol aqueous solution over titania nanoparticles with mesostructures," *Int. J. Hydrogen Energy*, vol. 33, no. 2, pp. 672–678, 2008, doi: https://doi.org/10.1016/j.ijhydene.2007.10.034.

[80] N. Lakshminarasimhan, E. Bae, and W. Choi, "Enhanced photocatalytic production of H2 on mesoporous TiO 2 prepared by template-free method: Role of interparticle charge transfer," *J. Phys. Chem. C*, vol. 111, no. 42, pp. 15244–15250, 2007, doi: 10.1021/jp0752724.

[81] J. Jitputti, S. Pavasupree, Y. Suzuki, and S. Yoshikawa, "Synthesis and photocatalytic activity for water-splitting reaction of nanocrystalline mesoporous titania prepared by hydrothermal method," *J. Solid State Chem.*, vol. 180, no. 5, pp. 1743–1749, 2007, doi: https://doi.org/10.1016/j.jssc.2007.03.018.

[82] W.-T. Chen, Y. Dong, P. Yadav, R. D. Aughterson, D. Sun-Waterhouse, and G. I. N. Waterhouse, "Effect of alcohol sacrificial agent on the performance of Cu/TiO2 photocatalysts for UV-driven hydrogen production," *Appl. Catal. A Gen.*, vol. 602, p.

117703, 2020, doi: https://doi.org/10.1016/j.apcata.2020.117703.

[83] I. Rossetti, “Hydrogen Production by Photoreforming of Renewable Substrates,” *ISRN Chem. Eng.*, vol. 2012, pp. 1–21, 2012, doi: 10.5402/2012/964936.

[84] F. Varas-Concha, D. Guzmán, M. Isaacs, and C. Sáez-Navarrete, “Operational Conditions Affecting Hydrogen Production by the Photoreforming of Organic Compounds using Titania Nanoparticles with Gold,” *Energy Technol.*, vol. 6, no. 2, pp. 416–431, 2018, doi: 10.1002/ente.201700546.

[85] M. Hakamizadeh, S. Afshar, A. Tadjarodi, R. Khajavian, M. R. Fadaie, and B. Bozorgi, “Improving hydrogen production via water splitting over Pt/TiO 2/activated carbon nanocomposite,” *Int. J. Hydrogen Energy*, vol. 39, no. 14, pp. 7262–7269, 2014, doi: 10.1016/j.ijhydene.2014.03.048.

CONCLUSION AND FUTURE WORK

Conclusion

The main aim of this study was to develop efficient photocatalytic materials for H_2 production from water. But because most reactions require the use of sacrificial reagents to obtain reasonable quantities of for H_2, methanol was used under mild conditions (>10%) as part of the study.

The first part of the project led to the development of a simple, Novel, one step method that was used in the synthesis of copper oxide nanoparticles, CuONPs at room temperature. The method was reproducible and the CuONPs synthesized using the method did not have to undergo further purification by calcination or annealing. Furthermore, the synthesized CuONPs were used to synthesize high quality carbon nanofibers, CNFs as shown in Chapter 3. The CNFs (as-synthesized) were functionalized and found to be of high purity, and thermal stability of 577ºC and comparable to other CNFs which have been synthesized by other methods.

The synthesis of TiO_2/F_CNFs composites were achieved in Chapter 4. The characterization of the synthesized structures were achieved by various techniques before performing photocatalytic water splitting. The loading of 20%TiO_2 onto the CNFs produced the highest H_2 production of 7203.50 μmol g^{-1} h^{-1}. 10% methanol was also tested for hydrogen production with water using the 20%TiO_2/CNFs photocatalyst but the results were not significantly different and therefore, the study recommended the use of the synthesized photocatalysts with distilled water without methanol addition because the use of methanol at 10% can be a threat to the environment via CO_2 emissions.

The loading of the TiO_2/F_CNFs composites with precious metals (Pt, Au or Ir) was achieved and discussed in Chapter 5. It was realized that compositing of CNFs with titania improved

the BET surface area of the TiO_2 from 73 m^2 g^{-1} to 126 m^2 g^{-1} 20%TiO_2/CNFs. Moreover, the BET surface area generally increased with the precious metal addition in which 20%TiO_2/CNFs/Pt photocatalyst obtained the highest surface area of 341 m^2 g^{-1}. The pore volume of the structures followed the same trend while pore diameter of the composites decrease. The increment was attributed to the fact that noble metals together with the CNFs efficiently tune the morphology of ^{TiO2} for higher surface area, larger pore volume and lower pore diameters thereby increasing the photocatalytic properties of the structures.

The XPS analysis was used to confirm the various elements in the heterostructures as Ti, O, C, N, F, Cl, Zn, and Cu. Therefore, it confirms the presence of Ti, O, C and the co-catalysts Zn and Cu for their quantities, chemical states, and morphology are important in photocatalytic water splitting processes, Chapter 6. From this study, we can concluded that Cu, Zn – TiO2/CNFs heterostructures have significant prospects for photocatalytic water splitting.

Future research

The output of this research has provided several routes that can be used to improve H_2 production from water. Besides, there are certain areas which may require improvement. Despite the fact that copper oxide nanoparticles, CuONPs were used in the synthesis of the carbon nanofibers, CNFs as catalysts, there could be other cheaper or better catalysts to be tried. Again, the CNFs (as-synthesized) had to be functionalized to obtain pure or functionalized CNFs, therefore, other methods of synthesis of CNFs should be explored to produce pure CNFs so that acid functionalization is avoided.

Loading of TiO_2 on CNFs should also be changed to check on the possibilities of getting better results than what is has been reported elsewhere and in in this project. The

hydrothermal method used in loading TiO_2 onto the CNFs has several steps to be followed, therefore, a simpler method should be tried.

Other than CNFs, there are other forms of carbons that can be tried to try enhance H_2 production. These materials include; activated carbon, carbon nanotubes and other forms of carbon. Non-carbonaceous can also be used as photocatalysts for water splitting because besides TiO_2, cadmium sulphite (CdS) has been used. Thus a comparison study should be conducted with $TiO_2$and non-carbonaceous materials.

Different precious metals and non-precious metals or metal oxides should also be tried with CNFs or other carbonaceous materials to improve the results obtained in this study and others that have been reported.

THE END